National Library of Canada
Acquisitions and Bibliographic Services Branch
395 Wellington Street
Ottawa, Ontario
K1A 0N4

Bibliothèque nationale du Canada
Direction des acquisitions et des services bibliographiques
395, rue Wellington
Ottawa (Ontario)
K1A 0N4

Your file Votre référence

Our file Notre référence

NOTICE

The quality of this microform is heavily dependent upon the quality of the original thesis submitted for microfilming. Every effort has been made to ensure the highest quality of reproduction possible.

If pages are missing, contact the university which granted the degree.

Some pages may have indistinct print especially if the original pages were typed with a poor typewriter ribbon or if the university sent us an inferior photocopy.

AVIS

La qualité de cette microforme dépend grandement de la qualité de la thèse soumise au microfilmage. Nous avons tout fait pour assurer une qualité supérieure de reproduction.

S'il manque des pages, veuillez communiquer avec l'université qui a conféré le grade.

La qualité d'impression de certaines pages peut laisser à désirer, surtout si les pages originales ont été dactylographiées à l'aide d'un ruban usé ou si l'université nous a fait parvenir une photocopie de qualité inférieure.

Canada

Surface Phenomena in Capillary Flow of Polymer Solutions

by

Pei Qiong Kuang

A thesis submitted to
the School of Graduate Studies and Research
in partial fulfillment of the requirements for
the degree of
DOCTOR OF PHILOSOPHY
in the Department of Chemical Engineering
at the University of Ottawa
Ottawa, Canada

ISBN 0-315-80007-0

UNIVERSITÉ D'OTTAWA
UNIVERSITY OF OTTAWA

Abstract

Evaluations of apparent slip and surface effects characterizing polymer adsorption are reported for laminar capillary flow of dilute aqueous solutions of three homologous compounds of Polyox, denoted by WSR 301, Coagulant and FRA. Measurements were carried out using very dilute solutions in the polymer concentration range 5 to 200 ppm and very fine glass capillary tubes with diameters varying from 0.0054 to 0.047 cm.

Results were obtained for glass capillary tubes coated with a silane compound (dimethyldiethoxysilane) as well as for the untreated glass tubes to provide a comparison between wall effects observed with a hydrophilic surface and a chemically modified surface.

The results indicate that flow enhancement characterized by a positive effective velocity at the wall is dominant at the very low polymer concentrations and flow retardation characterized by a negative effective velocity at the wall is dominant at the higher concentrations comprising the polymer concentration range investigated. In general, it was found that the magnitude of the effective velocity at the wall increases with increasing wall shear stress and the contribution to the total flow rate becomes more significant in the tubes of smaller diameter. A transition from a positive to a negative effective velocity at the wall was observed with increasing polymer concentration. The critical concentration marking the transition was found to be higher for the silane-treated tubes than for the untreated tubes.

The effective hydrodynamic thickness of the adsorbed polymer layer corresponding to zero shear was evaluated directly from the capillary flow data. The thickness in the plateau region at higher polymer concentrations was found to be greater than two times the root mean square radius of gyration of the polymer molecule for solutions of the three polymers in the untreated tubes while lower value was obtained

for the same solutions in the treated tubes.

A new analysis was applied to separate the contributions of polymer adsorption and slip in the evaluation of the effective velocity at the wall. In the analysis, the flow was modeled by postulating an adsorption isotherm for representation of the variation of the adsorbed layer thickness at zero shear with polymer concentration and assuming a linear dependence of the effective slip velocity on the wall shear stress. Effective hydrodynamic thicknesses of the adsorbed layers are presented as a function of the polymer concentration and wall shear stress for the three Polyox homologues investigated in the chemically treated and untreated glass tubes. The variation of the slip coefficients with polymer concentration of the solutions was also evaluated.

End effect corrections based on flow measurements obtained by varying the tube lengths of the capillaries in the L/D range 750 to 2000 were applied to the data using a modification of the Bagley plot.

Acknowledgements

The author would like to express her sincere appreciation to Dr. W. Kozicki for his supervision, constructive suggestions, valuable discussions and continuous assistance throughout this research program. Thanks are also due to Dr. Aragaki and Dr.Yim for their initial assistance, as well as to the Department's technicians for the construction of the experimental system.

The author gratefully appreciates the financial support provided by the Natural Sciences and Engineering Research Council of Canada.

The author is greatly indebted to her husband and parents as well as the family for their love and support.

Contents

List of Figures

List of Tables

Nomenclature

a	coefficients in Equation (3.36), cm^3/dynes.sec
$\bar{a}$	parameter in the MHS equation (3.53)
a_i	coefficient in Equation (3.13), $(cm^2/dynes)^{\alpha_i}$.cm/sec
A(c)	$du_w/d\tau_w$ at $\tau_w = 0$ in Equation (3.34), cm^3/dynes.sec
A_l, A_u	area of the collecting cup and the reservoir, respectively, cm^2
A_c	outer area of the capillary, cm^2
b	coefficients in Equation (3.36), $(cm^2/dynes)^{\alpha_i}$.cm/sec
c	polymer concentration, g/cm^3
d	exponent in Equation (3.36)
D	tube diameter, cm
D_e	equivalent diameter, cm
e_{vc}, e_{ve}	expansion & contraction friction loss factors at entrance and exit
$\hat{E}_v$	friction loss, cm^2/sec^2
$f(\tau)$	characteristic function of shear stress, sec^{-1}
g	acceleration due to gravity, cm/sec^2
$g(\tau, y)$	correction function in the wall region, sec^{-1}
h_l, h_u	liquid level in the receiver and the reservoir, respectively, cm
H	difference of liquid levels, cm
k	parameter in Equation (3.32), g/cm^3
$\bar{k}$	parameter in the MHS equation (3.53), $cm^3/g^{(\bar{a}+1)}$
k_h	Huggins constant
k_{s0}	proportionality coefficient in Equation (3.33), cm
K	fluid consistency coefficient in power law model, $(dynes/cm^2).sec^n$
K_1, K_2	parameters in Equation (B.4)
l_o	thickness of oil layer in the receiver, cm

L	tube length, cm
L_e	extra length required to account for end effects, cm
m	the degree of polymerization
M^t	reading from the balance at time t, g
M	average molecular weight
M_w	weight average molecular weight
M_v	viscosity average molecular weight
M_n	number average molecular weight
n	flow behavior index in power law model
n'	index defined for tube flow, Equation (3.21)
n_b	end correction factor
P_g	gas pressure, dynes/cm^2
ΔP	total potential difference, dynes/cm^2
ΔP_{ev}	evaluated value of total potential difference, dynes/cm^2
ΔP_{end}	total extra pressure losses, dynes/cm^2
ΔP_{en}	entrance pressure loss, dynes/cm^2
ΔP_{ex}	exit pressure loss, dynes/cm^2
Q	flow rate, cm^3/sec
Q_a	flow rate in the presence of adsorption, cm^3/sec
Q_s	flow rate in the presence of slip, cm^3/sec
R	radius of a capillary tube, cm
Re	Reynolds numbers
R_g	radius of gyration of polymer in solution, cm
r	radial coordinate, cm
$\sqrt{\langle r^2 \rangle}$	root mean square end-to-end distance, cm
u	velocity, cm/sec
$\langle u \rangle$	average velocity, cm/sec

u_w	effective velocity at the wall, cm/sec
u_{wa}	effective velocity at the wall due to polymer adsorption, cm/sec
u_{ws}	effective velocity of slip, cm/sec
W	actual weight of efflux, g
y	normal distance from the wall, y=R-r, cm

Greek Symbols

α	coefficient in Ellis model
α_i	coefficient in Equation (3.13)
$\dot{\gamma}$	magnitude of shear rate, sec^{-1}
δ	anomalous layer thickness, cm
δ_a	effective hydrodynamic thickness of adsorbed layer, cm
δ_{a0}	hydrodynamic thickness of adsorbed layer at zero shear, cm
δ_{ap}	plateau value of δ_{a0}, cm
δ_s	slip layer thickness, cm
ζ	slip coefficient, cm^3/dynes.sec
η_r	ratio of the viscosity of a solution to that of the solvent
η_R	Rabinowitsch viscosity, g/cm.sec
η_{sp}	specific viscosity
η_w	non-Newtonian viscosity evaluated at τ_w, g/cm.sec
η_0	lower limiting viscosity, g/cm.sec
$[\eta]$	intrinsic viscosity, cm^3/g
μ_s	solvent viscosity, g/cm.sec
Φ	Flory's universal constant
ρ	density of water or polymer solution, g/cm^3

ρ_{oil}	density of oil, g/cm^3
τ_w	wall shear stress, dynes/cm^2
$\tau_{1/2}$	Ellis fluid parameter, dynes/cm^2

Subscripts

a	adsorption
s	slip
w	at the wall

Superscripts

i	reading at initial time
t	value at time t

Chapter 1

Introduction

1.1 Introduction

The flow of polymer solutions in confined flow geometries, especially in packed beds or porous media with very large surface areas, may be significantly affected by surface phenomena. The dynamics of polymer solution flows near the solid surface is subject to influences by steric, repulsive, or attractive surface-polymer interactions. Attractive surface-molecular forces may lead to polymer adsorption onto the wall, which may affect the flow behavior of the solvent and free molecules in solution in proximity of the wall. The adsorption results in flow retardation. In contrast, steric effects, repulsive forces or deformation-induced-migration may lead to the formation of a thin depletion layer of polymer molecules with consequent flow enhancement. The phenomena involved are complicated further by the coupling of non-Newtonian as well as viscoelastic properties exhibited by the polymer solutions with influences from other factors. Surface phenomena are of practical importance in many areas such as in filtration (Kozicki, 1990), coating (Dutta and Mashelkar, 1982), enhanced oil recovery (Shah and Schechter, 1977; Sorbie, 1991), drag reduction in pipeline transport, waste treatment, rheology (Pilehvari and Clark, 1983; Yoshimura and Prud'homme, 1988) as well as in chemical, petroleum and environmental engineering (contaminant transfer). The diversity of these fields underlines the importance of systematic basic studies in the field of polymer adsorption and slip. The increas-

ing attention and research interest has been devoted to the subject in recent years. Because of the complexity of the systems involved, there is strong need for experimentation and analysis to further the understanding of the phenomena responsible for the observed flow anomalies.

In the following pages, the objectives of the present work are first outlined. A more detailed literature survey is then given in Chapter 2 which presents an overview of the developments and progress relating to surface phenomena in polymer solution flows. This is followed by a presentation of the analytical techniques employed and developed. In Chapter 4, a description of the equipment and experimental procedure employed is included. The experimental results are presented and discussed in the succeeding chapter. Finally, the conclusions and further work are summarized in Chapter 6.

1.2 Objectives

The goal of the research was to carry out measurements involving the flow of dilute aqueous Polyox solutions in small diameter capillary tubes to gain information relating to the adsorption of polymer onto the tube walls and apparent slip occurring during the flow. The experiments were performed using dilute aqueous solutions of the different molecular weight homologues WSR 301, Coagulant and Polyox FRA of Polyox. The flow measurements were carried out using glass capillary tubes whose surface was modified by chemical treatment with a silane compound (dimethyldiethoxysilane) as well as untreated glass tubes.

The objective of the study was to evaluate effective hydrodynamic thicknesses of the adsorbed polymer layers in contact with the polymer solutions as a function of the relevant parameters, viz. polymer concentration and shear stress, and to determine the effect of the macromolecular size and the surface treatment on the polymer adsorption characteristics. The evaluations, which necessitate accounting

for the slip velocities associated with polymer solution flows, were made by applying a new analysis which yielded the thicknesses of the adsorbed polymer layers and the effective slip velocities simultaneously.

Corrections for end effects, which could not be neglected in this work, were applied by an extension and refinement of Bagley's end correction method to account for the slight variations in the diameters of the tubes of different length having the same nominal diameter used in the experiments.

Chapter 2

Literature Review

The surface phenomena which are encountered in laminar flow of polymer solutions include polymer adsorption and apparent slip. The apparent viscosity of the fluid near the wall can be greater or less than that in the region of bulk flow depending upon the forces acting on the polymer molecules in the wall region. The surface phenomena exhibited by polymer solutions in laminar flow can be divided into two categories characterized by negative and positive effective velocities at the wall, respectively. Polymer solutions may also be considered to exhibit anomalous behavior in turbulent pipe flow, which is referred to as turbulent drag reduction. A small quantity of high molecular weight additive may cause a remarkable reduction in the pressure drop required to maintain the average velocity of the fluid in turbulent flow. This effect was first noticed by Toms (1949a) and has been studied extensively using a variety of polymers (Dodge and Metzner, 1959; Shaver and Merrill, 1959; Wells, 1965; Hoyt and Fabula, 1964; Meter, 1964). Several interpretations of the turbulent drag reduction phenomenon have been proposed involving laminar slip effects (Astarita, 1965), viscoelastic phenomena (Metzner and Park, 1964), and also adsorption effects. Kozicki and Tiu (1968) attributed turbulent drag reduction to two phenomena: (1) the anomalous behavior observed in laminar flow (adsorption or slip effect), and (2) a laminar sub-layer thickness greater than that applicable to the purely viscous non-Newtonian fluids. They presented

an analysis based on these concepts. In spite of numerous investigations there still appears to be no universally accepted mechanism for turbulent drag reduction.

The following presents an overview of previous work and the status of studies addressing surface effects exhibited by polymer solutions in laminar flows. One of the major factors affecting the evaluation of surface phenomena, viz. end effects, is also examined.

2.1 Apparent Wall Slip

Whenever a macromolecular solution flows in a bounded geometry, it encounters an inhomogeneous deformation field which promotes polymer molecular migration away from the wall in some cases. The migration results in a polymer depleted zone near the wall, which can manifest an apparent wall slip observed as an enhancement in the flow. Such wall slip can potentially play a significant role in controlling a variety of transport processes involving macromolecular systems.

The apparent slip phenomenon is not a new subject in the technical literature. In the early 20th century, slip effects had been observed in the flow of polymer solutions and dispersed phase fluids (Schofield and Scott Blair, 1930; Mooney, 1931; Toms, 1949b; Oldroyd, 1949). The early studies on apparent slip recognized that apparent slip effects are manifested by a decrease of the apparent viscosity with decreasing tube diameter at a fixed wall shear stress. Reiner (1931) demonstrated that a significant slip effect took place in the flow of a 1.7% nitrocellulose in dibutyl phthalate solution by comparing flow curves for different tube diameters. Slip effects in the flow of aqueous polymer solutions in capillary tubes have also been documented by Kozicki et al. (1970), Vinogradov and coworkers (1975), Vlasov and Kalashnikov (1973), as well as in porous medium flows (Kozicki and Tiu, 1967; Chauveteau, 1982). An example of an anomalous effect for the flow of polyethylene oxide solutions (WSR 301) in capillary tubes is demonstrated in figure 2.1 showing

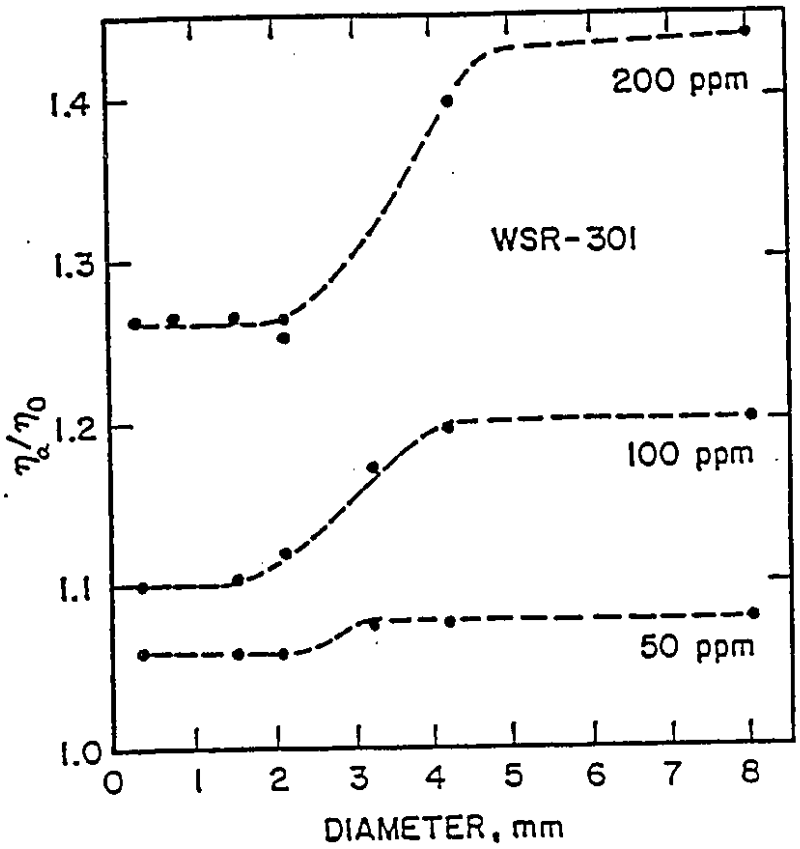

Figure 2.1 Diameter effects for the flow of aqueous polyethyleneoxide (WSR-301) solutions through capillary tubes. η_a is the apparent viscosity, and η_o is the solvent viscosity. Data of Kalashnikov & Vlasov (1978).

data reported by Kalashnikov and Vlasov (1978). The data clearly show that the relative viscosity decreases with decreasing capillary diameter. It should be noted that end effects were not taken into account in their work.

A more definitive illustration of apparent slip in capillary tube flow was given by Metzner et al. (1979), based on the data for tube flow of a 0.6% polyacrylamide solution. The slip for the flow of the polymer solutions in channels of dimensions much larger than the hydrodynamic macromolecular size was attributed to heterogeneous stress fields. Thus, no slip effects are assumed in a cone-and-plate viscometer in which the stress levels are constant everywhere. In a recent comprehensive paper, Cohen and Metzner (1985) quantified the flow enhancement due to slip in laminar flow of solutions of polystyrene, partially hydrolyzed polyacrylamide, and carboxymethylcellulose in small diameter stainless steel tubes. The experimental flow rates were considerably higher than the predictions based on viscometric cone-and-plate data. Figures 2.2-2.3 illustrate the flow curves obtained for two selected cases. The contribution of the effective slip velocity to the total flow rate for a given tube diameter was found to decrease with increasing wall stress and increase with decreasing tube diameter for a given wall stress. An empirical power-law relation was suggested to describe the relation between the effective slip velocity and the wall shear stress: $u_s = a_i \tau_w^{\alpha}$. An improved expression is $u_s = a_i(c)\tau_w^{\alpha}$, which accounts for the effect of the solution concentration. Similar relationships for the slip velocity have also been reported for film flow of polymer solutions (Mashelkar and Dutta, 1982; Carreau, et al., 1979).

Evaluations of slip for flow through capillaries have been reported recently for solutions of polyacrylamide and xanthan gum (De Vargas and Manero, 1989). These polymeric solutions represent macromolecules with different conformations during flow. Attention was directed to the influence of the molecular conformation of the polymer in solution upon the slip velocity. Larger effects were observed with steel

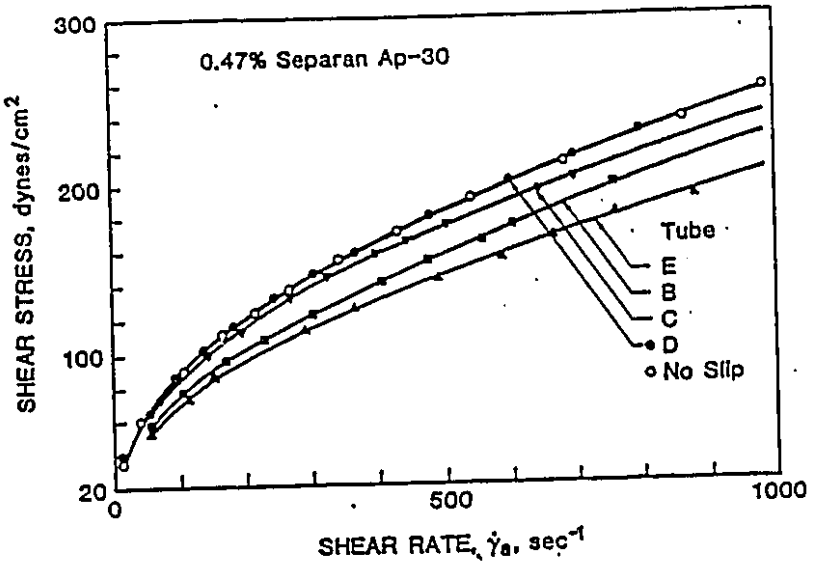

Figure 2.2 Capillary viscometer flow curves for the flow of 0.47% aqueous polyacrylamide (Separan AP30) solution. Demonstration of slip effects. Deviations from the uppermost curve (cone-and-plate data) are a measure of apparent slip effects. Data Cohen and Metzner [10]. Legend: E — D = 0.01906 cm, L/D = 1909; B — D = 0.02662 cm, L/D = 1996; C — D = 0.1097 cm, L/D = 997; (O)—cone-and-plate data.

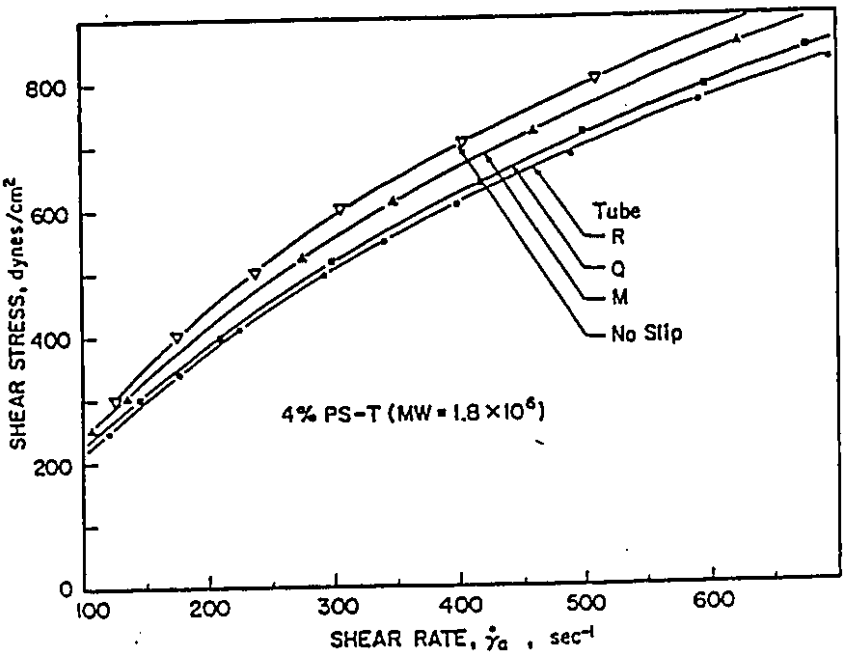

Figure 2.3 Capillary flow curves for 4% polystyrene-toluene solution (MW = 1.8 × 10⁶). Demonstration of slip effects. Deviations from the uppermost curve are a measure of apparent slip effects. Data of Cohen and Metzner [10]. Legend: R — D = 0.027 cm, L/D = 2013; Q — D = 0.052 cm, L/D = 1956; M — D = 0.084 cm, L/D = 1698.

capillaries and for the solutions of xanthan containing salt. This was explained in terms of the conformation adopted by the macromolecules in the region close to the wall and their interaction with the capillary material.

The detection of apparent slip is often complicated by the simultaneous adsorption of polymer onto the capillary wall. In order to minimize the interference of polymer adsorption with the slip phenomenon, a technique was introduced by Cohen and Metzner (1982) to chemically modify the silica surface. The method uses a bifunctional silane compound, dimethyldiethoxysilane. The silane can attach covalently to a silica surface (under appropriate solution conditions) through its hydrolyzable ethoxy functionalities, leaving its methyl groups exposed to the external environment (Arkles, 1977). Thus a "new" hydrophobic surface can be created on the silica surface. The modified silica surface minimizes polymer adsorption so apparent slip can be readily determined. The effectiveness of the surface treatment method has been utilized by Cohen and Metzner (1982, 1985), Cohen and Christ (1986a) in flow of polymer solutions through capillary tubes and porous media. On the other hand, studies (Taluder and Reuter, 1981; Hatzikiriakos and Dealy, 1991) have shown a significant effect of the nature of the solid surface on the observed slip.

To prove the existence of the slip layer, methods of directly detecting apparent wall slip have been developed. Because the slip layer is estimated to be of the order of a few microns in thickness, advanced and sophisticated measurement techniques in the vicinity of the wall are entailed. To date, laser differential microanemometry (LMA) and total reflection microscopy (TRM) (Mohnssen et al., 1987) and the techniques of total internal reflection (Ausserre et al., 1985) and evanescent-wave-induced fluorescence (EWIF) (Rondelez and Hervet, 1987; Kim et al., 1989) have been employed in detection of apparent slip. The detection of apparent slip is accomplished in the first two methods by measurement of the velocity profile and

in the latter two by determination of the polymer concentration profile near the wall of the channel. Mohnssen et al. (1990), using LMA and TRM (relying on tracking gold particles) to measure velocity profiles up to a minimum distance of 0.15 μm from the wall, revealed that the thickness of the slip layer δ_s sharply decreased with increasing concentration of aqueous polyacrylamide (PAM) and tended to a constant value at higher concentrations, in duct flows. At each concentration, the slip velocity increased linearly with shear stress at the wall and no threshold was found within the range of wall shear stress examined in the study. The slip coefficient denoting the ratio of the slip velocity to wall shear stress decreased with increasing concentration. Ausserre et al. (1986), using a light scattering method, have also found that the slip layer thickness decreased with concentration over the concentration range 100 to 1000 ppm for xanthan. Their result was confirmed by the recent study of Sorbie and Huang (1991), for the flow of xanthan solutions (30-160 ppm) through porous media. The apparent depleted layer thickness was estimated from rheological data which were analyzed using a simple two-fluid model expression (Chauveteau et al., 1982, 1984) as well as a recently published linear layer analytical model (Sorbie, 1990a).

The advent of the new EWIF technique has made it possible to directly probe the polymer concentration profile in the depletion layer adjacent to the wall. A recent EWIF study of the polymer concentration profile in shear flow reported shear-induced-thickening of the "depletion layers" (Ausserre et al., 1991). This has provoked initial interest of Duering and Rabin (1990) in the problem. They used computer simulation to study the conformation and concentration profiles of polymers in good solvents subjected to simple shear flow between repulsive walls. The result found for polymers with excluded volume interactions was that the width of the depletion layer near the wall decreases with shear rate.

To date, the reason for the polymer migration phenomenon is not clear and two

distinctly differing schools of thought exist, viz. due to wall-macromolecular interactions or migration under the action of shear gradients. Each of these mechanistic interpretations can explain some but not all of the wall slip behavior observed in macromolecular systems.

Steric effects due to electrostatic or hard-core repulsion of macromolecules from the wall may be partially responsible for the apparent slip phenomenon in small flow channels (Brunn, 1976; Aubert and Tirrell, 1982; Grisafi and Brunn, 1989). The latter proposed that in the presence of the wall, the configuration available to macromolecules near the wall would be restricted and therefore a polymer-depleted zone would exist. Since the thickness of the wall exclusion layer is of the order of the hydrodynamic size of the macromolecules, it is unlikely that such effects will be important in large channels. Brunn and coworkers (1985a-b) have conclusively shown, based on the linear elastic-dumbbell model of a macromolecule, that such wall effects in large channels may lead to a boundary layer region thickness of about $1.663R_o$, in which R_o is the equilibrium extension of the macromolecule. On the basis of the slip associated with the molecular exclusion at the surface, theoretical calculations have been presented on the rheological and transport properties of polymer solutions in capillaries and in network models of porous media (Sorbie, 1990a-b).

As indicated, an alternative explanation for apparent slip is linked to the existence of shear gradients in wall-bounded shear flows (Tirrell and Malone, 1977; Metzner and Cohen, 1979, 1982b). In any flow with a spatially dependent deformation rate, the molecular orientation and extension, and consequently, the free energy level vary with the position within a fluid. In order that the free energy becomes position independent at steady state, compensating concentration gradients are set up. Thus, in inhomogeneous flows, concentration gradients may be induced as the system tends toward an equalization of spatial free energy changes implied

by entropy gradients. The net effect is that the macromolecules tend to migrate towards regions of lower deformation rate levels. In capillary tube flow, for example, macromolecules will migrate away from the wall region, where shear stresses are higher. This diffusion phenomenon leads to depletion of polymer molecules in the wall region and consequently to the formation of the wall slip layer.

A theoretical analysis based on irreversible thermodynamics of deformation-induced migration of macromolecules was provided by Dutta and Mashelkar (1984), and by Cohen and Metzner (1986b). An approximation of the polymer concentration profile was obtained based on the thermodynamic diffusion model, which shows a significant decrease of the polymer concentration in the wall region.

2.2 Hydrodynamic Adsorption

Polymer adsorption onto a solid surface is of fundamental and practical importance in viscometry, oil recovery, filtration, wastewater treatment, medicine, liquid chromatography, etc.. A great deal of literature based on theoretical and experimental studies relating to polymer adsorption onto solid surface exists which concerns adsorption from quiescent solutions. In recent years, however, there has been a growing interest in polymer adsorption during flow (Dimarzio and Rubin, 1978; Hatano, 1984; Barham et al., 1986; Narh et al., 1986), since most practical processes in which polymer adsorption is important often involve a flow field above the adsorbing surface. It has been suggested that polymer adsorption can be significantly modified by external hydrodynamic or electrostatic forces (Lee and Fuller, 1985; Kawaguchi et al., 1988a; Besio et al., 1988; Miles et al., 1983).

It is well-known that polymer adsorption may result in a significant increase in the flow resistance due to the effective decrease in channel size. This flow retardation in capillary and porous media flows was reported earlier by Ohrn (1955), Takeda and Endo (1956), Tuijnman and Hermans (1957), Rowland and Eirich (1966a-b), and

Sadowski (1963) for a variety of systems. The phenomenon is the basis of methods developed to study the thickness of an adsorbed layer. Different techniques are now available for measuring the average adsorbed layer thickness. Included among the effective methods for studying hydrodynamic adsorption are ellipsometry (Lee and Fuller, 1984, 1985; Chin and Hoagland, 1991) and the hydrodynamic flow technique (Huque et al.,1959; Priel and Silberberg, 1978; Chauveteau et al., 1984). The two techniques provide different measures of the average adsorbed polymer layer thickness. The thickness measured by ellipsomery is an average over the entire segmental distribution above the surface. The hydrodynamic method, on the other hand, is considered to be more sensitive to the dangling ends and loops which extend furthest from the surface. The flow reduction due to adsorbed polymer is quantified in terms of an effective reduction in the flow cross-section which yields an effective hydrodynamic thickness (EHT) of the adsorbed polymer layer. In addition, the effect of polymer adsorption may also be characterized by a negative effective velocity at the wall, first proposed by Kozicki et al. (1967, 1970).

The early hydrodynamic flow studies were carried out at low shear rates and hence did not detect the effect of the applied pressure on the thickness of the adsorbed layers of polystyrene (Pefferkorn et al., 1978). The results are limited to adsorption of polymers of intermediate molecular weights at rather low pressure differences. In addition, the experimental technique usually compared the flow behavior of the solvent through a given capillary tube before and after the flow of the polymer solution (Chan and Robertson, 1970). The extra resistance to the flow of the solvent (due to the adsorbed polymer layer) was then expressed in terms of the hydrodynamic thickness of the residual adsorbed layer, δ_a (Varoqui and Dejardin, 1977),

$$\frac{\delta_a}{R} = 1 - (\frac{Q_a}{Q})^{1/4} \tag{2.1}$$

where Q and Q_a are the flow rates in the presence and absence of adsorption,

respectively. A relationship,

$$\delta_a \approx 2R_g \tag{2.2}$$

was found for the polymers of higher molecular weight, where R_g is the root mean square radius of gyration of the polymer molecule. This appears to be in good agreement with the results of Thomas (1976). It should be noted that some desorption may occur when the solvent is used in determination of the polymer adsorbed. Consequently, this method determines the resistance only of the residual adsorbed layer to the flow of the solvent.

Studies in the 1980's have shown that the thickness of the adsorbed layer is also a function of the wall shear stress. In solution flow, the question arises of the possible influence of interactions between the flowing polymers and the adsorbed polymers and whether this interaction is modified by the flow. Generally, the effect of hydrodynamic forces can be examined in two ways. In the first, the polymer chains are first adsorbed in a quiescent system and then subjected to the flow of the bulk liquid above the surface. Alternatively, the importance of the flow may be investigated by evaluating the adsorption from a flowing solution. In the former case, for a weakly adsorbed, high molecular weight, flexible chain, only a small proportion of the polymer segments is actually attached to the surface with the remainder extending away from the surface as dangling ends or loose loops. The imposition of hydrodynamic forces can result in distortion and alignment of those unattached segments. The latter case could result in flow-induced deformation and orientation of the polymer chains prior to attachment to the surface. It is possible that such changes in conformation could affect both the kinetics of the adsorption and the final conformation of the film.

Included among the early studies in this area which most convincingly demonstrate the effect of the flow on the deposited polymer films are those reported by Gramain and Myard (1981a) and by Cohen and Metzner (1982a). In both stud-

ies, the effective hydrodynamic thickness (EHT) of the adsorbed polymer layer was evaluated from the increased hydrodynamic resistance offered by the adsorbed polymer layer. The EHT is sensitive to both the density and spatial extent of adsorbed chains, particularly tail sections that protrude far into the solution. Gramain and Myard determined that the thickness of the residual adsorbed layer increased with flow rate for the flow of Newtonian solvents through the millipore filters used for both polyacrylmide-NaCl and polystyrene-toluene systems. It was indicated that both shear and extensional flows could occur during the solvent flow through the adsorbed polymer layer and the extensional component of the flow could be responsible for the increase in the EHT with increasing flow rate. However, the effective hydrodynamic thickness of the adsorbed layer, in the study of Cohen and Metzner using polystyrene-toluene, polystyrene-trans-decalin, and polyacrylamide-water solutions was reported to decrease with increasing shear rate in contrast to the dilatant behavior observed by Gramain and Myard. The latter result obtained with the adsorbed polymer in contact with the flowing polymer solution was attributed to the increased alignment of the polymer and/or tearing of adsorbed macromolecules from the surface with increasing shear stress at the wall. These results point to the need for more research in this area.

Adsorption and desorption of flexible polystyrene chains in flowing systems has been studied by Lee and Fuller (1984, 1985) and Chin et al. (1991) using ellipsometry. Lee and Fuller have found that hydrodynamic forces inhibit the adsorption of polymer chains from a moving fluid onto an initially clean surface and enhance desorption of high-molecular-weight, flexible polymer chains from preadsorbed layers; however, the thickness of the adsorbed layer did not change much due to the flow. In two different solvents, the results of Chin et al. show that flow had no effect on adsorption of polymer in decalin (a slightly good solvent); in contrast, there was a substantial shear flow effect in cyclohexane (a θ solvent), with flow reducing the

level of adsorbed polymer. Only the latter result is in agreement with the observation of Lee and Fuller. An initial reduction in the thickness of the adsorbed polymer layer with shear followed by a constant value was reported by Chang and Chung (1991) for the flow of polyethylene oxide solutions with nominal molecular weights of 1×10^5 and 9×10^5 of the polymer. The evaluations were carried out by means of photon correlation spectroscopy.

In a study of the adsorption of poly(acrylic acid) and polystyrenesulfonate from aqueous solutions in muscovite mica membranes, Idol and Andersen (1986) reported that the EHT may increase with increasing flow rate only in pores with diameters smaller than 800 $\dot{A}$. The results of a more recent study of Bagassi et al. (1989), however, indicate there is no apparent shear-thickening if the pores are straight with smooth walls (pure shear flow), for the flow of either pure solvent or polymer solutions over the adsorbed layer. Shear-thickening of the adsorbed layers was observed only in porous media with irregularities in the channel cross section or structure. The shear thickening was attributed to elongational-flow-induced "coil-stretch" transitions of the adsorbed macromolecules. Irregularities in pore structure are required to produce the local elongational flow. Shear flows produce small changes in molecular conformation in dilute solution compared to elongational flows which produce large conformational changes. Besio et al. (1988) have published the first study of elongational flow effects on polymer adsorption. The adsorption was found to be dramatically affected by elongational flow. Polymers adsorbed from elongational flow fields which are strong enough to produce stretched-state-conformations, result in highly compressed and dense adsorbed layers. Their results showed that for the polystyrene with $M_w = 20 \times 10^5$ and concentration of 700 ppm, the layer thickness decreased with increasing strain rate due to the compression of the adsorbed layer by the jet, however, the surface concentration in the adsorbed layer was not conserved but increased with time; for the polystyrene with $M_w =$

1.8×10^5 at 1000 ppm, the thickness of the adsorbed layer increased with increasing flow rate.

Cohen (1988) reported a transition from shear-thickening to shear-thinning of the adsorbed layer, for a polymer system at the θ-condition. Below a critical shear rate the drag force may be too small to drag the tails and loops closer to the surface; and as the shear rate increases, loops and trains that are anchored by floating trains (those whose attractive force might be weak) may be separated from the surface. Consequently, below the critical shear rate, the thickness of the adsorbed layer increased with increasing shear rate.

Significant levels of polymer adsorption have been observed in earlier work by Desremaux et al. (1971) as well as by Bryson et al. (1971), the latter based on a series of experimental observations and tracer study involving tubular flow of aqueous Polyox WSR 301. A wall thickness reported in the latter investigation was substantiated in an independent study (Kozicki et al., 1984) with the same polymer solution in which high adsorption-gelation levels were also determined. The thicknesses reported in an investigation by Cohen and Metzner (1982a) of the wall layer were larger than the end-to-end distances of the macromolecules by up to a factor of 5 for polyacrylamide and an order of magnitude for polystyrene. It appears that the associated flow reduction was more noticeable in the case of small tube diameters.

In an investigation (Hanna, 1977) of the adsorption characteries of Polyox solutions in beds packed with uniformly sized stainless steel spheres using three sphere sizes, the evaluations of the wall layer thicknesses showed a Langmuir-type polymer concentration dependence. It was also documented in the results of Kozicki et al. (1984) for the same polymer solution flowing in capillary tubes.

Evaluations of polymer adsorption-gel formation and pure solvent layer effective thicknesses as a function of the tube diameter, wall shear stress and polymer con-

centration for aqueous Natrosol 250G and 250HR solutions were studied based on a superposition model (Kozicki et al., 1987). The wall effect was found to undergo a change from one dominated by polymer adsorption-gel formation to one dominated by slip in a narrow range of the inverse of the tube radius 1/R.

The interfacial behaviour of polymer solutions, of course, can be strongly influenced by substrate surface chemistry and surface geometry (Kawaguchi and Arai, 1991). Chemical modification of a surface is a widely used method of obtaining desirable surface properties while retaining the mechanical and geometric properties of the substrate. Although a great deal of work has been done addressing static adsorption over the past several decades, relatively little work addressing polymer adsorption onto chemically modified surfaces has appeared in the literature (Gargallo and Cid, 1977; Cosgrove et al., 1986, 1988). Recently, Parnas and his coworkers (1989) have explored the experimental approach of modifying siliceous surfaces and the application of these surface to the study of polymer adsorption as a function of surface chemistry. In this study, the adsorption of polyvinylpyrrolidone onto untreated silica, silylated silica and polyvinylpyrrolidone-grafted silica was measured to determine the effect of the surface treatments on adsorption. Additionally, a limited number of adsorption experiments were conducted with polyethylene oxide using the untreated and the polyvinylpyrrolidone-grafted silica surfaces. The results indicate polyvinylpyrrolidone adsorption onto silica strongly depends on surface chemistry whereas polyethylene oxide with $\bar{M}_n$= 400,000 exhibits less dependence on surface chemistry. The study focused only on the static adsorption of polymer onto chemically modified surfaces. Effective hydrodynamic thickness measurements are lacking for chemically modified surfaces under controlled adsorption conditions, for comparison of the hydrodynamic characteristics of the polymer layers adsorbed onto surfaces of varying chemical functionality.

2.3 End Effects in Laminar Capillary Flows

Bagley (1957) developed a useful method for evaluation of entry and exit excess pressure losses required for evaluation of the surface effects and rheological behavior of the fluid from capillary flows. It is based on the assumption that at a constant shear rate, the shear stress at the wall should be constant and the total pressure applied to the reservoir of a capillary viscometer should be proportional to the ratio L/R (length over radius of the capillary). From the force balance,

$$\Delta P = \Delta P_{en} + \Delta P_{ex} + \frac{2\tau_w L}{R} \tag{2.3}$$

An extra tube length L_e may be defined in terms of the entrance and exit losses by

$$\Delta P_{en} + \Delta P_{ex} = \frac{2\tau_w L_e}{R} = 2\tau_w n_b \tag{2.4}$$

where n_b is the end correction representing the dimensionless extra length of tube (L_e/R) required to account for the entry and exit losses in fully developed flow. Thus, the wall shear stress τ_w may be expressed by:

$$\tau_w = \frac{\Delta P}{2(L/R + n_b)} \tag{2.5}$$

The end correction is determined by first plotting $R\Delta P/2L$ vs. $4\langle u\rangle/R$ on log-log coordinates. Different flow curves will be obtained for tubes with different L/R. Thus, ΔP can be determined as a function of L/R for given values of $4\langle u\rangle/R$. A linear plot of ΔP vs. L/R then is obtained. The end correction factor n_b is the intercept on the abscissa of this plot, which is obtained as a function of $4\langle u\rangle/R$.

Generally, the best theoretical result available for the end effect for a Newtonian fluid is $n_b = 0.854$. The end correction for the flow of a power-law fluid in a capillary rheometer varies with n and attains a very high value as n tends to zero (Boger et al., 1978).

The total excess pressure losses (end effects) in small capillary tubes were studied (Moan et al., 1979) for dilute hydrolyzed and non-hydrolyzed polyacrylamide

solutions. The total extra pressure loss was found to be proportional to the polymer concentration and to increase with the shear rate. Large total extra pressure losses ΔP_{end} ($=\Delta P_{en}+\Delta P_{ex}$) observed in capillary tubes at high flow rates were attributed to elastic effects. When inertia effects are negligible, the convergent entry flow is mainly governed by the elasticity of the polymer solution which may result in large extension of the polymer molecules; the energy dissipated by viscous friction on the stretched molecules can be represented by ΔP_{end}. The strong end effect found with dilute polymer solution was attributed by Chauveteau et al. (1984) to macromolecular elongation in the extensional flow at the entrance and the exit of the capillary. Separation of elastic and shear-thinning effects in the capillary rheometer was addressed by Boger and Binnington (1977). The end correction in the absence of shear thinning was found to be constant with shear rate in the lower shear rate region and to decrease slightly at higher shear rate; the influence of shear thinning in the presence of elasticity was found to increase the end effects. In a study by Ouibrahim (1979), ΔP_{end} was found to increase with tube diameter.

Another method for evaluating end pressure losses involves measurement of the pressure profile along a capillary or slit wall. The entrance and exit corrections can then be determined separately by extrapolating the linear part of the pressure profile to the entrance or the exit. This method was used by Han and coworkers (1970, 1971), and by Choplin and Carreau (1981). In the latter work, four fluid models, viz. Newtonian, inelastic shear thinning, elastic shear thinning and approximately second-order fluids, were used to study excess pressure losses in a slit. The results indicate that entrance losses are very important when the fluid exhibits both elastic and shear-thinning properties. In the absence of shear-thinning, the entrance losses were smaller or close to values obtained with Newtonian fluids (basically in agreement with the results of Boger and Binnington (1977)). Exit losses exhibited the same pattern as entrance losses which include kinetic energy and viscous dissipation

corrections and a correction due to the normal stress term in the fully developed flow region (stored elastic energy). Exit losses amounted to only 20-40% of entrance losses. The total correction factor corresponds to the Bagley factor, n_b.

Chapter 3

Theoretical Background

In the following, the analysis behind the methodologies employed in evaluation of the various flow characteristics including the rheological behavior of the fluid and the parameters characterizing the surface effects at the fluid-wall interface are presented. The analysis is confined to steady, uniform, laminar flow in capillary tubes which were used in this investigation.

3.1 Flow in a Capillary Tube

3.1.1 Evaluation of the Effective Velocity at the Wall

In steady, uniform, laminar flow of a fluid exhibiting a surface effect at the wall, the velocity gradient in the mainstream is given by

$$\frac{du}{dy} = f(\tau_{rz}) \tag{3.1}$$

and adjacent to the wall it may be represented by

$$\frac{du}{dy} = f(\tau_{rz}) + g(\tau_{rz}, y) \tag{3.2}$$

In the above, as shown in figure 3.1, y=R-r is the perpendicular distance from the wall; $f(\tau_{rz}) = \dot{\gamma_{rz}} = \tau_{rz}/\eta$ is the characteristic function of shear stress determined by the fluid model equation; and $g(\tau_{rz}, y)$ denotes the correction function introduced by Oldroyd (1949) which is applied to the wall region. The thickness of the anomalous zone is δ. Outside the region of anomalous flow, i.e. when $y \geq \delta$, $g(\tau_{rz}, y) = 0$.

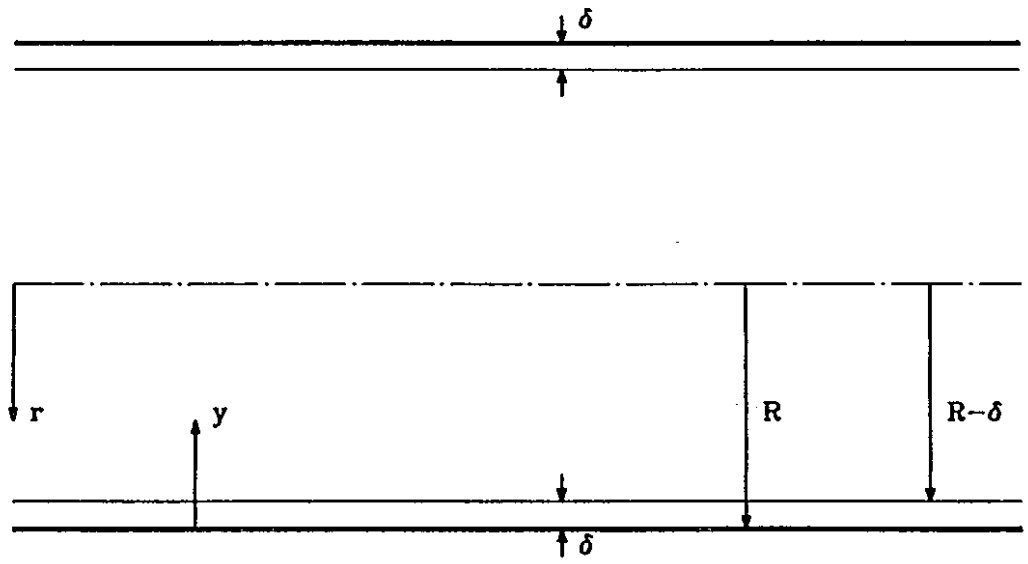

Figure 3.1 A schematic diagram of the anomalous layer in a capillary tube.

Integration of equation (3.2) with respect to y to beyond the region of anomalous flow yields the velocity expression:

$$u = \int_0^y f(\tau_{rz})dy + \int_0^\delta g(\tau_{rz}, y)dy \tag{3.3}$$

At the wall, y=0, equation (3.3) gives a finite velocity which characterizes the anomalous behavior of the fluid in the wall region and is designated the effective velocity at the wall:

$$u_w = \int_0^\delta g(\tau_{rz}, y)dy \tag{3.4}$$

This may be positive or negative corresponding to apparent slip or polymer adsorption, respectively, as depicted in figure 3.2.

The velocity distribution may therefore be represented by the usual expression for flow without a surface effect to which the effective velocity at the wall is added:

$$u = \int_0^y f(\tau_{rz})dy + u_w \tag{3.5}$$

For simplicity, in the following τ_{rz} will be denoted by τ.

Combination of equation (3.2) and the shear stress distribution $\tau/\tau_w = r/R$, with the tubular flow rate expression

$$Q = \pi \int_0^R r^2(-\frac{du}{dr})dr \tag{3.6}$$

produces

$$Q = \pi\{\frac{R^3}{\tau_w^3}\int_0^{\tau_w} \tau^2 f(\tau)d\tau + \int_{R-\delta}^R r^2 g(\tau, y)dr\} \tag{3.7}$$

For a very thin anomalous zone, $\delta/R \ll 1$ and r^2 inside the second integral may be replaced by R^2, which results in:

$$\langle u\rangle = \frac{R}{\tau_w^3}\int_0^{\tau_w} \tau^2 f(\tau)d\tau + \int_0^\delta g(\tau, y)dy \tag{3.8}$$

Combination with equation (3.4) finally yields the following expression (Oldroyd, 1949; Wilkinson, 1960; Kozicki et al., 1984):

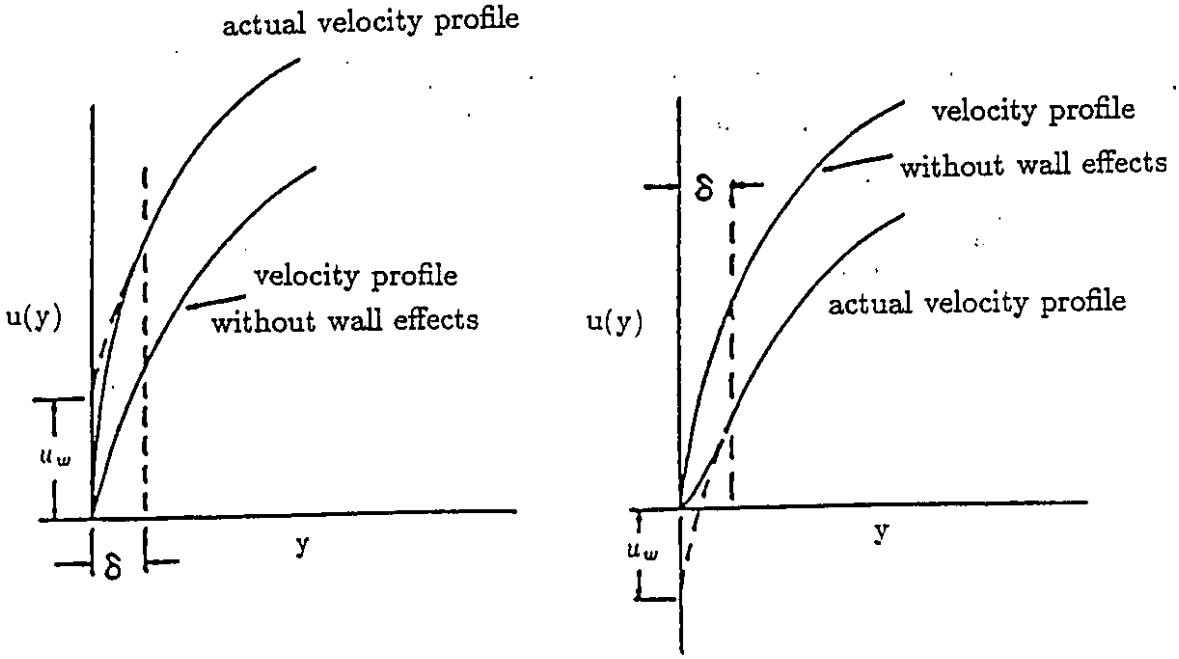

(a) Positive effective velocity at the wall

(b) Negative effective velocity at the wall

Figure 3.2: Positive and negative effective velocities at the wall

$$\frac{\langle u \rangle}{R} = \frac{1}{\tau_w^3} \int_0^{\tau_w} \tau^2 f(\tau) d\tau + \frac{u_w}{R} \tag{3.9}$$

which may be rewritten:

$$\frac{(\langle u \rangle - u_w)}{R} = \frac{1}{\tau_w^3} \int_0^{\tau_w} \tau^2 f(\tau) d\tau \tag{3.10}$$

Introduction of the Rabinowitsch viscosity given by

$$\eta_R = \frac{\tau_w^4}{4 \int_0^{\tau_w} \tau^2 f(\tau) d\tau} \tag{3.11}$$

produces

$$\frac{8\langle u \rangle}{D} = \frac{\tau_w}{\eta_R} + \frac{8u_w}{D} \tag{3.12}$$

As seen from equation (3.11), the Rabinowitsch viscosity is a function of the wall shear stress. For a Newtonian fluid, it reduces to the Newtonian viscosity.

Assuming the effective velocity at the wall due to a surface effect depends only on the wall shear stress, according to equation (3.12) a plot of $8\langle u \rangle / D$ vs. $1/D$ at constant τ_w will be linear, with slope equal to $8u_w$. Further, u_w can be evaluated as a function of the wall shear stress, which may be used to determine the relationship of $8(\langle u \rangle - u_w)/D$ to τ_w. This procedure for evaluation of the effective velocity at the wall implies that u_w is independent of the tube diameter. Recently, Kozicki et al. (1970, 1987) indicated that u_w may vary with tube diameter as well as wall shear stress. Both polymer adsorption-gel formation (a negative effective velocity at the wall) and polymer depletion (a positive effective velocity at the wall) phenomena may occur simultaneously. The relative extents depend upon the nature of the solid surface and polymer-solvent system.

For slip flow of polymer solutions, the fractional contribution of slip flow to the total flow rate (Q_s/Q) can be evaluated from a knowledge of the relationship between the slip velocity and the wall shear stress. An empirical relation for the effective slip velocity in terms of the wall shear stress was given by Cohen and Metzner (1985):

$$u_s = a_i \tau_w^{\alpha_i} \tag{3.13}$$

where the values of the parameters a_i and α_i can be determined from experimental data. Combination of equations (3.13) and (3.10) then gives:

$$\frac{u_s}{\langle u \rangle} = \frac{Q_s}{Q} = \{\frac{R}{a_i \tau_w^{3+\alpha_i}} \int_0^{\tau_w} \tau^2 f(\tau) d\tau + 1\}^{-1} \tag{3.14}$$

For a power-law fluid, $f(\tau) = (\tau/K)^{1/n}$, Q_s/Q becomes:

$$\frac{Q_s}{Q} = [(\frac{4n}{3n+1}) \frac{\tau_w^{(1/n)-\alpha_i}}{a_i K^{1/n}} D + 1]^{-1} \tag{3.15}$$

Equation (3.15) indicates that Q_s/Q increases with decreasing tube diameter as verified by the experiments of Cohen (1981). The slip phenomenon is therefore more important in small channels. The large enhancement in flow rate, up to 40%, demonstrates the potential importance of wall effects in research investigations and industrial applications.

3.1.2 Anomalous Zone Thickness

A positive u_w is referred to as an effective velocity of slip at the wall. If the slip is attributed to polymer depletion in the wall region, one may evaluate an effective solvent layer thickness manifesting the slip velocity. Thus, for a thin pure solvent layer at the wall in which any deviation of τ from τ_w is negligible, $du/dy = \tau_w/\mu_s$ and equation (3.2) gives:

$$g(\tau, y) = \frac{\tau_w}{\mu_s} - f(\tau) = \tau_w (\frac{1}{\mu_s} - \frac{1}{\eta_w}) \tag{3.16}$$

where μ_s is the solvent viscosity and η_w is the non-Newtonian viscosity of the bulk solution evaluated at the wall shear stress.

Substituting for $g(\tau, y)$ in equation (3.4) results in the solvent layer thickness as follows:

$$\delta_s = \frac{u_w}{\tau_w} (\frac{1}{\mu_s} - \frac{1}{\eta_w})^{-1} \tag{3.17}$$

It should be noted that assumption of a thin pure solvent layer at the wall results in a lower bound for the slip layer thickness.

In the case of a thin polymer adsorption-gel formation layer which results in a negative effective velocity at the wall, du/dy is assumed zero at the wall. Equation (3.2) then gives $g(\tau, y) = -\tau_w/\eta_w$. Making this substitution in equation (3.4) yields the thickness δ_a of the polymer adsorption-gel formation zone as follows:

$$\delta_a = -\frac{u_w \eta_w}{\tau_w} \tag{3.18}$$

As seen from the above equations, the thickness of the anomalous zone in each case is a function of the shear stress at the wall.

3.2 Characterization of Non-Newtonian Capillary Flow

Equation (3.10) may be differentiated with respect to τ_w to yield the Rabinowitsch-Mooney equation extended to include the effective velocity at the wall:

$$\dot{\gamma}_w = f(\tau_w) = \frac{1}{4}\tau_w \frac{d[8(\langle u \rangle - u_w)/D]}{d\tau_w} + \frac{3}{4}[\frac{8(\langle u \rangle - u_w)}{D}] \tag{3.19}$$

Equation (3.19) may be rearranged to:

$$\dot{\gamma}_w = (\frac{3n'+1}{4n'})[\frac{8(\langle u \rangle - u_w)}{D}] \tag{3.20}$$

where n' is given by:

$$n' = \frac{dln\tau_w}{dln[8(\langle u \rangle - u_w)/D]} \tag{3.21}$$

It is evaluated as the slope of the tangent to the curve obtained in a log-log plot of τ_w vs. $8(\langle u \rangle - u_w)/D$. For a power-law fluid, $f(\tau) = (\tau/K)^{1/n}$, equation (3.9) yields:

$$\tau_w = K(\frac{3n+1}{4n})^n[\frac{8(\langle u \rangle - u_w)}{D}]^n \tag{3.22}$$

Hence, for this fluid model the flow curve obtained in the log-log plot is linear with $n' = n$. In the case of a Newtonian fluid, the plot is linear with a slope of unity. Equation (3.20) enables one to deduce the shear stress-shear rate relationship of a fluid exhibiting a surface effect.

3.3 Evaluation of Properties in the Limit of Zero Shear

3.3.1 Zero Shear Viscosity

The basic equation (3.20) for non-Newtonian capillary flow may be utilized to evaluate the zero shear viscosity from capillary viscometer data. Thus, the non-Newtonian viscosity of the fluid may be represented by:

$$\eta = \frac{\tau_w}{\dot{\gamma}_w} = \tau_w / \{\frac{(3n'+1)}{4n'}[\frac{4(\langle u \rangle - u_w)}{R}]\} \tag{3.23}$$

where D in equation (3.20) has been replaced by R.

Recognizing that n' becomes unity in the limit as τ_w and $4(\langle u \rangle - u_w)/R$ approach zero, equation (3.23) yields the following expression for evaluation of the lower limiting viscosity:

$$\eta_0 = \lim_{\tau_w \& [4(\langle u \rangle - u_w)/R] \to 0} \frac{d\tau_w}{d[4(\langle u \rangle - u_w)/R]} \tag{3.24}$$

The zero shear viscosity is therefore the slope of the tangent to the curve denoting τ_w vs $4(\langle u \rangle - u_w)/R$ evaluated at the origin. This equation may be verified utilizing the Ellis fluid model for which:

$$\frac{1}{\eta} = \frac{1}{\eta_0}[1 + (\frac{\tau}{\tau_{1/2}})^{\alpha-1}] \tag{3.25}$$

and the average velocity for flow in a circular tube is given by:

$$\frac{4(\langle u \rangle - u_w)}{R} = \frac{\tau_w}{\eta_0}[1 + \frac{4}{\alpha+3}(\frac{\tau_w}{\tau_{1/2}})^{\alpha-1}] \tag{3.26}$$

Rearranging the latter to

$$\frac{4(\langle u\rangle - u_w)}{R} = \frac{\tau_w}{\eta_0} + G\tau_w^{\alpha} \tag{3.27}$$

where $G = \frac{4}{\eta_0(\alpha+3)}(\frac{1}{\tau_{1/2}})^{\alpha-1}$ and differentiating the equation with respect to τ_w yields:

$$\frac{d[4(\langle u\rangle - u_w)/R]}{d\tau_w} = \frac{1}{\eta_0} + \alpha G\tau_w^{\alpha-1} \tag{3.28}$$

Taking the limit as $\tau_w \to 0$ gives the expected limiting viscosity η_0 for a pseudoplastic fluid, $\alpha > 1$, in accordance with equation (3.24).

3.3.2 Thickness of the Adsorbed Polymer Layer at Zero Shear

In the following, we present the technique for evaluation of the effective hydrodynamic thickness of the adsorbed layer in the limit of zero shear, δ_{a0}, from capillary flow measurements of polymer solutions.

For polymer adsorption in the absence of slip flow, δ_{a0} can be calculated directly from equation (3.18) by taking the limit as $\tau_w \to 0$. Thus, applying l'Hopital's rule, one obtains:

$$\delta_{a0} = -\eta_0 \left(\frac{du_{wa}}{d\tau_w}\right)_{\tau_w=0} \tag{3.29}$$

Similarly, for slip flow, the effective hydrodynamic thickness of the solvent layer δ_{s0} obtained by applying l'Hopital's rule to equation (3.17) is

$$\delta_{s0} = \left(\frac{du_{ws}}{d\tau_w}\right)_{\tau_w=0} (\frac{1}{\mu_s} - \frac{1}{\eta_0})^{-1} \tag{3.30}$$

For the case in which polymer adsorption during tubular flow is accompanied by an effective velocity of slip at the wall, the experimental u_w represents a superposition of the effective velocities u_{wa} and u_{ws} characterizing polymer adsorption and slip, respectively.

Superposition, utilizing equations (3.29) and (3.30), produces:

$$\begin{aligned}\left(\frac{du_w}{d\tau_w}\right)_{\tau_w=0} &= \left(\frac{du_{ws}}{d\tau_w}\right)_{\tau_w=0} + \left(\frac{du_{wa}}{d\tau_w}\right)_{\tau_w=0} \\ &= -\frac{\delta_{a0}}{\eta_0} + \delta_{s0}(\frac{1}{\mu_s} - \frac{1}{\eta_0})\end{aligned} \tag{3.31}$$

where $(du_w/d\tau_w)_{\tau_w=0}$ is a function of the polymer concentration. It is assumed that the effective adsorbed layer thickness at zero shear may be represented by a Langmuir-type adsorption isotherm as follows:

$$\frac{\delta_{a0}}{\delta_{ap}} = \Theta = \frac{c}{k+c} \tag{3.32}$$

where δ_{ap} denotes the plateau value of the zero-shear thickness at high polymer concentrations.

It is also assumed that δ_{s0} is inversely related to the polymer coverage Θ as follows:

$$\delta_{s0} = k_{s0}(1-\Theta) = k_{s0}(1-\frac{c}{k+c}) \tag{3.33}$$

where k_{s0} is a proportionality coefficient.

Substitution of equations (3.33) and (3.32) into equation(3.31) results in:

$$A(c) = \left(\frac{du_w}{d\tau_w}\right)_{\tau_w=0} = -\frac{\delta_{ap}}{\eta_0}\frac{c}{(k+c)} + k_{s0}(\frac{1}{\mu_s}-\frac{1}{\eta_0})(1-\frac{c}{k+c}) \tag{3.34}$$

This equation can be solved by least-squares fitting to determine the parameters δ_{ap}, k and k_{s0}. The details are presented in Chapter 5. Using equation (3.32), the thickness of the adsorbed layer at zero shear δ_{a0} may be evaluated as a function of polymer concentration.

3.4 Effective Hydrodynamic Adsorbed Layer Thickness at Finite Shear

Simultaneous occurrence of adsorption and slip has already been observed in the earlier studies of Cohen et al. (1981, 1982a and 1988). In this section, we address the evaluation of hydrodynamic adsorption in the presence of slip.

The u_{ws} and u_{wa} characterizing the effective velocities at the wall due to slip and polymer adsorption are represented in terms of the wall shear stress by:

$$u_{ws} = \zeta \tau_w \tag{3.35}$$

and

$$u_{wa} = -a\tau_w - b\tau_w^d \tag{3.36}$$

where the slip coefficient ζ, and the parameters a, b and d are functions of the polymer concentration, and where $d > 1$.

Combination of equation (3.35) with equations (3.17) and (3.30) yields the following expression for the slip coefficient:

$$\zeta = \delta_s(\frac{1}{\mu_s} - \frac{1}{\eta_w}) = \delta_{s0}(\frac{1}{\mu_s} - \frac{1}{\eta_0}) \tag{3.37}$$

The second equality follows since ζ is independent of the wall shear stress. Note that at zero polymer concentration, $\eta_w = \eta_0 = \mu_s$ and equation (3.37) predicts a slip coefficient equal to zero. Solving equation (3.37) for δ_s yields

$$\delta_s = \delta_{s0}(\frac{1}{\mu_s} - \frac{1}{\eta_0})/(\frac{1}{\mu_s} - \frac{1}{\eta_w}) \tag{3.38}$$

Combination of equations (3.29) and (3.36) results in

$$\delta_{a0} = a\eta_0 \tag{3.39}$$

Thus, $a = \delta_{a0}/\eta_0$ which gives:

$$u_{wa} = -\frac{\delta_{a0}}{\eta_0}\tau_w - b\tau_w^d \tag{3.40}$$

and

$$u_w = u_{ws} + u_{wa} = \tau_w(\zeta - \frac{\delta_{a0}}{\eta_0}) - b\tau_w^d \tag{3.41}$$

The latter equation may be rewritten:

$$u_w = A(c)\tau_w - b\tau_w^d \tag{3.42}$$

where A(c)=$\zeta - \delta_{a0}/\eta_0$. This equation can be fitted directly to experimental evaluations of the effective velocity u_w at the wall as a function of the wall shear stress, to obtain A(c), b and d as a function of the polymer concentration. Substitution of A(c) in equation (3.34) is then used to calculate the constants δ_{ap}, k and k_{s0} from which δ_{a0} may be determined. Finally, u_{ws} and u_{wa} can be evaluated separately from equations (3.35) and (3.36). The effective hydrodynamic thickness of the adsorbed layer corrected for the slip is given by

$$\delta_a = -\frac{u_{wa}\eta_w}{\tau_w} = \eta_w(\frac{\delta_{a0}}{\eta_0} + b\tau_w^{d-1}) \tag{3.43}$$

3.5 End Effect Correction by Modified Bagley Method

3.5.1 A Modification of Bagley Plot

Because of the high precision requirements of the flow measurements, allowances have to be made for the slight differences in the diameters of the tubes with the same nominal diameter received from the supplier in evaluation of end effects. The following modification of Bagley plot was developed for this purpose.

The wall shear stress for steady, uniform, laminar flow in a tube is given by the following relation yielded by a momentum balance:

$$\tau_w = \frac{R}{2}\frac{\Delta P}{L} = \frac{R}{2}[\frac{\Delta P_{ev}}{L} - \frac{\rho\hat{E}_v}{L}] \tag{3.44}$$

where ΔP_{ev} is the total pressure drop evaluated directly from the experimental measurements and $\hat{E}_v$ is the friction loss at the entry and exit of the tube. Setting

$$\hat{E}_v = \frac{1}{2}\langle u\rangle^2(e_{vc} + e_{ve}) \tag{3.45}$$

where e_{vc} and e_{ve} are the contraction and expansion friction loss factors for the entrance and exit, respectively, yields

$$\tau_w = \frac{R}{2}[\frac{\Delta P_{ev}}{L} - \frac{1}{2}\frac{\rho}{L}\langle u\rangle^2(e_{vc} + e_{ve})] = \frac{D}{4L}[\Delta P_{ev} - \frac{1}{2}\rho\langle u\rangle^2(e_{vc} + e_{ve})] \tag{3.46}$$

Rearrangement results in:

$$\frac{\Delta P_{ev}}{\langle u \rangle^2} = 4\tau_w(\frac{L/D}{\langle u \rangle^2}) + \frac{1}{2}\rho(e_{vc} + e_{ve}) \tag{3.47}$$

It follows that ΔP_{end} is defined by

$$\Delta P_{end} = \frac{1}{2}\rho(e_{vc} + e_{ve})\langle u \rangle^2 \tag{3.48}$$

According to equation (3.47), a plot of $\Delta P_{ev}/\langle u \rangle^2$ vs. $(L/D)/\langle u \rangle^2$ at constant $8\langle u \rangle/D$ should be linear. The slope of the line yields the wall shear stress at the particular $8\langle u \rangle/D$; the friction loss parameter $(e_{ve} + e_{vc})$ is evaluated from the intercept at L/D=0. This data is utilized in the evaluation of the flow curves representing the relationship between the wall shear stress τ_w and $8\langle u \rangle/D$ used to evaluate the surface effects and rheological behavior of the fluid.

3.5.2 End Correction in the Presence of Slip

In this section, we provide an alterative method for correcting for end effects in the presence of slip. It also accounts for slight differences in the diameters of the tubes used.

The basic equation is:

$$\frac{4(\langle u \rangle - u_w)}{R} = \frac{\tau_w}{\eta_R} \tag{3.49}$$

Writing $u_w = \zeta\tau_w$ then gives

$$\begin{aligned} \frac{4\langle u \rangle}{R} &= \frac{4u_w}{R} + \frac{\tau_w}{\eta_R} \\ &= \frac{4\zeta\tau_w}{R} + \frac{\tau_w}{\eta_R} \end{aligned} \tag{3.50}$$

where ζ is the slip coefficient.

Substitution of $\tau_w = \frac{R}{2}(-\frac{dP}{dz})$ into equation 3.50 yields:

$$\frac{4\langle u \rangle}{R} = 2\zeta(-\frac{dP}{dz}) + \frac{1}{\eta_R}.\frac{R}{2}(-\frac{dP}{dz}) \tag{3.51}$$

Differentiation with respect to R at constant $(-dP/dz)$ produces:

$$\left[\frac{\partial(4\langle u\rangle/R)}{\partial R}\right]_{(-dP/dz)} = \frac{1}{2\eta_R}(-\frac{dP}{dz}) = \frac{1}{2\eta_R}\frac{(P_0 - P_L)}{L} \tag{3.52}$$

The variation in $4\langle u\rangle/R$ due to a small change ΔR in R is therefore given by

$$\Delta[\frac{4\langle u\rangle}{R}] = \frac{\Delta R}{2\eta_R}\frac{(P_0 - P_L)}{L} \tag{3.53}$$

An intermediate radius may be taken as a basis for the calculation. The corrected values of $4\langle u\rangle/R$ for the other tubes are determined from the original experimental values, at a particular $(-\Delta P/L)$. The flow curves corrected by this procedure are then used for end effect correction by application of Bagley plot.

3.6 Polymer Characterization

The intrinsic viscosity or limiting viscosity number of a polymer in a solution is defined by

$$[\eta] = \lim_{c\to 0}\frac{\eta_{sp}}{c} = \lim_{c\to 0}\frac{(\eta_r - 1)}{c} \tag{3.54}$$

where η_r is the ratio of the viscosity of the solution to the viscosity of the solvent, denoted as the relative viscosity; η_{sp} is the specific viscosity. The intrinsic viscosity is a measure of the contribution of the individual polymer molecule to the viscosity and is independent of polymer concentration.

A number of empirical relationships have been proposed, expressing essentially the concentration dependence of the viscosity number. The most widely used are the Huggins equation (1942):

$$\eta_{sp}/c = [\eta] + k_h[\eta]^2 c \tag{3.55}$$

Schulz and Blaschke formula (1941):

$$\eta_{sp}/c = [\eta] + k_h[\eta]^2\eta_{sp} \tag{3.56}$$

and Kraemer expression (1938):

$$ln(\eta_r)/c = [\eta] + (k_h - 0.5)[\eta]^2 c \tag{3.57}$$

For a given solvent medium and temperature, the intrinsic viscosity is related to the molecular weight of the polymer by the Mark-Houwink-Sakurada (MHS) equation:

$$[\eta] = \bar{k} M^{\bar{a}} \tag{3.58}$$

where the MHS parameters $\bar{a}$ and $\bar{k}$ are characteristic of the polymer at the particular conditions. With heterodisperse samples this gives the viscosity-average molecular weight, M_v. It is known that M_v lies between the number-average molecular weight M_n and the weight-average molecular weight M_w and is closer to M_w.

Flory and Fox (1951) proposed the following empirical relation for the flexible polymer:

$$[\eta] = \Phi(\sqrt{\langle r^2 \rangle})^3/M \tag{3.59}$$

where the theoretical value of Φ lies between 1.81×10^{21} to 3.62×10^{21} (Flory, 1953). The radius of gyration of the polymer in solution may be related to the intrinsic viscosity as follows (Yamakawa, 1971):

$$[\eta] = 6^{3/2} \Phi R_g^3/M \tag{3.60}$$

Combination of the latter equations yields (Bird et al., 1977):

$$R_g = (\sqrt{\langle r^2 \rangle})/\sqrt{6} \tag{3.61}$$

Chapter 4

Experimental

The experimental investigation essentially consisted in simultaneous evaluation of the flow rate and pressure drop for steady, uniform, laminar flow of dilute aqueous polymer solutions of varying concentration in capillary tubes of different lengths and diameters.

4.1 Equipment and Measurements

4.1.1 Experimental Flow System

The flow system used in this work is illustrated in figure 4.1. It includes a cylindrical plexiglas vessel 10cm long and 10.6cm in inner diameter which serves as the reservoir for the test solutions, with a connection to the capillary in the bottom plate. The connection to the pressure system providing the driving force for the flow was located in the top plate of the reservoir. The pressure system included a nitrogen cylinder, pressure regulator, surge tank for stabilization and maintenance of the desired pressure and a pressure gauge.

A constant temperature jacket with a coil through which water was circulated from a constant temperature bath served to maintain a constant temperature in the reservoir.

Two Mettler balances with different weighing ranges (100g and 400g) supplied by Mettler Instrument Corporation (N.J.), communicating directly with an IBM

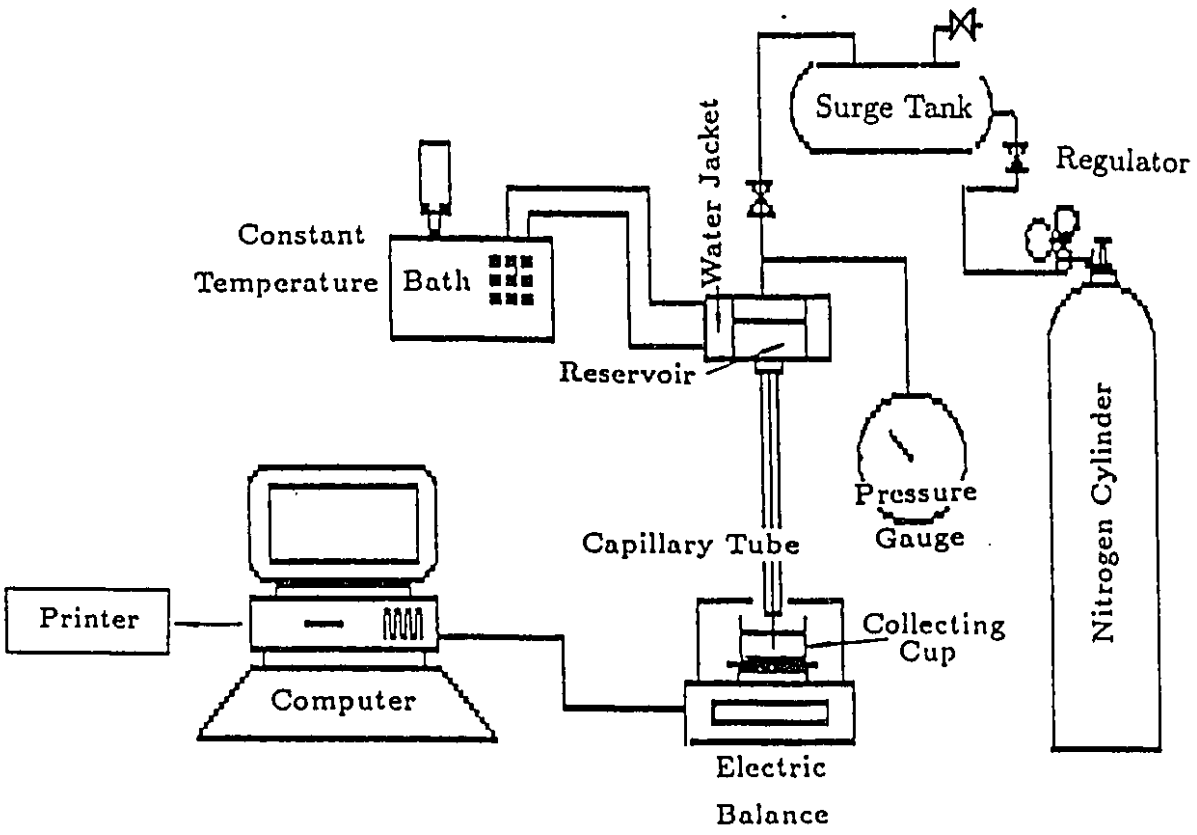

Figure 4.1: Schematic diagram of the experimental set-up

model PS2 microcomputer, were used for data acquisition consisting of the weight of fluid collected as a function of time, which provided the flow rate measurements.

The high precision bore glass capillary tubes supplied by Wilmad Glass Company (N.J.) ranged in diameter from 0.0054cm to 0.0466cm. Each glass tube was enclosed in a stainless steel tube with an epoxy resin seal to protect the tube and facilitate its handling. The connection to the reservoir was made through a connector which facilitated the removal and replacement of the tubes during the runs.

4.1.2 Pressure Drop Measurement

The pressure in the reservoir was monitored by either of two pressure gauges. A pressure gauge was used for pressure measurements in the range 344735-2068410 dynes/cm^2 (5-30 psi) and the other for pressure measurements from 2413145-3102615 dynes/cm^2 (35 to 45 psi). The first pressure gauge was calibrated with a fluid column manometer using water as the working fluid. The accuracy of the calibration was about 0.1% of the pressure gauge output. The second gauge was calibrated based on the calibrated one with the accuracy of 0.2%.

The pressure inside the reservoir was increased and adjusted to the desired level with compressed nitrogen from a cylinder equipped with a pressure regulator and pressure gauge. The pressure variations were normally held to less than 0.15% during an experimental run, by means of the fine adjustment valve mounted on the surge tank for stabilization of the pressure level.

The evaluation of the potential drop across the capillary includes the contributions due to the pressure drop, gravity and buoyancy forces. The effect of the slight level changes in the fluid reservoir and weighing vessel was also considered. The details of the calculation of the potential drop are given in Appendix B.

4.1.3 Flow Measurement

The determination of the mass flow rate of the fluid during a run consisted of directly recording the weight of the effluent collected as a function of time. This was performed with either a Mettler PM400 electronic balance accurate to 0.0005g or a Mettler AJ150 balance accurate to 0.00005g, linked to an IBM microcomputer. Each weight reading was fed to the microcomputer at predetermined intervals controlled by the computer. The flow rate was then evaluated from the calculated slope of the recorded weight as a function of time, based on 46 measured data points. Such measurements had good accuracy and the balance response allowed measurements of flow rates lower than 0.0001 g/s. An illustration of the linearity of the weight vs. time plot for two selected cases is shown in Appendix D.

To minimize errors associated with evaporation losses of particular importance in runs conducted with the very small diameter tubes at low flow rates, 20 ml of a non-volatile motor oil with a density of 0.874 was added in the collecting cup to produce a thin insoluble oil surface layer which effectively eliminated any change in weight of effluent due to evaporation.

4.1.4 Temperature Control

To facilitate the temperature control during a run, the equipment was located in a room whose temperature was thermostatically controlled at $25°C \pm 1.5°$. The fine temperature control was achieved by circulating water from a constant temperature bath through a water jacket surrounding the reservoir and a coil inside the reservoir. In this way, the experimental temperature could be controlled to within $\pm 0.1°C$ during the period of the experiment. The fluid temperature in the reservoir was monitored by means of a thermometer inserted into the reservoir center. The capillary tube enclosed in a stainless steel sleeve and sealed with epoxy resin was further insulated by wrapping two-three layers of polyurethane sponge to a thick-

ness of about 0.5 cm around the capillary tube. It was then secured with a plastic wrap ("stretch and cling" food wrap) and scotch tape. This insulation served to minimize temperature variation along the capillary tube.

4.1.5 Cannon Fenske Viscometer

Viscosity determinations were performed on polymer solutions using a calibrated Cannon Fenske viscometer with a specification size of 50 and a constant of 0.003984 at 25°C, made by Industrial Research Glassware Ltd. (N.J.). During the measurements, it was immersed in a constant temperature bath with temperature control to ±0.1°C. The kinematic viscosity in centistokes of the sample was obtained by multiplying the efflux time in seconds by the viscometer constant. Several measurements of efflux time were carried out on the same solution to obtain an average value. The viscometer was cleaned with the solvent acetone and periodically rinsed using chromic acid to remove traces of polymer deposits.

The measured data were used as a supplement to the results derived from the capillary flow measurements and employed to evaluate the intrinsic viscosity required for determination of the viscosity average molecular weight and the root mean square end-to-end distances of the polymers.

4.1.6 Cathetometer

Initial fluid levels in the reservoir and in the effluent receiver were measured by two cathetometers supplied by the Precision Tool Instrument Co. (England), with an accuracy of 0.001 cm. This information was used for evaluation of the potential drop across the tube (see Appendix B). The length of the tube was also measured by the cathetometers.

4.2 Polymers

The polymers used in this work were Polyox Coagulant, Polyox WSR-301 and Polyox FRA supplied by Union Carbide Corporation. A brief description of the properties of the polymers and the procedure used in preparation of the solutions is given in the following (Union Carbide Corp., 1973, 1981, 1983).

4.2.1 The Properties of the Polymers

The polymers of Polyox designated as WSR-301, Coagulant and FRA, are referred to as Polyox Water-Soluble Resins, having the following common structure:

$$-(O-CH_2CH_2)-_m$$

The degree of polymerization, m, varies from about 2000 to about 100,000. The Polyox Resins are similar in chemical structure differing in molecular weight and molecular weight distribution, solution rheology, and plastic properties in the solid state. They are nonionic poly(ethylene oxide) homopolymers ranging in molecular weight from 100,000 to several million. The molecular weights of the Polyox WSR 301, Coagulant and FRA are reported to be in the order of 4×10^6, over 5×10^6 and over 6×10^6 (James et al., 1975, 1982), respectively, with a broad distribution of molecular weights.

Polyox Resins, being polyethers, hydrogen-bond strongly with water and combine excellent water solubility and thermoplasticity. They are flexible, strong, and readily soluble.

The viscoelasticity of aqueous solutions of Polyox Resin varies with viscosity grade and concentration. Solutions of Polyox WSR-301, Polyox Coagulant and

Polyox FRA, are very viscoelastic. The viscoelasticity decreases, as the molecular weight of the resin decreases.

4.2.2 Preparation of Polymer Solutions

The most important step in the entire operation of dissolving Polyox Resins takes place in the first few seconds dispersing the Resins in solvent. In water, Polyox Resins are instantly wettable. If the Resin powder is not properly dispersed, the partially dissolved, wetted particles will agglomerate and form gels which will dissolve only with prolonged high speed agitation. However, high speed agitation produces shear degradation of the resins and should therefore be avoided.

In this work, 1% by weight solutions of Polyox Resins were prepared by direct addition of the dry resins to cold distilled water. The Polyox powder was slowly sprinkled over the surface of the distilled water and simultaneously stirred into the solution with a glass rod. This was repeated over a period of 30 to 60 minutes until all the powder was used. Care was taken to avoid the formation of lumps of powder. The stirring was also carried out gently to avoid degradation of the polymer. Once all the powder had been added, the slow stirring was continued for about one hour. The solution was then stored in a dark area for about 4 to 6 hours and again stirred at a low speed for an additional hour. The resulting solution serving as master solution should contain no visible gel structures. The master solution was stored in a dark place for use within 6 weeks.

A fresh solution was diluted by adding water to a predetermined volume of master solution for each test run. The mixture was gently stirred using a glass rod for about 15 to 20 minutes and then stored in an incubator for an hour. Before use, each freshly prepared dilute solution was filtered through a sieve (45 microns) to remove any microgels or particulate matter. It could be used for flow measurements within 8 hours. Additionally, the stirring time and standing time could be longer

for solutions with concentrations higher than 200 ppm.

The variation of the density of the dilute solution (in the concentration range 5 to 200 parts per million by weight in water), compared to water, was insignificant, and the water density was subsequently used in all calculations.

4.3 Factors Affecting Surface Effect Evaluations

4.3.1 End Effects

Failure to correct for pressure losses associated with flows at the entry and exit of the capillary may lead to erroneous evaluations of surface effects. For this reason, experiments with tubes of various lengths (L/D in the range 750 to 2000) were carried out and end effect corrections were evaluated and applied to all measurements. Additional details are presented in Chapter 5.

4.3.2 Polymer Degradation

Polymer degradation may occur due to aging, mechanical degradation, bacterial degradation and chemical degradation. Of particular concern are mechanical degradation due to high speed mixing and chemical degradation due mainly to interactions between polymer molecules and oxygen, catalyzed by a trace of metal ions and light (McGary, 1960). In order to reduce these potential problems, care was first taken in the preparation of the polymer solutions to avoid stirring at high speed; secondly contact between polymer molecules and air or metals was minimized; finally, fresh solutions were prepared each day and the solution in the reservoir was replaced within two hours.

4.3.3 Plugging

Complete or partial plugging of capillary tubes may occur when some solid or gelled particles remain and adhere onto the tubes. This is a possibility with the

smallest tubes and for flows at low rates. To avoid this problem, the fresh solutions were filtered and the capillary tubes were carefully washed immediately following each run.

4.4 Experimental Procedure

4.4.1 Flow through Capillary Tubes

The investigation of surface effects has been conducted utilizing flows of aqueous solutions of Polyox WSR 301, Coagulant and FRA in the concentration range from 5 ppm to 200 ppm (see Table 4.1), in untreated and silane-treated glass capillary tubes.

For each run, a freshly prepared polymer solution was placed in a constant temperature bath maintained at $25°C$ for an hour, filtered and then transfered slowly into the fluid reservoir. The solution in the reservoir was changed every two hours, to avoid any degradation of the dilute polymer solution due to light or to extended contact between the polymer solution and the metal in the reservoir. A selected capillary tube was then connected to the reservoir. After the desired fluid temperature was attained, fluid was driven through the tube by increasing the pressure of the nitrogen from the cylinder. The pressure in the reservoir was varied in steps from 5 psi to 45 psi. The flow rate was constant at each pressure drop and evaluated directly by the microcomputer from the readings of the weight of the fluid in the weighing vessel as a function of time.

After each run, the tube was rinsed first using 10% NaOH solution, then distilled water and dried with nitrogen.

4.4.2 Laminar Flow Measurements

All the experimental measurements were carried out in the laminar flow region based on the definition of laminar-turbulent transition at Reynolds number $Re \approx$

Table 4.1: Experimental Conditions Explored

Concentration	Polyox WSR 301		Polyox Coagulant		Polyox FRA	
(used)	(NST)	(ST)	(NST)	(ST)	(NST)	(ST)
5 ppm	×	×	×		×	×
10 ppm	×	×	×		×	×
15 ppm	×	×	×		×	×
20 ppm	×	×	×		×	×
30 ppm	×	×	×		×	×
60 ppm	×	×	×		×	×
100 ppm	×	×	×		×	×
130 ppm					×	
200 ppm	×	×	×		×	×

NST and ST designate the glass tubes without and with surface treatment using dimethyldiethoxysilane, respectively.

2000 (Bird et al., 1960). In the calibration runs carried out using distilled water to determine the tube diameters, the maximum driving pressure corresponding to a Reynolds number of about 1500 was first set for each tube. This pressure was not exceeded in the runs conducted with the polymer solutions to ensure laminar flow prevailed in all measurements. The maximum pressure was less than 3102615 dynes/cm^2 (45 psi) in the case of flows in large diameter tubes.

4.4.3 Capillary Diameter Calibration

As indicated, the preliminary calibration of the tube diameters was carried out using distilled water since water is a Newtonian fluid with known viscosity. Appropriate corrections for excess pressure losses were made in the calibration of the tube diameters. The details of the calibration procedure are described in Appendix C. The evaluated diameters for all of the tubes used in the experimental investigation are tabulated in Tables 4.2 and 4.3. These are in good agreement with the values provided by the supplier within the tolerance levels included.

4.4.4 Capillary Surface Treatment

Chemical modification of siliceous surfaces has been widely studied (Iler, 1979; Leyden, 1985) and silane compounds are often used to modify surfaces (Mungan, 1969). These surfaces then can be applied to the study of polymer adsorption as a function of surface chemistry. In the present work, some of the capillary tubes were chemically treated using a bifunctional silane compound, viz. dimethyldiethoxysilane. By reaction between the silane and a silica surface, a "new" surface or coating may be created on the silica surface (under appropriate conditions). The treatment method was first suggested by Arkles (1977), and has been successfully applied in the study of surface effects by Cohen et al. (1982, 1986). The details of the procedure used in the surface treatment are presented in Appendix D.

Table 4.2: Diameters for Untreated Capillary Tubes

Tubes	Length(cm)	Diameter (cm)	(L/D)	Recalibrated D
0.002A1	10.447	0.00531	1969.27	
0.002B1	12.835	0.00534	2405.81	
0.002A2	15.153	0.00536	2829.69	
0.003A1	10.366	0.00778	1332.39	
0.003B1	13.095	0.00803	1631.57	
0.003A2	15.208	0.00778	1955.26	
0.004A2	9.7560	0.01027	949.95	0.01027
0.004A1	16.151	0.01028	1571.11	0.01027
0.004B	25.431	0.01028	2473.83	
0.006A1	19.442	0.01559	1247.08	
0.006B1	25.633	0.01584	1618.24	0.01585
0.006A2	31.557	0.01547	2039.88	
0.006C1	30.751	0.01540	1996.82	
0.008A2	15.138	0.01906	794.22	0.01905
0.008B2	25.564	0.01922	1330.07	
0.008B2+	23.476	0.01922	1221.43	
0.008C1	31.275	0.01912	1635.72	
0.008D	50.976	0.01931	2639.88	
0.008E	50.957	0.01905	2674.91	
0.012C2	28.518	0.02967	961.17	0.02967
0.012A2	25.803	0.02870	899.06	0.02864
0.012A1	37.874	0.02866	1321.49	0.02864
0.012C1	35.169	0.02971	1183.74	0.02967
0.012B	63.682	0.02961	2150.69	
0.018A2	36.060	0.04677	771.01	0.04665
0.018C1	54.779	0.04758	1151.30	0.04749
0.018B	91.761	0.04658	1969.97	

Table 4.3: Diameters for Silane-Treated Capillary Tubes

Tubes	Length(cm)	Diameter (cm)	(L/D)	Recalibrated D
0.002C2	10.447	0.00535	1953.08	
0.002B2	12.802	0.00531	2410.47	
0.002C1	15.137	0.00533	2837.83	
0.003C2	10.577	0.00804	1315.87	
0.003B2	12.461	0.00802	1554.13	
0.003C1	14.982	0.00801	1871.11	
0.004D2	10.524	0.01058	994.71	
0.004D1	14.870	0.01052	1413.50	
0.004C	25.421	0.01033	2460.89	0.01038*
0.006C2	20.206	0.01550	1303.61	
0.006B2	25.296	0.01588	1592.95	0.01594*
0.006E2	31.232	0.01597	1955.67	
0.006F2	30.832	0.01595	1933.04	
0.008C2	19.582	0.01910	1025.24	0.01915*
0.008B1	25.418	0.01916	1326.62	
0.008A1	35.859	0.01912	1875.47	0.01905**
0.008G	51.001	0.01923	2652.16	
0.012E2	25.744	0.02952	872.09	
0.012F1	26.035	0.02970	876.59	
0.012E1	36.910	0.02953	1249.92	
0.012D	57.508	0.02931	1962.06	
0.012H	63.704	0.02987	2132.71	
0.018C2	36.714	0.04759	771.46	0.04749**
0.018A1	55.440	0.04664	1188.68	0.04665**
0.018D	91.581	0.04745	1930.05	

*– Diameter recalibrated after surface treatment.
**– Diameter recalibrated before surface treatment.

Chapter 5

Results and Discussion

The results of the study of surface phenomena in capillary flow of aqueous solutions of Polyox WSR 301, Polyox Coagulant and Polyox FRA at varying concentrations are reported in this Chapter. The analysis of the experimental data was based on the theoretical background presented in Chapter 3. All the plots and data relevant to the surface effects were obtained from calculations which included end effect corrections.

5.1 Polymer Molecular Weights and Average Dimensions

The viscosity average molecular weights were based on intrinsic viscosities determined from the viscosities measured with the Cannon-Fenske viscometer for the three polymers used. The polymer solutions used in the flow measurements were insufficient to predict the intrinsic viscosity (James et al., 1975). Additional solutions of higher concentration were prepared for the determination of the intrinsic viscosity. The viscometric data obtained are presented in figure 5.1. The plots show the expected linearity with Huggins constants of 0.36, 0.33 and 0.25 for Polyox WSR 301, Coagulant and FRA, respectively. The molecular weight of the polymers was determined from Shin's (1965) correlation: $[\eta] = 1.03 \times 10^{-4} M_n^{0.784}$. The root mean square end-to-end distances of the polymer molecules were then calculated accord-

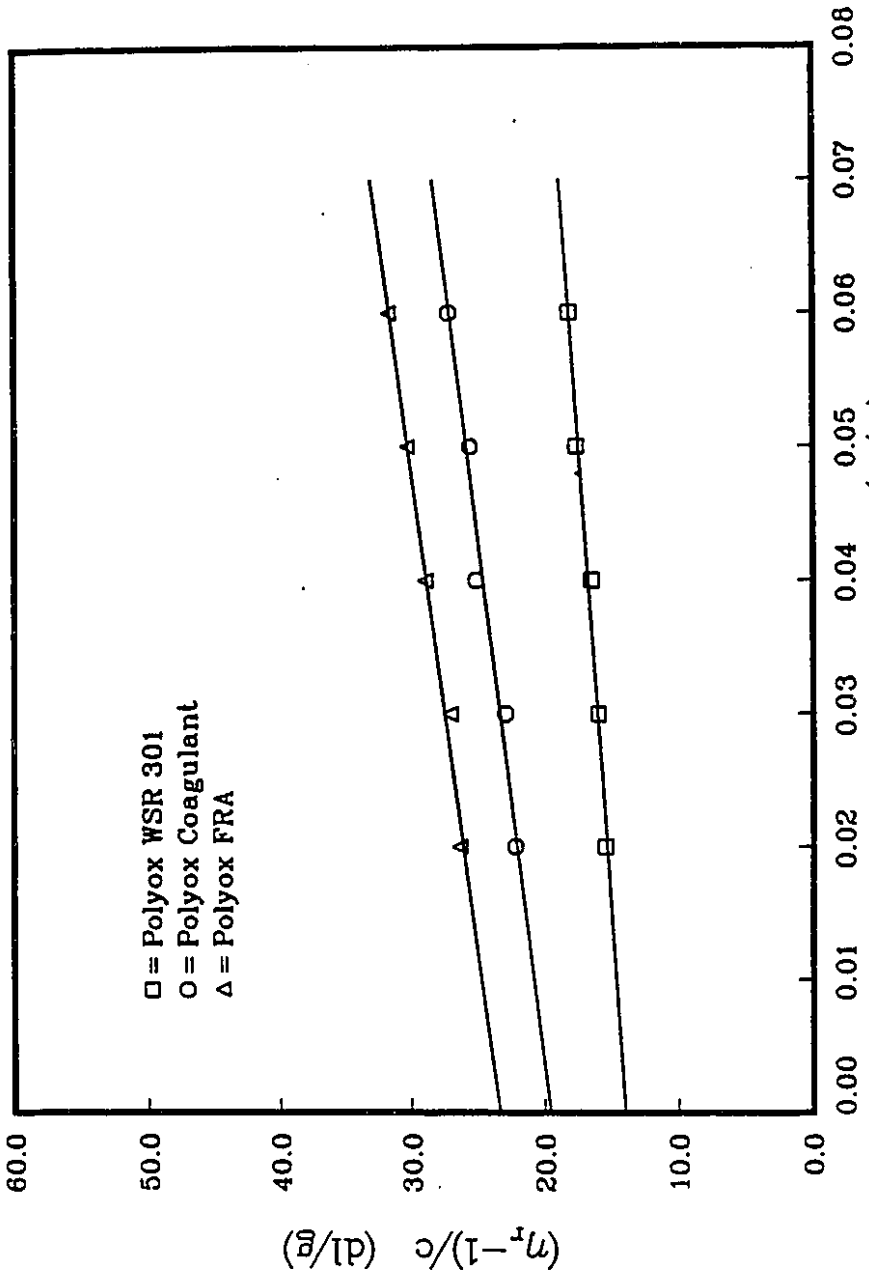

Figure 5.1 Plot of reduced viscosity vs. polymer concentration.

Table 5.1: Polymer Properties

Polyox	Average Molecular Weight	Intrinsic Viscosity	$\sqrt{\langle r^2 \rangle}$	$2R_g$
WSR 301	3.79×10^6	13.9 dl/g	2931 Å	2393 Å
Coagulant	5.85×10^6	19.6 dl/g	3791 Å	3095 Å
FRA	7.34×10^6	23.3 dl/g	4338 Å	3542 Å

ing to equation (3.59), using the value of 2.0×10^{21} for Flory's universal constant Φ. The characteristics determined for the Polyox solutions are summarized in Table 5.1.

5.2 Characterization of Excess Pressure Losses Due to End Effects

The analysis of wall effects is based on a precise determination of the wall shear stress which, however, is influenced directly by the excess pressure drop associated with the entry and exit regions of the tube. An example of the effect of the L/D ratio on the flow of 100 ppm aqueous Polyox FRA solution is shown in figure 5.2. The maximum errors in the shear stress data were estimated to be 1.5% for the shear rate range involved in the present work. It can be seen that the data points obtained for different tube lengths cannot be represented by a unique flow curve. Corrections to the flow curves for end effects, therefore, are important in evaluation

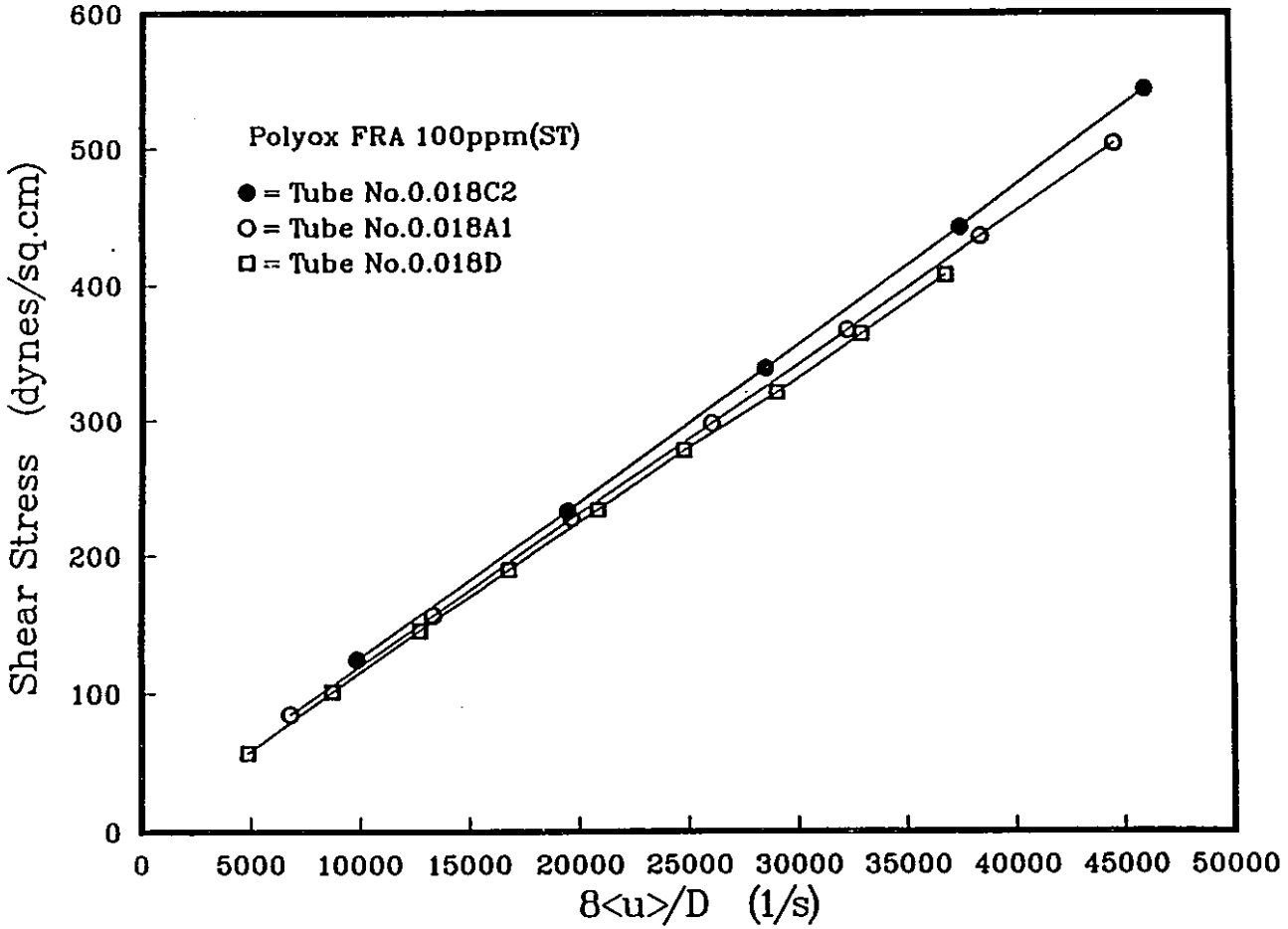

Figure 5.2 Demonstration of end effects on flow curves for 100 ppm Polyox FRA, at various L/D ratio.

of wall effects.

The length to diameter ratios of the tubes used in this study ranged from 750 to over 2000. The end effects were found to be negligible (no more than 2%) for the tube diameters smaller than 0.016cm for which L/D approached 1500 to 2000.

It should be mentioned that the evaluations of the end effects in the present work were made by the modified Bagley plot developed in section 3.5.1, since no significant differences were found using the method included in section 3.5.2, for the particular cases involved.

Figure 5.3 shows typical plots of $\Delta P/\langle u\rangle^2$ vs.(L/D)$/\langle u\rangle^2$ evaluated for the flow of 200 ppm Polyox Coagulant, which illustrate the technique employed for evaluation of excess pressure losses at various conditions.

The excess pressure losses for flow of polymer solutions in capillary tubes were found to vary with tube diameter, solute concentration and $8\langle u\rangle/D$. The variation of ΔP_{end} with $8\langle u\rangle/D$ is illustrated in figures 5.4 to 5.5 which show an increase in ΔP_{end} with increasing apparent shear rate. A power-law relationship may be used to represent the behavior with a power-law exponent which changes with tube diameter for a given solution. The figures also indicate that ΔP_{end} generally increases with tube diameter.

The effect of polymer concentration on ΔP_{end} is demonstrated in figures 5.6 and 5.7 in which an increasing trend with concentration was observed. This points to the importance of end effects in capillary flows of concentrated polymer solutions.

For the flow of a Newtonian fluid, the combined friction loss factor $(e_{vc} + e_{ve})$ is usually about 2 to 3. However, from the data collected, the values for the polymer solutions were found to be very high. The percent contribution of the extra pressure losses to the total pressure drop may approach 10% at high shear rate for an L/D ratio as high as 2000. Table 5.2 presents extra pressure losses for a variety of flow conditions involved in the experiments. The large end effect contributions to the

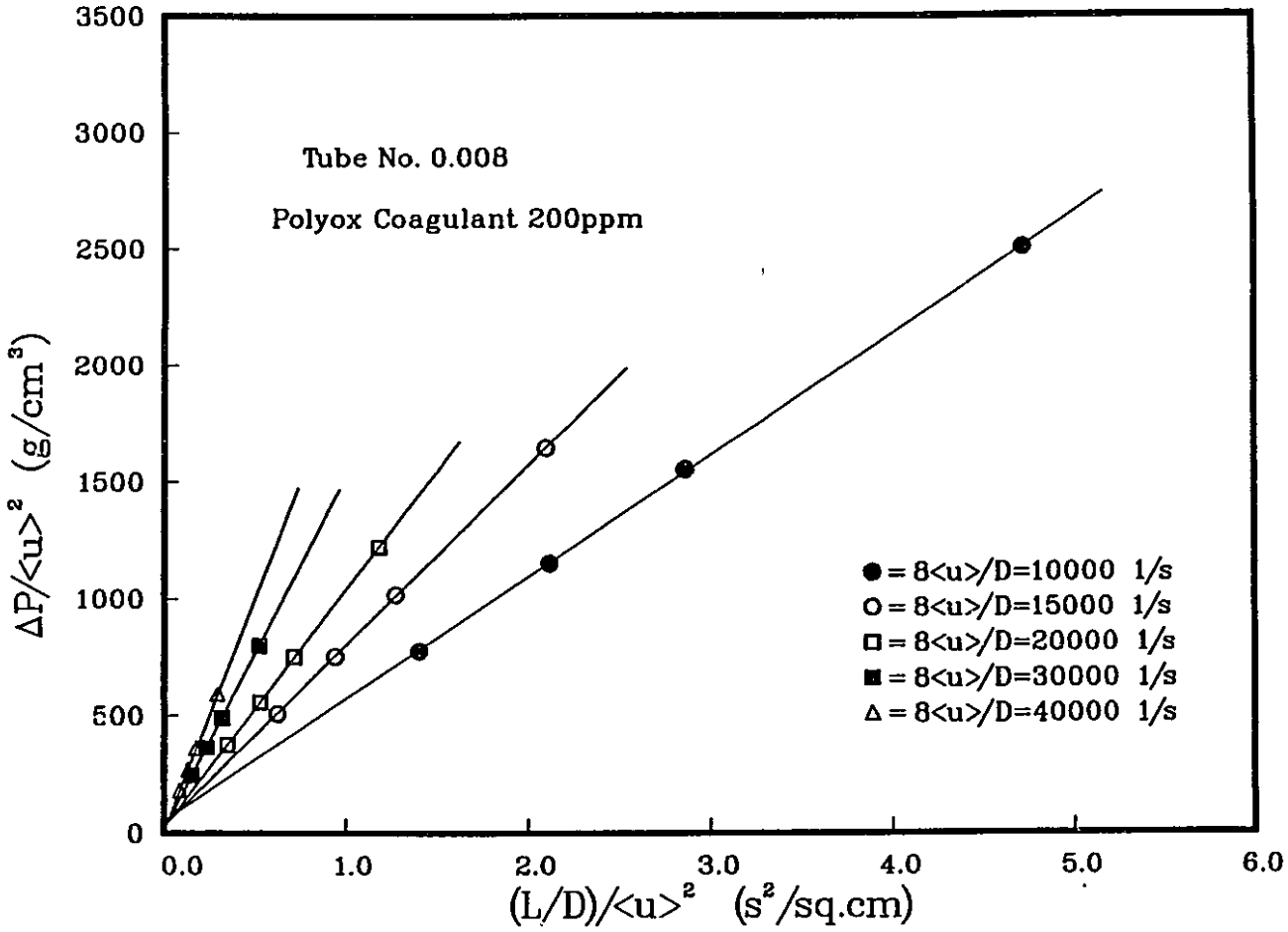

Figure 5.3 Plot of $\Delta P/\langle u\rangle^2$ vs. $L/D/\langle u\rangle^2$ for 200ppm Polyox Coagulant solution, depicting end correction technique.

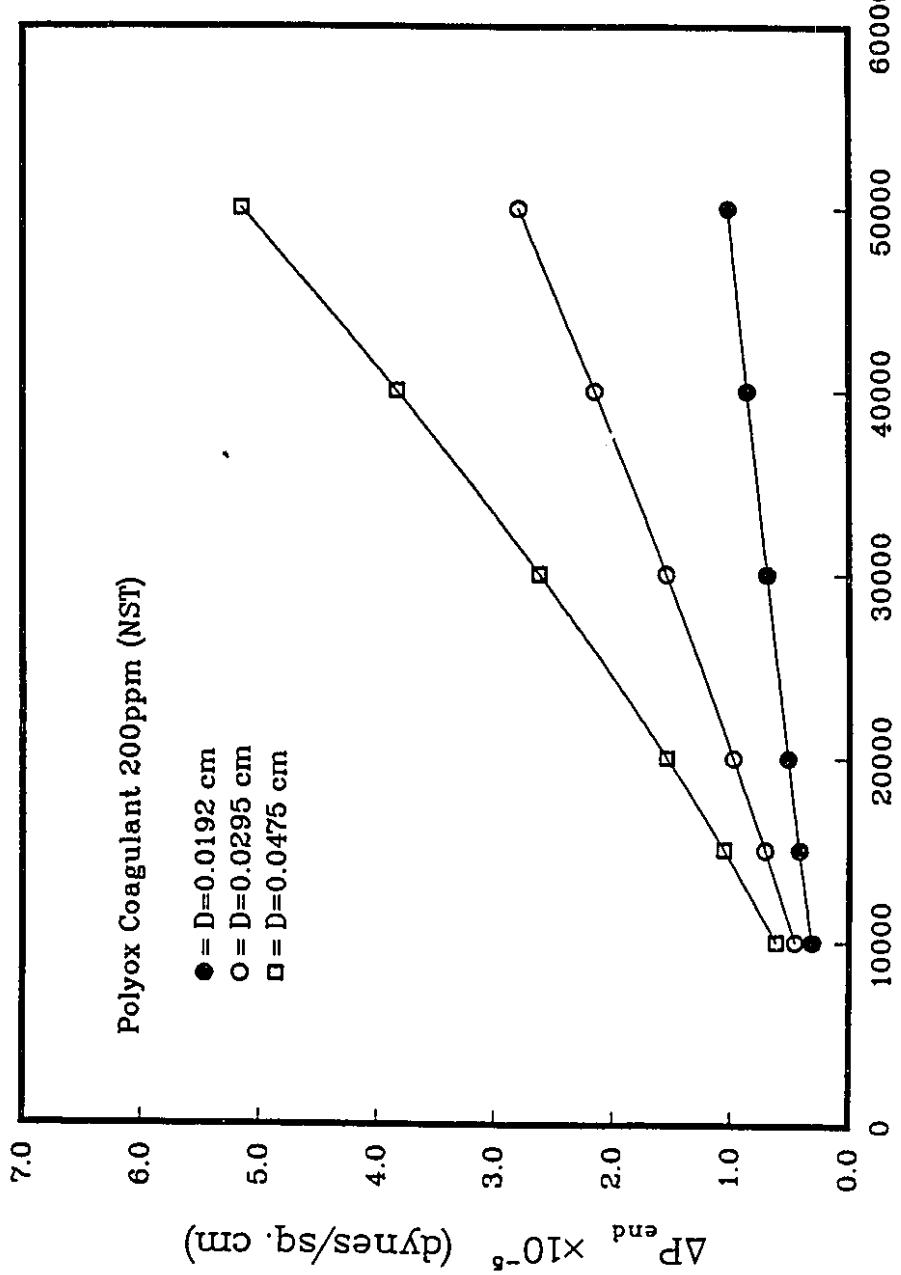

Figure 5.4 Variation of ΔP_{end} with $8\langle u\rangle/D$ for capillary flow of 200 ppm Coagulant solutions .

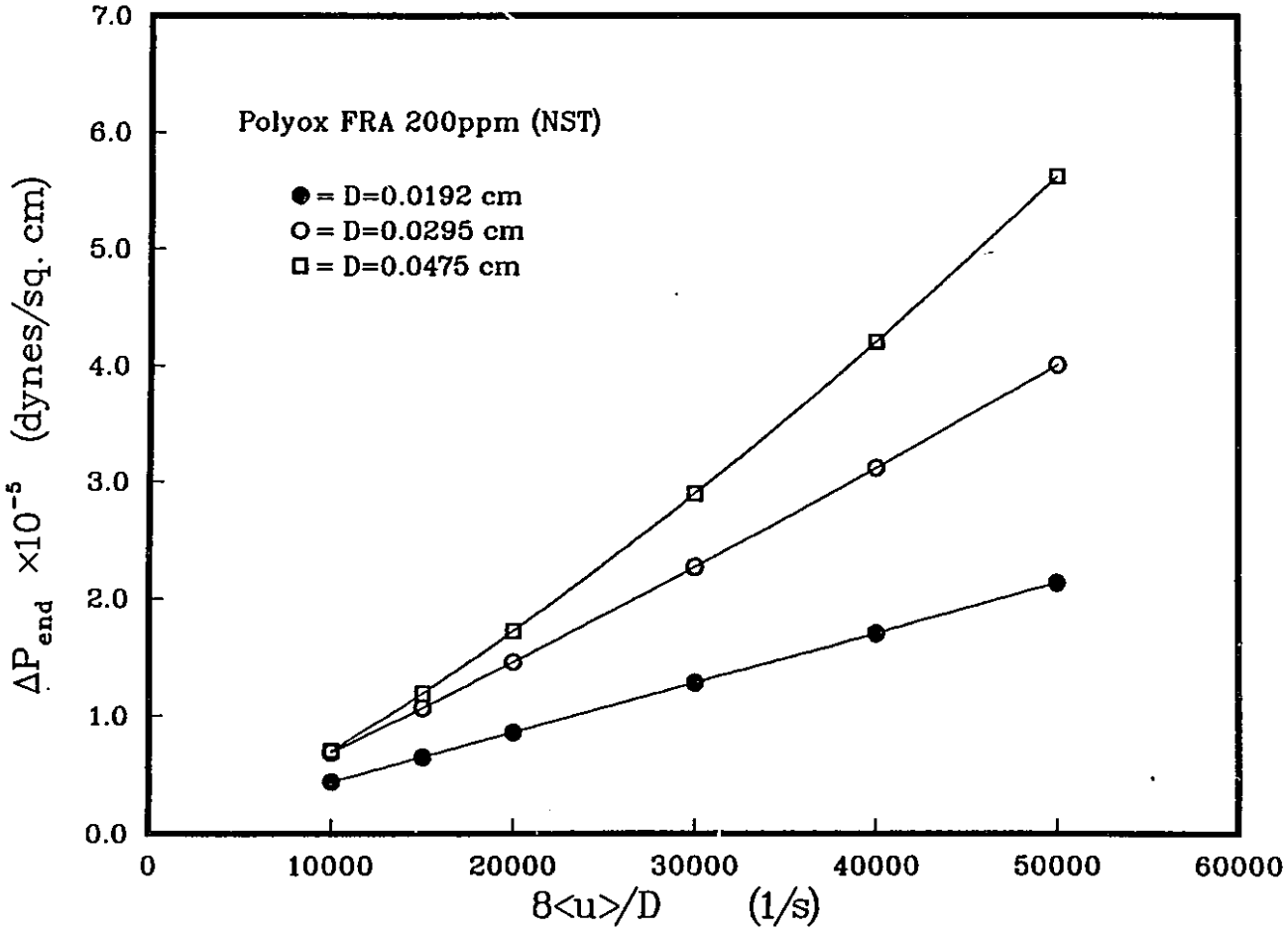

Figure 5.5 Variation of ΔP_{end} with $8\langle u\rangle/D$ for capillary flow of 200 ppm FRA solutions.

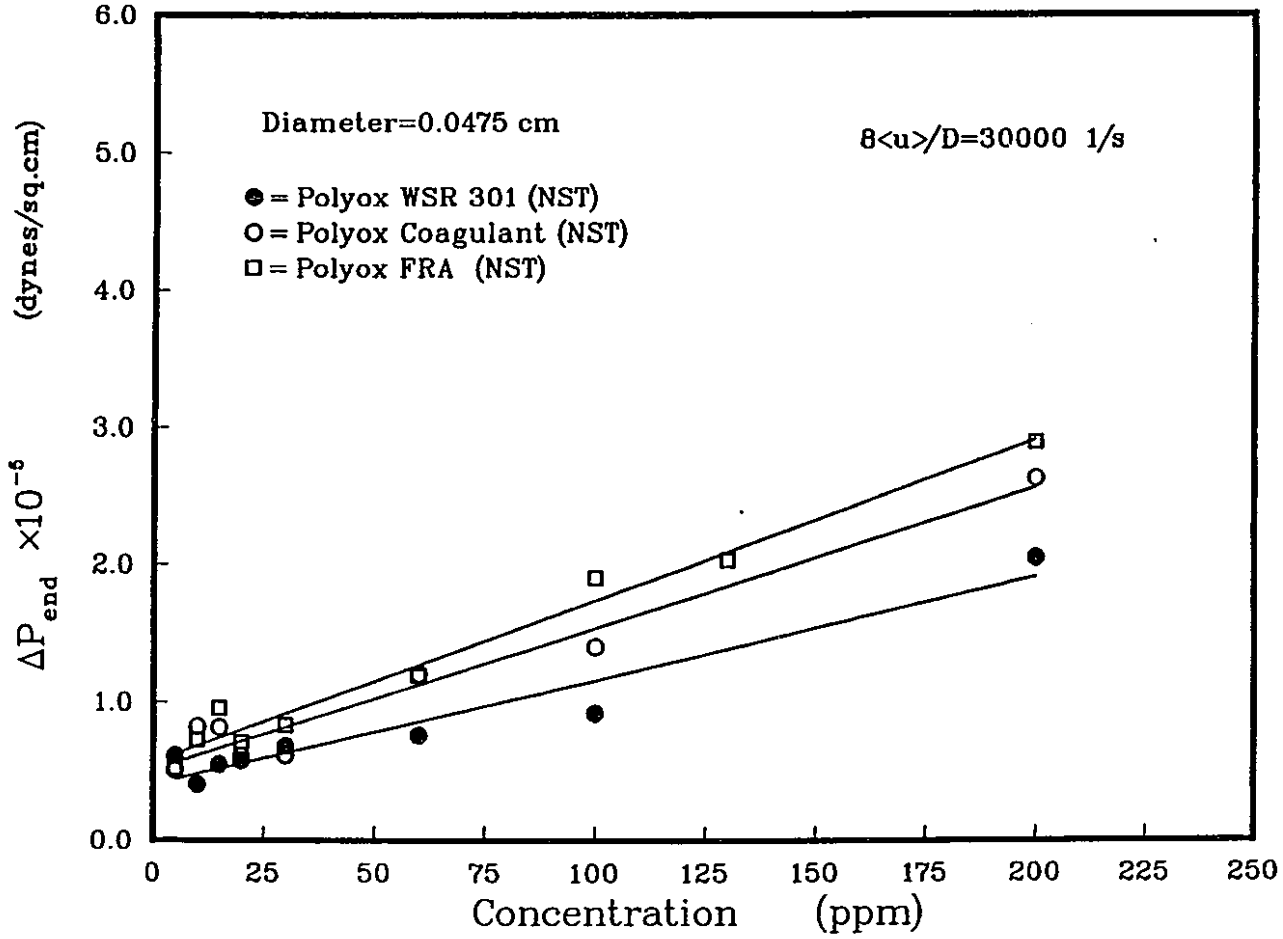

Figure 5.6 Variation of ΔP_{end} with concentration at 8<u>/D=30000 1/s (D=0.0465cm).

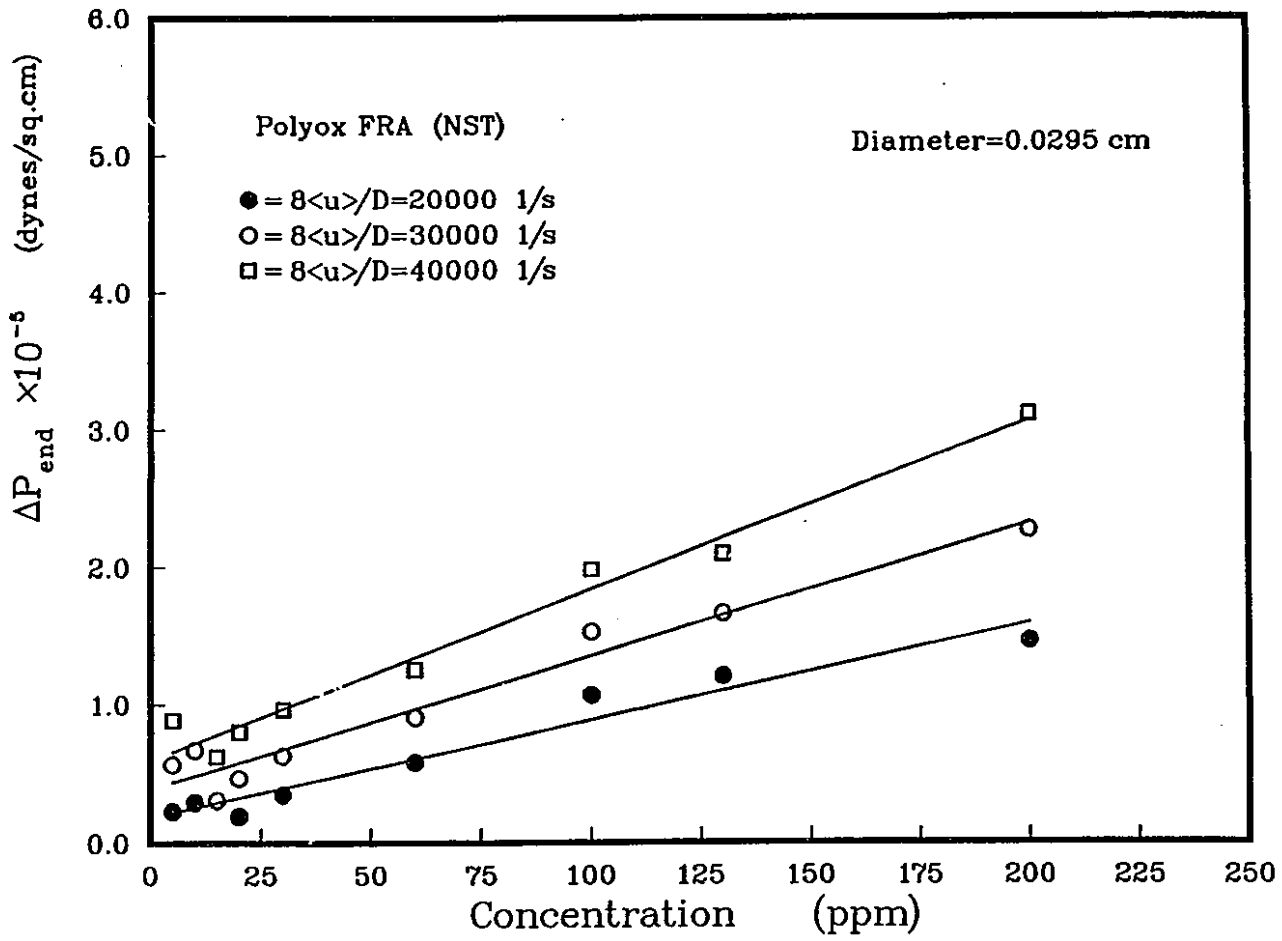

Figure 5.7 ΔP_{end} vs. concentration at various 8<u>/D for solutions of FRA (D=0.0295cm).

Table 5.2: Contribution of Excess Pressure Losses to the Total Pressure Drop

Polymer	Concentration	Diameter (cm)	$8\langle u\rangle$/D (1/s)	$\Delta P_{end}/\Delta P$ (%)
WSR 301	100ppm	0.0466	30000	3.7
	200ppm	0.0296	30000	4.5
	200ppm	0.0476	30000	6.9
	200ppm	0.0476	40000	7.2
Coagulant	100ppm	0.0466	30000	5.3
	200ppm	0.0296	30000	5.2
	200ppm	0.0466	30000	8.7
	200ppm	0.0466	40000	9.7
FRA	100ppm	0.0466	30000	7.6
	200ppm	0.0296	30000	7.5
	200ppm	0.0466	30000	9.4
	200ppm	0.0466	40000	10.4

All data were obtained from calculations based on L/D=2000.

flow might be attributed to shear thinning and viscoelasticity of the solutions. The results indicate that in general, an L/D ratio of 2000 may not be sufficient to neglect end effects in capillary flow of polymer solutions at some conditions. The ratio of L/D required to neglect end effects also depends on the tube diameter as well as shear rate. At the concentration of 200 ppm, for example, it seems that to minimize end effects sufficiently to render them insignificant, an L/D ratio approaching 2000 may be adequate for the tube 0.02 cm in diameter but not enough for the tube diameter greater than 0.05 cm. A larger critical ratio of L/D is then required for the larger diameter tubes at higher polymer concentration levels.

5.3 Evaluations of Effective Velocity at the Wall

A surface phenomenon accompanying the flow may be characterized in terms of the effective velocity at the wall u_w. This was accomplished by carrying out fits of the flow curves and using these to construct plots of the apparent shear rate $8\langle u\rangle/D$ vs. 1/D for different wall shear stresses. The slopes of the straight lines were used to determine the effective velocities at the wall. The analysis was performed numerically using least squares fitting procedures. The characteristic plots of $8\langle u\rangle/D$ vs. 1/D for selected cases are shown in figures 5.8 to 5.11. The figures display two anomalous effects. In the first two figures, slopes of the plots provided positive values, resulting in positive effective velocities at the wall corresponding to flow enhancement. However, negative slopes of the straight lines were found in the latter two cases, corresponding to negative effective velocities at the wall. These are consistent with flow reduction associated with polymer adsorption. The linearity of all the plots confirms that the effective velocity at the wall is independent of tube diameter for a given solution. No change in the sign of u_w with the tube diameter was observed over the diameter range involved in the experiments. It, however, implies that the contribution of wall effects to the total flow rate decreases with

increasing tube diameter.

In general, positive effective velocities at the wall were found at the lower polymer concentration levels studied, while negative values were obtained at higher polymer concentrations with the flows in the untreated glass tubes. The dependence of the effective velocity at the wall on polymer concentration over the entire concentration range investigated, with wall shear stress as a parameter, is shown in figures 5.12 to 5.14, for the untreated glass tubes. It is seen that the magnitude of the negative effective velocity at the wall increases initially with polymer concentration and proceeds to level off at higher concentration levels. The behavior is contrasted with that for the treated surface tubes, in which the positive effective velocity at the wall shows a rapid decrease with increasing polymer concentration, as seen in figure 5.15. This is supported by the measurements of Mohnsse et al. (1990) obtained using the laser-differential microanemometer. Furthermore, it is in qualitative agreement with the trends in slip layer thicknesses with polymer concentration reported in general findings of Aussere et al. (1986), and Sorbie and Huang (1991) observed by various methods.

Variation of the effective velocities at the wall with wall shear stress was observed for all the systems studied. The magnitude of the effective velocity at the wall increases with shear stress at the wall in most cases. The behavior of u_w over a range of wall shear stresses and polymer concentrations is represented in figures 5.16 to 5.20 for the three polymers for flow in the chemically treated and untreated tubes. The data points shown were determined at each τ_w from the slopes of the straight lines of $8\langle u\rangle/D$ vs. 1/D. It can be seen that they displayed a very good trend and remarkably consistent pattern of variation of the effective velocities at the wall with the wall shear stresses and polymer concentrations. The smooth curves which are plots of the equation $u_w = A(c)\tau_w - b\tau_w^d$ illustrate the fits obtained using the parameter evaluation by least squares fitting. The parameters A(c), b

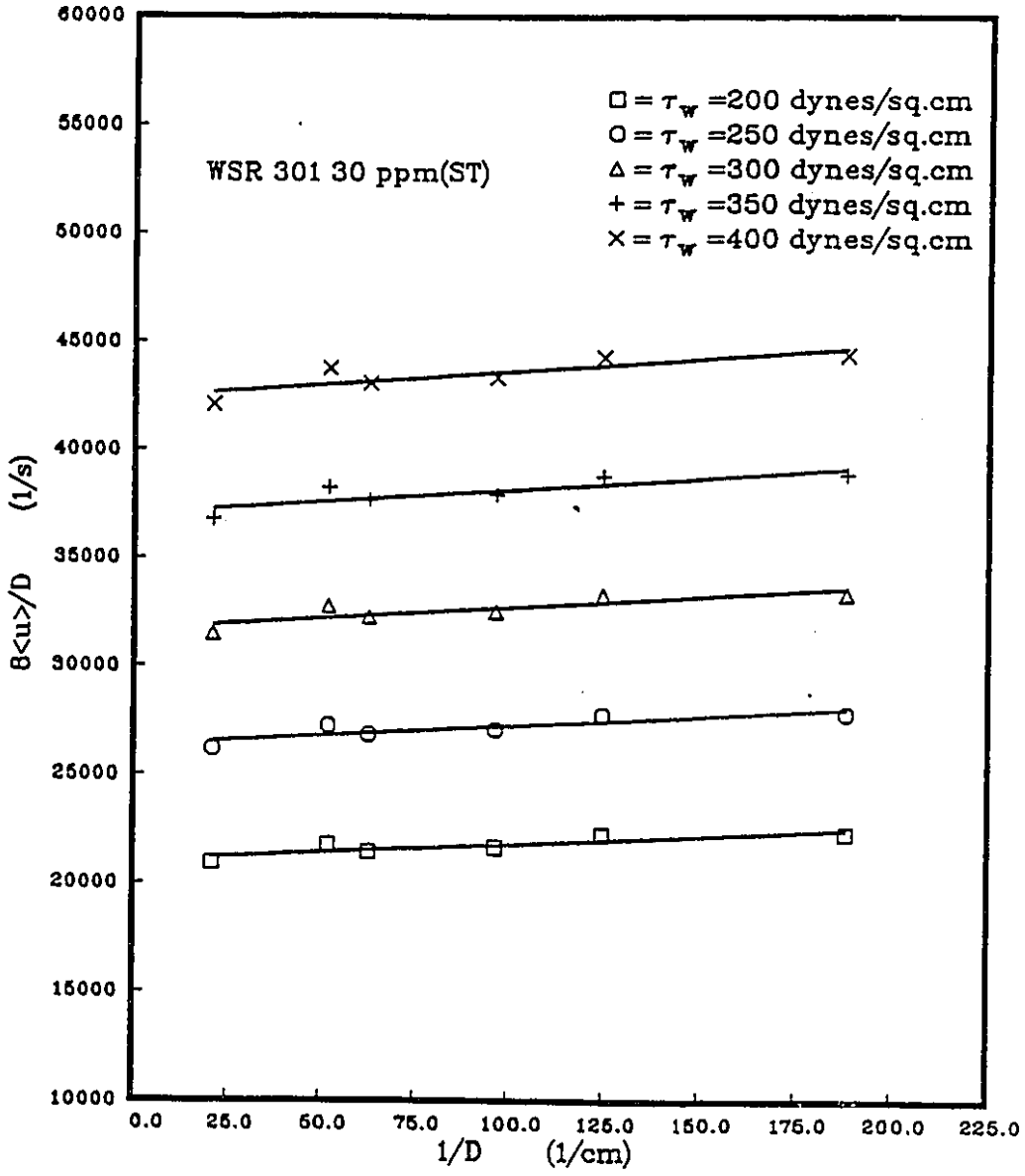

Figure 5.8: Apparent shear rate vs. 1/D, 30 ppm Polyox WSR 301.

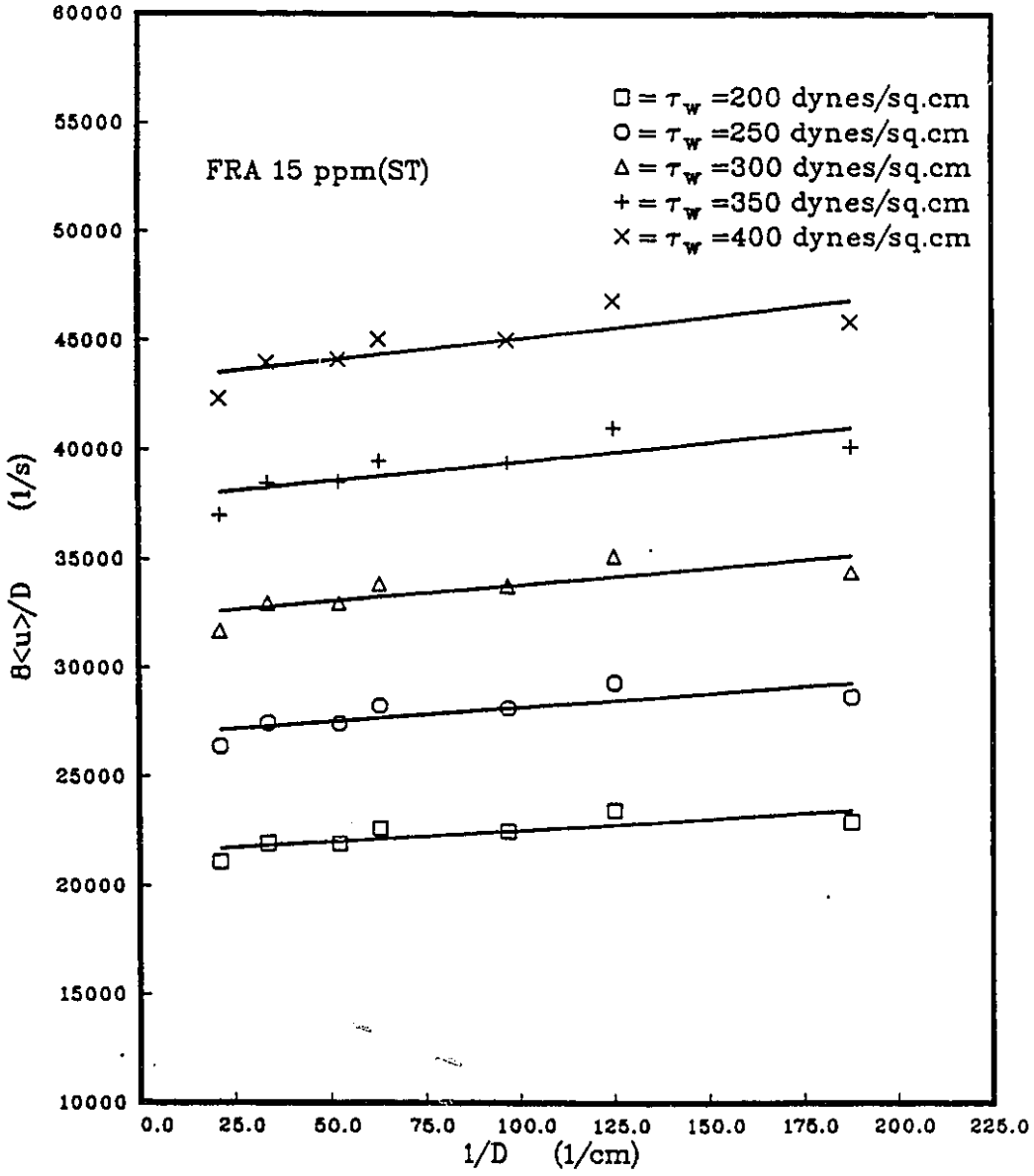

Figure 5.9: Apparent shear rate vs. 1/D, 15 ppm Polyox FRA.

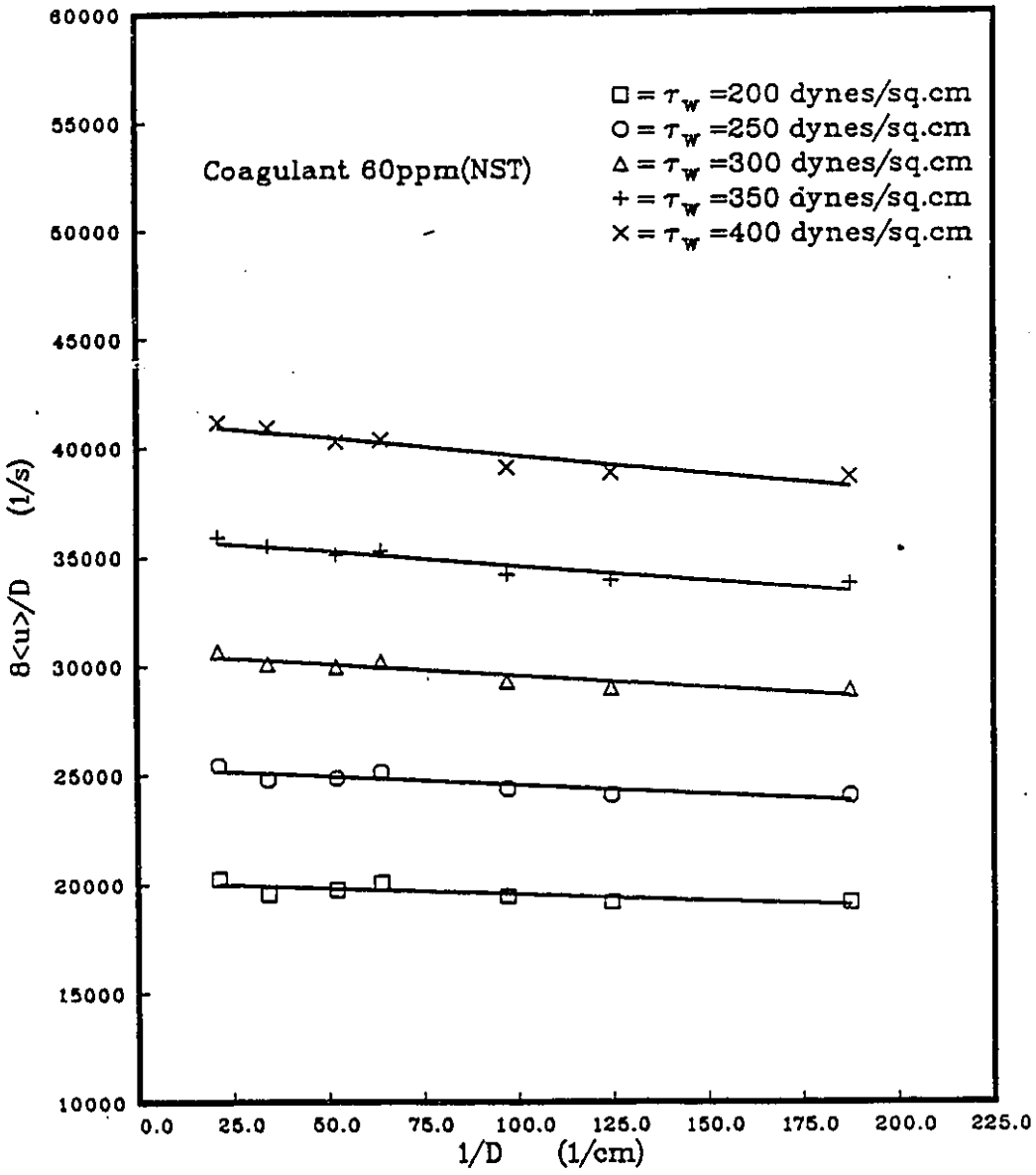

Figure 5.10: Apparent shear rate vs. 1/D, 60 ppm Polyox Coagulant.

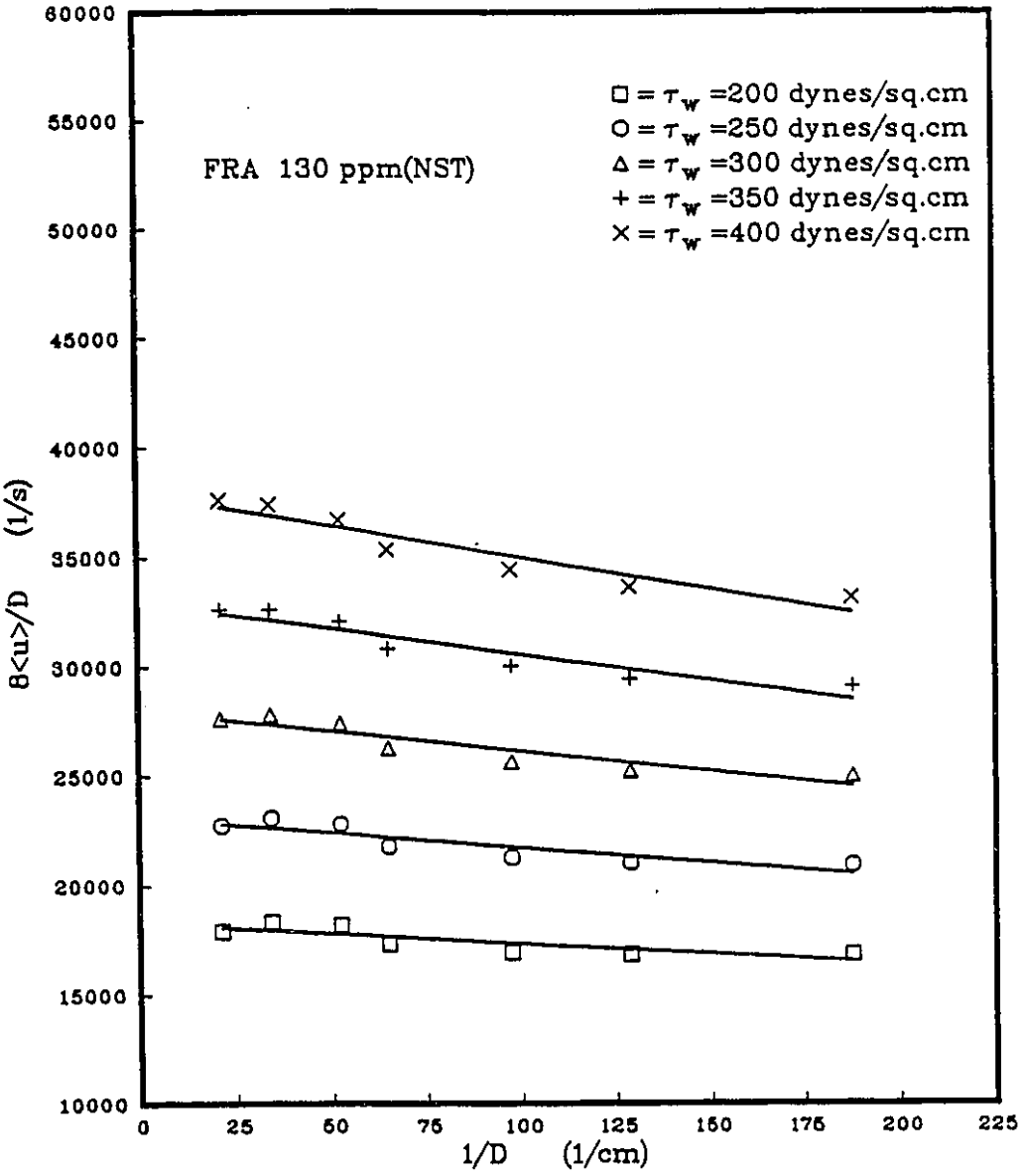

Figure 5.11: Apparent shear rate vs. 1/D, 130 ppm Polyox FRA.

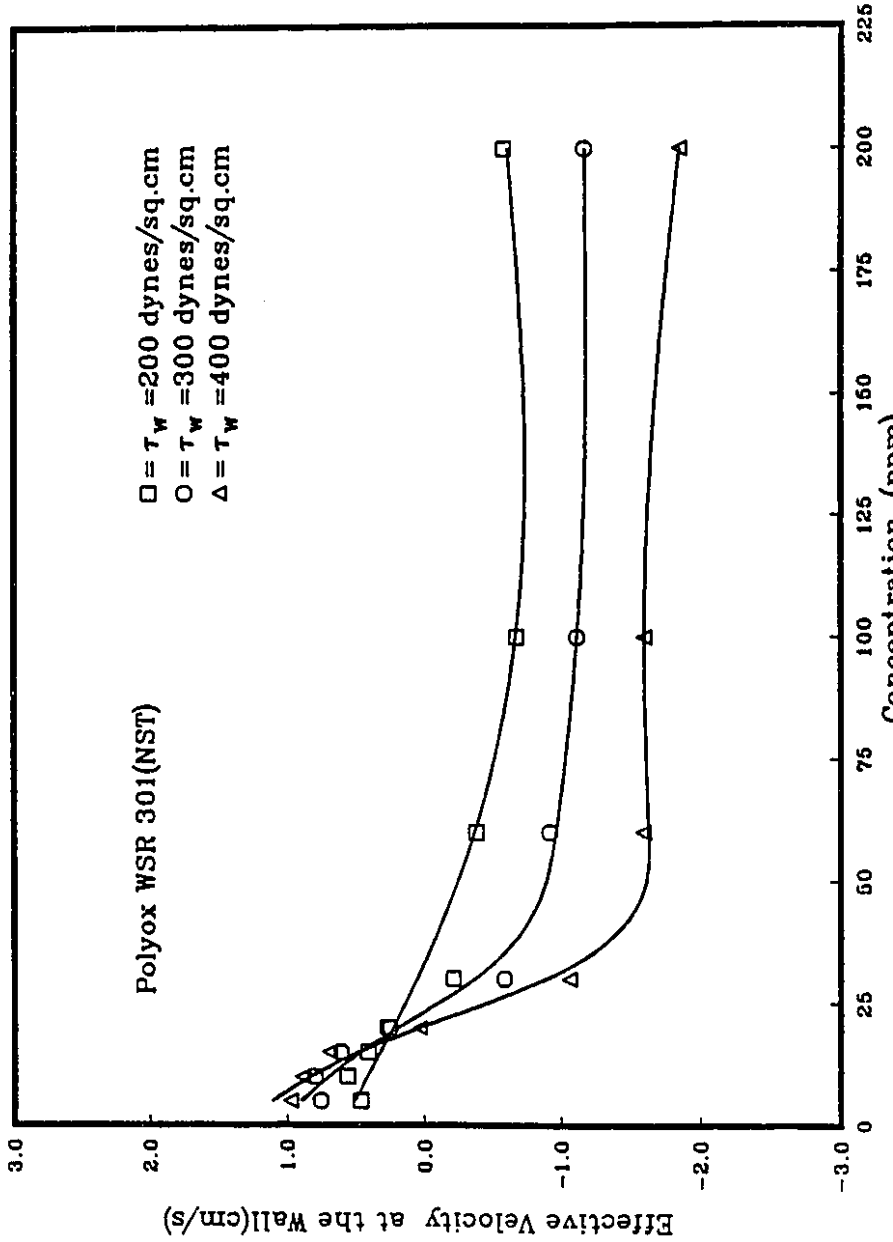

Figure 5.12 Dependence of effective velocity at the wall on concentration for Polyox WSR 301 solutions flowing in untreated tubes.

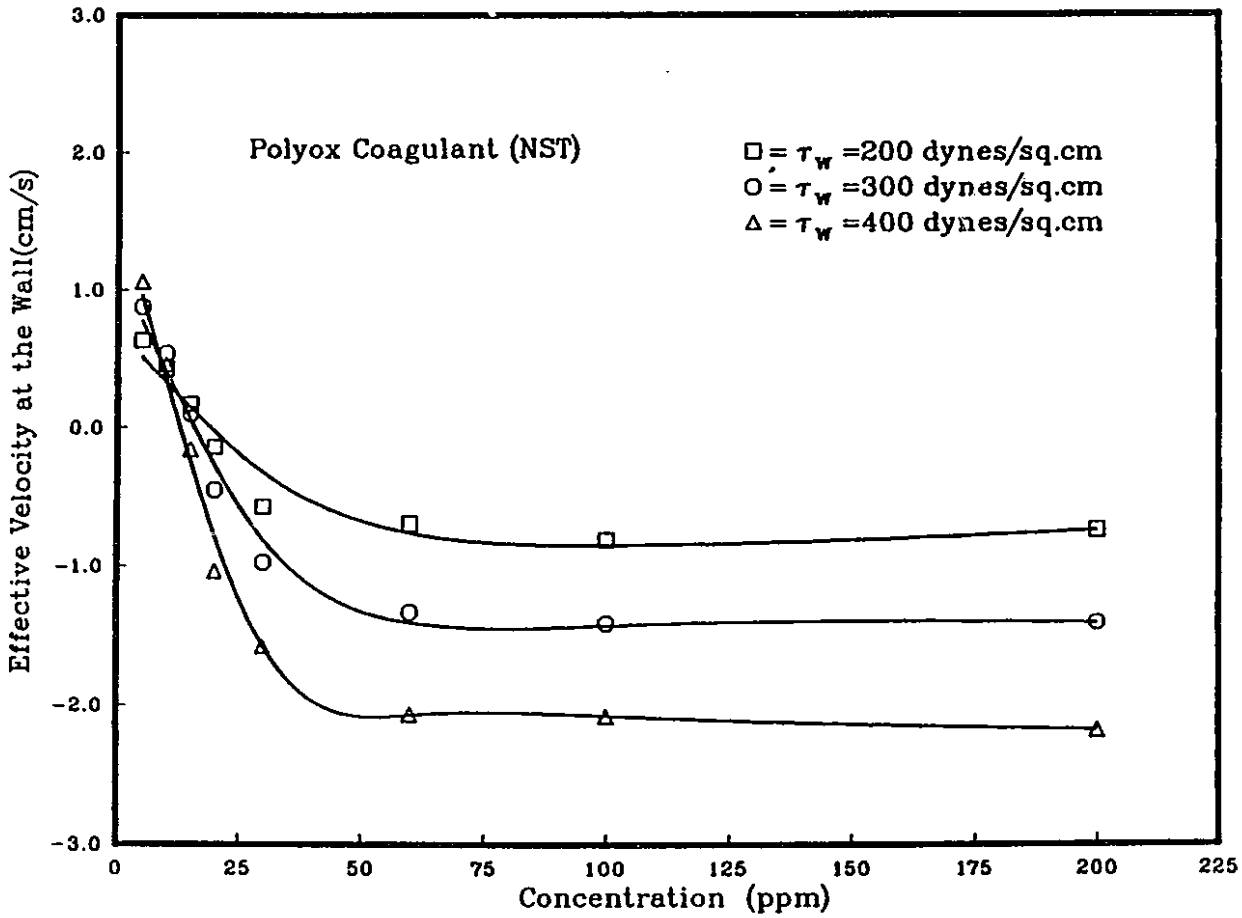

Figure 5.13 Dependence of effective velocity at the wall on concentration for Polyox Cagulant solutions flowing in untreated tubes.

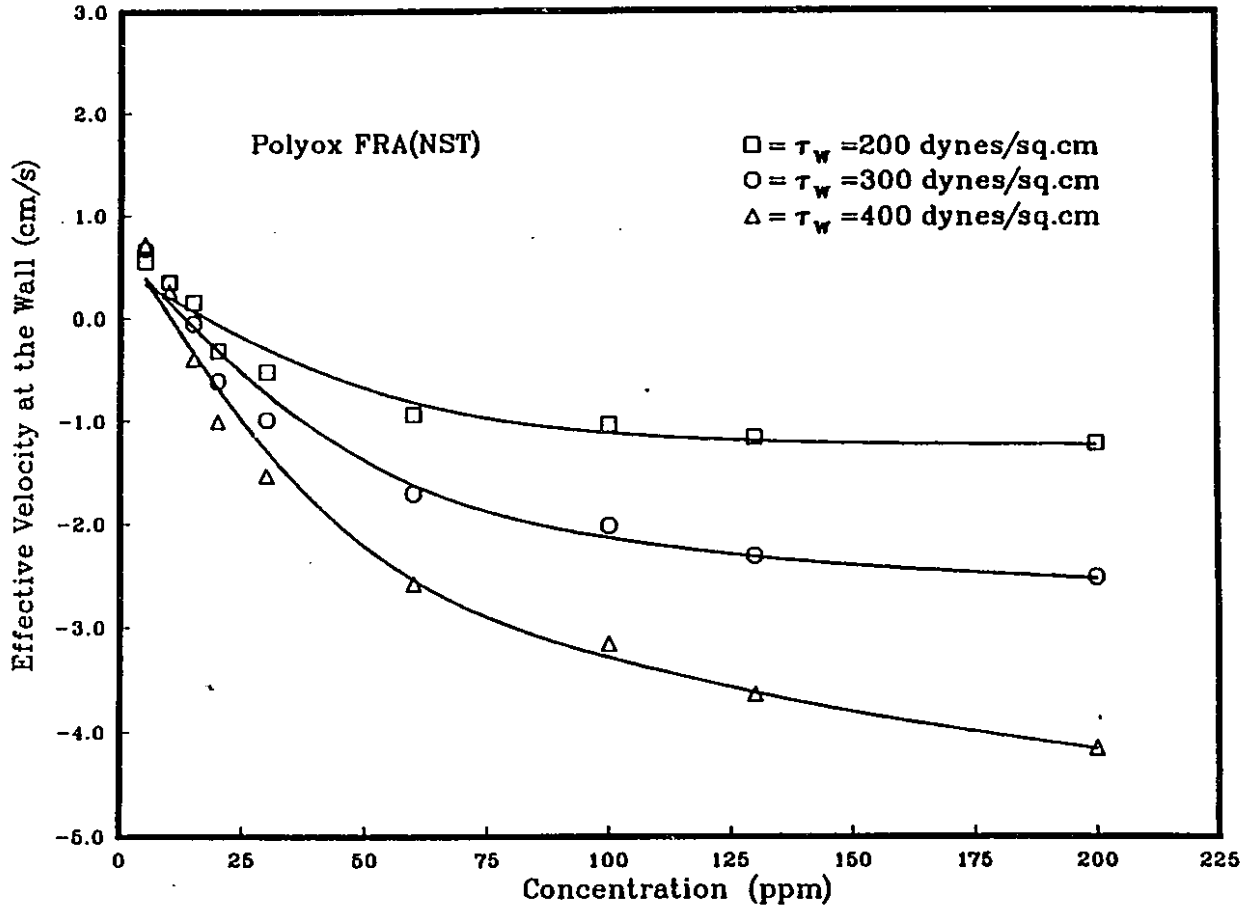

Figure 5.14 Dependence of effective velocity at the wall on concentration for Polyox FRA solutions flowing in untreated tubes.

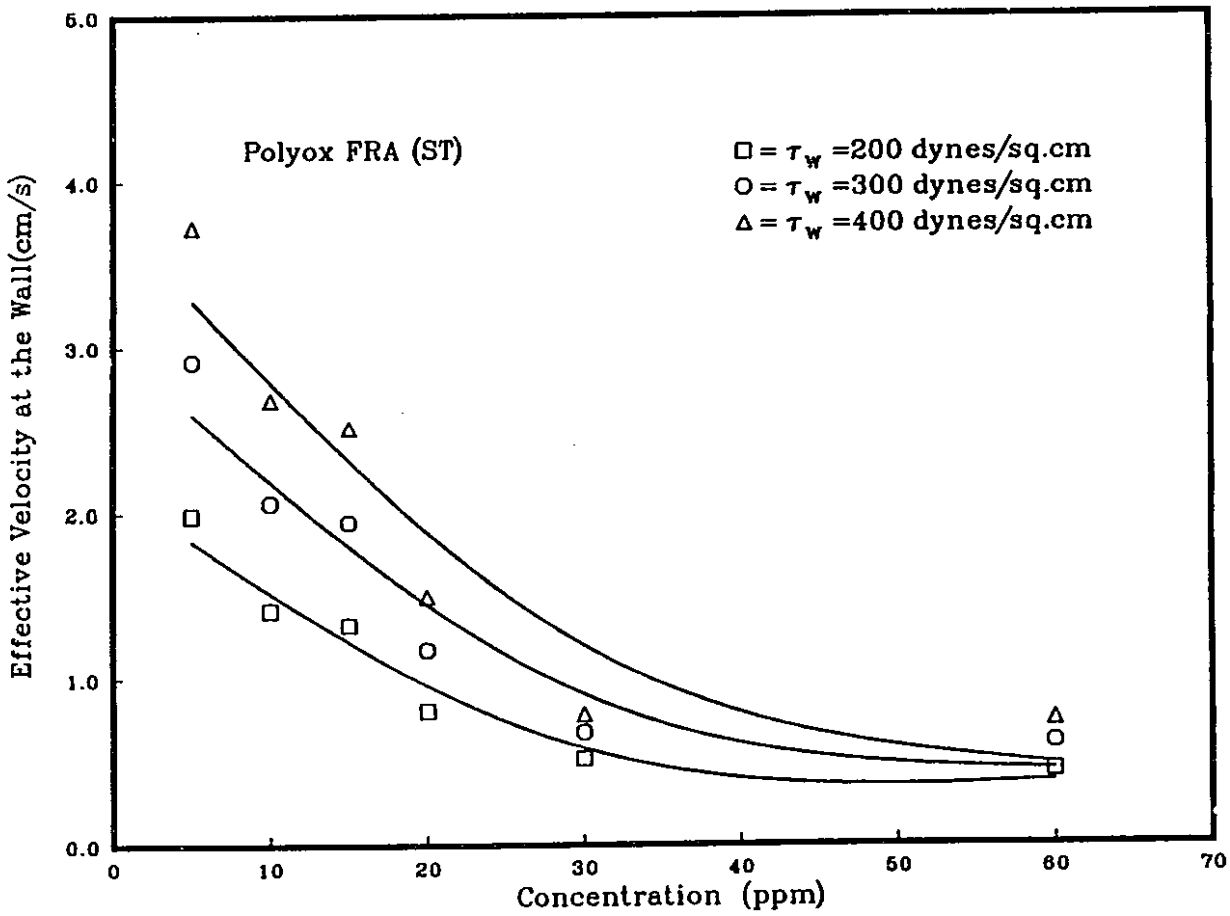

Figure 5.15 Dependence of effective velocity at the wall on concentration for Polyox FRA solutions flowing in silane treated tubes.

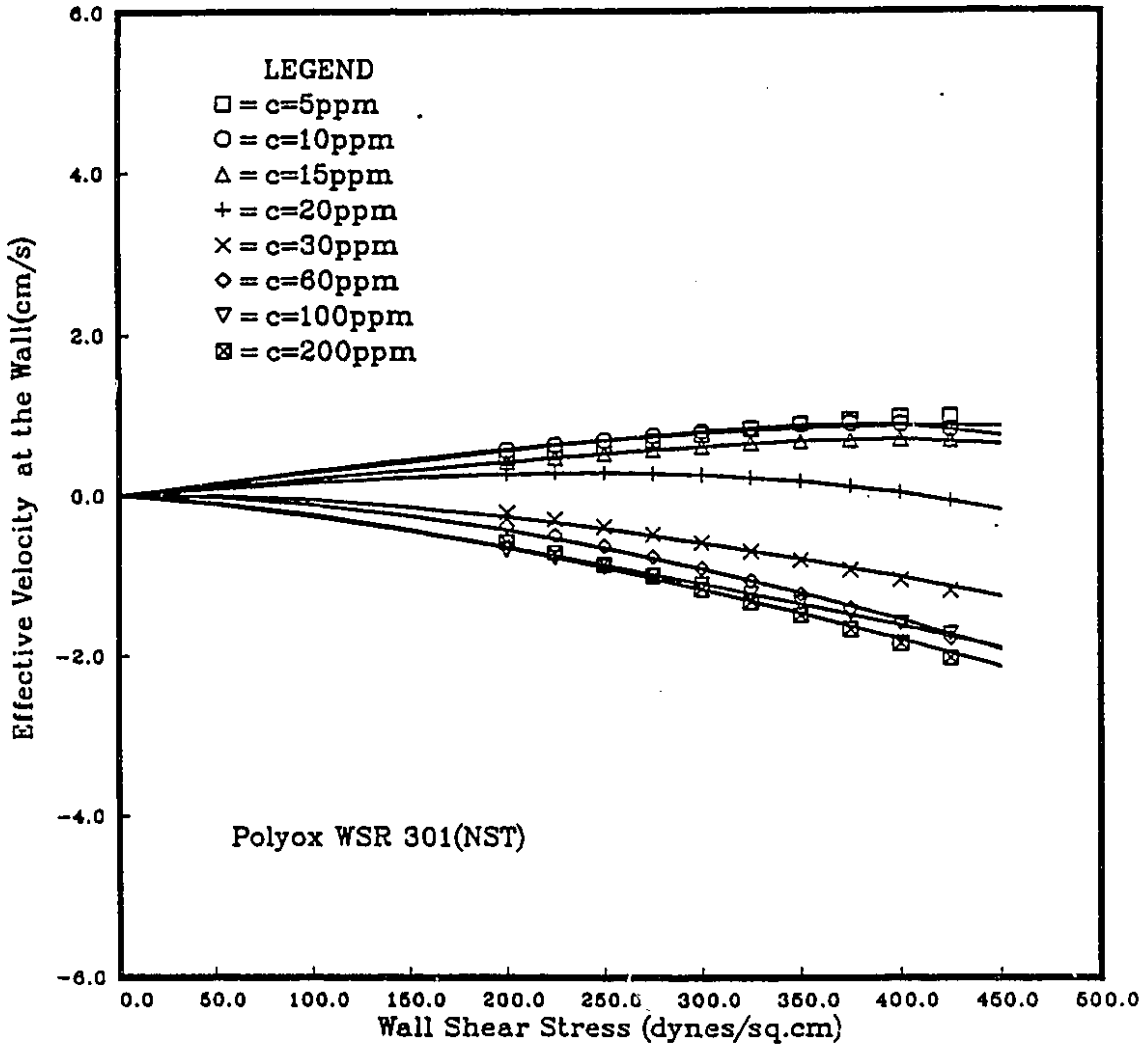

Figure 5.16 Variation of effective velocity at the wall with wall shear stress for Polyox WSR 301 solutions (no surface treatment).

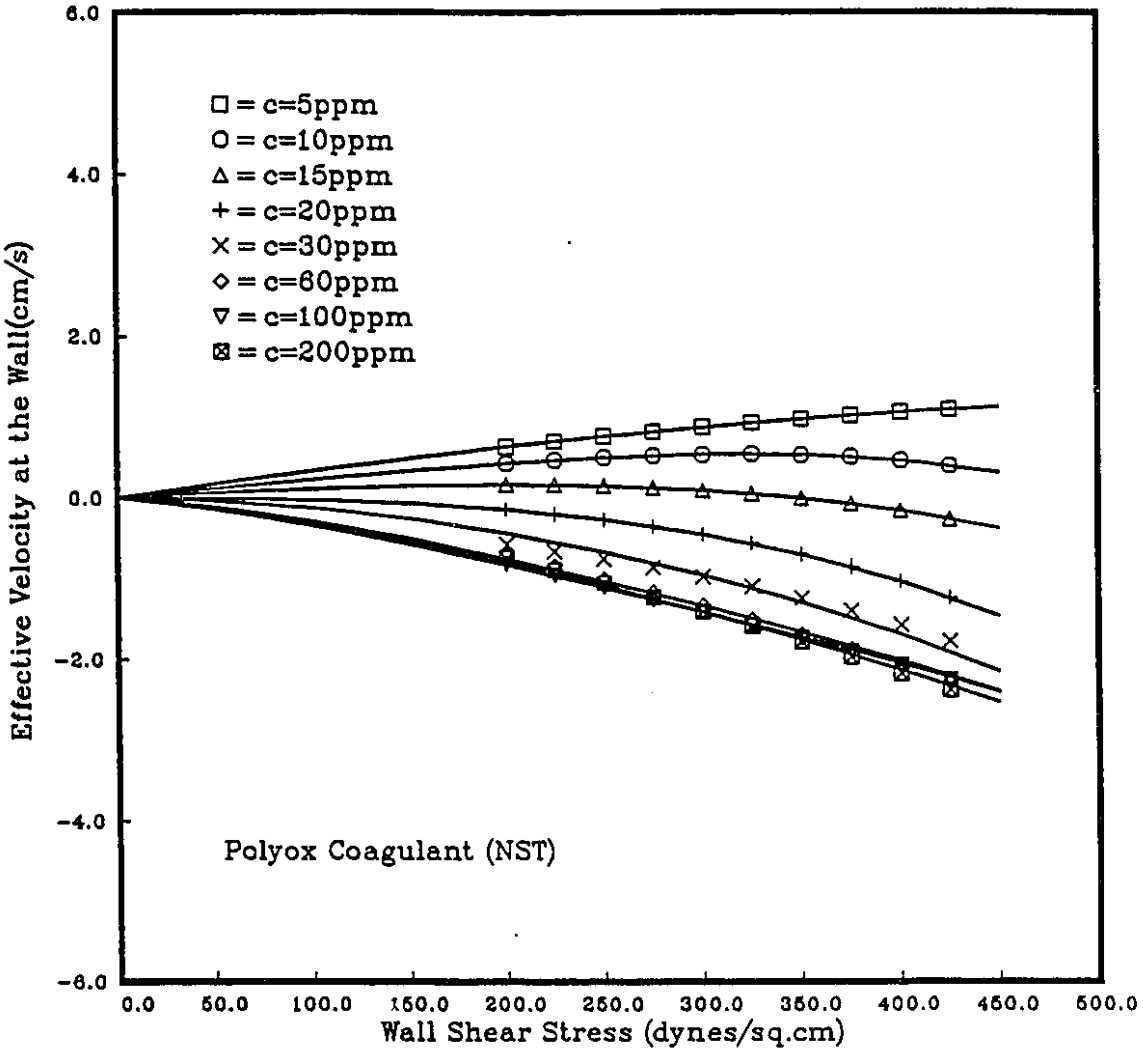

Figure 5.17 Variation of effective velocity at the wall with wall shear stress for Polyox Coagulant solutions (no surface treatment).

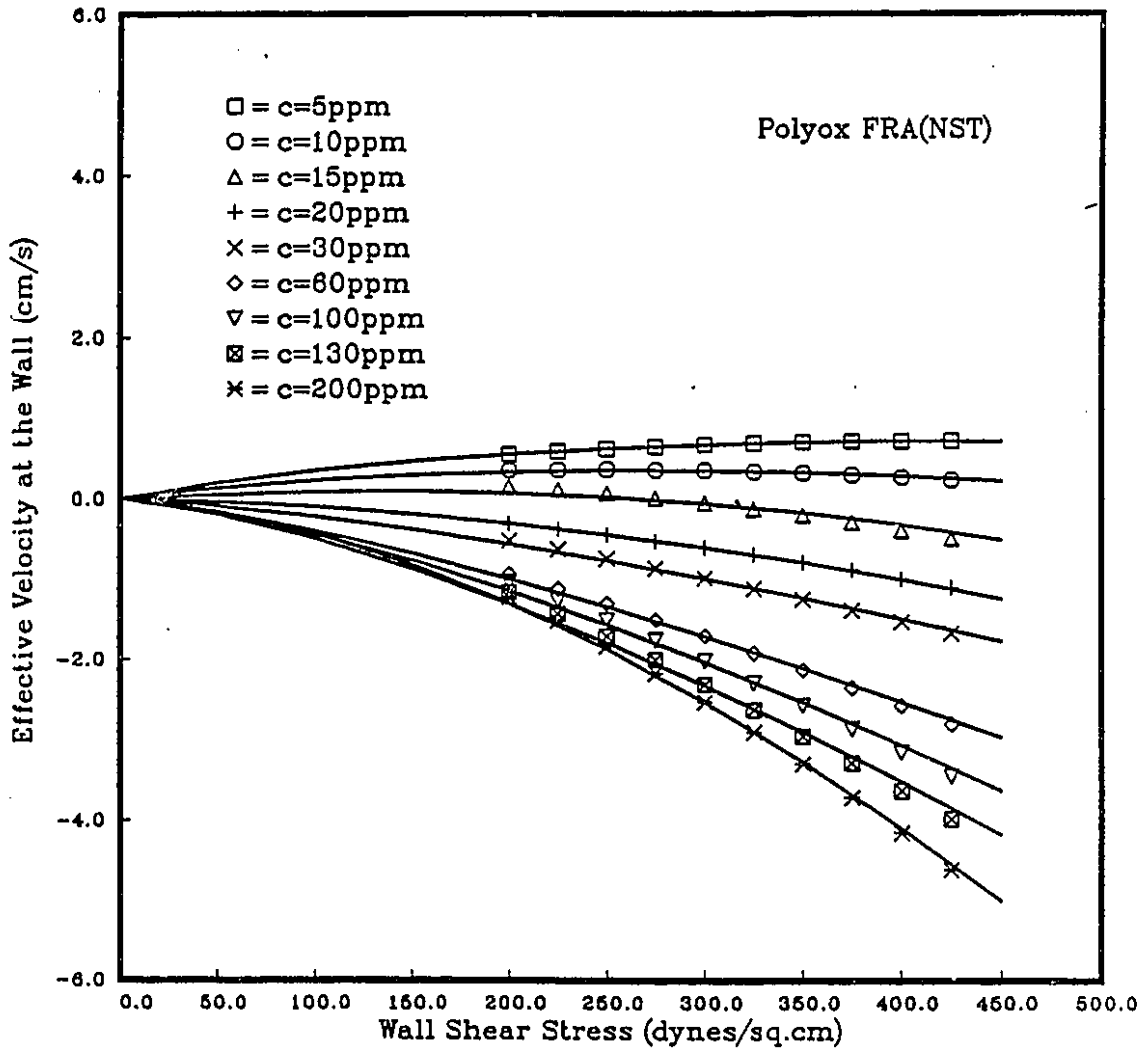

Figure 5.18 Variation of effective velocity at the wall with wall shear stress for Polyox FRA solutions (no surface treatment).

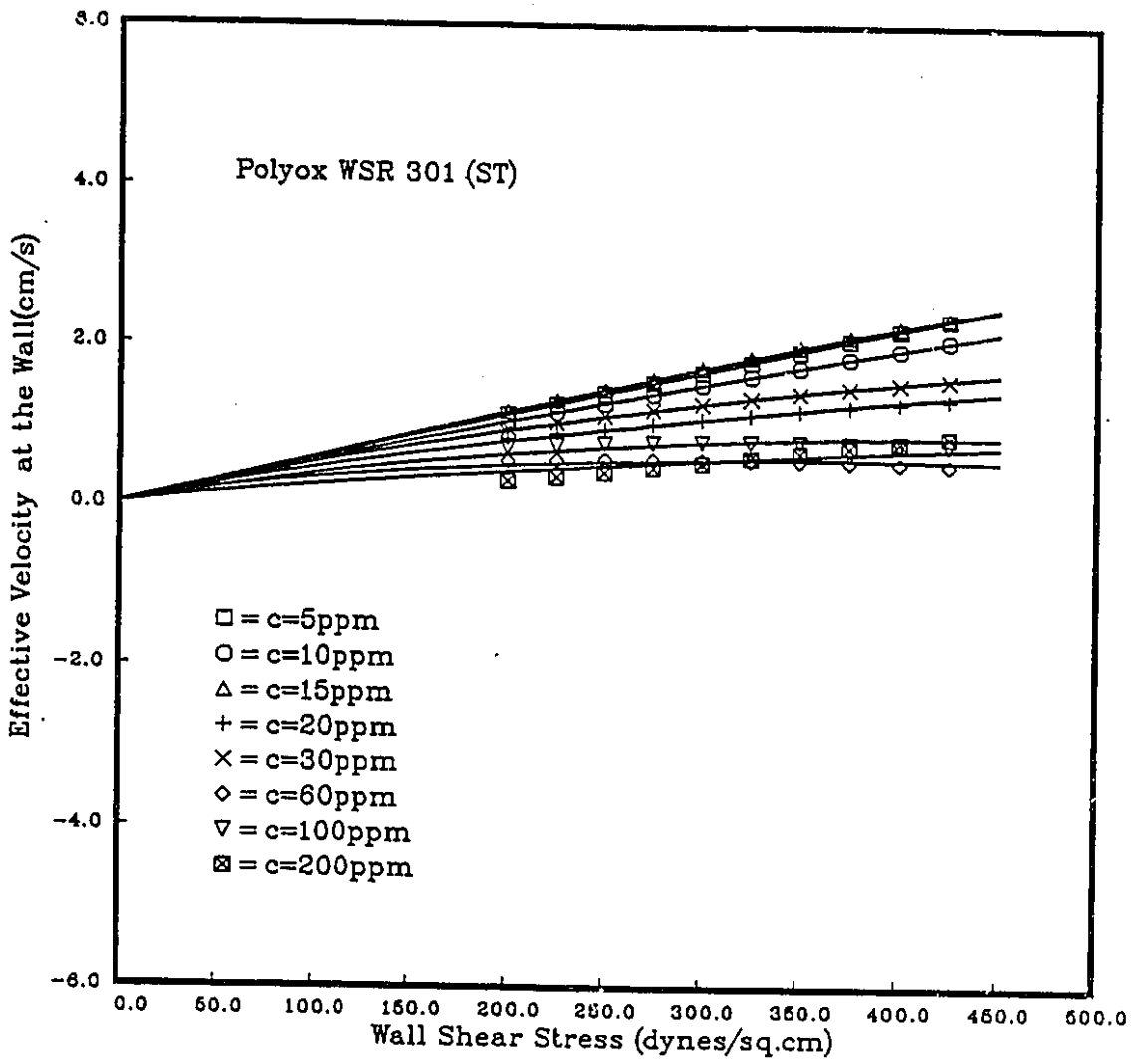

Figure 5.19 Variation of effective velocity at the wall with wall shear stress for Polyox WSR 301 solutions in treated tubes.

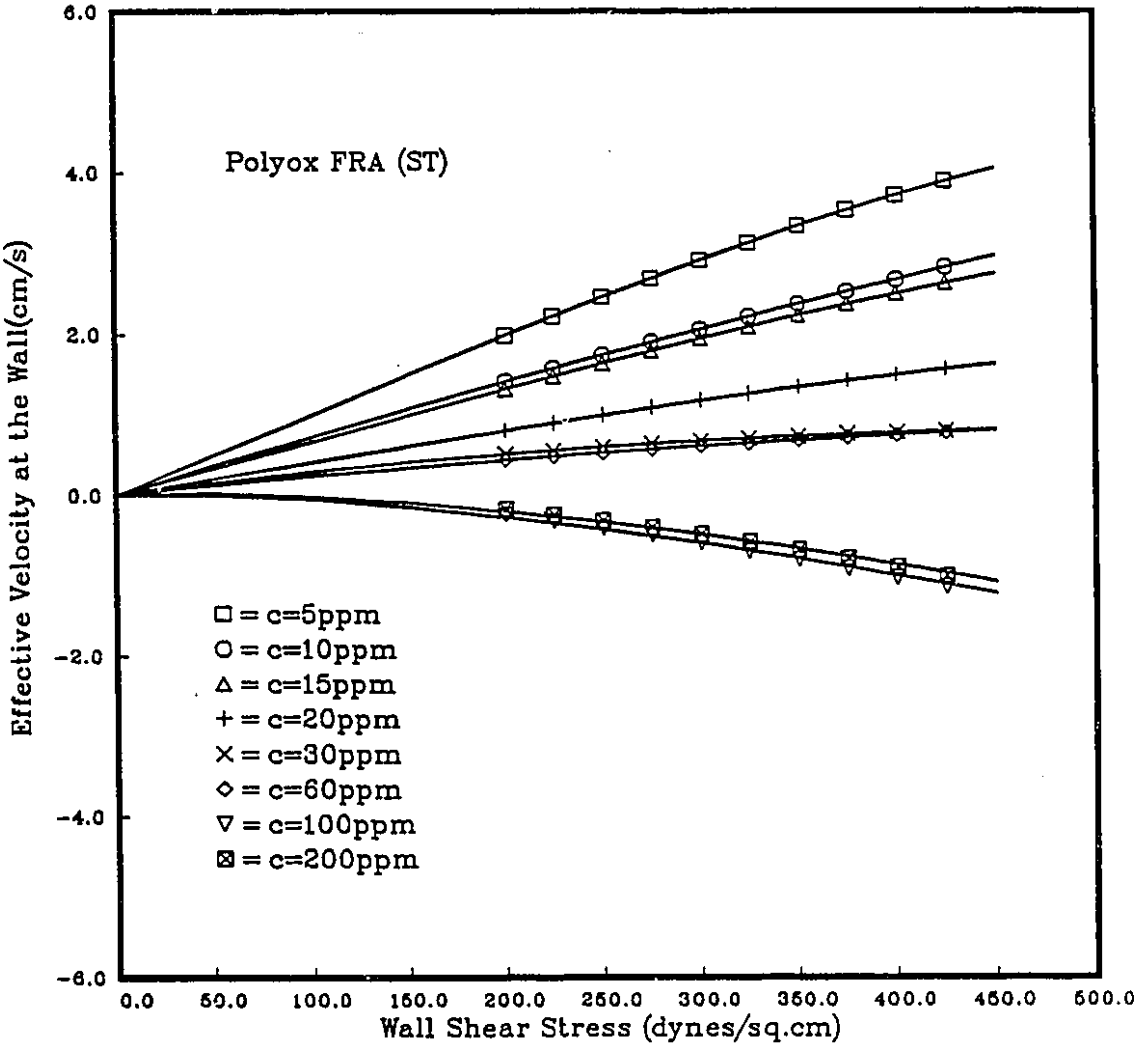

Figure 5.20 Variation of effective velocity at the wall with wall shear stress for Polyox FRA solutions in treated tubes.

and d are functions of the polymer concentration for a given polymer-solid surface system and were evaluated by means of the following iterative algorithm. A value of d greater than 1 was assumed first. The parameters A(c), b and corresponding standard deviation then were evaluated by least squares fitting of the equation. The procedure was repeated for a series of d in the range $1 \leq d \leq d^*$, where d^* was finite. The desired values of d, A(c) and b were those yielding the minimum standard deviation for the particular system. It is seen that the experimental points are well described by the fitted curves. The fitted equation furthermore is available for evaluation of the first derivative of u_w at zero shear which, as seen from the analysis in Chapter 3, is required for determination of the thickness of the adsorbed polymer layer at zero shear. A power-law expression for u_w in terms of τ_w in the literature (Cohen, 1981) is incapable of providing the same information.

The contribution of the wall effects to the total flow rate may be determined by substitution of the expression for u_w in the flow expression for a particular flow model. Thus, substituting for u_w in the Ellis model flow expression given by equation (3.27) yields:

$$\frac{u_w}{\langle u \rangle} = \left[\frac{(\frac{\tau_w}{\eta_0} + G\tau_w^\alpha)D}{8(A\tau_w - b\tau_w^d)} + 1\right]^{-1} \tag{5.1}$$

The ratio $u_w/\langle u \rangle$ is inversely proportional to the capillary diameter, indicating that surface phenomena may be important in flow of polymer solutions through fine tubes.

5.4 Transition From Slip to Polymer Adsorption

As noticed in figures 5.16 to 5.20, an increase in the polymer concentration of the solution over the range of 5 ppm to 200 ppm may be accompanied by a change in sign from positive to negative of the effective velocity at the wall. It is seen more clearly from the plots of u_w vs. concentration presented in figures

5.12 through 5.14. As indicated in Chapter 3, the change is associated with a transition from a wall effect dominated by slip flow to one dominated by polymer adsorption onto the capillary wall. The experimental data for the different solutions of the three polymers studied indicate that the transition usually occurs in the 15 to 20 ppm polymer concentration range for the untreated tubes. Interestingly, the concentrations marking the transition correspond to the concentration range at which the maximum drag reduction in turbulent flow is reached (Hanna, 1977) or the concentrations at which the large increase of drag reduction with polymer concentration tends to taper off (Arunachalam and Fulford, 1971), in turbulent flow of the same polymer solutions. The transition depicted in the figures is seen to be gradual, not abrupt.

Figure 5.21 presents the behavior in the transition region for the flow of aqueous Polyox FRA in the silane-treated glass tubes. The critical concentration is higher, compared to that observed with the untreated tubes. In the case of flow of Polyox WSR 301 aqueous solutions, however, no transition to polymer adsorption in the treated tubes was detected up to the maximum polymer concentration of 200 ppm studied. The flow was found to be accompanied only by a positive effective velocity at the wall.

Figure 5.22 showing the variation of u_w with wall shear stress over the transition region is representative of the three polymers studied in the untreated glass tubes (NST). The behavior in the transition region is consistent with the increase in magnitude of a negative u_w with increasing wall shear stress observed outside this region. This is not the case with slip flow corresponding to a positive u_w. In the absence of a transition to polymer adsorption, the positive u_w increases with increasing wall shear stress, as earlier reported by numerous workers. The behavior is seen to be reversed in the region of the transition from slip flow to polymer adsorption. It is evident from these results, that the onset of the transition varies

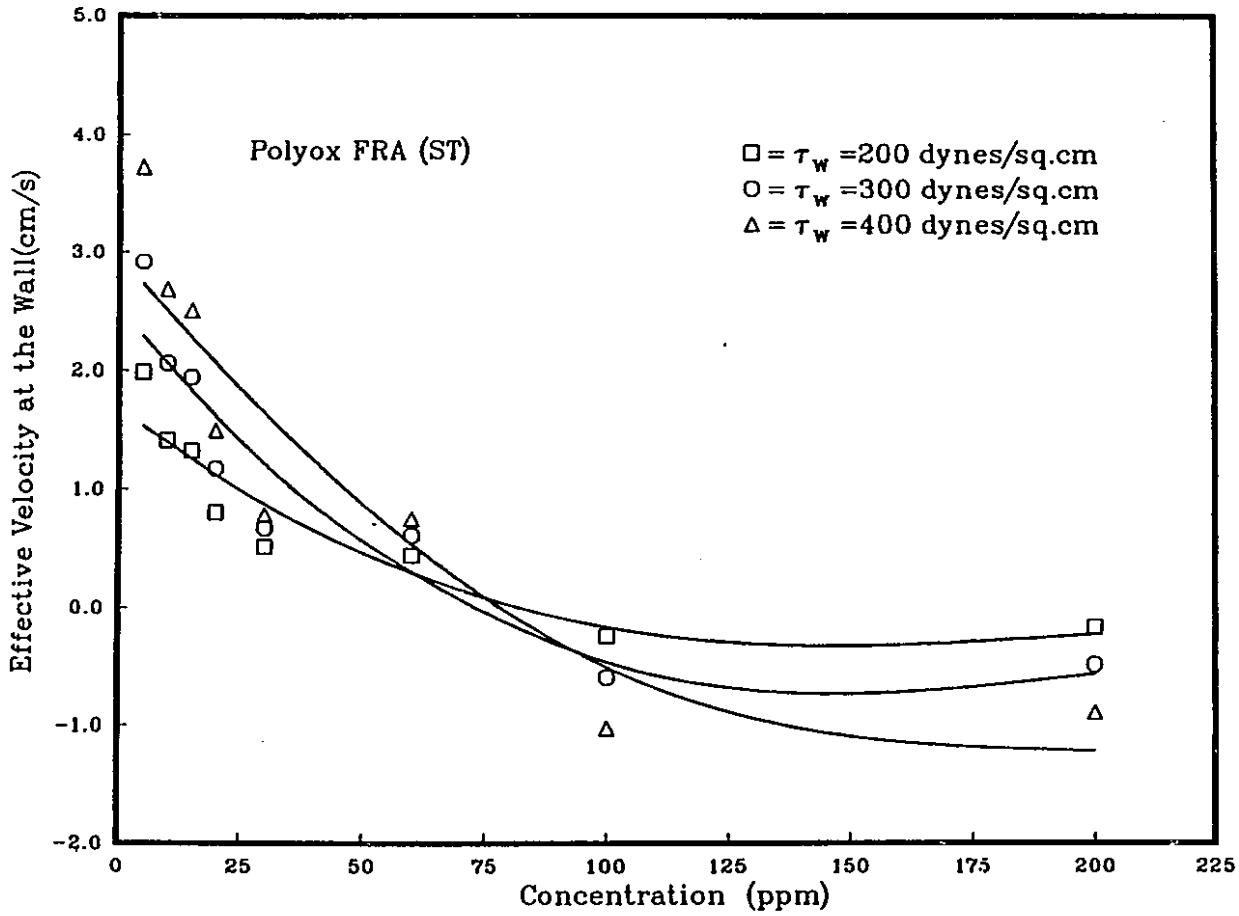

Figure 5.21 Demonstration of the transition behavior in terms of the effective velocity at the wall vs. concentration, for Polyox FRA solution flowing in treated tubes.

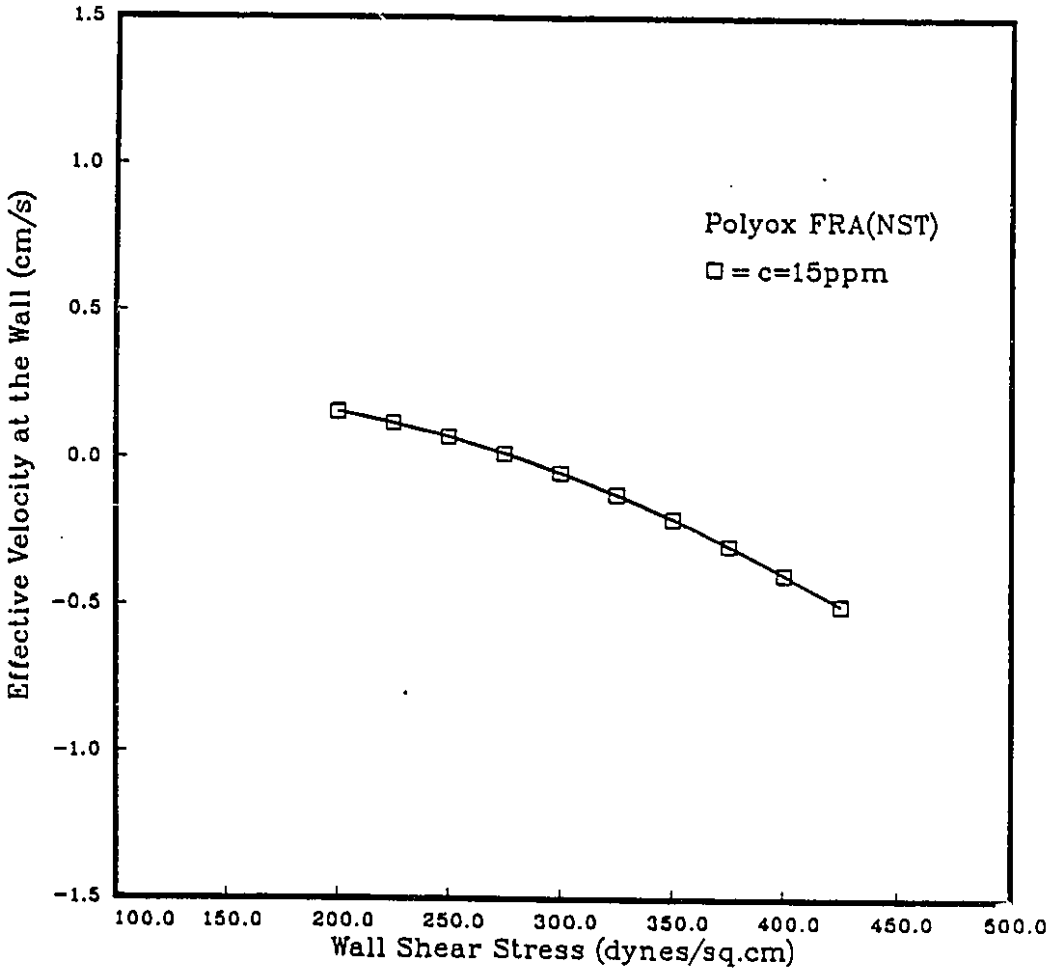

Figure 5.22 Plot of effective velocity at the wall vs. wall shear stress at the critical concentration of 15 ppm Polyox FRA.

with the wall shear stress, type of polymer and molecular weight as well as the state of the solid surface.

The transition of the effective velocity at the wall from a positive to a negative value does not appear to have previously been reported in the literature. This may result from the fact that more concentrated polymer solutions and fewer concentrations were investigated in earlier reported studies. It would be of interest to determine if other polymer systems exhibit transition from positive to negative effective velocities at the wall.

5.5 Hydrodynamic Adsorption in Capillary Flow

The analysis in Chapter 3 was applied in the evaluation of the effective hydrodynamic thicknesses of the adsorbed polymer layers from the effective velocities at the wall obtained directly from the experimental measurements. It accounts for the slip effects associated with flow of polymer solutions in addition to the polymer adsorption.

5.5.1 Parameter Evaluation

As seen from figures 5.16 to 5.20, the variation of u_w with τ_w is successfully represented by the equation (3.42) $u_w = A(c)\tau_w - b\tau_w^d$, which was used in the curve fits. The parameters in the equation vary with the polymer concentration and the composition of the tube wall. The $A(c)$, which is equal to $du_w/d\tau_w$ in the limit of zero shear, was utilized directly in equation (3.34) used in the determination of the polymer adsorption characteristics corresponding to a condition of zero shear. For the purpose of parameter evaluation, the equation may be rearranged as follows:

$$Y(c) = b_0 + b_1 X_1(c) + b_2 X_2(c) \tag{5.2}$$

where

$$Y(c) = \eta_0 A(c) \tag{5.3}$$

$$X_1(c) = \frac{\eta_0 A(c)}{c} \tag{5.4}$$

$$X_2(c) = \frac{(\eta_0/\mu_s - 1)}{c} \tag{5.5}$$

with

$$\begin{aligned} b_0 &= -\delta_{ap} \\ b_1 &= -k \\ b_2 &= k_{s0}k \end{aligned}$$

Since Y(c), $X_1(c)$ and $X_2(c)$ are provided by experiment as a function of the polymer concentration in the range 5-200 ppm, b_0, b_1 and b_2 are amenable to evaluation by linear regression.

Equation (3.27) was used for determination of η_0 and rewritten as:

$$Y^*(c) = b_0^* + b_1^* X_1^*(c) \tag{5.6}$$

where

$$Y^*(c) = \frac{8(\langle u \rangle - u_w)}{D}/\tau_w \tag{5.7}$$

$$X_1^*(c) = \tau_w^{\alpha-1} \tag{5.8}$$

and with constants:

$$\begin{aligned} b_0^* &= \frac{1}{\eta_0} \\ b_1^* &= G \end{aligned}$$

Equations (5.6) to (5.8), utilizing the results for the average velocity corrected for wall effects versus τ_w, were solved by least squares fitting through an iterative

algorithm. The constant b_0^* then gives the value of η_0 for the particular polymer solution. The iterative procedure was the same as that used to predict A(c) using equation (3.42), described in section 5.3, except for the additional constraint that b_0^* must be positive.

The evaluations of A(c) for all the cases studied are shown plotted in figure 5.23, as a function of the polymer concentration. The open and closed points represent experiments in the untreated and in the treated tubes, respectively. The data points were obtained from the fits of $u_w = A\tau_w - b\tau_w^d$ and the curves were calculated according to equation (5.2) using the parameters determined for each concentration. The values of A(c) increase with decreasing polymer concentration to a maximum and then as predicted by equation (3.34), decrease to zero for pure water, as suggested by the data for the solutions of WSR 301 flowing in the silane-treated tubes. The good fits obtained in the plots support the analysis upon which the method for evaluation of the adsorption characteristics is based.

Typical results of slip coefficients yielded by equation (3.37) are given in figure 5.24. The behavior and trends are similar to that of A(c) and consistent with the results of Mohnssen et al. (1991). The values of ζ are also tabulated in Appendix G.

An approximate method for solving equation (3.34) when there is a shortage of experimental data is given in appendix E. In this case, the problem is reduced to the solution of two single-variable equations.

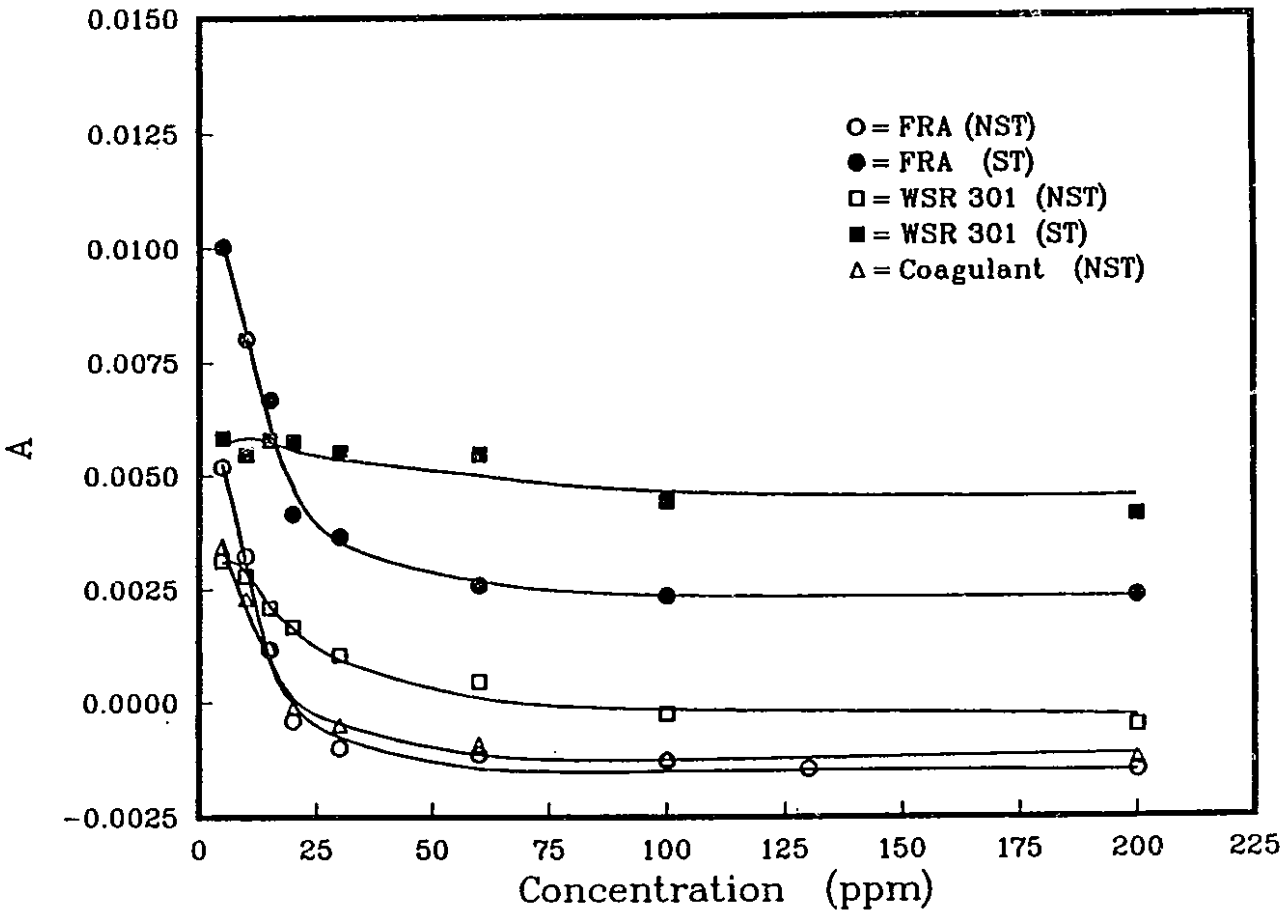

Figure 5.23 Behavior of A(c) vs. concentration for the three polymers.

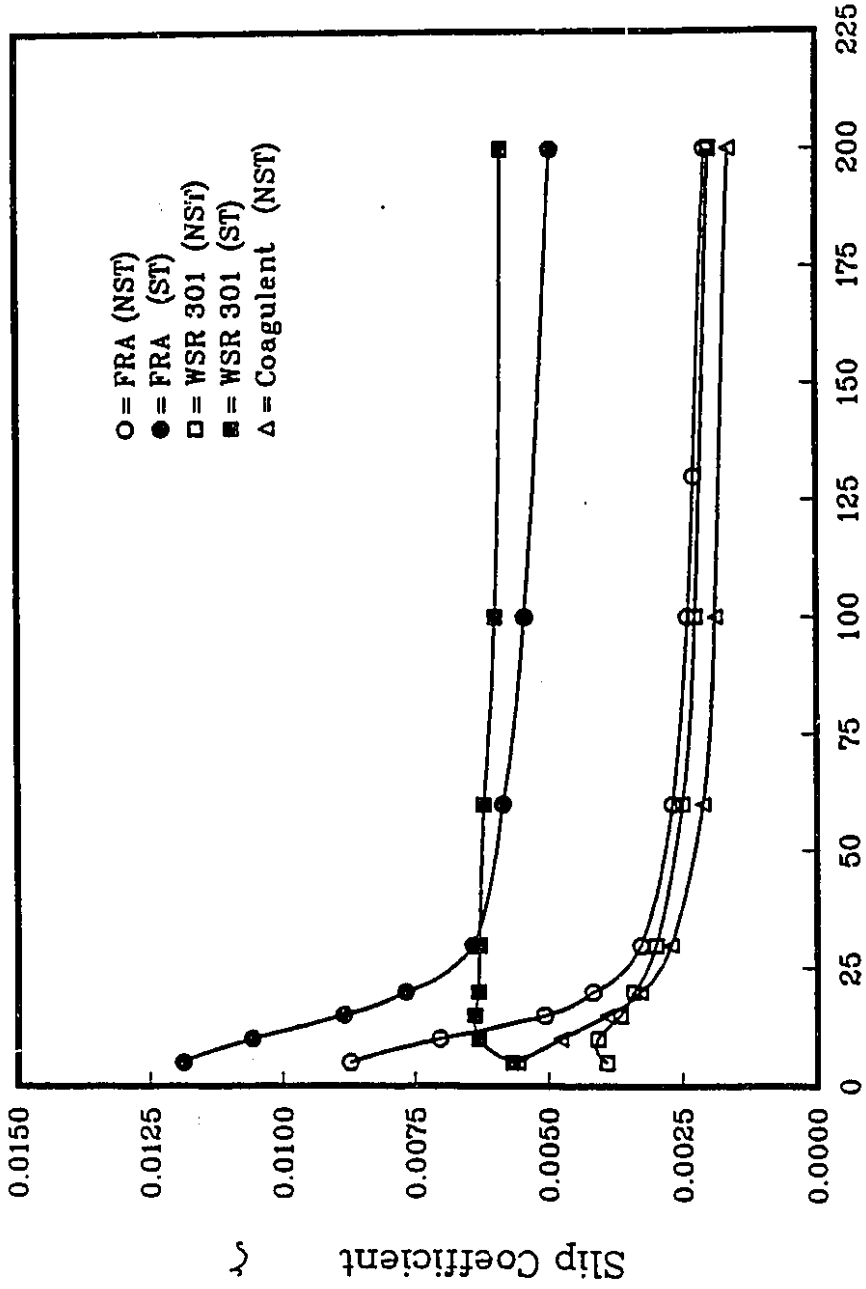

Figure 5.24 Plot of slip coefficient vs. conentration for the POLYOX.

5.5.2 Evaluation of Explicit Effective Velocities at the Wall

In the present study, slip flow is implied when the polymer solution flow is accompanied by a positive u_w or u_{ws}. Similarly, polymer adsorption is associated with a negative u_w or u_{wa}. It is important that the meaning of the various kinds of effective velocities at the wall be understood and the distinction between u_{ws}, u_{wa} and u_w be recognized. It can be recalled in Chapter 3 that u_w is represented as a sum of u_{ws} and u_{wa}. It is also yielded directly by experiment. A positive u_w refers to the experimental result found when the slip phenomenon is dominant in the presence of polymer adsorption whereas u_{ws} is the effective velocity at the wall directly ascribable to the slip phenomenon. A negative u_w is found when polymer adsorption is dominant in the presence of slip while a negative u_{wa} denotes the effective velocity at the wall attributable directly to polymer adsorption. The following expressions for u_{ws} and u_{wa} were derived from the equations in Chapter 3:

$$u_{ws} = k_{s0}(1 - \frac{c}{k+c})(\frac{1}{\mu_s} - \frac{1}{\eta_0}) \tag{5.9}$$

$$u_{wa} = \delta_{ap}(\frac{c}{k+c})\frac{\tau_w}{\eta_0} - b\tau_w^d \tag{5.10}$$

while the evaluation of the parameters was discussed in the previous section. The behavior of the effective velocity at the wall u_w as well as the distinct wall velocities u_{ws} and u_{wa} as a function of polymer concentration are illustrated in figures 5.25 to 5.29. Generally, the maximum slip effect occurs at lower concentrations while polymer adsorption shows an increasing effect with concentration until the plateau is reached. This produces the gradual change observed in the effective velocity at the wall, including a transition from a positive to a negative value with increasing polymer concentration. As the concentration approaches zero the u_w, u_{ws} and u_{wa} vanish, as expected for pure water. A peak in the curve is just discernible in the

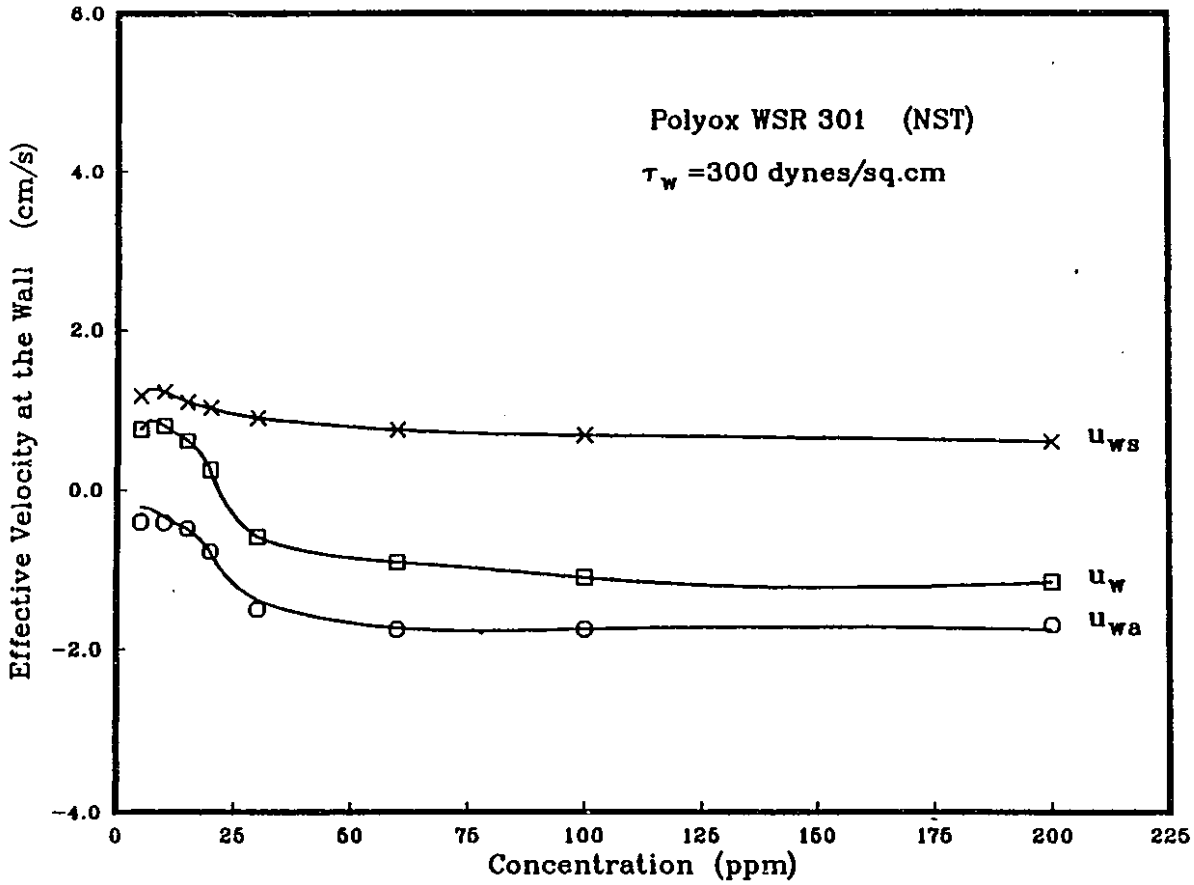

Figure 5.25 Plot of u_w, u_{wa} and u_{ws} vs. concentration for Polyox WSR 301 solutions, at τ_w =300 dynes/sq.cm.

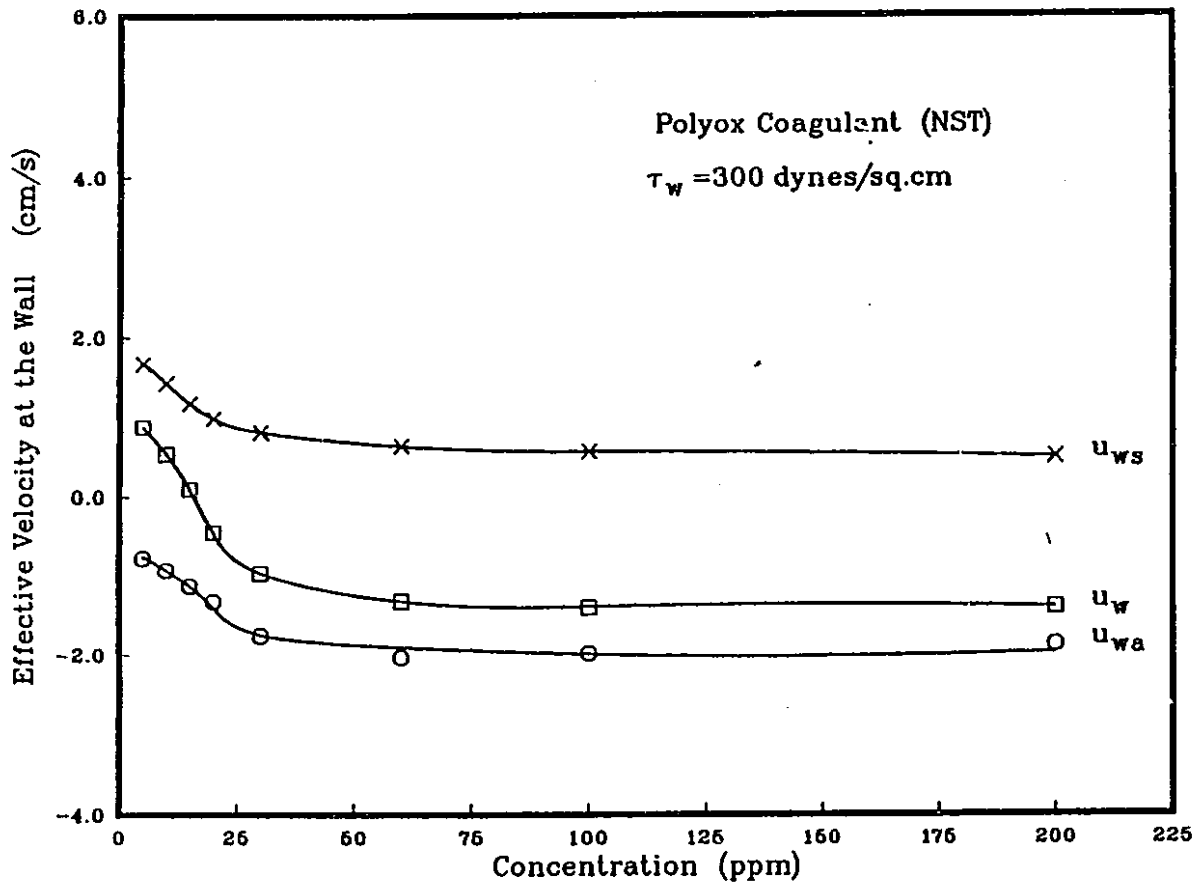

Figure 5.26 Plot of u_w, u_{wa} and u_{ws} vs. concentration for Polyox Coagulant solutions, at τ_w =300 dynes/sq.cm.

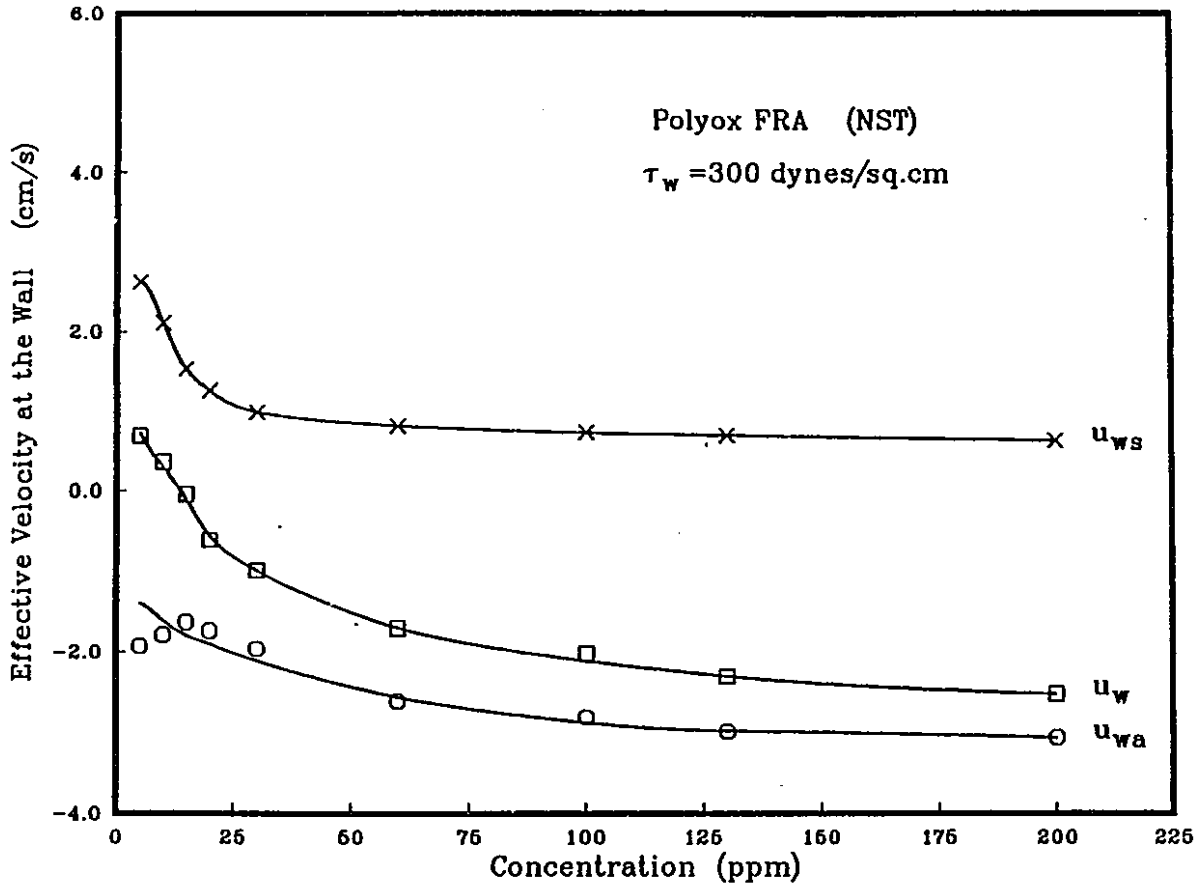

Figure 5.27 Plot of u_w, u_{wa} and u_{ws} vs. concentration for Polyox FRA solutions, at τ_w =300 dynes/sq.cm.

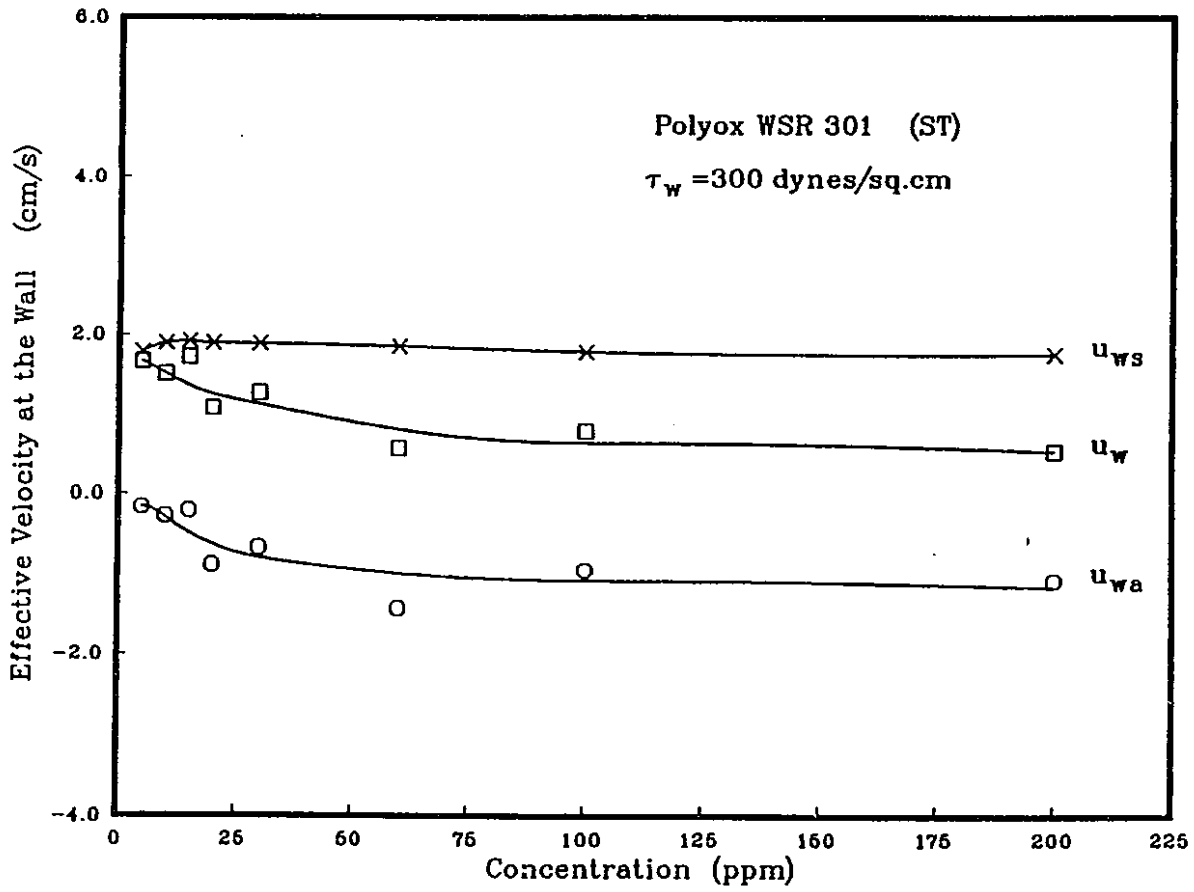

Figure 5.28 Plot of u_w, u_{wa} and u_{ws} vs. concentration for Polyox WSR 301 solutions in treated tubes, at τ_w=300 dynes/sq.cm.

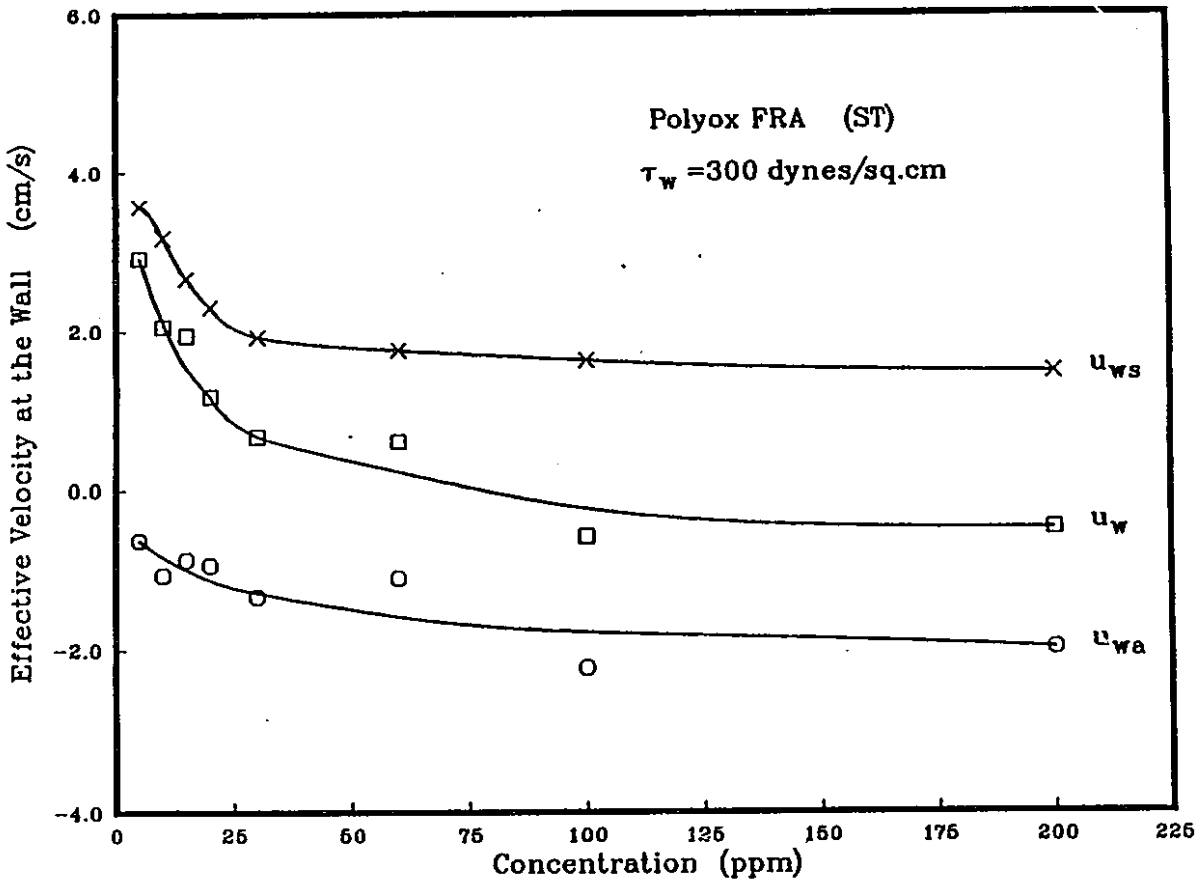

Figure 5.29 Plot of u_w, u_{wa} and u_{ws} vs. concentration for Polyox FRA solutions in treated tubes, at τ_w=300 dynes/sq.cm.

results for the flow of WSR 301 solutions, whereas for the other cases it is not shown since it is supposed to occur at concentration lower than 5 ppm. Over a wide range of higher concentration up to 200 ppm, the u_{ws} and u_{wa} are less dependent on the polymer concentration. In the limit as the concentration approaches infinity, the prediction is that u_{ws} approaches zero and u_w approaches its maximum magnitude u_{wa}.

Although the effective velocity at the wall is sensitive to the polymer concentration at low concentrations, the sensitivity was also dependent upon the molecular weight of the polymer. Greater variation was found for the Polyox FRA having the highest molecular weight, whereas little change with polymer concentration in u_{ws} was exhibited by the WSR 301 having the lowest molecular weight.

5.5.3 Effective Hydrodynamic Thicknesses of Adsorbed Polymer Layers

Evaluations of the effective hydrodynamic thickness of adsorbed polymer layers were carried out using equation (3.18) and/or equation (3.43). Equation (3.43) yields effective thicknesses of the adsorbed polymer layers corrected for slip whereas equation (3.18) gives the thicknesses without slip correction. It should be noted that the evaluations by both equations yield the thicknesses for the actual flow conditions in the presence of the polymer solution. This is in contrast with those provided by the method in which the solvent alone flows past the adsorbed polymer previously deposited in a polymer solution passed through the capillary. The latter method yields a residual adsorbed polymer layer. For this reason and the possibility of interaction between adsorbed macromolecules with those in the flowing solution, the results yielded by the latter method may be expected to differ from the present evaluations.

The effective hydrodynamic thickness of the adsorbed layers evaluated from the explicit effective velocity at the wall u_{wa} including the slip correction is presented in

figures 5.30 through 5.34. The data is represented by the closed points, together with the results based on u_w without the slip correction. The corrected data display the variation with polymer concentration characteristic of adsorption isotherms showing a rapid initial rise of the effective hydrodynamic thickness with increasing concentration and approaching a plateau region, at higher concentrations. The values of δ_a in the plateau region are observed to be up to several times the end to end distance of the polymer molecules consistent with multilayer adsorption (Son, 1978). Furthermore, the effective hydrodynamic thickness of the adsorbed layers increases with an increase in molecular weight of the polymer. Thicker adsorbed layers were obtained with the Polyox FRA solution flows.

It is seen that the coupling of polymer adsorption and slip flow results in an underprediction of the adsorption effect. The difference becomes smaller with increasing polymer concentration due to a reduction in slip at the higher concentration levels. However, the gap was found to be still significant even at the plateau levels in the concentration range examined. Figure 5.35 illustrates the effect of the slip correction on the evaluation of the adsorbed layer thickness δ_a. In the flow of the 200 ppm solutions through the untreated tubes, the correction in the plateau value of the thickness was 35% in the case of the WSR 301 and 16% in the case of the FRA, at the shear stress $\tau_w = 400\ dynes/cm^2$.

It should be noted that the curves corrected for slip in figures 5.30 to 5.34 pass through the origin consistent with expected adsorption isotherm behavior; on the other hand, the uncorrected curves representing the open data points intercept the polymer concentration axis as a result of the slip effect.

The effective hydrodynamic thicknesses of the adsorbed polymer layers increase with increasing wall shear stress over the shear stress range involved. This behavior is in qualitative agreement with the observations of Gramain and Myard (1981a). It has been widely accepted that parts of the adsorbed polymer chains make direct

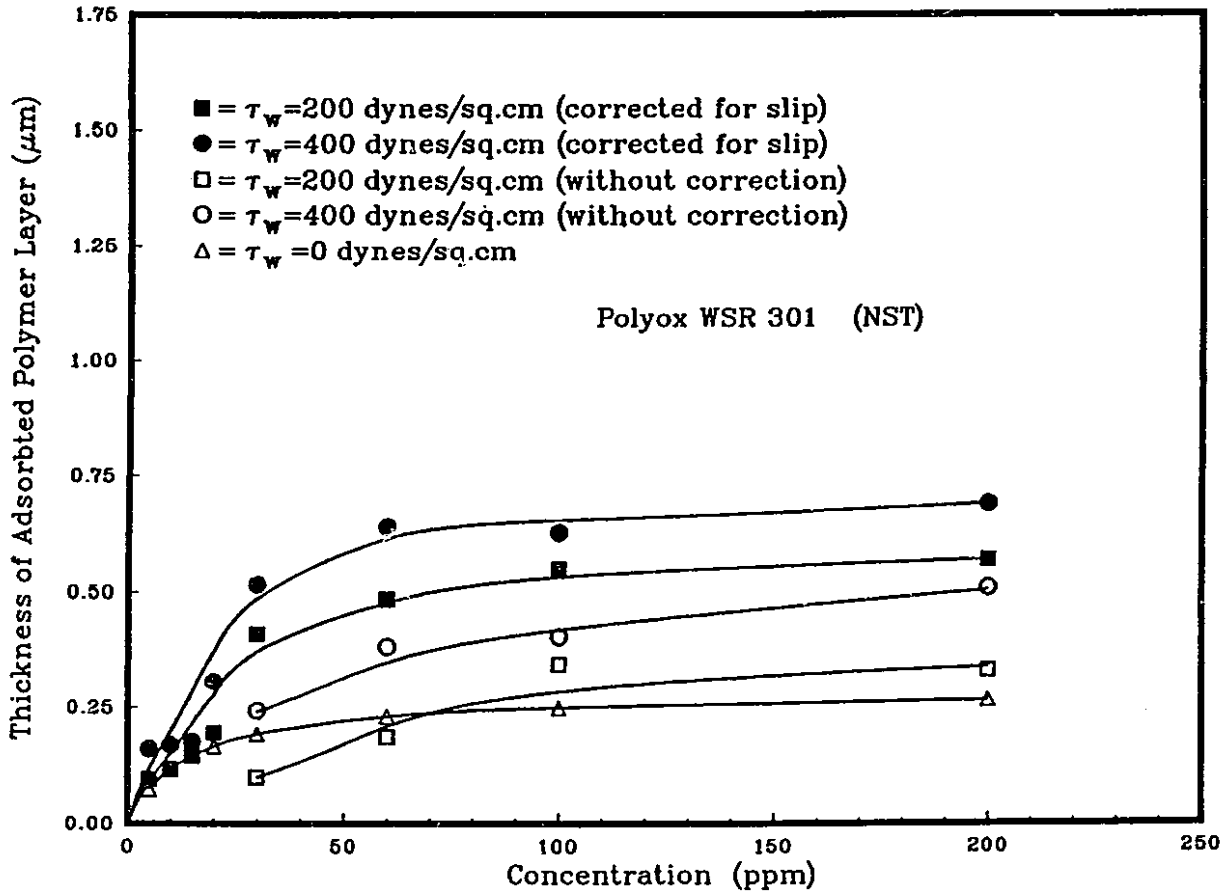

Figure 5.30 Demonstration of adsorption free of slip effect for Polyox WSR 301 solutions.

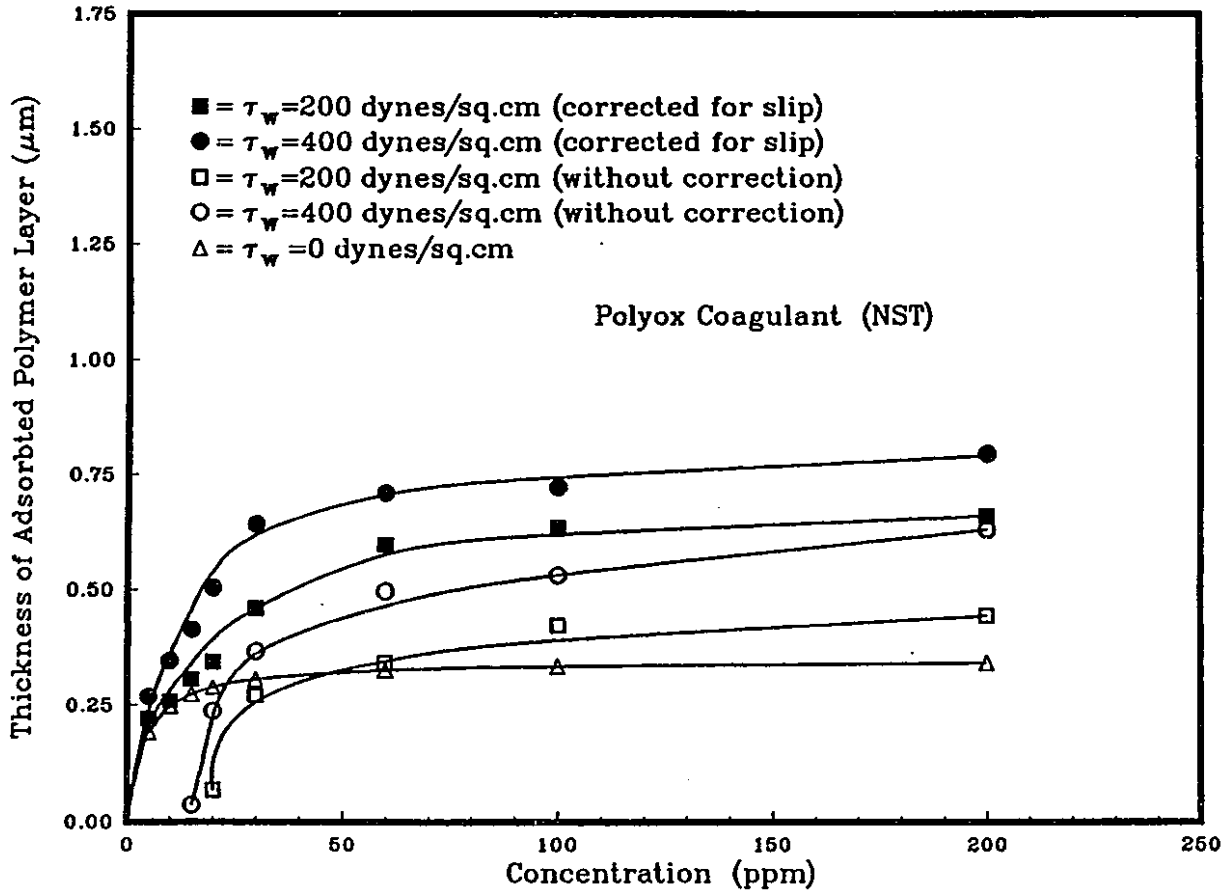

Figure 5.31 Demonstration of adsorption free of slip effect for Polyox Coagulant solutions.

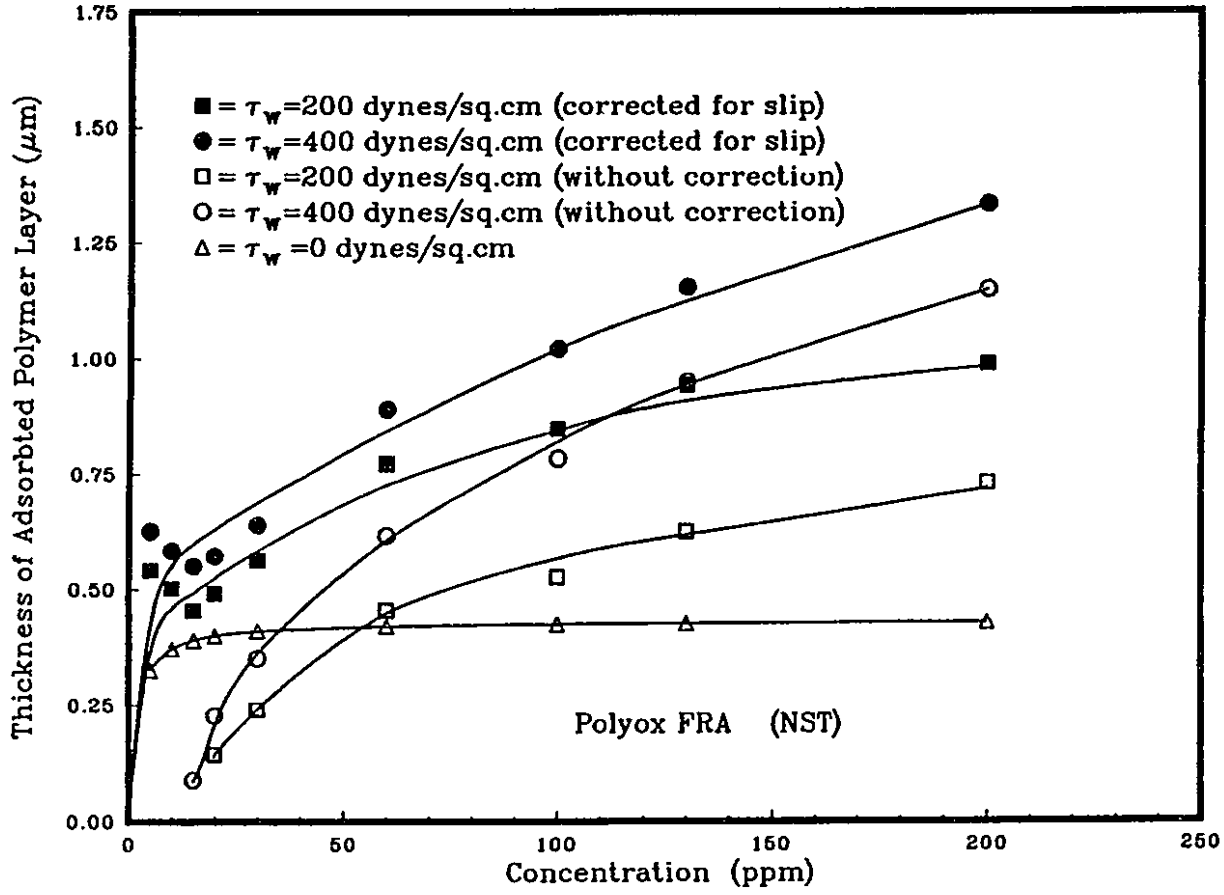

Figure 5.32 Demonstration of adsorption free of slip effect for Polyox FRA solutions.

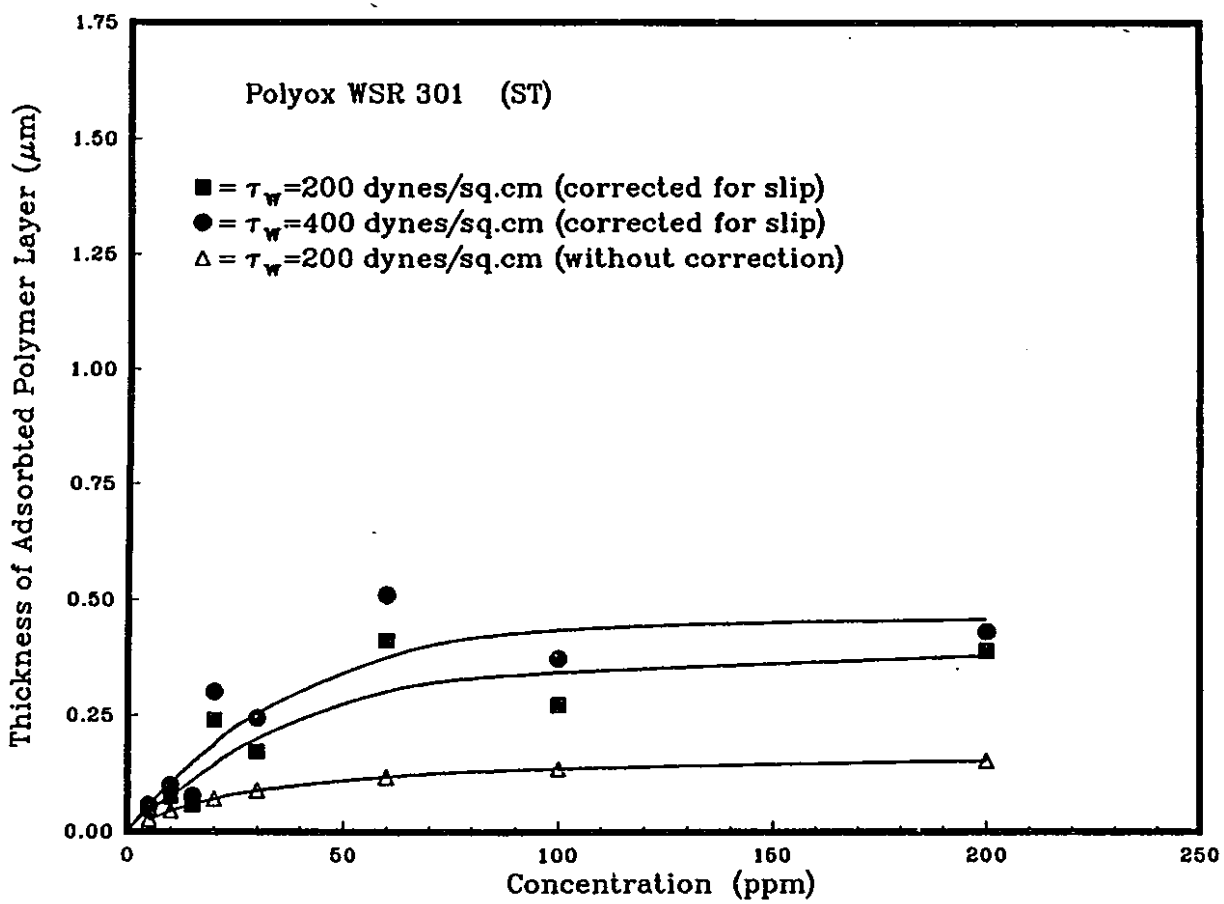

Figure 5.33 Demonstration of adsorption free of slip effect for Polyox WSR 301 solutions in treated tubes.

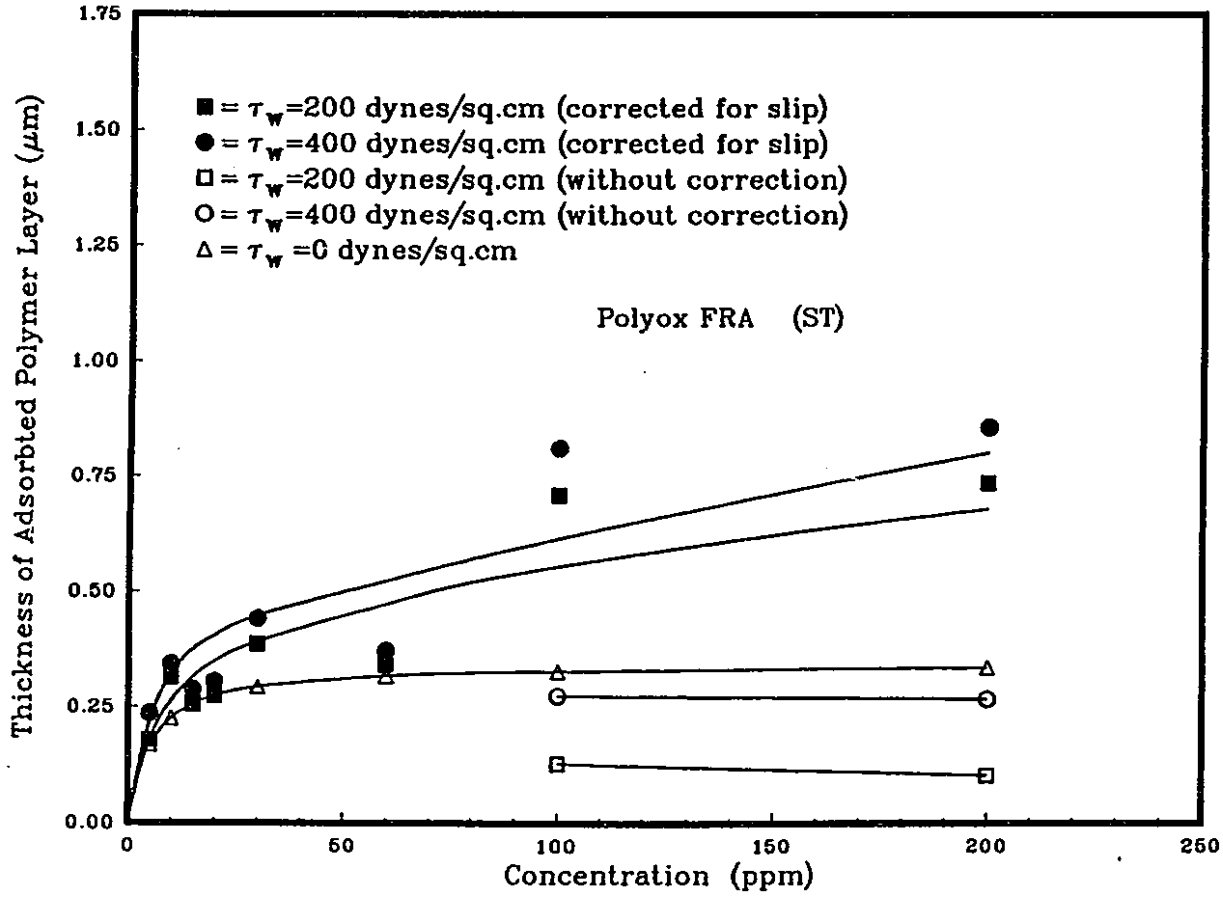

Figure 5.34 Demonstration of adsorption free of slip effect for Polyox FRA solutions in treated tubes.

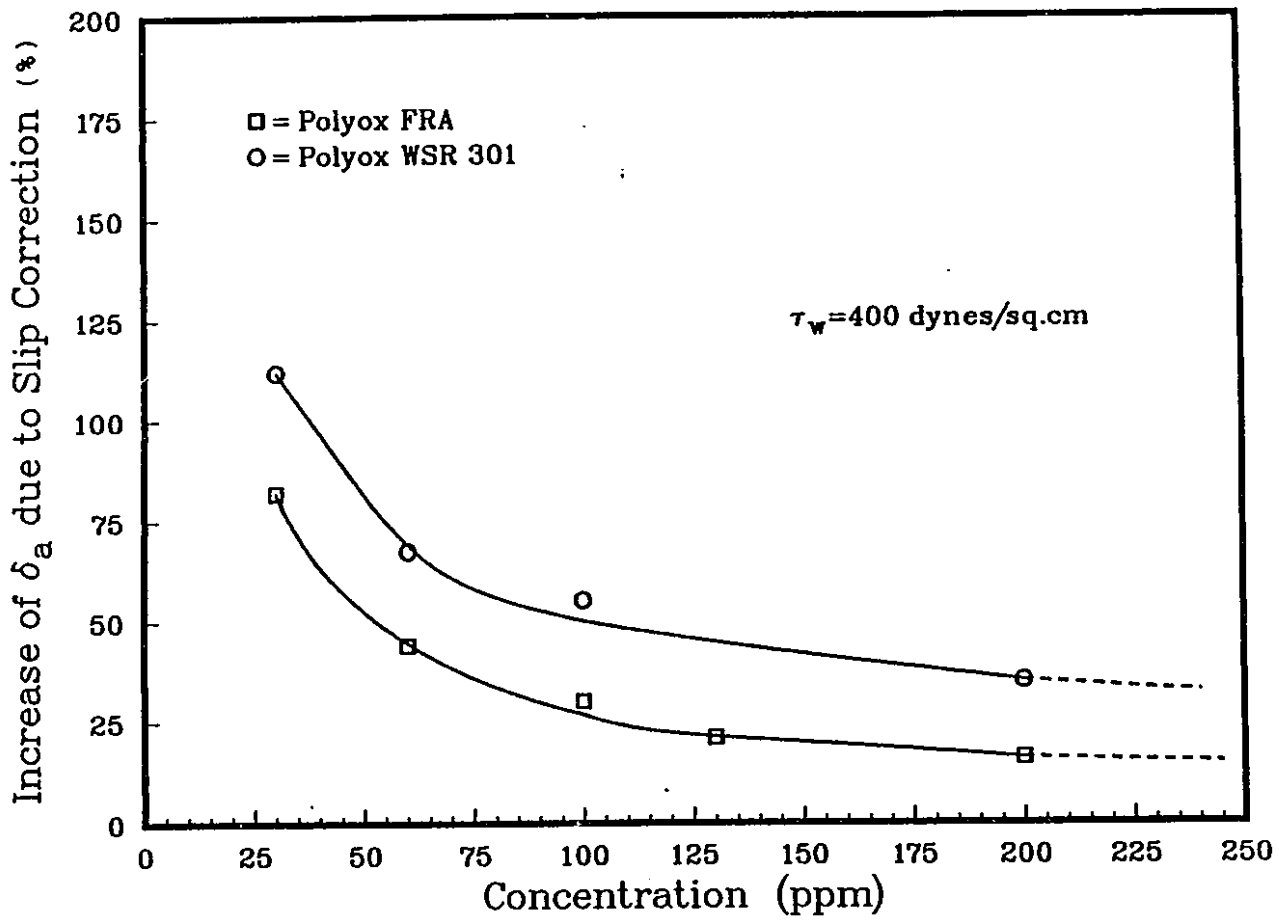

Figure 5.35 Plot of percentage increase of δ_a by correction for slip.

contact with the surface as trains, while other segments extend into the solution as loops and tails leading to a thick adsorbed layer (Hesselink, 1975; Lax, 1974). The tails in particular make a substantial contribution to the thickness of the layer produced by the adsorbed polymer chain (Feigin and Napper, 1979). At the high velocity gradients involved in our experiments, the indication is that the adsorbed layers become substantially extended with the consequence that the friction factor of the larger segments (which contribute most significantly to the flow resistance) may no longer be constant. Therefore, the apparent thickening of the adsorbed layers could be attributed to stretching or swelling of the adsorbed molecules with solvent percolating into the adsorbed layer as the wall shear stress increases.

Also included in figures 5.30 to 5.34 are the predictions of the effective hydrodynamic thickness corresponding to a condition of zero shear stress, represented by the triangles. These were obtained directly from the analysis of the data obtained from the flow experiments. In the analysis of Chapter 3, the adsorption characteristics at zero shear are characterized by the adsorption isotherm: $\delta_{a0}/\delta_{ap} = c/(k+c)$. The plateau values of the thickness in the limit of zero shear, δ_{ap}, were found to be 0.29 μm for Polyox WSR 301, 0.32 μm for Coagulant, and 0.44 μm for FRA solutions in the untreated tubes and 0.19 μm for WSR 301 and 0.38 μm for FRA solution flowing in the silane-treated tubes, respectively. A log-log plot of δ_{ap} as a function of the molecular weight of the Polyox homologue is presented in figure 5.36, for the flow in the untreated tubes. The slope of the linear curve through the points is 0.52. Similar behavior has been documented in the work of Kawaguchi et al. (1984, 1988b) for narrow molecular weight fractions of polyethylene, adsorbed onto cellulose ester millipore filters, at M_w=4×10^4 to 1.2×10^6. They reported an exponent describing the variation in thickness with molecular weight of 0.4 in water (good solvent) and 0.68 in aqueous 0.45 M K_2SO_2 solution (poor solvent) at 35°C, from volumetric flow rate measurements. The slight difference in the exponents may

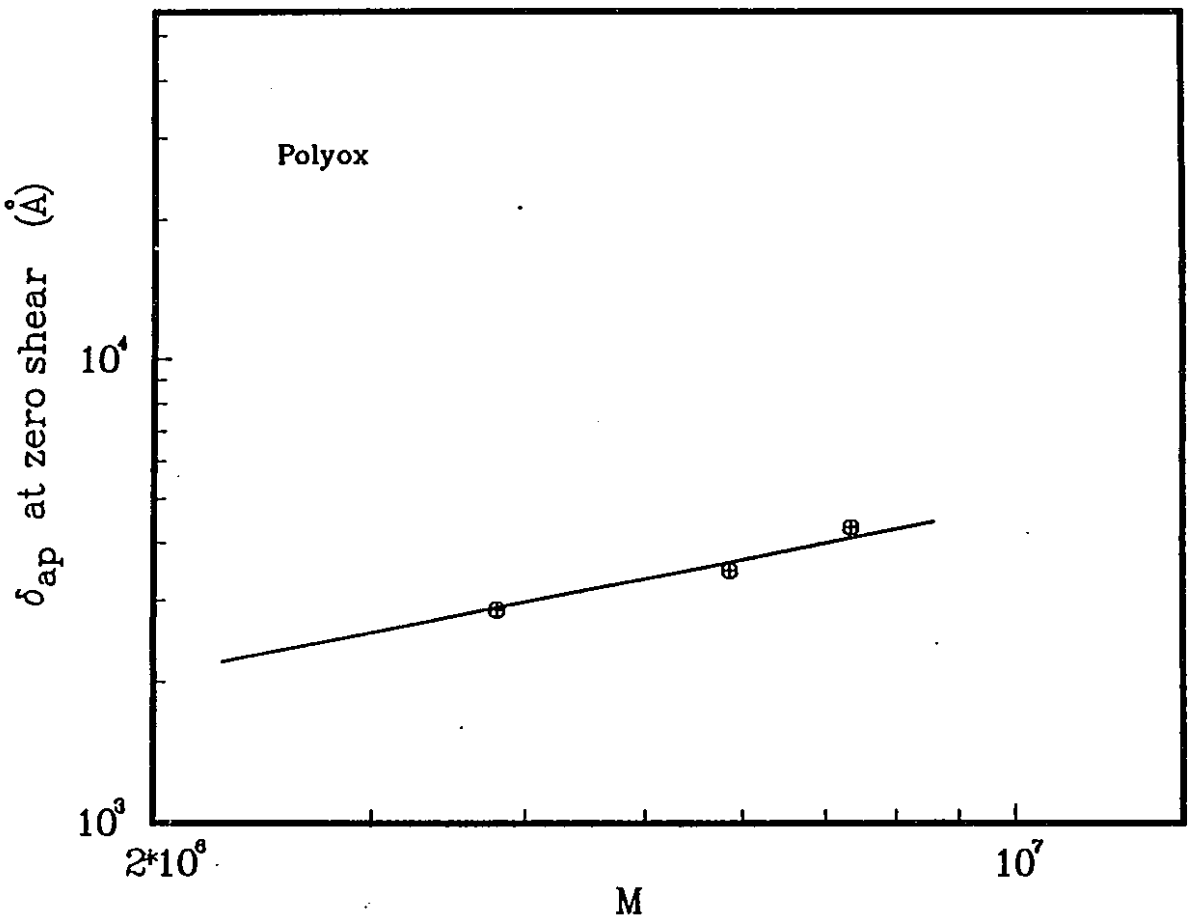

Figure 5.36 Plot of the thickness of the adsorbed Polyox layer on untreated glass vs. molecular weight.

be due to the difference in the surface geometry, the molecular weight distribution and the experimental conditions. The approximate slope of 0.5 in the present work suggests that δ_{ap} varies with the square root of the molecular weight, as seen in figure 5.37. A variation in the adsorbed layer thickness which is proportional to the square root of the molecular weight has been predicted for polymer adsorption by Hoeve (1966), Silberberg (1968) and Scheutjens and Fleer (1979). It has also been confirmed by Smith and Stromberg (1975), Killmann (1976), and Takahashi et al. (1980) using polystyrene with molecular weights up to 13×10^6, by means of the ellipsometry. The agreement with the earlier investigations provides support for the present method for evaluation of the polymer adsorption characteristics in the limit of zero shear stress from capillary flow measurements.

Some comparison between the plateau thickness of the adsorbed layer δ_{ap} at zero shear and the radius of gyration R_g of the free coil in solution is possible. It has generally been accepted in previous studies that in a θ solvent $\delta_{ap} \approx 2R_g$ (Rowland and Eirich, 1966a, 1966b; Varoqui and Dejardin, 1977) while δ_{ap} can be much greater than $2R_g$ for high molecular weight polymers in good solvents (Gramain and Myard, 1981a-b; Cohen Stuart et al., 1984). For polyethylene adsorbed onto polystyrene latex particles, the δ_{ap} obtained from photo correlation spectroscopy (Cosgrove et al., 1984) was less than $2R_g$ for molecular weights of less than about 6.6×10^5 but exceeded the value of $2R_g$ at higher molecular weights. In the present work, the values of $2R_g$ are given by 0.24 μm for WSR 301, 0.31 μm for Coagulant and 0.35 μm for FRA, respectively. This results in plateau thicknesses at zero shear of $2.4R_g$ for WSR 301, $2.06R_g$ for Coagulant and $2.5R_g$ for FRA. Thus, the current results indicate that in the flow through the untreated glass tubes, δ_{ap} is greater than $2R_g$ for the three polymers in the good solvent (water), with molecular weights in the order of 4×10^6 and higher. As expected, lower δ_{ap} values were found for the flows of the same polymer solutions through silane-treated tubes.

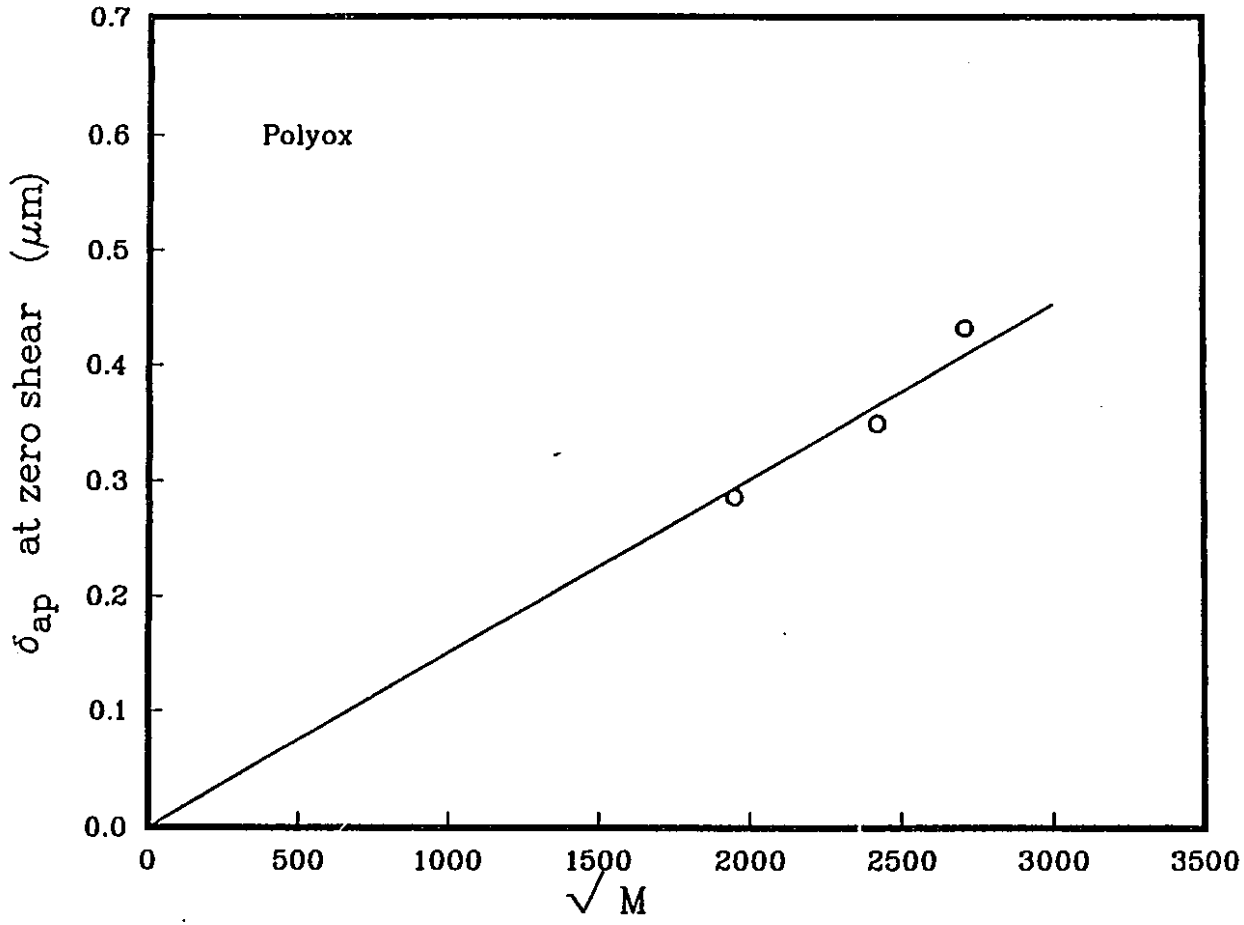

Figure 5.37 Thickness of the adsorbed Polyox layer on untreated surface as a function of the sqaure root of the molecular weight.

5.6 Dependence of Wall Effects on the Surfaces

A comparison of the effect of surface modification by silane treatment on the polymer adsorption characteristics has been presented. The literature (Parnas et al., 1989; Hatzikiriakos and Dealy, 1991) also reports on the dependence of the wall effects upon the material properties of the substrate. In the following we illustrate the effect of the surface modification on the resultant flow curves obtained in the capillary flows. Figures 5.38 and 5.39 compare the flow behavior in the treated tubes labeled ST with that obtained using the clean untreated glass tubes (NST). The apparent shear rate $8\langle u\rangle/D$ at a given shear stress is seen to be higher for the silane treated (ST) tubes. The silane treatment therefore provides an effective means for influencing the flow behavior at the wall.

In terms of the effective velocity at the wall, positive values were obtained with both surfaces (ST and NST) and exhibited the same trend with polymer concentration. The influence of the solid surface however was reflected in the magnitude of u_w, with a higher u_w obtained in the case of the treated tubes, due to the higher slip velocity manifested by the treated surface. For the Polyox FRA solutions with solute concentrations greater than 60 ppm, negative effective velocities at the wall were observed with silane-treated tubes, as well as with the untreated tubes. However, the magnitude of the negative u_w was much smaller in the case of the treated tubes. Table 5.3 compares the u_w determined for the two surfaces using aqueous Polyox WSR 301 and Polyox FRA. The negative u_w for Polyox FRA at 100 ppm to 200 ppm was confirmed by repeating the measurements with the tubes subjected to the silane treatment. The results indicate that although surface treatment minimized polymer adsorption, it did not always eliminate the effect at the higher concentrations. In spite of the strong adsorption in the untreated glass tubes, slip flow still dominated in the low concentration range. The critical concentration marking the

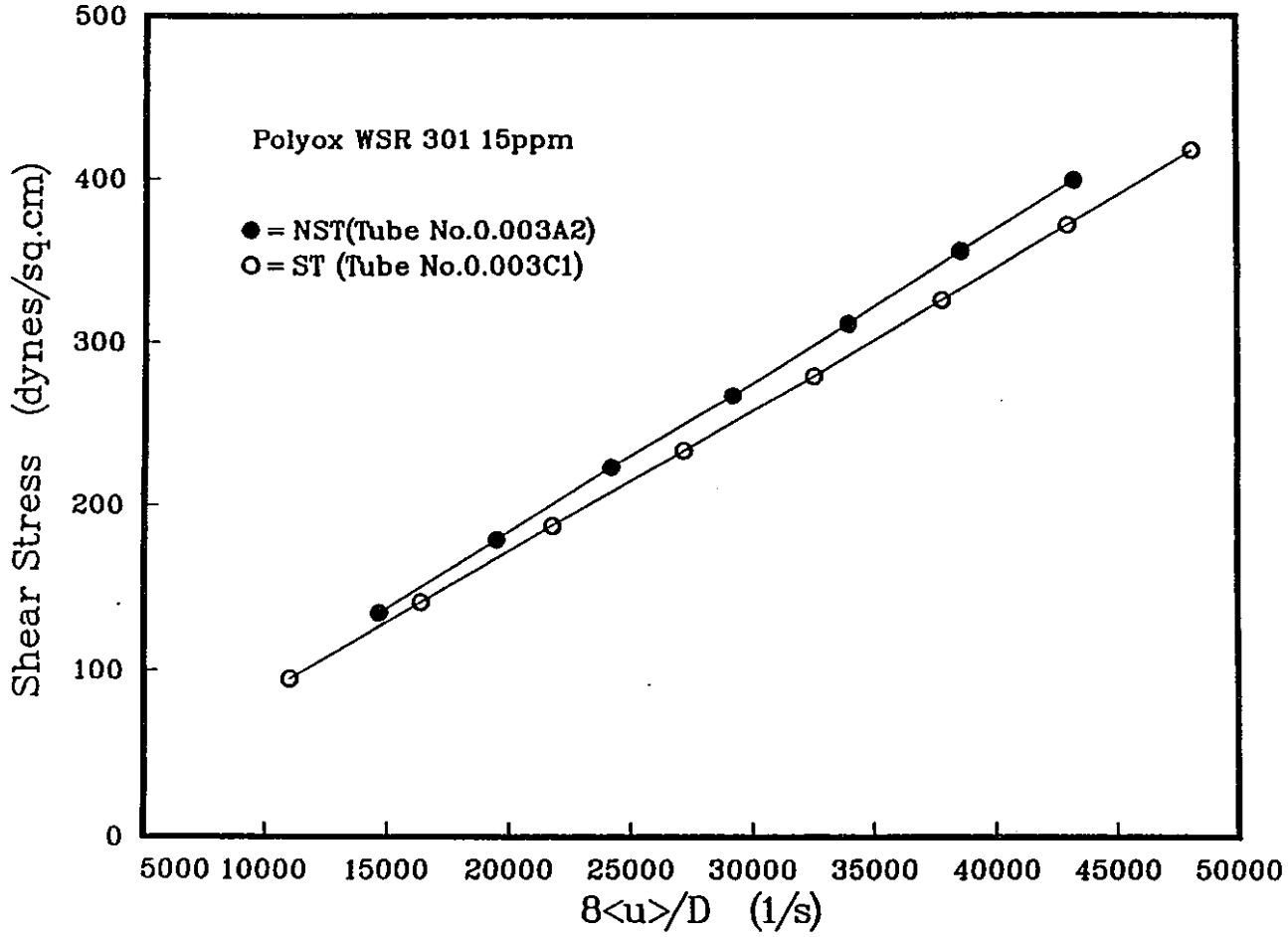

Figure 5.38 Flow curves for 15ppm aqueous Polyox WSR 301 in silane treated and untreated tubes.

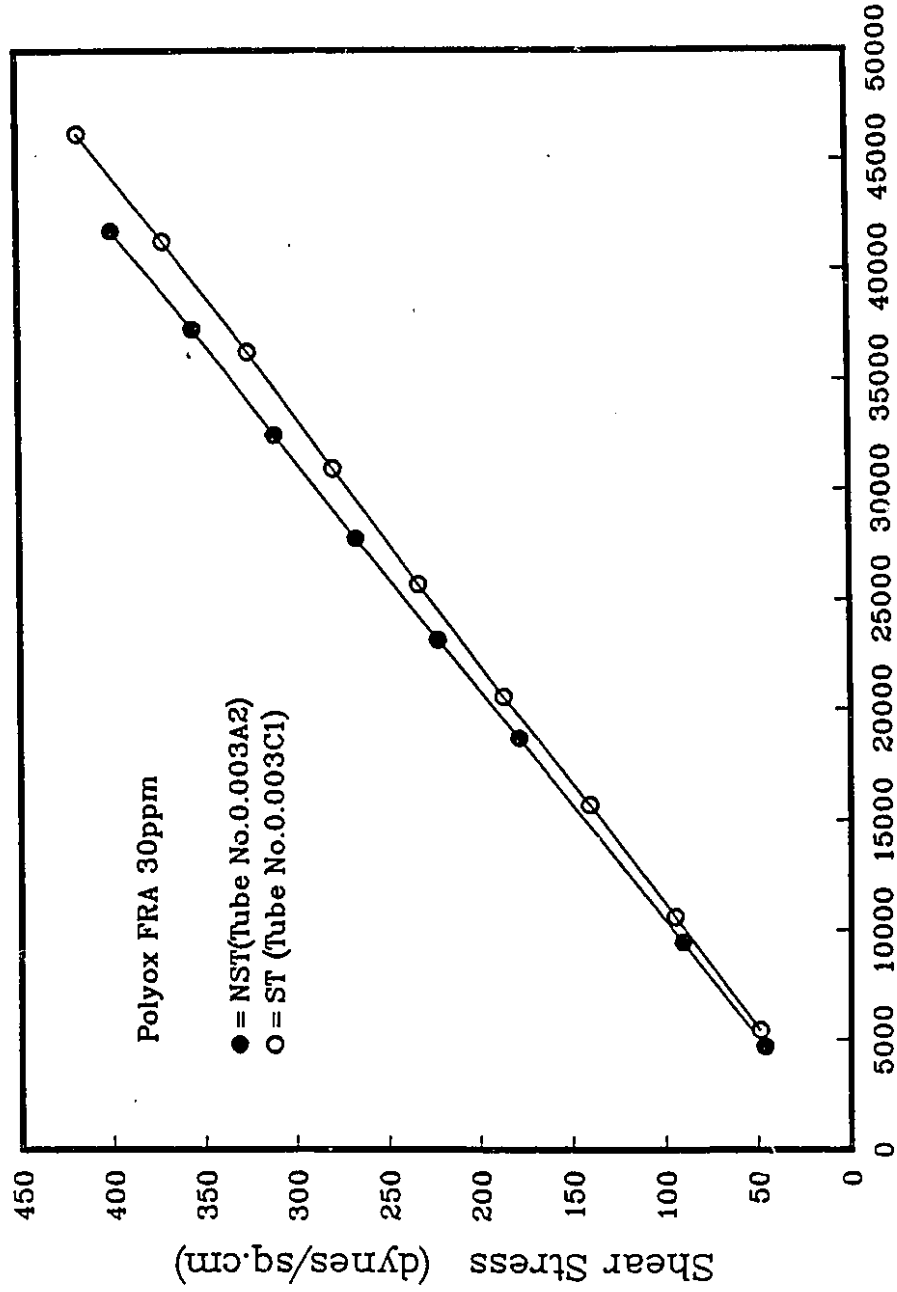

Figure 5.39 Flow curves for 30ppm aqueous Polyox FRA in silane treated and untreated tubes.

Table 5.3: Comparison of Effective Velocities at the Wall for Treated and Untreated Surfaces

Polyox	Concentration	τ_w (dynes/cm^2	u_w (cm/s)	
			(ST)	(NST)
WSR 301	5 ppm	200	1.12	0.47
		300	1.66	0.76
		400	2.20	0.98
	10 ppm	200	1.03	0.56
		300	1.50	0.80
		400	1.95	0.89
	15 ppm	200	1.15	0.41
		300	1.71	0.61
		400	2.24	0.69
	20 ppm	200	0.82	0.27
		300	1.07	0.25
		400	1.28	0.034
FRA	5 ppm	200	1.99	0.56
		300	2.92	0.67
		400	3.72	0.72
	10 ppm	200	1.41	0.36
		300	2.06	0.35
		400	2.68	0.27
	15 ppm	200	1.32	0.16
FRA	100 ppm	200	-0.25	-1.03
		300	-0.60	-2.02
		400	-1.02	-3.15
	200 ppm	200	-0.17	-1.23
		300	-0.49	-2.52
		400	-0.89	-4.16

NST and ST designate the glass tubes without and with surface treatment using dimethyldiethoxysilane.

transition from positive to negative u_w was greater for the silane treated tubes.

A comparison of u_{ws} and u_{wa} evaluated for the two cases confirms that the surface treatment resulted in an increased effective velocity of slip and a reduced negative effective velocity at the wall due to polymer adsorption. The data indicates an increase in u_{ws} up to 100% in the plateau region for both polymers used. The percentage increase goes up with increasing polymer concentration; however, it remains almost constant with varying wall shear stress. The magnitude of u_{wa} for the treated tubes was 35% and 37% lower for the FRA and WSR 301 solutions than those obtained in the untreated tubes at the concentration of 200 ppm. This resulted in the same percentage reduction in the effective hydrodynamic thickness of the adsorbed polymer layers. It appears that the percentage reduction is independent of the molecular weight.

Parnas et al. (1989) on the basis of static adsorption experiments have reported that the adsorption of polyvinylpyrrolidone could be either increased or decreased by chemical modification of the silica substrate employed in the experiments. The present results based on hydrodynamic adsorption experiments confirm the dependence of polymer adsorption on surface chemistry. The adsorption of Polyox of high molecular weight was greatly reduced by the silane treatment of the glass tubes. The results were also extended to the adsorption of Polyox at zero shear from the hydrodynamic data.

5.7 Internal Consistency

A comparison of the final flow curves for the same polymer solutions flowing in the untreated and treated glass tubes, after correction for the effective velocities at the wall, is seen in figures 5.40 to 5.41. Since the wall effect has been subtracted out in each case, the curves should match to within the experimental uncertainty, which is confirmed by the final curves.

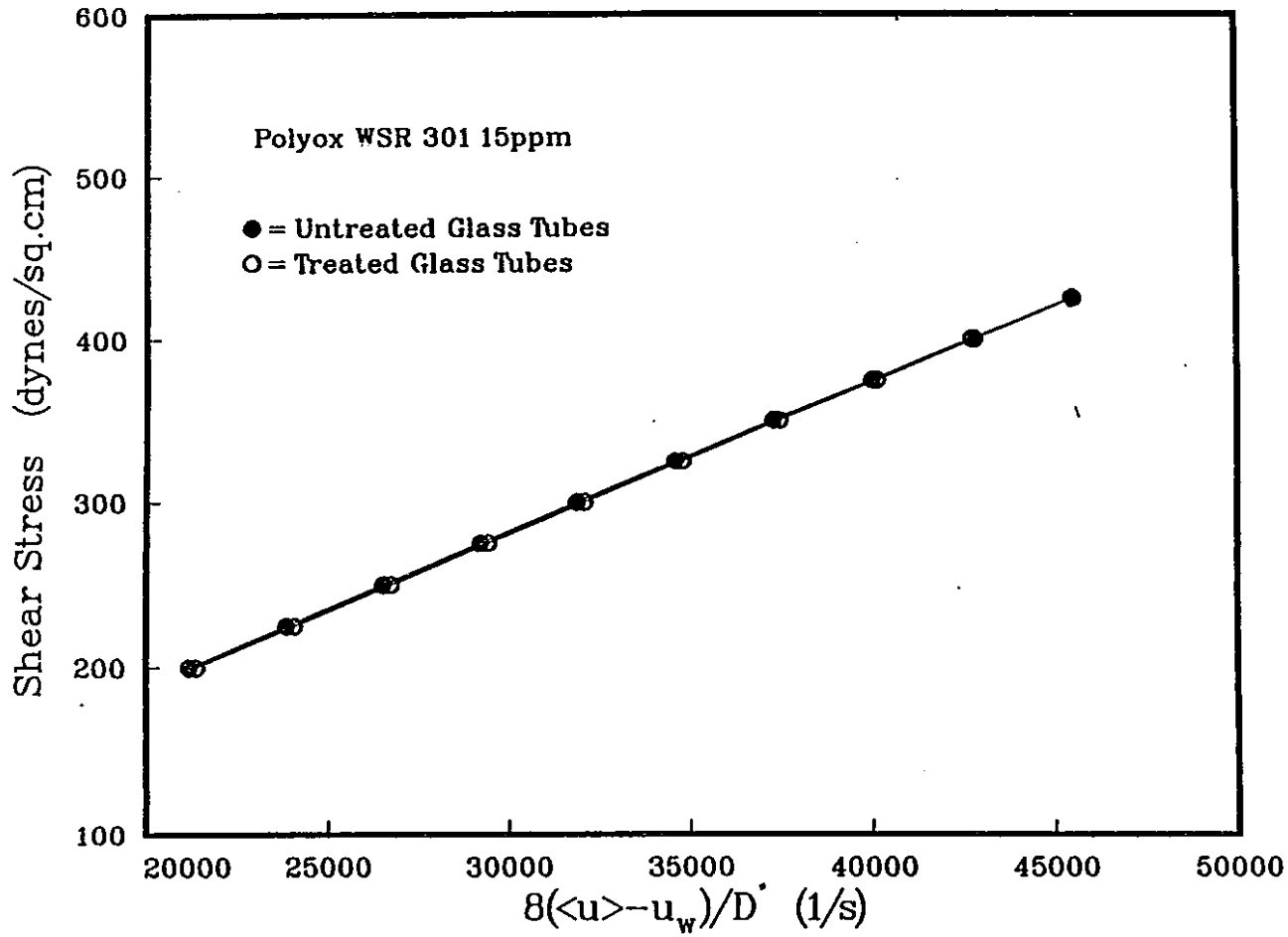

Figure 5.40 Flow curves corrected for wall effects, for 15ppm WSR 301 in treated and untreated tubes.

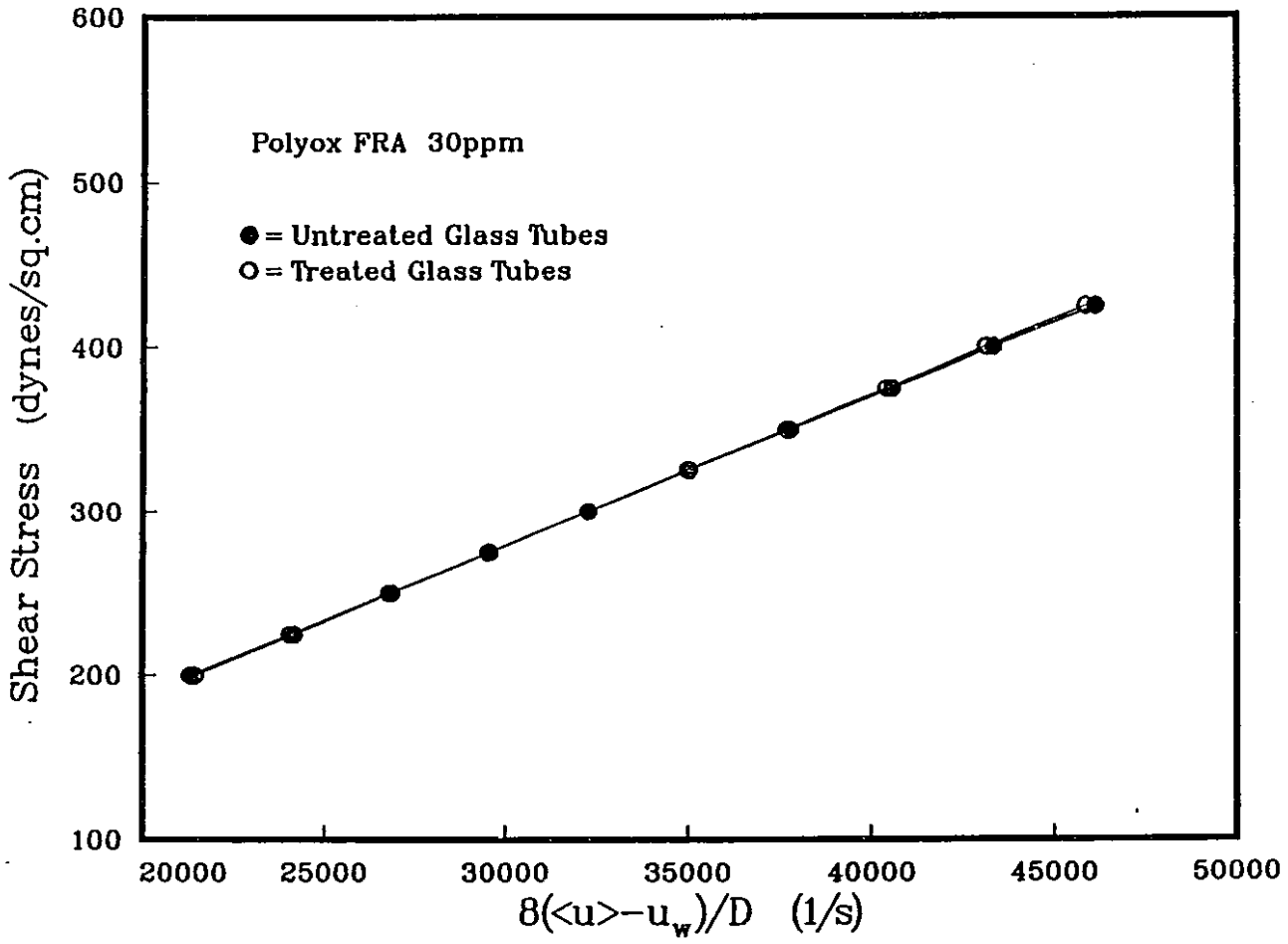

Figure 5.41 Flow curves corrected for wall effects for 30ppm Polyox FRA in treated and untreated tubes.

Chapter 6

Conclusions and Recommendations

Evaluations of the parameters associated with surface phenomena which accompany capillary flows of high molecular weight aqueous polymer solutions have been carried out. The experimental study was devoted to flows of very dilute solutions (5-200 ppm of polymers) in capillary tubes of varying diameter (0.0054-0.0465 cm) at varying shear stresses up to 500 dynes/cm^2. The results agree with trends of related work reported in the literature and provide some additional findings which may lead to an improved understanding and interpretation of surface phenomena encountered in capillary flow of dilute polymer solutions.

In the present work, a transition from a positive effective velocity at the wall at very dilute polymer concentration to a negative effective velocity at the wall was observed with an increase in polymer concentration. This was interpreted as a transition from a slip dominated mechanism at the wall to one dominated by polymer adsorption, at higher polymer concentrations. It is of interest that the critical concentration marking the transition falls in the range yielding the maximum drag reduction in turbulent flow of the same polymer solutions (Hanna, 1977). The critical concentration was found to be higher for the silane-treated tubes due to more pronounced slip flow.

In general, the magnitude of the effective velocity at the wall characterizing the wall effect was found to increase with an increase in the wall shear stress over the shear stress range studied. The correlation was well described by the relation $u_w = A\tau_w - b\tau_w^d$ which was utilized in evaluation of the separate contributions of u_{wa} and u_{ws} to the effective velocity u_w at the wall. The ratio of u_w to the total flow rate decreases as the tube diameter is increased. The contribution of the wall effects to the flow was greater for the tubes of smaller diameter.

A method for utilization of capillary flow measurements for determination of the adsorption characteristics in the limit of zero shear was used in the present work. It allows for the direct evaluation of the zero-shear-viscosity of a non-Newtonian fluid as well as the thickness of the adsorbed polymer layer at zero shear, δ_{a0}, based on a Langmuir type adsorption isotherm. The predictions of the δ_{ap} plateau values were found to be marginally greater than twice the root-mean-square radius of gyration of the polymer molecule, $2R_g$, for the three polymers with the untreated tubes while lower values were found with the silane-treated tubes. A log-log plot of δ_{ap} versus the molecular weight of the polymers yielded a slope of 0.52, on the basis of the flow measurements. This leads to an approximately linear relationship between δ_{ap} and the square root of the polymer molecular weight.

Silane treatment of the glass surface resulted in a reduction of the level of polymer adsorption onto the surface and an enhancement of slip flow characterized by an effective slip velocity.

An analysis has been presented which allows for evaluation of hydrodynamic adsorption in the presence of slip. A correction for slip was applied in evaluation of the effective hydrodynamic thickness of the polymer adsorbed onto the capillary walls. The relevant slip information, viz. slip coefficient and effective slip velocity, was also yielded simultaneously. Computer programs were developed for evaluation of the parameters associated with polymer adsorption in the presence of slip. The

success of the analysis in describing the experimental adsorption and slip data provides further support for the simultaneous occurrence of polymer adsorption and slip in capillary flow.

Sufficiently far removed from zero concentration, with an increase in polymer concentration, the magnitude of u_{wa} attributed to polymer adsorption increases while u_{ws} due to pure slip flow generally decreases. Superposition of the two effects accounts for the transition of the effective velocity at the wall u_w from a positive to a negative value, with increasing polymer concentration.

A thickening of the adsorbed polymer layer with an increase in wall shear stress was observed for the three polymers studied in the concentration range involved. The effective hydrodynamic thickness was also increased with polymer bulk concentration, showing a steep rise of δ_a at low concentration and levelling off to a plateau value at higher concentrations, which is characteristic of adsorption isotherm behavior. The zero thickness intercept with the polymer concentration was shifted from zero to 15-20 ppm when the slip correction was not included in the thickness evaluation. The adsorbed polymer layer thickness increased with the molecular weight of the polymer.

A modification of Bagley's method for determination of excess pressure losses in entry and exit flows was employed in this work. The end effect corrections for excess pressure losses were greater for the flows at the higher polymer concentration solutions, in larger diameter tubes and at higher shear rates (up to 10% of the pressure drop in the tube, in some cases).

The following recommendations are based on the results of this investigation:

It would be of interest to extend the present work involving polymer adsorption in polymer solution flows to other polymer systems at a series of concentrations including dilute and concentrated solutions.

It is suggested that more data should be collected for a series of very dilute solutions of polymers in flows through very fine tubes, the study being focused on the transition region.

A study of the effect on polymer adsorption and slip flow of polymer solution flows in capillary tubes subjected to different surface treatments, using silane compounds with different functional groups is proposed for future work. It will be practically useful to determine whether a silane compound that completely eliminates polymer adsorption on the treated surface can be found. The effect of silane treatment on the adsorption properties of different substrates should also be examined.

Consideration should be given to extending the experimental technique and analysis used in the present work to studies of polymer adsorption and slip in porous medium flows.

References

1. Arkles, B., Chemtech., **7**, 766-777 (1977).
2. Arunachalam, VR. and G.D. Fulford, Chem. Eng. Sci., **26**, 1065-1073 (1971).
3. Astarita, G., Ind. Eng. Chem. Fundls., 4, 354-356 (1965).
4. Aubert, J.H. and M. Tirrell, J. Chem. Phys., **77**, 553-561 (1982).
5. Ausserre, D., H. Hervet and F. Rondelez, Phys. Rev. Lett., **54** , 1948-1951 (1985).
6. Ausserre, D., H. Hervet and F. Rondelez, Macromolecules, **19**, 85-88 (1986).
7. Ausserre, D., J. Edwards, J. Lecourtier, H. Hervet and F. Rondelez, Europhys. Lett., **14**, 33-38 (1991).
8. Bagassi, M., G. Chauveteau, J. Lecourtier, J. Englert and M. Tirrell, Macromolecules, **22**, 262-266 (1989).
9. Bagley, E.B., J. Appl. Phys., **28**, 624-627 (1957).
10. Barham, P.J., R.A.M. Hikmet, K.A. Narh and A. Keller, Colloid Polymer Sci., **264**, 515-521 (1986).
11. Besio, G.J., R.K. Prud'homme and J.B. Benziger, Macromolecules, **21**, 1070-1074 (1988).
12. Bird, R.B., W.E. Steward and E. Lightfoot, "Transport Phenomena", J. Wiley and Sons, New York (1960).
13. Bird, R.B., R.C. Armstrong and O. Hassager, "Dynamics of Polymeric Liquids", Vol.1, J. Wiley and Sons, New York (1977).
14. Boger, D.V. and R. Binnington, Trans. Soc. Rheol., **21**, 515-534 (1977).

15. Boger, D.V., R. Gupta and R.I. Tanner, J. Non-Newt. Fluid Mech., 4, 239-248 (1978).

16. Brunn, P.O., Rheol. Acta., **15**, 23-29 (1976).

17. Brunn, P.O., J. Rheol., **29**, 859-886 (1985a).

18. Brunn, P.O. and S. Grisafi, Chem Eng. Commun., **36**, 367-383 (1985b).

19. Bryson, A.W., V. Arunachalam and G.D. Fulford, J. Fluid Mech., **47**, 209-230 (1971).

20. Carreau, P.J., Q.H. Bui and P. Leroux, Rheol. Acta, **18**, 600-608 (1979).

21. Chan, F.S. and A.A. Robertson, J. Colloid Interface Sci., **33**, 598-602 (1970).

22. Chang, S.H. and I. J. Chung, Macromolecules, **24**, 567-571 (1991).

23. Chauvteau, G., J. Rheol., **26**, 111-142 (1982).

24. Chauveteau, G., M. Moan and A. Magueur, J. Non-Newt. Fluid Mech., **16**, 315-327 (1984).

25. Chauveteau, G., M. Tirrell and A. Omari, J. Colloid Interface Sci., **100**, 41-45 (1984).

26. Chin, Susana and D.A. Hoagland, Macromolecules, **24**, 1876-1882 (1991).

27. Choplin, L. and P.J. Carreau, J. Non-Newt. Fluid Mech., **9**, 119-146 (1981).

28. Cohen, Y., " The Behavior of Polymer Solutions in Non-Uniform Flows", Ph.D Thesis, Univ. of Delaware (1981).

29. Cohen, Y. and A.B. Metzner, Macromolecules, **15**, 1425-1429 (1982a).

30. Cohen, Y. and A.B. Metzner, AIChE Symp., Series **78**, 77-85 (1982b).

31. Cohen Stuart, M.A., F.H.W.H. Waajen, T. Cosgrove, B. Vincent and T.L. Crowley, Macromolecules, **7**, 1825-1830 (1984).

32. Cohen, Y. and A.B. Metzner, J. Rheol., **29**, 67-102 (1985).

33. Cohen, Y. and F.R. Christ, SPE Reservoir Eng., **1**, 113-118 (1986a).

34. Cohen, Y. and A.B. Metzner, Rheol. Acta, **25**, 28-35 (1986b).

35. Cohen, Y., Macromolecules, **21**, 494-499 (1988).

36. Cosgrove, T., T.L. Crowley and M.A.S. Cohen, in "Polymer Adsorption and Dispersion Stability", Goddard, E.D and B. Vincent, Eds., ACS Symposium Serie, ACS (1984).

37. Cosgrove, T. and B. Vincent, "Fluid Interfacial Phenomena", Wiley, New York (1986).

38. Cosgrove, T., N. Finch, B. Vincent and J. Webster, Adv. Colloid Interface Sci., **31**, 33-35 (1988).

39. Denn, M.M., "Process Fluid Mechanics", Prentice-Hall, Inc., Englewood Cliffs, New Jersey (1980).

40. Desremaux, L., G. Chauveteau and M. Martin, Rev. Inst. Franc. Petrole., **26**, 495-520 (1971).

41. De Vargas, L. and O. Manero, Polymer Eng. Sci., **29**, 1232-1236 (1989).

42. Dimarzio, E.A. and R.J. Rubin, J. Polymer Sci., Polym. Phys. Ed., **16**, 457-466 (1978).

43. Dodge, D.W. and A.B. Metzner, AIChE J., **5**, 189-204 (1959).

44. Dutta, A. and R.A. Mashelkar, Rheol. Acta, **21**, 52-61 (1982).

45. Dutta, A. and R.A. Mashelkar, J. Non-Newt. Fluid Mech., **16**, 279-302 (1984).

46. Duering, E. and Y. Rabin, Macromolecules, **23**, 2232-2237 (1990).

47. Feigin, R.I. and D.H. Napper, J. Colloid Interface Sci., **71**, 117-129 (1979).

48. Flory, P.J. and T.G. Jr. Fox, J. Am. Chem. Soc., **73**, 1904-1910 (1951).

49. Flory, P.J., "Principles of Polymer Chemistry", Cornell Univ. Press, Ithaca, N.Y. (1953).

50. Gargallo, L. and E. Cid, Colloid Polym. Sci., **255**, 556-559 (1977)

51. Gramain, Ph. and Ph. Myard, Macromolecules, **14**, 180-184 (1981a).

52. Gramain, Ph. and Ph. Myard, J. Colloid Interface Sci., **84**, 114-126 (1981b).

53. Grisafi, S. and P.O. Brunn, J. Rheol., **33**, 47-67 (1989).

54. Han, C.D., M. Charles and W. Philippoff, Trans. Soc. Rheol., **13**, 455-466 (1969).

55. Han, C.D., M. Charles and W. Philippoff, Trans. Soc. Rheol., **14**, 393-408 (1970).

56. Han, C.D. and M. Charles, Trans. Soc. Rheol., **15**, 371-384 (1971).

57. Hanna, M.R., "Flow of Active Additives through Packed Beds", Ph.D Thesis, Univ. of Ottawa, Canada (1977).

58. Hatano, A., Polymer, **25**, 1198-1202 (1984).

59. Hatzikiriakos, S.G and J.M. Dealy, J. Rheol., **35**, 497-523 (1991).

60. Hesselink, F.T., J Colloid Interface Sci., **50**, 606-608 (1975).

61. Hoeve, C.A.J., J. Chem. Phys., **44**, 1505-1509 (1966).

62. Hoyt, J. W. and A.G. Fabula, 5th Symp. on Naval Hydrodynamics, Bergen, Norway (1964).

63. Huggins, M.L., J. Am. Chem. Soc., **64**, 2716-2718 (1942).

64. Huque, M.M., M. Fishman and D.A.I. Goring, J. Phys. Chem., **63**, 766-768 (1959).

65. Idol, W.K. and J.L. Anderson, J. Membrane Sci., **28**, 269-286 (1986).

66. Iler, R.K., "The Chemistry of Silica", Wiley, New York (1979).

67. James, D.F. and D.R. Mclaren, J. Fluid Mech., **70**, 733-752 (1975).

68. James, D.F. and J.H. Saringer, J. Non-Newt. Fluid Mech., **11**, 317-339 (1982).

69. Kalashnikov, V.N. and S.A. Vlasov, Rheol. Acta, **17**, 296-302 (1978).

70. Kawaguchi, M., M. Mikura and A. Takahashi, Macromolecules, **17**, 2063-2065 (1984).

71. Kawaguchi, M., K. hayashi and A. Takahashi, Macromolecules, **21**, 1016-1020 (1988a).

72. Kawaguchi, M., C. Suzuki and A. Takahashi, J. Colloid Interface Sci., **121**, 585-589 (1988b).

73. Kawaguchi, M. and T. Arai, Macromolecules, **24**, 889-892 (1991).

74. Killmann, E., Croat. Chem. Acta, **48**, 463-468 (1976).

75. Kim, M.W., D.G. Peiffer, W. Chen, H. Hsiung, T. Rasing and Y.R. Shen, Macromolecules, **22**, 2682-2686 (1989).

76. Kozicki, W. and C. Tiu, Chem. Eng. Sci., **22**, 487-502 (1967).

77. Kozicki, W. and C. Tiu, Chem. Eng. Sci., **23**, 231-242 (1968).

78. Kozicki, W., S.N. Parari, A.R.K. Rao and C. Tiu, Chem. Eng. Sci., **25**, 41-52 (1970).

79. Kozicki, W., J.E. Son and M.R. Hanna, Chem. Eng. J., **29**, 171-181 (1984).

80. Kozicki, W., C.J. Hsu and S.N. Pasari, Chem. Eng. Comm., **59**, 137-160 (1987).

81. Kozicki, W., Can. J. Chem. Eng., **68**, 69-80 (1990).

82. Kraemer, E.O., Ind. Eng. Chem., **30**, 1200-1203 (1938).

83. Lax, M., Macromolecules, **7**, 660-666 (1974).

84. Lee, J.J. and G.G. Fuller, Macromolecules, **17**, 375-380 (1984).

85. Lee, J.J. and G.G. Fuller, J. Colloid Interface Sci., **103**, 569-577 (1985).

86. Leyden, D.E. (Ed.), "Silanes, Surface and Interfaces", Gordon & Breach, New York (1985).

87. Mashelkar, R.A. and A. Dutta, Chem. Eng. Sci., **37**, 969-985 (1982).

88. McGary, C.W., J. Poly. Sci., **46**, 51-57 (1960).

89. Meter, D. M., AIChE J., **10**, 881-887 (1964).

90. Metzner, A.B. and G. Park, J. Fluid Mech., **20**, 291-303 (1964).

91. Metzner, A.B., Y. Cohen and C.R. Nafaile, J. Non-Newt. Fluid Mech., **5**, 449-462 (1979).

92. Miles, M.T.; K. Tanaka and A. Keller, Polymer, **24**, 1081-1088 (1983).

93. Moan, M., G. Chauveteau and S. Ghoniem, J. Non-Newt. Fluid Mech., **5**, 463-474 (1979).

94. Mohnssen, H., H.P. Lobl and W. Schauerte, J. Rheol., **31**, 323-336 (1987).

95. Mohnssen, H., D. Weiss and A. Tippe, J. Rheol., **34**, 223-244 (1990).

96. Mooney, M., J. Rheol., **2**, 210-222 (1931).

97. Mungan, N., J. Can. Petrol. Technol., **8**, 45-50 (1969).

98. Narh, K.A., P.J. Barham, R.A.M. Hikmet and A. Keller, Colloid Polymer Sci., **264**, 507-514 (1986).

99. Ohrn, O. E., J. Polymer. Sci., **17**, 137-140 (1955).

100. Oldroyd, J.G., J. Colloid Sci., 4, 333-342 (1949).

101. Ouibrahim, A., Phys. Fluids, **22**, 784-785 (1979).

102. Parnas, R.S., M. Chaimberg, V. Taepaisitphongse and Y. Cohen, J. Colloid Interfacial Sci., **129**, 441-450 (1989).

103. Pefferkorn, E., P. Dejardin and R. Varoqui, J. Colloid Interfacial Sci., **63**, 353-361 (1978).

104. Pilehavari, A. and P.E. Clark, "Rheology of Fracturing Fluids: Wall Slip during Viscosuty Measurement", Paper SPE 12029 (1983).

105. Priel, Z. and A. Silberberg, J. Polym. Sci., Polym. Phys. Ed., **16**, 1917-1925 (1978).

106. Reiner, M., J. Rheol., **2**, 337-350 (1931).

107. Rondelez, F., D. Ausserre and H. Hervet, Annu. Rev. Phys. Chem., **38**, 317-347 (1987)

108. Rowland, F.W. and F.R. Eirich, J. Polym. Sci., Polym. Chem. Ed., 4, 2033-2040 (1966a).

109. Rowland, F.W. and F.R. Eirich, J. Polym. Sci., Polym. Chem. Ed., 4, 2401-2421 (1966b).

110. Sadowski, T.J., "Non-Newtonian Flow through Porous Media", Ph.D Thesis, University of Wisconsin (1963).

111. Scheutjens, J.M.H.M. and G.T. Fleer, J. Phys. Chem., **83**, 1619-1635 (1979).

112. Schofield, R.K. and G.W. Scott Blair, J. Phys. Chem., **34**, 248-262 (1930).

113. Schulz, G.L. and F. Blaschke, J. Prakt. Chem., **158**, 130-135 (1941).

114. Shah, D.O. and R.S. Schechter (eds), "Improved Oil Recovery by Surfactant and Polymer Flooding", Academic Press, New York (1977).

115. Shaver, R. G. and E.W. Merrill, AIChE J., **5**, 181-188 (1959).

116. Shin, N., Ph.D Thesis, Massachusetts Institute of Technology (1965).

117. Silberberg, A., J. Chem. Phys., **48**, 2835-2851 (1968).

118. Smith, L.E. and R.R. Stromberg, In Conference on Polymers at the Liquid-Solid Interface, Loughborough (1975).

119. Sorbie, K.S., J. Colloid Interface Sci., **139**, 299-314 (1990a).

120. Sorbie, K.S., J. Colloid Interface Sci., **139**, 315-323 (1990b).

121. Sorbie, K.S., "Polymer Improved Oil Recovery", Blackie and Son, Glasgow (1991).

122. Sorbie, K.S. and Y. Huang, J. Interface Sci., **145**, 74-89 (1991).

123. Son, J.E., "Polymer Adsorption in Laminar Tube Flow of Drag Reducing Fluids", Ph.D Thesis, University of Ottawa (1978).

124. Takahashi, A., M. Kawaguchi, H. Hirota and T. Kato, Macromolecules, **13**, 884-889 (1980).

125. Takeda, M. and R. Endo, J. Phys. Chem., **60**, 1202-1204 (1956).

126. Talukder, N. and B. Reuter, Biomed. Thechn., **26**, 120 (1981).

127. Thomas, C.P., Soc. Pet. Eng. J., **16**, 130-136 (1976).

128. Tirrell, M. and M.F. Malone, J. Polym. Sci., Polym. Phy. Ed., **15**, 1569-1583 (1977).

129. Tiu, C., W. Kozicki and T.Q. Phung, Can. J. Chem. Eng., **46**, 389-393 (1968).

130. Toms, B.A., Proc. Int. Congr. Rheol., part 2, 135-138, Noeth-Holland (1949a).

131. Toms, B.A., J. Colloid Sci., 4, 511-521 (1949b).

132. Tuijnman, C.A.F. and J.J. Hermans, J. Polymer. Sci., **25**, 385-401 (1957).

133. Union Carbide Corp., "Polyox: Look Polyox water-Soluble Resins to Solve Your Problems", U.S.A. (1973, 1981).

134. Union Carbide Corp., "Polyox: How To Dissolve Polyox Water-Soluble Resins", U.S.A. (1983).

135. Varoqui, R. and P. Dejardin, J. Chem. Phys., **66**, 4395-4399 (1977).

136. Vinogradov, G.V., G.B. Froishteter, K.K. Trilisky and E.L. Smorodinsky, Rheol. Acta, **14**, 765-775 (1975).

137. Vlasov, S.A. and V.N. Kalashnikov, Fluid Mech. Soviet Res., **12**, 104-107 (1973).

138. Wells, C. S., Am. Inst. Aeronautics Astronautics J., **3**, 1800-1805 (1965).

139. Wilkinson, W. L., "Non-Newtonian Flow Fluids", Pergamon Press, New York (1960).

140. Yamakawa, H., "Modern Theory of Polymer Solutions", Harper and Row, New York (1971).

141. Yoshimura, A. and R.K. Prud'homme, J. Rheo., **32**, 53-67 (1988).

Appendix A

Calculation of Total Pressure Drop

A schematic diagram of the capillary tube assembly is shown in figure A.1a. A mechanical energy balance yields the total pressure drop through a capillary tube as follows:

$$\Delta P = P_g + \rho g \langle H \rangle - \frac{1}{2}\rho \langle u \rangle^2 (e_{ve} + e_{vc}) \tag{A.1}$$

Accounting for the buoyancy force, the weight of fluid collected in the weighing cup is given by:

$$W^t - W^i = \rho g A_l (h_l^t - h_l^i) f^* = g(M^t - M^i).f^* \tag{A.2}$$

or by

$$W^t - W^i = \rho g A_u (h_u^i - h_u^t) \tag{A.3}$$

where $f^* = 1 - A_c/A_l$. h_u^i and h_u^t refer to the levels of the fluid in the reservoir and h_l^i and h_l^t are the liquid levels in the collecting cup, measured at initial time and at an instant time, respectively. Combination of the above two equations yields:

$$\frac{W^t - W^i}{\rho g}\{\frac{1}{f^* A_l} + \frac{1}{A_u}\} = (h_1^i - h_0^i) - (h_u^t - h_l^t) \tag{A.4}$$

From equation (A.2), $(W^t - W^i)/g = f^*(M^t - M^i)$ gives

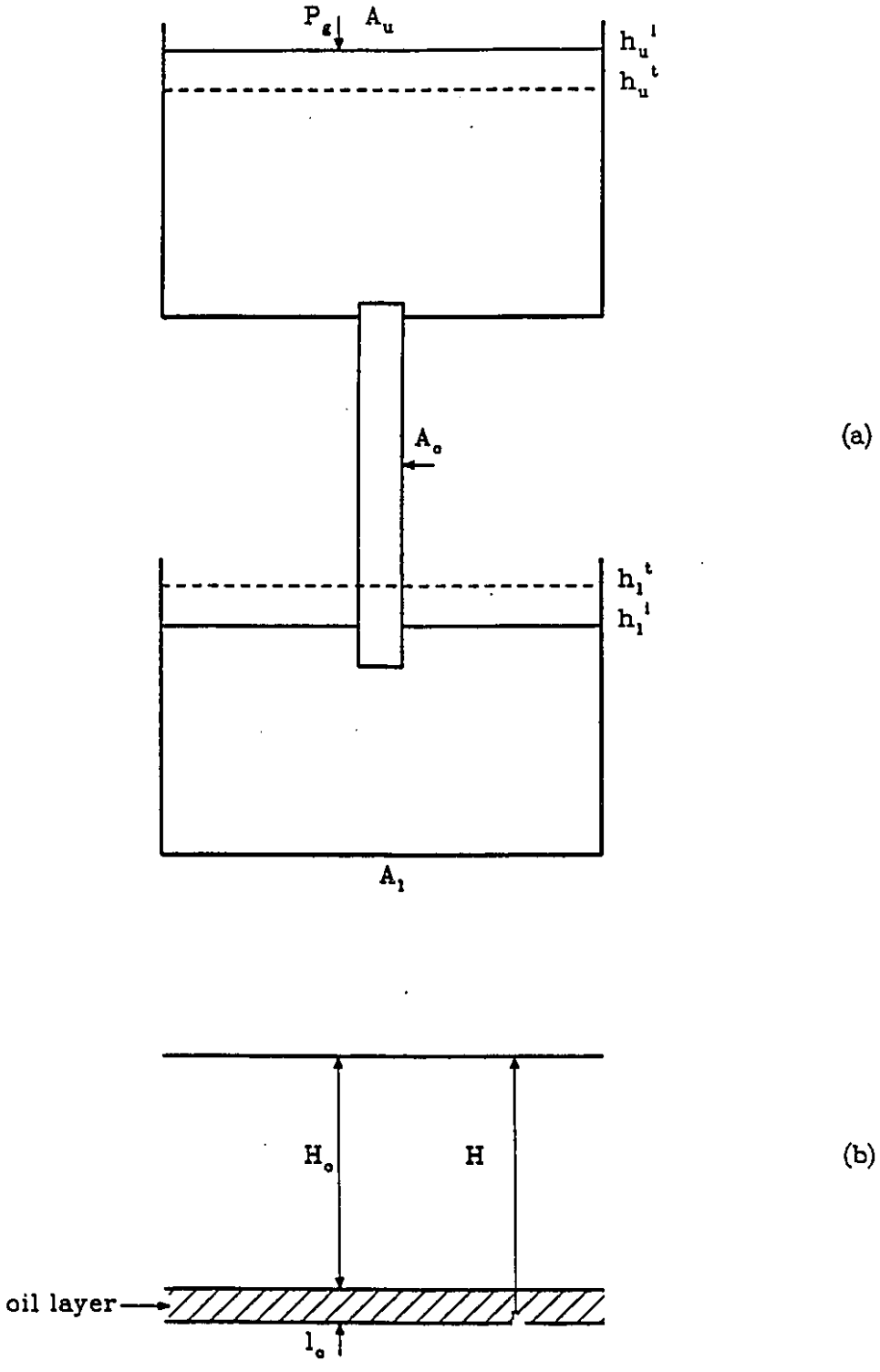

Figure A.1 A schematic diagram of the capillary tube assembly.

$$(h_u^t - h_l^t) = (h_1^i - h_0^i) - \frac{M^t - M^i}{\rho}\{\frac{1}{A_l} + \frac{f^*}{A_u}\} \tag{A.5}$$

In terms of the difference in liquid levels, H, this becomes:

$$H^t = H^i - \frac{M^t - M^i}{\rho}\{\frac{1}{A_l} + \frac{f^*}{A_u}\} \tag{A.6}$$

Similarly, at time $t = t + \Delta t$, we may write

$$H^{t+\Delta t} = H^i - \frac{M^{t+\Delta t} - M^i}{\rho}\{\frac{1}{A_l} + \frac{f^*}{A_u}\} \tag{A.7}$$

The average value of H may be evaluated as

$$\langle H \rangle = \frac{1}{2}(H^t + H^{t+\Delta t}) = H^i - \frac{\langle M \rangle - M^i}{\rho}\{\frac{1}{A_l} + \frac{f^*}{A_u}\} \tag{A.8}$$

where $\langle M \rangle = (M^t + M^{t+\Delta t})/2$.

To account for the thickness of the oil film in the weighing cup, the pressure drop expression may be written as

$$\Delta P = P_g + \rho g \langle H \rangle - \rho_{oil} l_o g - \frac{1}{2}\rho \langle u \rangle^2 (e_{ve} + e_{vc}) \tag{A.9}$$

where H represents the difference in liquid levels. If the actual reading of the lower level in the weighing cup is taken from the oil surface, then $H = H_o + l_o$ and $H^i = H_o^i + l_o$ (seen in figure A-1b). The following expression is finally obtained for evaluation of the total pressure drop:

$$\begin{aligned} \Delta P &= P_g + \rho g H_o^i - g(\langle M \rangle - M^i)(\frac{1}{A_l} + \frac{f^*}{A_u}) + (\rho - \rho_{oil}) g l_0 - \frac{1}{2}\rho \langle u \rangle^2 (e_{ve} + e_{vc}) \\ &= P_g + \rho g \langle H_o \rangle - (\rho - \rho_{oil}) l_o g - \frac{1}{2}\rho \langle u \rangle^2 (e_{ve} + e_{vc}) \end{aligned} \tag{A.10}$$

Appendix B

Capillary Diameter Calibration

From the mechanical energy balance, the following equation can be obtained:

$$\Delta P_{ev} = 2\tau_w \frac{L}{R} + \frac{1}{2}\rho(e_{vc} + e_{ve})\langle u\rangle^2 \tag{B.1}$$

Substituting $\tau_w = \mu 4Q/\pi R^3$ for a Newtonian fluid results in:

$$\frac{\Delta P_{ev}}{L} = \frac{8\mu Q}{\pi R^4} + \frac{\rho Q^2}{2\pi^2 L R^4}(e_{vc} + e_{ve}) \tag{B.2}$$

which may be rewritten

$$\frac{\Delta P_{ev}/L}{Q} = \frac{8\mu}{\pi R^4} + \frac{\rho(e_{vc} + e_{ve})}{2\pi^2 L R^4} Q \tag{B.3}$$

Assuming $(e_{vc} + e_{ve})$ is constant, a plot of the experimental data in the form $\frac{\Delta P_{ev}/L}{Q}$ vs. Q should be a straight line. The tube diameter may be evaluated from the intercept at Q=0 and $(e_{vc} + e_{ve})$ from the slope of the line.

The values of $(e_{vc} + e_{ve})$ may vary with shear rate or Reynolds Number Re. The relationship may be described by:

$$(e_{vc} + e_{ve}) = K_1 + \frac{K_2}{Re} \tag{B.4}$$

For a Newtonian fluid in capillary flow, we have:

$$Re = \frac{D\langle u\rangle\rho}{\mu} = \frac{2Q\rho}{\pi\mu R} \tag{B.5}$$

Combination of equations (B.3) and (B.5) finally yields:

$$\frac{\Delta P_{ev}/L}{Q} = \frac{8\mu}{\pi R^4}[1 + \frac{K_2}{32(L/R)}] + \frac{\rho K_1}{2\pi^2 L R^4} Q \tag{B.6}$$

From Denn's "Process Fluid Dynamics" (1980), $(e_{vc} + e_{ve})$ is given by:

$$(e_{vc} + e_{ve}) = 2.3(1 + \frac{9.4}{Re}) = 2.3 + \frac{21.6}{Re} \tag{B.7}$$

The parenthetical term in equation (B.6) then becomes:

$$1 + \frac{K_2}{32(L/R)} = 1 + \frac{21.6}{32(L/R)} \tag{B.8}$$

For $L/R = 1000$, the above term is equal to 1.000675. In our measurements, the minimum value of L/R is about 1500. Thus the equation (B.3) with constant $(e_{vc} + e_{ve})$ was simply used to evaluate the tube diameters.

Appendix C

Surface Treatment

All the tubes used for surface treatment were brand new and were not previously used in the adsorption experiments. The surface treatment procedure follows:

a) The tubes were prewashed with distilled water and dried with nitrogen.

b) They were then washed using pure ethanol (100%) and also dried with nitrogen.

c) Subsequently, the clean tubes were treated using a solution of 2% dimethyldiethoxysilane in an ethanol-5% water solution adjusted to a pH of 4.5-5.5 with acetic acid.

d) Finally, they were washed with ethanol (100%) and dried again to remove any excess silane solution.

The treated tubes were then cured for 24 hours at room temperature.

If necessary, the tubes may be retreated. Before repeating the above treatment procedure, the used tubes should be washed by an aqueous 10% NaOH solution, followed by distilled water.

Appendix D

Check on the Linearity of Weight vs. Time

Flow rate measurements were conducted by using an electric balance linked with a computer. The measurement governed by the computer provided a precise determination of the flow rate in small diameter capillary flow. The data for two runs shown in figures D.1 and D.2 illustrate the linearity of the plots of effluent weight vs. time.

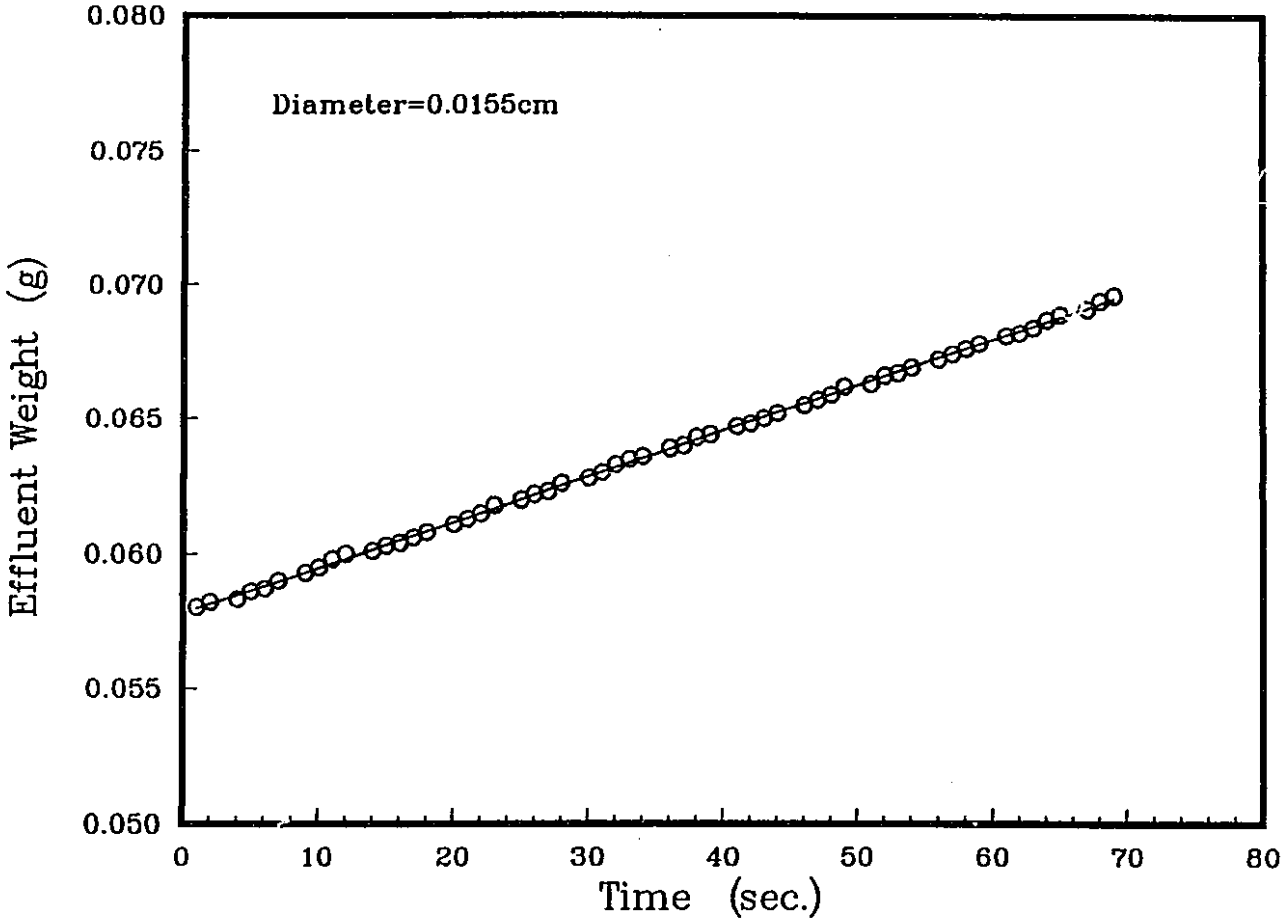

Figure D.1 Effluent weight vs. time for the tube of D=0.0155 cm.

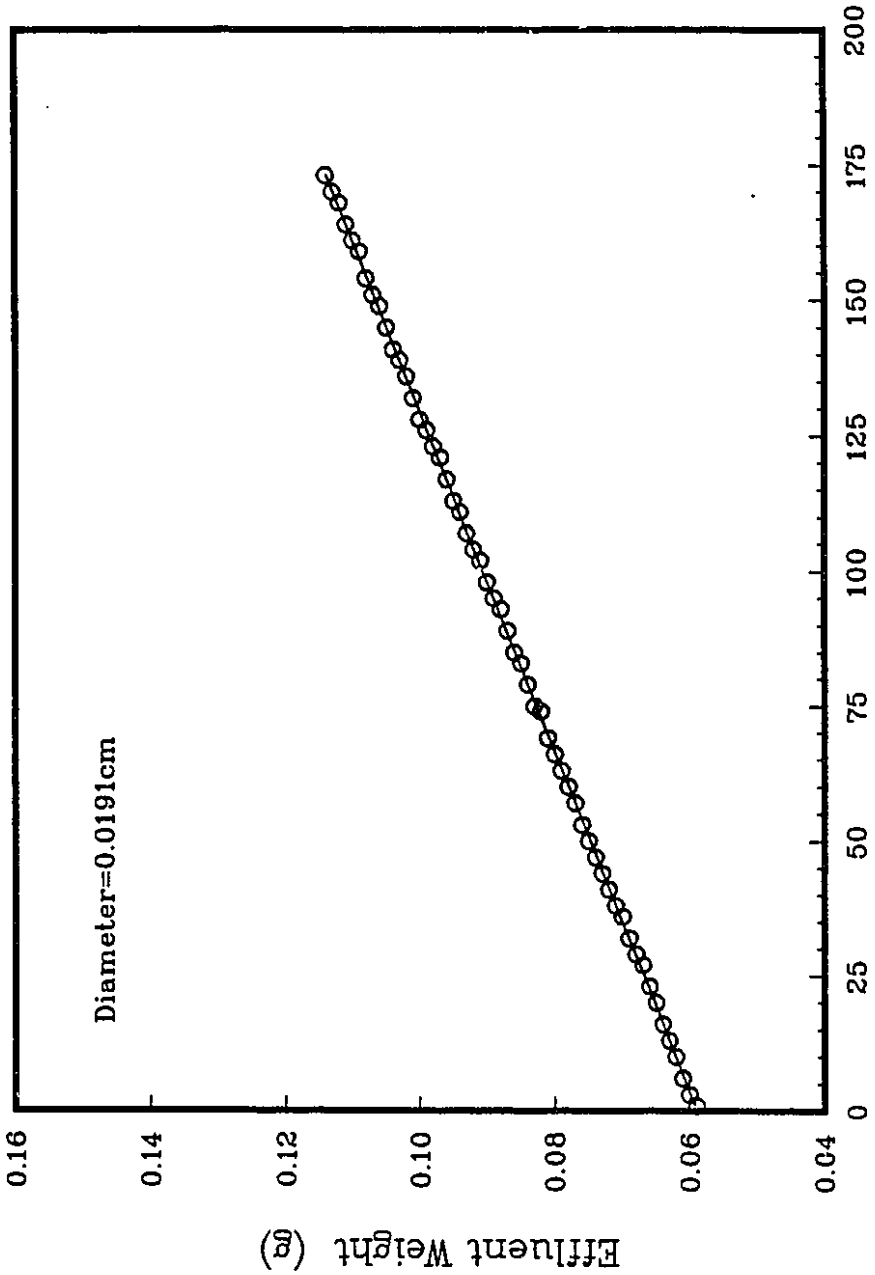

Figure D.2 Effluent Weight vs. time for the tube of D=0.0191 cm.

Appendix E

Method for Determination of Parameters from Limited Data

In the case where limited data is available, an approximate method may be used for evaluation of the parameters in equation (3.34) associated with wall effects. The method utilizes experimental data from the low concentration and the high concentration regimes.

Evaluation of Parameters from Data at Low Concentrations

In the low concentration region, equation (3.34) simplifies to

$$A(c) = -\frac{\delta_{ap}}{\eta_0}\frac{c}{k} + k_{s0}\left(\frac{1}{\mu_s} - \frac{1}{\eta_0}\right) \tag{E.1}$$

which may be rewritten

$$Y_l(c) = b_{l0} + b_{l1}X_l(c) \tag{E.2}$$

where

$$Y_l(c) = A(c)\eta_0/c \tag{E.3}$$

$$X_l(c) = \left(\frac{\eta_o}{\mu_s} - 1\right)/c \tag{E.4}$$

with the parameters

$$b_{l0} = -\delta_{ap}/k \tag{E.5}$$

and

$$b_{l1} = k_{s0} \tag{E.6}$$

Least squares fitting is used to evaluate k_{s0} and δ_{ap}/k.

Evaluation of Parameters from Data at High Concentrations

At the high polymer concentrations corresponding to the plateau region of the adsorption isotherm, equation (3.34) becomes:

$$A(c) = -\frac{\delta_{ap}}{\eta_0} + k_{s0}(\frac{1}{\mu_s} - \frac{1}{\eta_0})(\frac{k}{c}) \tag{E.7}$$

which may also be expressed in the same form as equation (E.2):

$$Y_h(c) = b_{h0} + b_{h1}X_h(c) \tag{E.8}$$

where, in this case,

$$Y_h(c) = A(c)\eta_0 \tag{E.9}$$

$$X_h(c) = (\frac{\eta_o}{\mu_s} - 1)/c \tag{E.10}$$

and

$$b_{h0} = -\delta_{ap} \tag{E.11}$$

and

$$b_{h1} = kk_{s0} \tag{E.12}$$

k_{s0} is provided by the previous analysis of the data at low concentrations. The separate analyses of the data at low and high polymer concentrations provide all

the parameters in equation (3.34). They can be applied in further evaluation of wall effects.

For a better accuracy, the following procedure may be used. For a given k yielded from the above calculation, equation (3.34) could be used to reevaluate k_{s0} and δ_{ap} by least squares fitting. Repeat the procedure till the minimum deviation is reached. The values of k, k_{s0} and δ_{ap} then could be obtained at this deviation.

Appendix F

Errors and Uncertainties in Measurements

Errors and experimental uncertainties are always involved in experimental work. They may play a great role in the evaluation of experimental results and may lead to a misinterpretation of the physical phenomena studied. Therefore, the principle of designing an experimental system is to keep errors and uncertainties to a minimum level so as to minimize their influence, in order to obtain meaningful results.

Evaluations of the errors and uncertainties involved in the present work are summarized in the following, which have also been indicated in the appropriate sections of the text.

During the measurements, experimental temperature was controlled at $25 \pm 0.1^{\circ}C$, utilizing a thermometer with an accuracy of $0.05^{\circ}C$.

Flow rates were measured using the two electronic balances with accuracies in the weight measurements of 0.0005 g and 0.00005 g, based on the evaluations of 46 measurements, seen in figures D.1 and D.2. The average error in a flow measurement by this method was estimated to be 0.5%. The pressure drop measurements were carried out using the two calibrated pressure gauges for the different pressure ranges. The maximum error involved in a measurement was not more than 0.5%.

The reproducibility involved in the calibration of the tube diameters was found to fall within 0.5%, as illustrated in Tables 4.2 and 4.3.

The evaluations of the shear stress at the wall involved the measurement of the pressure drop, tube diameter and the length of the tube. The maximum error introduced in these measurements was then estimated to be 1.5% for the shear stress range involved.

End corrections were made using a modified Bagley plot, as seen in figure 5.3. The values of $(e_{ve}+e_{vc})$ were obtained from the intercept at L/D=0. The uncertainty in the intercept evaluations was estimated to be within 2.0%. This led to a maximum uncertainty of 2.0% in the end corrections (ΔP_{end}), on the basis of the total pressure drop.

Appendix G

Experimental Data and Additional Relevant Plots

Table G.1: Cannon-Fenske Viscometer Evaluations of η_r

Concentration	Polyox WSR 301	Polyox Coagulant	Polyox FRA
200 ppm	1.3093	1.4435	1.5275
300 ppm	1.4799	1.6871	1.8124
400 ppm	1.6598	2.0037	2.1562
500 ppm	1.8814	2.2783	2.5129
600 ppm	2.0891	2.6266	2.9003

Table G.2: Slip Coefficients

Concentration (used)	Polyox WSR 301		Polyox Coagulant		Polyox FRA	
	(NST)	(ST)	(NST)	(ST)	(NST)	(ST)
5 ppm	0.0039	0.0057	0.0056		0.0087	0.0119
10 ppm	0.0041	0.0063	0.0048		0.0070	0.0106
15 ppm	0.0037	0.0064	0.0040		0.0051	0.0086
20 ppm	0.0034	0.0063	0.0033		0.0042	0.0077
30 ppm	0.0030	0.0063	0.0027		0.0033	0.0064
60 ppm	0.0025	0.0062	0.0021		0.0027	0.0058
100 ppm	0.0022	0.0060	0.0019		0.0024	0.0054
130 ppm					0.0023	
200 ppm	0.0020	0.0059	0.0016		0.0021	0.0049

NST and ST designate the glass tubes without and with surface treatment using dimethyldiethoxysilane.

Table G.3

Experimental Data for Capillary Flows

(The data shown are the original results of the measurements, without corrections for end effects or wall effects)

(i) Untreated glass tubes, p. 141-180.

(i) Silane-treated glass tubes, p. 181-202.

Flow of Polyox WSR 301 Solutions in Untreated Tubes

Concentration: 5ppm
Tube: 0.002B1

Q (cm^3/s)	ΔP ($dynes/cm^2$)
0.00012	707761
0.00018	1052502
0.00024	1397241
0.00030	1741981
0.00035	2086720
0.00042	2431458
0.00047	2776197
0.00053	3120935

Concentration: 5ppm
Tube: 0.003A2

Q (cm^3/s)	ΔP ($dynes/cm^2$)
0.00024	365429
0.00046	710168
0.00069	1054907
0.00091	1399644
0.00114	1744375
0.00136	2089110
0.00160	2433843
0.00181	2778572
0.00204	3123303

Concentration: 5ppm
Tube: 0.004B

Q (cm^3/s)	ΔP ($dynes/cm^2$)
0.00044	375701
0.00086	720437
0.00126	1065167
0.00166	1409893
0.00207	1754613
0.00249	2099334
0.00291	2444043
0.00332	2788758
0.00372	3133474

Concentration: 5ppm
Tube: 0.006C1

Q (cm^3/s)	ΔP ($dynes/cm^2$)
0.00187	381189
0.00356	725904
0.00523	1070618
0.00693	1415321
0.00868	1759993
0.01036	2104676
0.01215	2449341
0.01393	2793999
0.01559	3138635

Concentration: 5ppm
Tube: 0.008A2

Q (cm^3/s)	ΔP ($dynes/cm^2$)
0.00847	365560
0.01658	710235
0.02456	1054873
0.03263	1399460
0.04050	1744013
0.04833	2088523
0.05638	2432968
0.06354	2777377
0.07107	3121789

Concentration: 5ppm
Tube: 0.008B2+

Q (cm^3/s)	ΔP ($dynes/cm^2$)
0.01108	717916
0.01642	1062582
0.02174	1407204
0.02706	1751711
0.03229	2096248
0.03768	2440673
0.04279	2785192

Concentration: 5ppm
Tube: 0.008C1

Q (cm^3/s)	ΔP ($dynes/cm^2$)
0.00825	725069
0.01216	1069710
0.01608	1414338
0.02008	1758763
0.02403	2103368
0.02805	2447812
0.03188	2792314
0.03568	3136839

Concentration: 5ppm
Tube: 0.012B

Q (cm^3/s)	ΔP ($dynes/cm^2$)
0.0133	414621
0.0245	759255
0.0356	1103853
0.0470	1448300
0.0581	1792819
0.0690	2137255
0.0801	2481720
0.0907	2826127

Concentration: 5ppm
Tube: 0.012C1

Q (cm^3/s)	ΔP ($dynes/cm^2$)
0.0227	386612
0.0431	731198
0.0630	1075723
0.0831	1420171
0.1027	1764420
0.1212	2108737
0.1406	2452937
0.1589	2797176
0.1768	3141246

Concentration: 5ppm
Tube: 0.018A2

Q (cm^3/s)	ΔP ($dynes/cm^2$)
0.1307	385530
0.2400	729610
0.3430	1073095
0.4435	1416444
0.5368	1759830

Concentration: 5ppm
Tube: 0.012C2

Q (cm^3/s)	ΔP ($dynes/cm^2$)
0.0279	379829
0.0535	724284
0.0779	1068730
0.1021	1413125
0.1257	1757463
0.1486	2101676
0.1724	2445587
0.1948	2789514
0.2164	3133244

Concentration: 5ppm
Tube: 0.018C1

Q (cm^3/s)	ΔP ($dynes/cm^2$)
0.0990	405712
0.1806	749838
0.2568	1093757
0.3327	1437350
0.4045	1780709
0.4740	2123653

Concentration: 5ppm
Tube: 0.018B

Q (cm^3/s)	ΔP ($dynes/cm^2$)
0.0590	441789
0.1059	786158
0.1505	1130392
0.1955	1474550
0.2380	1818362
0.2807	2162006
0.3245	2505581
0.3642	2848988
0.4030	3192885

Concentration: 10ppm
Tube: 0.004B

Q (cm^3/s)	ΔP ($dynes/cm^2$)
0.00043	375412
0.00084	720149
0.00124	1064885
0.00164	1409619
0.00205	1754349
0.00246	2099076
0.00288	2443803
0.00328	2788525
0.00369	3133246

Concentration: 10ppm
Tube: 0.002A1

Q (cm^3/s)	ΔP ($dynes/cm^2$)
0.00007	360334
0.00014	705075
0.00022	1049815
0.00028	1394556
0.00035	1739295
0.00056	2773506
0.00062	3118243

Concentration: 10ppm
Tube: 0.006C1

Q (cm^3/s)	ΔP ($dynes/cm^2$)
0.00185	380654
0.00354	725380
0.00520	1070095
0.00691	1414802
0.00861	1759495
0.01032	2104179
0.01211	2448807
0.01379	2793471
0.01553	3138116

Concentration: 10ppm
Tube: 0.003A2

Q (cm^3/s)	ΔP ($dynes/cm^2$)
0.00023	365384
0.00046	710125
0.00067	1054863
0.00091	1399596
0.00113	1744331
0.00135	2089060
0.00158	2433793
0.00179	2778523
0.00201	3123251

Concentration: 10ppm
Tube: 0.008A2

Q (cm^3/s)	ΔP ($dynes/cm^2$)
0.00839	366111
0.02451	1055305
0.03254	1399848
0.04046	1744347
0.04819	2088828
0.05627	2433271
0.06369	2777677
0.07098	3121715

Concentration: 10ppm
Tube: 0.008B2+

Q (cm^3/s)	ΔP ($dynes/cm^2$)
0.00568	373067
0.01098	717742
0.01638	1062400
0.02166	1407038
0.02690	1751641
0.03225	2096212
0.03769	2440760
0.04269	2785309
0.04789	3129804

Concentration: 10ppm
Tube: 0.012C2

Q (cm^3/s)	ΔP ($dynes/cm^2$)
0.0279	380077
0.0534	724666
0.0783	1068957
0.1029	1413314
0.1259	1757461
0.1493	2101685
0.1722	2445986
0.1941	2790201
0.2147	3134246

Concentration: 10ppm
Tube: 0.008C1

Q (cm^3/s)	ΔP ($dynes/cm^2$)
0.00423	381031
0.00811	725702
0.01200	1070340
0.01596	1414996
0.01989	1759625
0.02400	2104232
0.02813	2448704
0.03197	2793280
0.03582	3137777

Concentration: 10ppm
Tube: 0.012B

Q (cm^3/s)	ΔP ($dynes/cm^2$)
0.0130	413992
0.0241	758659
0.0352	1103293
0.0464	1447838
0.0575	1792356
0.0684	2136808
0.0800	2481227
0.0906	2825666

Concentration: 10ppm
Tube: 0.012C1

Q (cm^3/s)	ΔP ($dynes/cm^2$)
0.0222	385824
0.0426	730427
0.0626	1074961
0.0829	1419266
0.1023	1763705
0.1214	2108070
0.1407	2452370
0.1585	2796586
0.1759	3140746

Concentration: 10ppm
Tube: 0.018A2

Q (cm^3/s)	ΔP ($dynes/cm^2$)
0.1324	385792
0.2427	730846
0.3426	1074651
0.4398	1418027
0.5330	1761126

Concentration: 10ppm
Tube: 0.018C1

Q (cm^3/s)	ΔP ($dynes/cm^2$)
0.0982	405990
0.1799	749982
0.2568	1093625
0.3291	1437306
0.4004	1780785
0.4689	2124021

Concentration: 30ppm
Tube: 0.003A2

Q (cm^3/s)	ΔP ($dynes/cm^2$)
0.00022	366883
0.00043	711624
0.00065	1056363
0.00106	1745834
0.00128	2090570
0.00151	2435305
0.00171	2780039
0.00191	3124772

Concentration: 10ppm
Tube: 0.018B

Q (cm^3/s)	ΔP ($dynes/cm^2$)
0.0592	441654
0.1056	785962
0.1482	1130320
0.1916	1473690
0.2345	1817847
0.2772	2161880
0.3200	2505780
0.3583	2849716
0.3998	3193473

Concentration: 30ppm
Tube: 0.004B

Q (cm^3/s)	ΔP ($dynes/cm^2$)
0.00043	376316
0.00082	721055
0.00121	1065788
0.00160	1410523
0.00199	1755256
0.00238	2099985
0.00280	2444715
0.00318	2789442
0.00357	3134161

Concentration: 30ppm
Tube: 0.002B1

Q (cm^3/s)	ΔP ($dynes/cm^2$)
0.00012	709401
0.00017	1054142
0.00023	1398883
0.00028	1743623
0.00034	2088364
0.00039	2433103
0.00045	2777842
0.00051	3122582

Concentration: 30ppm
Tube: 0.006C1

Q (cm^3/s)	ΔP ($dynes/cm^2$)
0.00176	381999
0.00336	726725
0.00495	1071441
0.00654	1416146
0.00816	1760843
0.00983	2105512
0.01158	2450156
0.01321	2794827
0.01488	3139496

Concentration: 30ppm
Tube: 0.008A2

Q (cm^3/s)	ΔP ($dynes/cm^2$)
0.00811	365332
0.01559	710003
0.02310	1054636
0.03067	1399208
0.03806	1743749
0.05290	2432518
0.06011	2776681
0.06743	3121119

Concentration: 30ppm
Tube: 0.012C1

Q (cm^3/s)	ΔP ($dynes/cm^2$)
0.0216	386423
0.0412	731050
0.0609	1075643
0.0805	1419881
0.1003	1764334
0.1198	2108509
0.1395	2452886
0.1586	2796896
0.1766	3140760

Concentration: 30ppm
Tube: 0.008B2$^+$

Q (cm^3/s)	ΔP ($dynes/cm^2$)
0.00543	373919
0.01052	718613
0.01549	1063252
0.02083	1407881
0.02620	1752495
0.03242	2097090
0.03690	2441664
0.04207	2786220
0.04711	3130654

Concentration: 30ppm
Tube: 0.012A2

Q (cm^3/s)	ΔP ($dynes/cm^2$)
0.0250	377389
0.0484	721975
0.0716	1066532
0.0942	1411006
0.1172	1755393
0.1390	2099688
0.1620	2443990
0.1827	2788159
0.2030	3131960

Concentration: 30ppm
Tube: 0.008C1

Q (cm^3/s)	ΔP ($dynes/cm^2$)
0.00410	381892
0.00788	726584
0.01161	1071257
0.01552	1415903
0.01939	1760518
0.02336	2105136
0.02733	2449743
0.03110	2794328
0.03476	3138908

Concentration: 30ppm
Tube: 0.012B

Q (cm^3/s)	ΔP ($dynes/cm^2$)
0.0125	413331
0.0233	758005
0.0340	1102575
0.0447	1447181
0.0560	1791746
0.0667	2136301
0.0784	2480801
0.0887	2825271
0.0993	3169711

Concentration: 30ppm
Tube: 0.018A2

Q (cm^3/s)	ΔP ($dynes/cm^2$)
0.1298	387090
0.2439	731129
0.3470	1074742
0.4399	1418069
0.5272	1761369

Concentration: 60ppm
Tube: 0.002B1

Q (cm^3/s)	ΔP ($dynes/cm^2$)
0.00016	1054033
0.00021	1398774
0.00027	1743514
0.00032	2088255
0.00037	2432995
0.00043	2777734
0.00048	3122475

Concentration: 30ppm
Tube: 0.018C1

Q (cm^3/s)	ΔP ($dynes/cm^2$)
0.0962	405952
0.1782	750227
0.2576	1094183
0.3305	1437900
0.3989	1780548
0.4659	2123903

Concentration: 60ppm
Tube: 0.003B1

Q (cm^3/s)	ΔP ($dynes/cm^2$)
0.00026	364547
0.00052	709285
0.00076	1054024
0.00102	1398759
0.00131	1743494
0.00157	2088229
0.00188	2432962
0.00212	2777694
0.00238	3122414

Concentration: 30ppm
Tube: 0.018B

Q (cm^3/s)	ΔP ($dynes/cm^2$)
0.0573	442232
0.1036	786702
0.1487	1130915
0.1945	1475141
0.2381	1819183
0.2807	2162986
0.3218	2506911
0.3607	2850728
0.3959	3194061

Concentration: 60ppm
Tube: 0.004B

Q (cm^3/s)	ΔP ($dynes/cm^2$)
0.00040	375198
0.00078	719933
0.00115	1064667
0.00152	1409401
0.00190	1754128
0.00227	2098860
0.00267	2443591
0.00302	2788318
0.00341	3133045

Concentration: 60ppm
Tube: 0.006C1

Q (cm^3/s)	ΔP ($dynes/cm^2$)
0.00169	381811
0.00325	726537
0.00477	1071258
0.00630	1415965
0.00787	1760666
0.00942	2105358
0.01112	2450048
0.01272	2794740
0.01424	3139392

Concentration: 60ppm
Tube: 0.008C1

Q (cm^3/s)	ΔP ($dynes/cm^2$)
0.00386	382885
0.00729	727580
0.01075	1072262
0.01427	1416924
0.01787	1761568
0.02155	2106192
0.02546	2450798
0.02932	2795384
0.03292	3139990

Concentration: 60ppm
Tube: 0.008A2

Q (cm^3/s)	ΔP ($dynes/cm^2$)
0.01487	710978
0.02206	1055608
0.02949	1400186
0.03692	1744692
0.04435	2089200
0.05219	2433723
0.05920	2778161
0.06641	3122516

Concentration: 60ppm
Tube: 0.012C1

Q (cm^3/s)	ΔP ($dynes/cm^2$)
0.0205	386808
0.0395	731444
0.0583	1076053
0.0759	1420595
0.0950	1765052
0.1135	2109428
0.1329	2453803
0.1513	2798133
0.1698	3142335

Concentration: 60ppm
Tube: 0.008B2+

Q (cm^3/s)	ΔP ($dynes/cm^2$)
0.00525	374938
0.00992	719635
0.01470	1064310
0.01960	1408853
0.02459	1753480
0.02959	2098072
0.03480	2442606
0.03963	2787182
0.04460	3131730

Concentration: 60ppm
Tube: 0.012A2

Q (cm^3/s)	ΔP ($dynes/cm^2$)
0.0240	377649
0.0461	722244
0.0662	1066821
0.0879	1411287
0.1099	1755707
0.1318	2099947
0.1545	2444263
0.1748	2788583
0.1957	3132851

Concentration: 60ppm
Tube: 0.012B

Q (cm^3/s)	ΔP ($dynes/cm^2$)
0.0119	415082
0.0223	759730
0.0324	1104392
0.0431	1448957
0.0536	1793510
0.0635	2138069
0.0744	2482534
0.0846	2826999
0.0950	3171452

Concentration: 60ppm
Tube: 0.018B

Q (cm^3/s)	ΔP ($dynes/cm^2$)
0.0540	441942
0.0978	786421
0.1412	1130708
0.1856	1474767
0.2290	1818665
0.2727	2162496
0.3178	2506195
0.3611	2849674
0.3990	3193592

Concentration: 60ppm
Tube: 0.018A2

Q (cm^3/s)	ΔP ($dynes/cm^2$)
0.1235	387058
0.2315	731050
0.3365	1074610
0.4306	1418032
0.5247	1761196

Concentration: 100ppm
Tube: 0.002A1

Q (cm^3/s)	ΔP ($dynes/cm^2$)
0.00012	708101
0.00018	1052841
0.00024	1397581
0.00031	1742320
0.00036	2087061
0.00043	2431799
0.00049	2776538

Concentration: 60ppm
Tube: 0.018C1

Q (cm^3/s)	ΔP ($dynes/cm^2$)
0.0900	405792
0.1687	750135
0.2465	1094227
0.3240	1437746
0.3995	1781312
0.4741	2124694

Concentration: 100ppm
Tube: 0.003A2

Q (cm^3/s)	ΔP ($dynes/cm^2$)
0.00020	366748
0.00040	711488
0.00058	1056226
0.00078	1400964
0.00095	1745700
0.00115	2090435
0.00135	2435170
0.00154	2779904
0.00173	3124637

Concentration: 100ppm
Tube: 0.004B

Q (cm^3/s)	ΔP ($dynes/cm^2$)
0.00038	376668
0.00072	721405
0.00108	1066139
0.00142	1410872
0.00176	1755603
0.00211	2100333
0.00249	2445063
0.00283	2789787
0.00318	3134512

Concentration: 100ppm
Tube: 0.008C1

Q (cm^3/s)	ΔP ($dynes/cm^2$)
0.00368	381742
0.00698	726451
0.01014	1071146
0.01351	1415829
0.01700	1760495
0.02053	2105132
0.02421	2449766
0.02777	2794380
0.03119	3138959

Concentration: 100ppm
Tube: 0.006C1

Q (cm^3/s)	ΔP ($dynes/cm^2$)
0.00159	380986
0.00303	725712
0.00445	1070421
0.00589	1415135
0.00733	1759825
0.00884	2104492
0.01044	2449159
0.01202	2793849
0.01342	3138531

Concentration: 100ppm
Tube: $0.008B2^+$

Q (cm^3/s)	ΔP ($dynes/cm^2$)
0.00494	374606
0.00934	719308
0.01379	1063910
0.01844	1408563
0.02330	1753179
0.02815	2097776
0.03313	2442339
0.03789	2786916
0.04235	3131460

Concentration: 100ppm
Tube: 0.008A2

Q (cm^3/s)	ΔP ($dynes/cm^2$)
0.00701	366904
0.01337	711492
0.02026	1056144
0.02754	1400741
0.03460	1745299
0.04153	2089818
0.04890	2434339
0.05600	2778738
0.06278	3123164

Concentration: 100ppm
Tube: 0.012A2

Q (cm^3/s)	ΔP ($dynes/cm^2$)
0.0220	377501
0.0411	722139
0.0615	1066685
0.0822	1411182
0.1034	1755563
0.1231	2099851
0.1452	2444068
0.1643	2788291
0.1835	3132512

Concentration: 100ppm
Tube: 0.012C1

Q (cm^3/s)	ΔP ($dynes/cm^2$)
0.0194	386519
0.0358	731146
0.0532	1075710
0.0710	1420215
0.0890	1764579
0.1063	2108985
0.1255	2452904
0.1429	2797037
0.1607	3141212

Concentration: 100ppm
Tube: 0.012B

Q (cm^3/s)	ΔP ($dynes/cm^2$)
0.0111	415011
0.0206	759695
0.0299	1104343
0.0395	1448960
0.0493	1793492
0.0594	2138043
0.0698	2482407
0.0793	2826902
0.0890	3171359

Concentration: 100ppm
Tube: 0.018A2

Q (cm^3/s)	ΔP ($dynes/cm^2$)
0.1164	387372
0.2092	731491
0.3093	1075398
0.4062	1418856
0.5003	1762009
0.5906	2104329

Concentration: 100ppm
Tube: 0.018C1

Q (cm^3/s)	ΔP ($dynes/cm^2$)
0.0855	404805
0.1603	749088
0.2256	1093313
0.2998	1437204
0.3718	1780797
0.4437	2124174
0.5150	2467810

Concentration: 100ppm
Tube: 0.018B

Q (cm^3/s)	ΔP ($dynes/cm^2$)
0.0504	441736
0.0915	786216
0.1325	1130422
0.1735	1474686
0.2127	1818749
0.2542	2162756
0.2968	2506564
0.3368	2850320
0.3772	3194001

Flow of Polyox Coagulant Solutions in Untreated Tubes

Concentration: 5ppm
Tube: 0.002B1

Q (cm^3/s)	ΔP ($dynes/cm^2$)
0.00012	704593
0.00018	1049334
0.00024	1394075
0.00029	1738815
0.00035	2083552
0.00041	2428289
0.00047	2773026
0.00053	3117764

Concentration: 5ppm
Tube: 0.006B

Q (cm^3/s)	ΔP ($dynes/cm^2$)
0.00248	375358
0.00477	720075
0.00704	1064778
0.00936	1409467
0.01171	1754242
0.01867	2788027
0.02097	3132662

Concentration: 5ppm
Tube: 0.003A2

Q (cm^3/s)	ΔP ($dynes/cm^2$)
0.00023	361829
0.00045	706569
0.00067	1051307
0.00088	1396041
0.00111	1740777
0.00134	2085505
0.00157	2430230
0.00180	2774959
0.00200	3119686

Concentration: 5ppm
Tube: 0.008A2

Q (cm^3/s)	ΔP ($dynes/cm^2$)
0.00853	366201
0.01668	710808
0.02472	1055411
0.03276	1399982
0.04060	1744515
0.04832	2088973
0.05636	2433408
0.06390	2777806
0.07089	3121996

Concentration: 5ppm
Tube: 0.004B

Q (cm^3/s)	ΔP ($dynes/cm^2$)
0.00043	373136
0.00084	717874
0.00124	1062609
0.00164	1407343
0.00204	1752075
0.00245	2096803
0.00284	2441530
0.00326	2786258
0.00365	3130981

Concentration: 5ppm
Tube: 0.008B2+

Q (cm^3/s)	ΔP ($dynes/cm^2$)
0.00574	372744
0.01112	717425
0.01648	1062094
0.02186	1406706
0.02723	1751300
0.03256	2095856
0.03811	2440371
0.04326	2784883
0.04838	3129368

Concentration: 5ppm
Tube: 0.008C1

Q (cm^3/s)	ΔP ($dynes/cm^2$)
0.00422	380848
0.00810	725537
0.01196	1070211
0.01592	1414850
0.01996	1759399
0.02384	2103981
0.02800	2448475
0.03115	2792859
0.03475	3137275

Concentration: 5ppm
Tube: 0.012B

Q (cm^3/s)	ΔP ($dynes/cm^2$)
0.0126	414016
0.0233	758686
0.0338	1103312
0.0448	1447886
0.0558	1792441
0.0666	2136835
0.0777	2481356
0.0881	2825860
0.0984	3170288

Concentration: 5ppm
Tube: 0.012C1

Q (cm^3/s)	ΔP ($dynes/cm^2$)
0.0226	386241
0.0432	730827
0.0631	1075323
0.0827	1419600
0.10213	1764010
0.1216	2108082
0.1407	2452312
0.1581	2796522
0.1761	3140596

Concentration: 5ppm
Tube: 0.018A2

Q (cm^3/s)	ΔP ($dynes/cm^2$)
0.1333	386356
0.2440	730395
0.3454	1074093
0.4436	1417381
0.5382	1760628

Concentration: 5ppm
Tube: 0.012C2

Q (cm^3/s)	ΔP ($dynes/cm^2$)
0.0278	379501
0.0531	724072
0.0780	1068533
0.1033	1412809
0.1261	1757070
0.1497	2100990
0.1728	2444948
0.1950	2789068
0.2164	3133102

Concentration: 5ppm
Tube: 0.018C1

Q (cm^3/s)	ΔP ($dynes/cm^2$)
0.0993	405200
0.1805	749406
0.2579	1093322
0.3318	1436340
0.4040	1780065
0.4749	2123385

Concentration: 5ppm
Tube: 0.018B

Q (cm^3/s)	ΔP ($dynes/cm^2$)
0.0590	440711
0.1059	785149
0.1506	1129439
0.1947	1473576
0.2384	1817636
0.2804	2161565
0.3249	2505387
0.3634	2849242
0.4039	3193090

Concentration: 10ppm
Tube: 0.004B

Q (cm^3/s)	ΔP ($dynes/cm^2$)
0.00044	375348
0.00083	720086
0.00123	1064822
0.00163	1409554
0.00203	1754286
0.00243	2099015
0.00285	2443740
0.00323	2788463
0.00363	3133179

Concentration: 10ppm
Tube: 0.002A2

Q (cm^3/s)	ΔP ($dynes/cm^2$)
0.00021	1052639
0.00028	1397378
0.00035	1742116
0.00043	2086854
0.00050	2431590
0.00056	2776329
0.00063	3121067

Concentration: 10ppm
Tube: 0.006A1

Q (cm^3/s)	ΔP ($dynes/cm^2$)
0.00295	369766
0.00573	714482
0.00850	1059171
0.01135	1403858
0.01411	1748540
0.01689	2093203
0.01972	2437840
0.02250	2782474
0.02517	3127057

Concentration: 10ppm
Tube: 0.003A2

Q (cm^3/s)	ΔP ($dynes/cm^2$)
0.00023	365399
0.00045	710140
0.00067	1054875
0.00089	1399612
0.00112	1744348
0.00134	2089083
0.00157	2433812
0.00179	2778546
0.00200	3123270

Concentration: 10ppm
Tube: 0.008A2

Q (cm^3/s)	ΔP ($dynes/cm^2$)
0.00836	365490
0.01635	710138
0.02436	1054736
0.03228	1399299
0.04014	1743787
0.04788	2088238
0.05595	2432654
0.06359	2777024
0.07089	3121383

Concentration: 10ppm
Tube: 0.008B2+

Q (cm^3/s)	ΔP ($dynes/cm^2$)
0.00566	374359
0.01094	719042
0.01624	1063693
0.02164	1408316
0.02694	1752900
0.03230	2097412
0.03773	2441876
0.04292	2786346
0.04796	3130435

Concentration: 10ppm
Tube: 0.012C1

Q (cm^3/s)	ΔP ($dynes/cm^2$)
0.0427	730882
0.0629	1075241
0.0828	1419717
0.1026	1764115
0.1219	2108350
0.1411	2452653
0.1591	2796745
0.1767	3140807

Concentration: 10ppm
Tube: 0.008C1

Q (cm^3/s)	ΔP ($dynes/cm^2$)
0.00421	380387
0.00806	725081
0.01199	1069663
0.01590	1414321
0.01980	1758949
0.02373	2103514
0.02787	2447993
0.03166	2792554
0.03551	3137081

Concentration: 10ppm
Tube: 0.012C2

Q (cm^3/s)	ΔP ($dynes/cm^2$)
0.0531	724128
0.0779	1068679
0.1267	1757350
0.1497	2101506
0.1724	2445698
0.1939	2789732
0.2147	3133777

Concentration: 10ppm
Tube: 0.008E

Q (cm^3/s)	ΔP ($dynes/cm^2$)
0.00272	399950
0.00505	744666
0.00739	1089365
0.00977	1434054
0.01214	1778713
0.01462	2123369
0.01706	2468014
0.01944	2812653
0.02178	3157085

Concentration: 10ppm
Tube: 0.012B

Q (cm^3/s)	ΔP ($dynes/cm^2$)
0.0129	414115
0.0240	758763
0.0351	1103391
0.0462	1447961
0.0574	1792487
0.0685	2136980
0.0802	2481473
0.0908	2825949
0.1011	3170358

Concentration: 10ppm
Tube: 0.018A2

Q (cm^3/s)	ΔP ($dynes/cm^2$)
0.1329	386376
0.2443	730262
0.3444	1073788
0.4388	1416883

Concentration: 15ppm
Tube: 0.002B1

Q (cm^3/s)	ΔP ($dynes/cm^2$)
0.00017	1051308
0.00023	1396048
0.00029	1740788
0.00035	2085527
0.00041	2430267
0.00046	2775003
0.00052	3119743

Concentration: 10ppm
Tube: 0.018C1

Q (cm^3/s)	ΔP ($dynes/cm^2$)
0.1802	749207
0.2560	1092995
0.3290	1436340
0.3987	1779820
0.4662	2123357

Concentration: 15ppm
Tube: 0.003A2

Q (cm^3/s)	ΔP ($dynes/cm^2$)
0.00066	1056055
0.00087	1400792
0.00109	1745527
0.00131	2090260
0.00153	2434993
0.00174	2779725
0.00195	3124454

Concentration: 10ppm
Tube: 0.018B

Q (cm^3/s)	ΔP ($dynes/cm^2$)
0.1053	785246
0.1956	1473450
0.2391	1817313
0.2803	2161119
0.3214	2504947
0.3612	2848818
0.4010	3192639

Concentration: 15ppm
Tube: 0.004B

Q (cm^3/s)	ΔP ($dynes/cm^2$)
0.00043	374684
0.00083	719417
0.00123	1064153
0.00163	1408885
0.00202	1753613
0.00242	2098330
0.00284	2443040
0.00322	2787762
0.00363	3132481

Concentration: 15ppm
Tube: 0.006C1

Q (cm^3/s)	ΔP ($dynes/cm^2$)
0.00181	380171
0.00345	724895
0.00505	1069605
0.00670	1414310
0.00838	1758999
0.01003	2103663
0.01175	2448309
0.01351	2792885
0.01511	3137518

Concentration: 15ppm
Tube: 0.008C1

Q (cm^3/s)	ΔP ($dynes/cm^2$)
0.00419	379796
0.00799	724466
0.01180	1069137
0.01566	1413786
0.01947	1758387
0.02340	2102919
0.02739	2447323
0.03106	2791680
0.03486	3136102

Concentration: 15ppm
Tube: 0.008A2

Q (cm^3/s)	ΔP ($dynes/cm^2$)
0.00827	365580
0.01629	710234
0.02395	1054809
0.03177	1399385
0.03950	1743847
0.04714	2088288
0.05500	2432721
0.06254	2777087
0.06983	3121362

Concentration: 15ppm
Tube: 0.012C1

Q (cm^3/s)	ΔP ($dynes/cm^2$)
0.0222	385627
0.0447	730251
0.0616	1074460
0.0810	1418870
0.1010	1763309
0.1203	2107561
0.1400	2451759
0.1581	2795934
0.1748	3139370

Concentration: 15ppm
Tube: 0.008B2+

Q (cm^3/s)	ΔP ($dynes/cm^2$)
0.00562	373039
0.01071	717671
0.01588	1062291
0.02105	1406867
0.02620	1751424
0.03136	2095928
0.03670	2440448
0.04171	2784896
0.046733	3129276

Concentration: 15ppm
Tube: 0.012C2

Q (cm^3/s)	ΔP ($dynes/cm^2$)
0.0274	380012
0.0529	724447
0.0776	1068759
0.1021	1413164
0.1265	1757368
0.1506	2101519
0.1731	2445345
0.1938	2789422
0.2143	3133232

Concentration: 15ppm
Tube: 0.012B

Q (cm^3/s)	ΔP ($dynes/cm^2$)
0.0128	414541
0.0236	759198
0.0347	1103628
0.0458	1448207
0.0569	1792738
0.0679	2137170
0.0795	2481636
0.0900	2825984
0.1007	3170227

Concentration: 15ppm
Tube: 0.018B

Q (cm^3/s)	ΔP ($dynes/cm^2$)
0.0580	441192
0.1044	785643
0.1503	1129919
0.1962	1473964
0.2392	1817720
0.2796	2161552
0.3219	2505138
0.3605	2848994

Concentration: 15ppm
Tube: 0.018A2

Q (cm^3/s)	ΔP ($dynes/cm^2$)
0.1303	386559
0.2414	730273
0.3421	1073465
0.4346	1417096
0.5226	1760529

Concentration: 20ppm
Tube: 0.002B1

Q (cm^3/s)	ΔP ($dynes/cm^2$)
0.00006	363052
0.00011	707793
0.00017	1052534
0.00023	1397275
0.00028	1742015
0.00034	2086755
0.00040	2431495
0.00045	2776234
0.00050	3120974

Concentration: 15ppm
Tube: 0.018C1

Q (cm^3/s)	ΔP ($dynes/cm^2$)
0.0981	405496
0.1813	749773
0.2580	1093642
0.3318	1437082
0.3998	1780405
0.4662	2123544

Concentration: 20ppm
Tube: 0.003A2

Q (cm^3/s)	ΔP ($dynes/cm^2$)
0.00022	365199
0.00044	709939
0.00064	1054677
0.00086	1399414
0.00107	1744149
0.00128	2088883
0.00150	2433612
0.00171	2778339
0.00191	3123071

Concentration: 20ppm
Tube: 0.004B

Q (cm^3/s)	ΔP ($dynes/cm^2$)
0.00082	719771
0.00121	1064508
0.00160	1409243
0.00199	1753973
0.00239	2098701
0.00279	2443419
0.00318	2788140
0.00358	3132859
0.00399	3477575

Concentration: 20ppm
Tube: 0.006A1

Q (cm^3/s)	ΔP ($dynes/cm^2$)
0.00286	368846
0.00553	713560
0.00819	1058257
0.01093	1402964
0.01369	1747614
0.01644	2092264
0.019340	2436908
0.02195	2781494
0.02468	3126082

Concentration: 20ppm
Tube: 0.008A2

Q (cm^3/s)	ΔP ($dynes/cm^2$)
0.00829	366073
0.01612	710747
0.02379	1055364
0.03144	1399929
0.03915	1744423
0.04698	2088905
0.05481	2433257
0.06235	2777643
0.06946	3121727

Concentration: 20ppm
Tube: 0.008B2+

Q (cm^3/s)	ΔP ($dynes/cm^2$)
0.00551	372412
0.01071	717105
0.01583	1061761
0.02108	1406384
0.02625	1750985
0.03148	2095546
0.03688	2440089
0.04190	2784599
0.04696	3129060

Concentration: 20ppm
Tube: 0.008C1

Q (cm^3/s)	ΔP ($dynes/cm^2$)
0.00413	379677
0.00797	724380
0.01174	1069061
0.01572	1413700
0.01962	1758327
0.02339	2102931
0.02745	2447527
0.03121	2792074
0.03501	3136586

Concentration: 20ppm
Tube: 0.012A1

Q (cm^3/s)	ΔP ($dynes/cm^2$)
0.0175	387796
0.0336	732399
0.0493	1076971
0.0650	1421473
0.0810	1765888
0.0964	2110250
0.1132	2454589
0.1279	2798933
0.1430	3143062

Concentration: 20ppm
Tube: 0.012C2

Q (cm^3/s)	ΔP ($dynes/cm^2$)
0.0267	379322
0.0513	723901
0.0756	1068397
0.0999	1412795
0.1236	1757141
0.1474	2101403
0.1943	2789739

Concentration: 20ppm
Tube: 0.018C1

Q (cm^3/s)	ΔP ($dynes/cm^2$)
0.1784	749562
0.2583	1093471
0.3335	1437166
0.4026	1780615

Concentration: 20ppm
Tube: 0.012B

Q (cm^3/s)	ΔP ($dynes/cm^2$)
0.0124	413542
0.0231	758209
0.0340	1102836
0.0450	1447393
0.0561	1791944
0.0668	2136436
0.0780	2480867
0.0885	2825322
0.0995	3169504

Concentration: 20ppm
Tube: 0.018B

Q (cm^3/s)	ΔP ($dynes/cm^2$)
0.1030	786211
0.1494	1130452
0.1952	1474608
0.2398	1818603
0.2827	2162589
0.3255	2506537
0.3631	2850497

Concentration: 20ppm
Tube: 0.018A2

Q (cm^3/s)	ΔP ($dynes/cm^2$)
0.2425	730284
0.3451	1073906
0.4369	1417019

Concentration: 60ppm
Tube: 0.002B1

Q (cm^3/s)	ΔP ($dynes/cm^2$)
0.00005	362886
0.00010	707627
0.00016	1052368
0.00021	1397108
0.00026	1741848
0.00031	2086588
0.00036	2431328
0.00041	2776068
0.00047	3120808

Concentration: 60ppm
Tube: 0.003B1

Q (cm^3/s)	ΔP ($dynes/cm^2$)
0.00027	362714
0.00052	707453
0.00078	1052185
0.00104	1396920
0.00130	1741651
0.00157	2086383
0.00183	2431098
0.00211	2775828
0.00238	3120549

Concentration: 60ppm
Tube: 0.004B

Q (cm^3/s)	ΔP ($dynes/cm^2$)
0.00039	374588
0.00075	719325
0.00111	1064060
0.00146	1408775
0.00182	1753504
0.00220	2098232
0.00258	2442959
0.00294	2787663
0.00331	3132384

Concentration: 60ppm
Tube: 0.006A1

Q (cm^3/s)	ΔP ($dynes/cm^2$)
0.00257	368290
0.00488	712996
0.00727	1057694
0.00984	1402371
0.01243	1747031
0.01506	2091665
0.01777	2436209
0.02037	2780846
0.02293	3125453

Concentration: 60ppm
Tube: 0.006B1

Q (cm^3/s)	ΔP ($dynes/cm^2$)
0.00214	374654
0.00406	719371
0.00600	1064065
0.00807	1408740
0.01021	1753407
0.01229	2098068
0.01450	2442727
0.01662	2787384
0.01876	3132023

Concentration: 60ppm
Tube: 0.006C1

Q (cm^3/s)	ΔP ($dynes/cm^2$)
0.00162	379369
0.00308	724091
0.00451	1068801
0.00600	1413492
0.00752	1758160
0.00910	2102825
0.01081	2447355
0.01240	2792033
0.01397	3136694

Concentration: 60ppm
Tube: 0.008B2$^+$

Q (cm^3/s)	ΔP ($dynes/cm^2$)
0.00503	373872
0.00950	718558
0.01435	1063199
0.01937	1407764
0.02450	1752358
0.02940	2096974
0.03465	2441551
0.03966	2786094
0.04432	3130620

Concentration: 60ppm
Tube: 0.008C1

Q (cm^3/s)	ΔP ($dynes/cm^2$)
0.00381	381301
0.00708	725974
0.01051	1070633
0.01409	1415278
0.01765	1759691
0.02137	2104282
0.02514	2448887
0.02853	2793475
0.03219	3138046

Concentration: 60ppm
Tube: 0.012A1

Q (cm^3/s)	ΔP ($dynes/cm^2$)
0.0192	388512
0.0357	733177
0.0524	1077701
0.0702	1422049
0.0877	1766379
0.1050	2110412
0.1232	2454534

Concentration: 60ppm
Tube: 0.008E

Q (cm^3/s)	ΔP ($dynes/cm^2$)
0.00241	399593
0.00457	744311
0.00660	1089013
0.00874	1433694
0.01094	1778312
0.01314	2122945
0.01640	2467525
0.01774	2812003
0.02002	3156621

Concentration: 60ppm
Tube: 0.012B

Q (cm^3/s)	ΔP ($dynes/cm^2$)
0.0110	412869
0.0208	757542
0.0306	1102170
0.0407	1446782
0.0508	1791361
0.0616	2135602
0.0729	2480079
0.0822	2824542
0.0932	3168950

Concentration: 60ppm
Tube: 0.012C2

Q (cm^3/s)	ΔP ($dynes/cm^2$)
0.0233	377788
0.0454	722369
0.0682	1066892
0.0912	1411325
0.1138	1755706
0.1368	2099946
0.1596	2444216
0.1816	2788436
0.2029	3132463

Concentration: 60ppm
Tube: 0.018A2

Q (cm^3/s)	ΔP ($dynes/cm^2$)
0.1120	387053
0.2159	731008
0.3201	1074369
0.4192	1417757
0.5135	1760774

Concentration: 60ppm
Tube: 0.018C1

Q (cm^3/s)	ΔP ($dynes/cm^2$)
0.0839	405331
0.1567	749542
0.2307	1093467
0.3047	1436980
0.3768	1780178
0.4447	2123522

Concentration: 100ppm
Tube: 0.003A2

Q (cm^3/s)	ΔP ($dynes/cm^2$)
0.00020	365764
0.00039	710504
0.00057	1055243
0.00076	1399980
0.00097	1744716
0.00116	2089452
0.00135	2434187
0.00151	2778920
0.00174	3123653

Concentration: 60ppm
Tube: 0.018B

Q (cm^3/s)	ΔP ($dynes/cm^2$)
0.0519	437826
0.0929	782041
0.1343	1126406
0.1771	1470394
0.2206	1814533
0.2638	2158425
0.3080	2502391
0.3493	2846246

Concentration: 100ppm
Tube: 0.004A1

Q (cm^3/s)	ΔP ($dynes/cm^2$)
0.00111	712335
0.00166	1057063
0.00221	1401790
0.00276	1746515
0.00331	2091241
0.00388	2435966
0.00448	2780662
0.00506	3125374

Concentration: 100ppm
Tube: 0.002B1

Q (cm^3/s)	ΔP ($dynes/cm^2$)
0.00010	708071
0.00014	1052812
0.00019	1397553
0.00023	1742293
0.00028	2087033
0.00033	2431773
0.00038	2776510
0.00042	3121248

Concentration: 100ppm
Tube: 0.006C1

Q (cm^3/s)	ΔP ($dynes/cm^2$)
0.00155	381603
0.00291	726329
0.00425	1071041
0.00569	1415741
0.00716	1760431
0.00864	2105102
0.01038	2449725
0.01190	2794398
0.01341	3139067

Concentration: 100ppm
Tube: 0.006A1

Q (cm^3/s)	ΔP ($dynes/cm^2$)
0.00248	369956
0.00463	714639
0.00690	1059332
0.00949	1404014
0.01199	1748650
0.01459	2093272
0.01718	2437917
0.01964	2782520
0.02209	3127077

Concentration: 100ppm
Tube: 0.008C1

Q (cm^3/s)	ΔP ($dynes/cm^2$)
0.00353	381430
0.00652	726097
0.00974	1070761
0.01320	1415366
0.01669	1759990
0.02020	2104587
0.02381	2449169
0.02729	2793740
0.03059	3138176

Concentration: 100ppm
Tube: 0.008A2

Q (cm^3/s)	ΔP ($dynes/cm^2$)
0.00658	364730
0.01300	709409
0.01991	1054038
0.02673	1398621
0.03389	1743183
0.04075	2087659
0.04778	2432128
0.05461	2776527
0.06126	3120837

Concentration: 100ppm
Tube: 0.008D

Q (cm^3/s)	ΔP ($dynes/cm^2$)
0.00239	400639
0.00446	745364
0.00647	1090084
0.00867	1434762
0.01092	1779458
0.01317	2124124
0.01550	2468780
0.01774	2813465
0.01999	3158155

Concentration: 100ppm
Tube: 0.008B2$^+$

Q (cm^3/s)	ΔP ($dynes/cm^2$)
0.00458	373235
0.00859	717904
0.01321	1062557
0.01792	1407180
0.02250	1751763
0.02742	2096279
0.03242	2440809
0.03703	2785305
0.04166	3129595

Concentration: 100ppm
Tube: 0.012C1

Q (cm^3/s)	ΔP ($dynes/cm^2$)
0.0177	385020
0.0341	729663
0.0513	1074261
0.0690	1418706
0.0866	1763151
0.1042	2107515
0.1220	2451819
0.1394	2796123
0.1557	3140003

Concentration: 100ppm
Tube: 0.012C2

Q (cm^3/s)	ΔP ($dynes/cm^2$)
0.0212	378965
0.0428	723465
0.0646	1067974
0.0850	1412409
0.1068	1756700
0.1280	2100968
0.1511	2445241
0.1716	2789369
0.1906	3132942

Concentration: 100ppm
Tube: 0.018C1

Q (cm^3/s)	ΔP ($dynes/cm^2$)
0.0766	405349
0.1471	749570
0.2177	1093496
0.2874	1437184
0.3556	1780649
0.4251	2123951

Concentration: 100ppm
Tube: 0.012B

Q (cm^3/s)	ΔP ($dynes/cm^2$)
0.0107	414265
0.0384	1448181
0.0482	1792743
0.0581	2137253
0.0683	2481745
0.0778	2826097
0.0871	3170472

Concentration: 100ppm
Tube: 0.018B

Q (cm^3/s)	ΔP ($dynes/cm^2$)
0.0472	441648
0.0855	786093
0.1248	1130448
0.1657	1474698
0.2052	1818712
0.2452	2162616
0.2862	2506264
0.3271	2849974
0.3653	3193617

Concentration: 100ppm
Tube: 0.018A2

Q (cm^3/s)	ΔP ($dynes/cm^2$)
0.1024	387062
0.2005	731094
0.2942	1074954
0.3876	1418198
0.4758	1761062

Concentration: 200ppm
Tube: 0.002B1

Q (cm^3/s)	ΔP ($dynes/cm^2$)
0.00008	705935
0.00012	1050676
0.00020	1740157
0.00024	2084897
0.00028	2429638
0.00033	2774378
0.00038	3119118

Concentration: 200ppm
Tube: 0.003B1

Q (cm^3/s)	ΔP ($dynes/cm^2$)
0.00022	363644
0.00043	708384
0.00063	1053123
0.00084	1397860
0.00108	1742591
0.00130	2087325
0.00154	2432057
0.00176	2776791
0.00197	3121523

Concentration: 200ppm
Tube: 0.008A2

Q (cm^3/s)	ΔP ($dynes/cm^2$)
0.00573	366840
0.01086	711475
0.01670	1056120
0.02259	1400736
0.02855	1745258
0.03451	2089760
0.04080	2434186
0.04647	2778594
0.05241	3123051

Concentration: 200ppm
Tube: 0.004B

Q (cm^3/s)	ΔP ($dynes/cm^2$)
0.00030	376059
0.00060	720796
0.00090	1065495
0.00120	1410230
0.00150	1754962
0.00181	2099692
0.00214	2444421
0.00245	2789158
0.00275	3133876

Concentration: 200ppm
Tube: 0.008C1

Q (cm^3/s)	ΔP ($dynes/cm^2$)
0.00285	381597
0.01097	1415726
0.01388	1760419
0.01687	2105106
0.02005	2449790
0.02315	2794395

Concentration: 200ppm
Tube: 0.006B1

Q (cm^3/s)	ΔP ($dynes/cm^2$)
0.00172	376753
0.00336	721477
0.00838	1755211
0.01013	2099682
0.01195	2444558
0.01374	2789230
0.01551	3133887

Concentration: 200ppm
Tube: 0.008B2$^+$

Q (cm^3/s)	ΔP ($dynes/cm^2$)
0.00389	374862
0.01112	1064276
0.01499	1408927
0.01904	1753594
0.02313	2098258
0.02744	2442870
0.03147	2787488
0.03535	3131982

Concentration: 200ppm
Tube: 0.008E

Q (cm^3/s)	ΔP ($dynes/cm^2$)
0.0183	398754
0.0349	743489
0.0510	1088217
0.0672	1432941
0.0844	1777653
0.1019	2122354
0.1187	2467057
0.1395	2811721
0.1570	3156408

Concentration: 200ppm
Tube: 0.012B

Q (cm^3/s)	ΔP ($dynes/cm^2$)
0.0087	411878
0.0160	756543
0.0239	1101165
0.0323	1445608
0.0407	1790180
0.0498	2134732
0.0583	2479213
0.0665	2823684
0.0750	3168093

Concentration: 200ppm
Tube: 0.012A1

Q (cm^3/s)	ΔP ($dynes/cm^2$)
0.0124	385742
0.0229	730258
0.0344	1074790
0.0469	1419370
0.0586	1763893
0.0717	2108119
0.0849	2452547
0.0963	2796627
0.1081	3140925

Concentration: 200ppm
Tube: 0.018A2

Q (cm^3/s)	ΔP ($dynes/cm^2$)
0.0839	387369
0.1663	731279
0.2435	1075194
0.3227	1418902
0.3993	1762360
0.4664	2105447

Concentration: 200ppm
Tube: 0.012C2

Q (cm^3/s)	ΔP ($dynes/cm^2$)
0.0173	380018
0.0350	724415
0.0529	1068759
0.0712	1413156
0.0900	1757283
0.1088	2101368
0.1278	2445541
0.1463	2789776
0.1617	3133152

Concentration: 200ppm
Tube: 0.018C1

Q (cm^3/s)	ΔP ($dynes/cm^2$)
0.0618	405240
0.1230	749658
0.1835	1093711
0.2448	1437804
0.3037	1781545
0.4163	2125292

Concentration: 200ppm
Tube: 0.018B

Q (cm^3/s)	ΔP ($dynes/cm^2$)
0.0380	441517
0.0708	785866
0.1060	1130315
0.1408	1474555
0.1756	1818716
0.2113	2162330
0.2471	2506290
0.2807	2850184
0.3143	3193876

Flow of Polyox FRA Solutions in Untreated Tubes

Concentration: 15ppm
Tube: 0.002B1

Q (cm^3/s)	ΔP ($dynes/cm^2$)
0.00006	363186
0.00012	707927
0.00018	1052668
0.00023	1397408
0.00029	1742148
0.00035	2086889
0.00041	2431629
0.00046	2776368
0.00052	3121108

Concentration: 15ppm
Tube: 0.006C1

Q (cm^3/s)	ΔP ($dynes/cm^2$)
0.00182	380529
0.00348	725252
0.00516	1069971
0.00686	1414685
0.00849	1759388
0.01017	2104083
0.01194	2448756
0.01366	2793419
0.01527	3138083

Concentration: 15ppm
Tube: 0.003A2

Q (cm^3/s)	ΔP ($dynes/cm^2$)
0.00023	365305
0.00045	710045
0.00067	1054784
0.00090	1399517
0.00112	1744252
0.00133	2088984
0.00157	2433715
0.00178	2778449
0.00199	3123179

Concentration: 15ppm
Tube: 0.008A2

Q (cm^3/s)	ΔP ($dynes/cm^2$)
0.00820	366525
0.02351	1055777
0.03126	1400265
0.03900	1744769
0.04663	2089272
0.05531	2433714
0.06292	2778157
0.07019	3122443

Concentration: 15ppm
Tube: 0.004B

Q (cm^3/s)	ΔP ($dynes/cm^2$)
0.00043	375276
0.00083	720015
0.00123	1064751
0.00163	1409486
0.00203	1754217
0.00241	2098947
0.00285	2443676
0.00324	2788400
0.00364	3133125

Concentration: 15ppm
Tube: 0.008C1

Q (cm^3/s)	ΔP ($dynes/cm^2$)
0.00416	381219
0.00799	725930
0.01187	1070614
0.01579	1415268
0.01970	1759914
0.02365	2104539
0.02763	2449138
0.03152	2793676
0.03529	3138240

Concentration: 15ppm
Tube: 0.008B2+

Q (cm^3/s)	ΔP ($dynes/cm^2$)
0.00560	374077
0.01083	718766
0.01612	1063433
0.02133	1408067
0.02663	1752681
0.03190	2097258
0.03744	2441810
0.04253	2786332
0.04750	3130783

Concentration: 15ppm
Tube: 0.012B

Q (cm^3/s)	ΔP ($dynes/cm^2$)
0.0128	414383
0.0236	759061
0.0345	1103705
0.0456	1448332
0.0566	1792891
0.0679	2137398
0.0792	2481877
0.0900	2826355
0.1004	3170775

Concentration: 15ppm
Tube: 0.012A2

Q (cm^3/s)	ΔP ($dynes/cm^2$)
0.0257	377442
0.0494	722028
0.0723	1066541
0.0955	1411010
0.1187	1755385
0.1407	2099701
0.1831	2788086
0.2024	3132066

Concentration: 15ppm
Tube: 0.018A2

Q (cm^3/s)	ΔP ($dynes/cm^2$)
0.1326	386891
0.2475	730919
0.3474	1074568
0.4394	1417734
0.5302	1760908

Concentration: 15ppm
Tube: 0.012C1

Q (cm^3/s)	ΔP ($dynes/cm^2$)
0.0223	386724
0.0426	731340
0.0625	1075886
0.0826	1420366
0.1024	1764778
0.1222	2109145
0.1422	2453437
0.1607	2797709
0.1784	3141825

Concentration: 15ppm
Tube: 0.018C1

Q (cm^3/s)	ΔP ($dynes/cm^2$)
0.0977	405576
0.1808	749843
0.2595	1093719
0.3327	1437487
0.4011	1781038
0.4675	2124503
0.5361	2468024

Concentration: 15ppm
Tube: 0.018B

Q (cm^3/s)	ΔP ($dynes/cm^2$)
0.0583	441986
0.1050	786385
0.1511	1130689
0.1974	1474887
0.2403	1818726
0.2819	2161924
0.3243	2506140
0.3627	2849768
0.3988	3193549

Concentration: 30ppm
Tube: 0.004B

Q (cm^3/s)	ΔP ($dynes/cm^2$)
0.00042	376670
0.00080	721408
0.00118	1066143
0.00156	1410877
0.00195	1755606
0.00234	2100337
0.00275	2445067
0.00314	2789791
0.00352	3134514

Concentration: 30ppm
Tube: 0.002B1

Q (cm^3/s)	ΔP ($dynes/cm^2$)
0.00011	707528
0.00017	1052269
0.00022	1397009
0.00028	1741749
0.00033	2086488
0.00039	2431227
0.00044	2775965
0.00050	3120704

Concentration: 30ppm
Tube: 0.006C1

Q (cm^3/s)	ΔP ($dynes/cm^2$)
0.00173	381622
0.00334	726348
0.00493	1071065
0.00651	1415761
0.00814	1760463
0.00977	2105150
0.01156	2449809
0.01313	2794463
0.01480	3139083

Concentration: 30ppm
Tube: 0.003A2

Q (cm^3/s)	ΔP ($dynes/cm^2$)
0.00022	364872
0.00044	709606
0.00086	1399077
0.00107	1743812
0.00128	2088546
0.00150	2433276
0.00172	2778007
0.00193	3122737

Concentration: 30ppm
Tube: 0.008A2

Q (cm^3/s)	ΔP ($dynes/cm^2$)
0.00766	365998
0.01465	710673
0.02201	1055306
0.02982	1399901
0.03741	1744329
0.04507	2088828
0.05293	2433283
0.06040	2777677
0.06741	3121886

Concentration: 30ppm
Tube: 0.008B2+

Q (cm^3/s)	ΔP ($dynes/cm^2$)
0.00538	374559
0.01028	719294
0.01526	1063962
0.02038	1408594
0.02559	1753188
0.03066.	2097726
0.03630	2442272
0.04130	2786749
0.04630	3131199

Concentration: 30ppm
Tube: 0.012A2

Q (cm^3/s)	ΔP ($dynes/cm^2$)
0.0246	377536
0.0460	722121
0.0686	1066679
0.0915	1411191
0.1139	1755618
0.1365	2099944
0.1598	2444269
0.1796	2788508
0.2014	3132662

Concentration: 30ppm
Tube: 0.008C1

Q (cm^3/s)	ΔP ($dynes/cm^2$)
0.00404	382349
0.00772	727000
0.01134	1071639
0.01513	1416280
0.01890	1760886
0.02276	2105469
0.02673	2450005
0.03046	2794519
0.03430	3139040

Concentration: 30ppm
Tube: 0.012B

Q (cm^3/s)	ΔP ($dynes/cm^2$)
0.0123	414803
0.0230	759459
0.0337	1104107
0.0442	1448707
0.0549	1793243
0.0659	2137753
0.0767	2482239
0.0875	2826695
0.0982	3171133

Concentration: 30ppm
Tube: 0.012C1

Q (cm^3/s)	ΔP ($dynes/cm^2$)
0.0214	386658
0.0409	731293
0.0591	1075837
0.0788	1420322
0.0982	1764738
0.1181	2109215
0.1376	2453532
0.1565	2797787
0.1746	3141888

Concentration: 30ppm
Tube: 0.018A2

Q (cm^3/s)	ΔP ($dynes/cm^2$)
0.1281	387501
0.2398	731595
0.3417	1075322
0.4435	1418284
0.5413	1761173

Concentration: 30ppm
Tube: 0.018C1

Q (cm^3/s)	ΔP ($dynes/cm^2$)
0.0934	405656
0.1735	749940
0.2508	1093885
0.3298	1437022
0.4059	1780663
0.4771	2123973

Concentration: 60ppm
Tube: 0.003A2

Q (cm^3/s)	ΔP ($dynes/cm^2$)
0.00021	363923
0.00040	708662
0.00059	1053401
0.00079	1398139
0.00099	1742876
0.00118	2087612
0.00139	2432349
0.00160	2777082
0.00180	3121815

Concentration: 30ppm
Tube: 0.018B

Q (cm^3/s)	ΔP ($dynes/cm^2$)
0.0560	441886
0.1011	786301
0.1457	1130579
0.1911	1474747
0.2373	1818695
0.2819	2162553
0.3266	2506335
0.3697	2850167
0.4112	3193789

Concentration: 60ppm
Tube: 0.004B

Q (cm^3/s)	ΔP ($dynes/cm^2$)
0.00040	376898
0.00076	721637
0.00111	1066374
0.00146	1411110
0.00183	1755843
0.00220	2100575
0.00259	2445304
0.00297	2790022
0.00333	3134747

Concentration: 60ppm
Tube: 0.002B1

Q (cm^3/s)	ΔP ($dynes/cm^2$)
0.00011	706765
0.00020	1396247
0.00025	1740988
0.00031	2085729
0.00036	2430469
0.00041	2775210
0.00046	3119949

Concentration: 60ppm
Tube: 0.006C1

Q (cm^3/s)	ΔP ($dynes/cm^2$)
0.00166	382143
0.00313	726871
0.00460	1071588
0.00606	1416308
0.00761	1761017
0.00914	2105706
0.01098	2450379
0.01255	2795053
0.01411	3139703

Concentration: 60ppm
Tube: 0.008A2

Q (cm^3/s)	ΔP ($dynes/cm^2$)
0.00707	367106
0.01407	711632
0.02112	1056299
0.02872	1400809
0.03589	1745364
0.04329	2089875
0.05070	2434394
0.05740	2778822
0.06438	3123282

Concentration: 60ppm
Tube: 0.012C1

Q (cm^3/s)	ΔP ($dynes/cm^2$)
0.0197	385781
0.0373	730440
0.0555	1075029
0.0742	1419529
0.0929	1763949
0.1120	2108398
0.1308	2452770
0.1482	2797113
0.1654	3141374

Concentration: 60ppm
Tube: 0.008B2+

Q (cm^3/s)	ΔP ($dynes/cm^2$)
0.00501	374555
0.00948	719270
0.01434	1063949
0.01936	1408559
0.02435	1753205
0.02939	2097801
0.03458	2442399
0.03936	2786971
0.04430	3131476

Concentration: 60ppm
Tube: 0.012A2

Q (cm^3/s)	ΔP ($dynes/cm^2$)
0.0221	377329
0.0432	721905
0.0642	1066418
0.0861	1410871
0.1076	1755292
0.1287	2099685
0.1504	2443977
0.1708	2788266
0.1914	3132453

Concentration: 60ppm
Tube: 0.008C1

Q (cm^3/s)	ΔP ($dynes/cm^2$)
0.00384	381762
0.00716	726463
0.01064	1071160
0.01430	1415850
0.01793	1760511
0.02164	2105145
0.02554	2449761
0.02917	2794338
0.03273	3138913

Concentration: 60ppm
Tube: 0.012B

Q (cm^3/s)	ΔP ($dynes/cm^2$)
0.0117	414886
0.0212	759562
0.0310	1104217
0.0413	1448848
0.0517	1793435
0.0621	2137960
0.0731	2482503
0.0832	2827012
0.0933	3171410

Concentration: 60ppm
Tube: 0.018A2

Q (cm^3/s)	ΔP ($dynes/cm^2$)
0.1111	387092
0.2164	731229
0.3163	1075068
0.4143	1418729
0.5105	1762042

Concentration: 100ppm
Tube: 0.002B1

Q (cm^3/s)	ΔP ($dynes/cm^2$)
0.00005	360235
0.00010	704976
0.00015	1049717
0.00020	1394458
0.00024	1739199
0.00029	2083939
0.00034	2428680
0.00038	2773420
0.00044	3118157

Concentration: 60ppm
Tube: 0.018C1

Q (cm^3/s)	ΔP ($dynes/cm^2$)
0.0880	405461
0.1582	749793
0.2347	1093480
0.3091	1437111
0.3825	1780769
0.4540	2124130
0.5269	2467838

Concentration: 100ppm
Tube: 0.003A2

Q (cm^3/s)	ΔP ($dynes/cm^2$)
0.00020	361661
0.00038	706402
0.00055	1051139
0.00073	1395876
0.00093	1740614
0.00112	2085349
0.00131	2430084
0.00151	2774820
0.00171	3119553

Concentration: 60ppm
Tube: 0.018B

Q (cm^3/s)	ΔP ($dynes/cm^2$)
0.0524	441625
0.0924	786076
0.1346	1130422
0.1774	1474662
0.2211	1818763
0.2630	2162582
0.3076	2506498
0.3488	2850224
0.3910	3193969

Concentration: 100ppm
Tube: 0.004B

Q (cm^3/s)	ΔP ($dynes/cm^2$)
0.00036	375746
0.00070	720485
0.00103	1065221
0.00137	1409956
0.00168	1754687
0.00202	2099419
0.00240	2444148
0.00275	2788874
0.00310	3133592

Concentration: 100ppm
Tube: 0.006A1

Q (cm^3/s)	ΔP ($dynes/cm^2$)
0.00248	370413
0.00458	715134
0.00697	1059849
0.00934	1404552
0.01182	1749251
0.01438	2093925
0.01684	2438593
0.01935	2783260
0.02164	3127915

Concentration: 100ppm
Tube: 0.008A2

Q (cm^3/s)	ΔP ($dynes/cm^2$)
0.00617	366471
0.01256	711169
0.01893	1055827
0.02562	1400451
0.03242	1745038
0.03880	2089598
0.04565	2434135
0.05169	2778637
0.05793	3123061

Concentration: 100ppm
Tube: 0.006B1

Q (cm^3/s)	ΔP ($dynes/cm^2$)
0.00200	375731
0.00378	720454
0.00558	1065165
0.00755	1409869
0.00957	1754561
0.01159	2099256
0.01376	2443876
0.01573	2788530
0.01775	3133165

Concentration: 100ppm
Tube: 0.008B2$^+$

Q (cm^3/s)	ΔP ($dynes/cm^2$)
0.00457	374789
0.00862	719496
0.01307	1064167
0.01773	1408819
0.02227	1753445
0.02715	2098056
0.03203	2442646
0.03652	2787193
0.04109	3131730

Concentration: 100ppm
Tube: 0.006C1

Q (cm^3/s)	ΔP ($dynes/cm^2$)
0.00151	381212
0.00287	725941
0.00417	1070660
0.00561	1415367
0.00708	1760075
0.00859	2104775
0.01021	2449428
0.01166	2794115
0.01319	3138790

Concentration: 100ppm
Tube: 0.008C1

Q (cm^3/s)	ΔP ($dynes/cm^2$)
0.00351	381718
0.00649	726430
0.00969	1071127
0.01311	1415808
0.01645	1760469
0.02005	2105113
0.02368	2449715
0.02713	2794278
0.03045	3138861

Concentration: 100ppm
Tube: 0.012C1

Q (cm^3/s)	ΔP ($dynes/cm^2$)
0.0171	386597
0.0336	731244
0.0507	1075786
0.0679	1420259
0.0857	1764626
0.1026	2108969
0.1206	2453371
0.1369	2797735
0.1520	3141757

Concentration: 100ppm
Tube: 0.018A2

Q (cm^3/s)	ΔP ($dynes/cm^2$)
0.1006	386821
0.1959	731125
0.2864	1075086
0.3759	1418702
0.4652	1762289

Concentration: 100ppm
Tube: 0.012A2

Q (cm^3/s)	ΔP ($dynes/cm^2$)
0.0190	377795
0.0382	722430
0.0586	1067000
0.0790	1411407
0.0992	1755886
0.1195	2100280
0.1396	2444574
0.1565	2788780
0.1735	3132961

Concentration: 100ppm
Tube: 0.018C1

Q (cm^3/s)	ΔP ($dynes/cm^2$)
0.0757	405805
0.1473	750169
0.2169	1094266
0.2860	1437953
0.3538	1781614
0.4233	2125153
0.4909	2468542

Concentration: 100ppm
Tube: 0.012B

Q (cm^3/s)	ΔP ($dynes/cm^2$)
0.0105	414463
0.0189	759161
0.0279	1103817
0.0378	1448449
0.0477	1793027
0.0574	2137593
0.0675	2482125
0.0771	2826654
0.0866	3171068

Concentration: 100ppm
Tube: 0.018B

Q (cm^3/s)	ΔP ($dynes/cm^2$)
0.0474	441927
0.0852	786456
0.1250	1130440
0.1648	1474743
0.2063	1818845
0.2451	2162871
0.2874	2506763
0.3252	2850430
0.3625	3194045

Concentration: 130ppm
Tube: 0.002B1

Q (cm^3/s)	ΔP ($dynes/cm^2$)
0.00005	364086
0.00009	708827
0.00014	1053568
0.00019	1398309
0.00024	1743049
0.00028	2087789
0.00033	2432529
0.00038	2777268
0.00043	3122008

Concentration: 130ppm
Tube: 0.003A2

Q (cm^3/s)	ΔP ($dynes/cm^2$)
0.00018	362414
0.00036	707154
0.00053	1051893
0.00069	1396631
0.00086	1741369

Concentration: 130ppm
Tube: 0.004B

Q (cm^3/s)	ΔP ($dynes/cm^2$)
0.00033	372452
0.00064	717190
0.00095	1061926
0.00127	1406662
0.00159	1751396
0.00192	2096128
0.00224	2440859
0.00258	2785589
0.00291	3130317

Concentration: 130ppm
Tube: 0.006C1

Q (cm^3/s)	ΔP ($dynes/cm^2$)
0.00146	382107
0.00277	726834
0.00399	1071554
0.00532	1416271
0.00676	1760966
0.00824	2105656
0.00980	2450349
0.01120	2795030
0.01259	3139716

Concentration: 130ppm
Tube: 0.008A2

Q (cm^3/s)	ΔP ($dynes/cm^2$)
0.00596	365967
0.01204	710621
0.01800	1055279
0.02508	1399922
0.03160	1744538
0.03811	2089105
0.04524	2433618
0.05146	2778117
0.05766	3122564

Concentration: 130ppm
Tube: $0.008B2^+$

Q (cm^3/s)	ΔP ($dynes/cm^2$)
0.00447	374532
0.00819	719231
0.01255	1063920
0.01688	1408589
0.02141	1753234
0.02584	2097825
0.03054	2442402
0.03498	2786963
0.03933	3131475

Concentration: 130ppm
Tube: 0.008C1

Q (cm^3/s)	ΔP ($dynes/cm^2$)
0.00333	381994
0.00617	726707
0.00923	1071408
0.01246	1416091
0.01582	1760766
0.01908	2105426
0.02265	2450019
0.02586	2794637
0.02910	3139230

Concentration: 130ppm
Tube: 0.012B

Q (cm^3/s)	ΔP ($dynes/cm^2$)
0.0101	414570
0.0182	759251
0.0270	1103911
0.0361	1448542
0.0453	1793150
0.0544	2137739
0.0643	2482291
0.0737	2826841
0.0828	3171386

Concentration: 130ppm
Tube: 0.012C1

Q (cm^3/s)	ΔP ($dynes/cm^2$)
0.0161	386508
0.0320	731086
0.0480	1075673
0.0643	1420248
0.0809	1764617
0.0974	2108469
0.1146	2452917
0.1312	2797320
0.1474	3141658

Concentration: 130ppm
Tube: 0.018A2

Q (cm^3/s)	ΔP ($dynes/cm^2$)
0.0941	387152
0.1854	731286
0.2740	1075385
0.3574	1418925
0.4446	1762330

Concentration: 130ppm
Tube: 0.012A2

Q (cm^3/s)	ΔP ($dynes/cm^2$)
0.0182	376957
0.0364	721595
0.0553	1066170
0.0744	1410686
0.0939	1755210
0.1132	2099697
0.1318	2444069
0.1498	2788456
0.1648	3132746

Concentration: 130ppm
Tube: 0.018C1

Q (cm^3/s)	ΔP ($dynes/cm^2$)
0.0702	405604
0.1369	749953
0.2017	1094157
0.2691	1438081
0.3309	1781871
0.3934	2125378
0.4567	2468894

Concentration: 130ppm
Tube: 0.018B

Q (cm^3/s)	ΔP ($dynes/cm^2$)
0.0433	441894
0.0793	786246
0.1168	1130396
0.1552	1474680
0.1934	1818875
0.2329	2162851
0.2722	2506832
0.3076	2850589
0.3467	3194387

Flow of Polyox WSR 301 Solutions in Silane-Treated Tubes

Concentration: 15ppm
Tube: 0.002B2

Q (cm^3/s)	ΔP ($dynes/cm^2$)
0.00012	709594
0.00018	1054335
0.00024	1399076
0.00030	1743816
0.00036	2088557
0.00042	2433297
0.00048	2778035
0.00053	3122775

Concentration: 15ppm
Tube: 0.006B2

Q (cm^3/s)	ΔP ($dynes/cm^2$)
0.00257	374816
0.00493	719536
0.00727	1064240
0.00961	1408910
0.01200	1753597
0.01436	2098275
0.01681	2442953
0.01916	2787624
0.02148	3132268

Concentration: 15ppm
Tube: 0.003C1

Q (cm^3/s)	ΔP ($dynes/cm^2$)
0.00055	712017
0.00083	1056756
0.00110	1401493
0.00137	1746227
0.00164	2090962
0.00190	2435695
0.00217	2780425
0.00243	3125156

Concentration: 15ppm
Tube: 0.008C2

Q (cm^3/s)	ΔP ($dynes/cm^2$)
0.00672	368926
0.01304	713487
0.01917	1058139
0.02554	1402763
0.03185	1747363
0.03805	2091965
0.04445	2436543
0.05032	2781099
0.05638	3125621

Concentration: 15ppm
Tube: 0.004C

Q (cm^3/s)	ΔP ($dynes/cm^2$)
0.00047	376702
0.00089	721440
0.00130	1066177
0.00173	1410910
0.00216	1755640
0.00258	2100372
0.00302	2445100
0.00343	2789830
0.00384	3134551

Concentration: 15ppm
Tube: 0.008B1

Q (cm^3/s)	ΔP ($dynes/cm^2$)
0.00536	374780
0.01026	719480
0.01512	1064159
0.02000	1408829
0.02506	1753481
0.02995	2098108
0.03501	2442713
0.03976	2787293
0.04430	3131849

Concentration: 15ppm
Tube: 0.008G

Q (cm^3/s)	ΔP ($dynes/cm^2$)
0.00287	401890
0.00531	746612
0.00773	1091288
0.01014	1435984
0.01254	1780671
0.01499	2125336
0.01764	2469974
0.01995	2814613
0.02237	3159239

Concentration: 15ppm
Tube: 0.012D

Q (cm^3/s)	ΔP ($dynes/cm^2$)
0.0132	414343
0.0241	759016
0.0348	1103672
0.0456	1448298
0.0564	1792866
0.0670	2137367
0.0784	2481905
0.0887	2826270
0.0994	3170748

Concentration: 15ppm
Tube: 0.012E2*

Q (cm^3/s)	ΔP ($dynes/cm^2$)
0.0292	377144
0.0556	721706
0.0814	1066220
0.1065	1410669
0.1312	1754829
0.1547	2098935
0.1783	2443202
0.2002	2787300
0.2205	3131383

Concentration: 15ppm
Tube: 0.018A1

Q (cm^3/s)	ΔP ($dynes/cm^2$)
0.0908	405998
0.1659	750332
0.2363	1094498
0.3037	1438261
0.3682	1781919
0.4306	2125555
0.4940	2469094

Concentration: 15ppm
Tube: 0.012E1

Q (cm^3/s)	ΔP ($dynes/cm^2$)
0.0214	388103
0.0401	732747
0.0589	1077351
0.0772	1421855
0.0956	1766273
0.1136	2110613
0.1308	2455002

Concentration: 15ppm
Tube: 0.018C2

Q (cm^3/s)	ΔP ($dynes/cm^2$)
0.1393	387700
0.2559	731931
0.3585	1075924
0.4570	1419579
0.5509	1762994

Concentration: 15ppm
Tube: 0.018D

Q (cm^3/s)	ΔP ($dynes/cm^2$)
0.0649	441086
0.1149	785498
0.1632	1129855
0.2099	1474040
0.2557	1819836
0.3001	2162095
0.3442	2505611
0.3864	2849194

Concentration: 20ppm
Tube: 0.004C

Q (cm^3/s)	ΔP ($dynes/cm^2$)
0.00045	376046
0.00087	720785
0.00128	1065520
0.00170	1410255
0.00212	1754987
0.00254	2099717
0.00298	2444445
0.00339	2789168
0.00379	3133884

Concentration: 20ppm
Tube: 0.002B2

Q (cm^3/s)	ΔP ($dynes/cm^2$)
0.00006	363494
0.00012	708236
0.00018	1052977
0.00023	1397718
0.00035	2087198
0.00041	2431938
0.00053	3121416

Concentration: 20ppm
Tube: 0.006B2

Q (cm^3/s)	ΔP ($dynes/cm^2$)
0.00253	375820
0.00485	720527
0.00716	1065235
0.00947	1409894
0.01178	1754587
0.01419	2099274
0.01656	2443940
0.01891	2788600
0.02115	3133220

Concentration: 20ppm
Tube: 0.003C1

Q (cm^3/s)	ΔP ($dynes/cm^2$)
0.00028	365809
0.00054	710548
0.00080	1055285
0.00107	1400018
0.00133	1744749
0.00159	2089478
0.00186	2434208
0.00212	2778937
0.00238	3123669

Concentration: 20ppm
Tube: 0.008C2

Q (cm^3/s)	ΔP ($dynes/cm^2$)
0.00669	370981
0.01295	715666
0.01920	1060314
0.02542	1404944
0.03158	1749480
0.03775	2094030
0.04408	2438548
0.05015	2783071
0.05605	3127595

Concentration: 20ppm
Tube: 0.008B1

Q (cm^3/s)	ΔP ($dynes/cm^2$)
0.00521	375862
0.00995	720554
0.01472	1065247
0.01937	1409924
0.02426	1754545
0.02906	2099125
0.03405	2443724
0.03875	2788294
0.04337	3132717

Concentration: 20ppm
Tube: 0.012E1

Q (cm^3/s)	ΔP ($dynes/cm^2$)
0.0212	387246
0.0399	731889
0.0588	1076476
0.0771	1420993
0.0957	1765434
0.1137	2109830
0.1322	2453821
0.1488	2798102
0.1652	3142401

Concentration: 20ppm
Tube: 0.008A1

Q (cm^3/s)	ΔP ($dynes/cm^2$)
0.00383	386551
0.00723	731258
0.01066	1075935
0.01414	1420570
0.01757	1765217
0.02103	2109825
0.02466	2454424
0.02806	2799040
0.03151	3143619

Concentration: 20ppm
Tube: 0.012D

Q (cm^3/s)	ΔP ($dynes/cm^2$)
0.0130	414380
0.0238	759049
0.0345	1103688
0.0453	1448281
0.0563	1792849
0.0667	2137350
0.0781	2481884
0.0889	2826415
0.0995	3170850

Concentration: 20ppm
Tube: 0.012E2"

Q (cm^3/s)	ΔP ($dynes/cm^2$)
0.0282	376860
0.0536	721448
0.0785	1066012
0.1030	1410522
0.1270	1754578
0.1495	2098909
0.2011	2786839
0.2224	3130860

Concentration: 20ppm
Tube: 0.018A1

Q (cm^3/s)	ΔP ($dynes/cm^2$)
0.0903	406738
0.1657	751139
0.2370	1095257
0.3045	1439243
0.3678	1782905
0.4299	2126341
0.4924	2469933

Concentration: 20ppm
Tube: 0.018C2

Q (cm^3/s)	ΔP ($dynes/cm^2$)
0.1396	387404
0.2563	731554
0.3581	1075354
0.4573	1419069
0.5481	1762362

Concentration: 60ppm
Tube: 0.003C1

Q (cm^3/s)	ΔP ($dynes/cm^2$)
0.00026	366423
0.00050	711162
0.00074	1055901
0.00098	1400639
0.00122	1745374
0.00147	2090106
0.00172	2434841
0.00196	2779573
0.00221	3124306

Concentration: 20ppm
Tube: 0.018D

Q (cm^3/s)	ΔP ($dynes/cm^2$)
0.0645	441414
0.1152	785877
0.1634	1130117
0.2106	1474349
0.2564	1818388
0.3011	2162359
0.3445	2506085
0.3864	2849796
0.4268	3193654

Concentration: 60ppm
Tube: 0.004C

Q (cm^3/s)	ΔP ($dynes/cm^2$)
0.00042	376017
0.00082	720756
0.00120	1065493
0.00159	1410227
0.00197	1754961
0.00237	2099693
0.00277	2444423
0.00316	2789152
0.00355	3133879

Concentration: 60ppm
Tube: 0.002B2

Q (cm^3/s)	ΔP ($dynes/cm^2$)
0.00012	709575
0.00017	1054315
0.00022	1399056
0.00039	2433272
0.00044	2778009
0.00050	3122748

Concentration: 60ppm
Tube: 0.006B2

Q (cm^3/s)	ΔP ($dynes/cm^2$)
0.00239	377084
0.00459	721807
0.00672	1066525
0.00887	1411213
0.01107	1755911
0.01323	2100552
0.01549	2445238
0.01770	2789895
0.01995	3134546

Concentration: 60ppm
Tube: 0.008C2

Q (cm^3/s)	ΔP ($dynes/cm^2$)
0.00624	371264
0.01187	715963
0.01747	1060631
0.02315	1405276
0.02902	1749896
0.03494	2094506
0.04101	2439063
0.04682	2783584
0.05238	3128110

Concentration: 60ppm
Tube: 0.012E2*

Q (cm^3/s)	ΔP ($dynes/cm^2$)
0.0271	376997
0.0515	721620
0.0758	1066180
0.1002	1410651
0.1245	1755069
0.1479	2099344
0.1727	2443690
0.1966	2787887
0.2188	3132105

Concentration: 60ppm
Tube: 0.008A1

Q (cm^3/s)	ΔP ($dynes/cm^2$)
0.00357	386493
0.00678	731207
0.00992	1075906
0.01312	1420595
0.01631	1765256
0.01961	2109906
0.02297	2454547
0.02614	2799161
0.02942	3143748

Concentration: 60ppm
Tube: 0.012E1

Q (cm^3/s)	ΔP ($dynes/cm^2$)
0.0195	388186
0.0372	732842
0.0545	1077408
0.0721	1421942
0.0881	1766400
0.1057	2110792
0.1244	2454948
0.1417	2799151
0.1587	3143382

Concentration: 60ppm
Tube: 0.008G

Q (cm^3/s)	ΔP ($dynes/cm^2$)
0.00261	401464
0.00485	746189
0.00712	1090895
0.00942	1435569
0.01158	1780262
0.01385	2124939
0.01615	2469604
0.01849	2814250
0.02071	3158837

Concentration: 60ppm
Tube: 0.012D*

Q (cm^3/s)	ΔP ($dynes/cm^2$)
0.0129	408439
0.0240	753123
0.0350	1097772
0.0463	1442396
0.0577	1786989
0.0690	2131534
0.0803	2476020
0.0911	2820564
0.1025	3165026

Concentration: 60ppm
Tube: 0.018A1

Q (cm^3/s)	ΔP ($dynes/cm^2$)
0.0838	406377
0.1557	750644
0.2267	1094804
0.2973	1438596
0.3682	1782311
0.4361	2125958

Concentration: 100ppm
Tube: 0.002C1

Q (cm^3/s)	ΔP ($dynes/cm^2$)
0.00005	366868
0.00009	711610
0.00014	1056351
0.00018	1401092
0.00023	1745833
0.00028	2090573
0.00032	2435313
0.00037	2780053
0.00041	3124793

Concentration: 60ppm
Tube: 0.018C2

Q (cm^3/s)	ΔP ($dynes/cm^2$)
0.1314	388058
0.2450	732203
0.3559	1076137
0.4630	1419640

Concentration: 100ppm
Tube: 0.003C1

Q (cm^3/s)	ΔP ($dynes/cm^2$)
0.00024	366108
0.00048	710848
0.00070	1055584
0.00093	1400320
0.00115	1745057
0.00139	2089792
0.00163	2434528
0.00184	2779263
0.00208	3123994

Concentration: 60ppm
Tube: 0.018D

Q (cm^3/s)	ΔP ($dynes/cm^2$)
0.0593	441722
0.1064	786237
0.1536	1130546
0.2003	1474700
0.2475	1818590
0.2961	2162471
0.3446	2506089
0.3899	2849548
0.4325	3193284

Concentration: 100ppm
Tube: 0.004D1

Q (cm^3/s)	ΔP ($dynes/cm^2$)
0.00072	367169
0.00139	711906
0.00204	1056641
0.00270	1401372
0.00336	1746100
0.00405	2090823
0.00479	2435545
0.00545	2780264
0.00616	3124979

Concentration: 100ppm
Tube: 0.006C2

Q (cm^3/s)	ΔP ($dynes/cm^2$)
0.00247	371003
0.00472	715724
0.00691	1060429
0.00925	1405114
0.01156	1749795
0.01406	2094466
0.01653	2439096
0.01890	2783738
0.02124	3128366

Concentration: 100ppm
Tube: 0.008A1

Q (cm^3/s)	ΔP ($dynes/cm^2$)
0.00329	386473
0.00625	731190
0.00907	1075884
0.01202	1420575
0.01510	1765235
0.01813	2109898
0.02150	2454504
0.02454	2799140
0.02766	3143766

Concentration: 100ppm
Tube: 0.008C2

Q (cm^3/s)	ΔP ($dynes/cm^2$)
0.00584	370144
0.01088	714835
0.01610	1059516
0.02179	1404175
0.02736	1748793
0.03304	2093368
0.03889	2437939
0.04422	2782486
0.04965	3126994

Concentration: 100ppm
Tube: 0.012E2*

Q (cm^3/s)	ΔP ($dynes/cm^2$)
0.0253	376626
0.0459	721229
0.0678	1065733
0.0903	1410174
0.1135	1754546
0.1366	2098854
0.1602	2443214
0.1820	2787149
0.2022	3130945

Concentration: 100ppm
Tube: 0.008B1

Q (cm^3/s)	ΔP ($dynes/cm^2$)
0.00456	376253
0.00862	720960
0.01255	1065646
0.01683	1410266
0.02113	1754894
0.02571	2099522
0.03030	2444075
0.03450	2788669
0.03894	3133127

Concentration: 100ppm
Tube: 0.012E1

Q (cm^3/s)	ΔP ($dynes/cm^2$)
0.0183	388347
0.0339	732989
0.0498	1077595
0.0662	1422140
0.0828	1766573
0.0998	2110932
0.1168	2455067
0.1327	2799371
0.1494	3143535

Concentration: 100ppm
Tube: 0.012D*

Q (cm^3/s)	ΔP ($dynes/cm^2$)
0.0121	408341
0.0226	753024
0.0325	1097648
0.0429	1442251
0.0538	1786791
0.0642	2131276
0.0752	2475812
0.0859	2820220
0.0966	3164691

Concentration: 100ppm
Tube: 0.018D

Q (cm^3/s)	ΔP ($dynes/cm^2$)
0.0554	441319
0.1001	785806
0.1443	1130187
0.1894	1474327
0.2311	1818225
0.2766	2161981
0.3232	2505298
0.3661	2849067
0.4093	3192903

Concentration: 100ppm
Tube: 0.018A1

Q (cm^3/s)	ΔP ($dynes/cm^2$)
0.0790	406434
0.1470	750731
0.2136	1094737
0.2752	1438700
0.3435	1782358
0.4103	2125788

Concentration: 200ppm
Tube: 0.002C1

Q (cm^3/s)	ΔP ($dynes/cm^2$)
0.00004	365679
0.00008	710420
0.00012	1055162
0.00016	1399903
0.00020	1744644
0.00025	2089385
0.00029	2434125
0.00033	2778865
0.00036	3123605

Concentration: 100ppm
Tube: 0.018C2

Q (cm^3/s)	ΔP ($dynes/cm^2$)
0.1224	387629
0.2306	731837
0.3245	1075639
0.4267	1419239
0.5220	1762215

Concentration: 200ppm
Tube: 0.003C1

Q (cm^3/s)	ΔP ($dynes/cm^2$)
0.00022	366098
0.00043	710838
0.00063	1055578
0.00085	1400312
0.00105	1745047
0.00125	2089781
0.00149	2434515
0.00169	2779248
0.00190	3123979

Concentration: 200ppm
Tube: 0.004D1

Q (cm^3/s)	ΔP ($dynes/cm^2$)
0.00062	366109
0.00122	710846
0.00179	1055579
0.00236	1400310
0.00294	1745035
0.00355	2089754
0.00423	2434473
0.00483	2779185
0.00547	3123903

Concentration: 200ppm
Tube: 0.008B1

Q (cm^3/s)	ΔP ($dynes/cm^2$)
0.00405	376153
0.00757	720866
0.01105	1065564
0.01496	1410239
0.01880	1754904
0.02278	2099537
0.02701	2444150
0.03082	2788764
0.03472	3133360

Concentration: 200ppm
Tube: 0.006B2

Q (cm^3/s)	ΔP ($dynes/cm^2$)
0.00201	377103
0.00396	721824
0.00558	1066503
0.00732	1411196
0.00919	1755879
0.01124	2100562
0.01326	2445240
0.01519	2789887
0.01711	3134529

Concentration: 200ppm
Tube: 0.008A1

Q (cm^3/s)	ΔP ($dynes/cm^2$)
0.00286	3886644
0.00558	731360
0.00805	1076074
0.01064	1420764
0.01335	1765452
0.01622	2110109
0.01927	2454742
0.02194	2799389
0.02471	3143964

Concentration: 200ppm
Tube: 0.008C2

Q (cm^3/s)	ΔP ($dynes/cm^2$)
0.00506	371231
0.00930	715892
0.01387	1060563
0.01890	1405220
0.02397	1749816
0.02903	2094365
0.03432	2438878
0.03929	2783351
0.04439	3127847

Concentration: 200ppm
Tube: 0.012E2*

Q (cm^3/s)	ΔP ($dynes/cm^2$)
0.0191	377618
0.0568	1066830
0.0756	1411318
0.0935	1755743
0.1124	2100077
0.1324	2444295
0.1517	2788423
0.1700	3132613

Concentration: 200ppm
Tube: 0.012E1

Q (cm^3/s)	ΔP ($dynes/cm^2$)
0.0158	388642
0.0294	733318
0.0437	1077925
0.0587	1422467
0.0734	1766923
0.0883	2111344
0.1303	3144322

Concentration: 200ppm
Tube: 0.018C2

Q (cm^3/s)	ΔP ($dynes/cm^2$)
0.0983	388310
0.1880	732482
0.2806	1076587
0.3681	1420436
0.4523	1763716

Concentration: 200ppm
Tube: 0.012D*

Q (cm^3/s)	ΔP ($dynes/cm^2$)
0.0112	408986
0.0204	753674
0.0291	1098334
0.0384	1442935
0.0480	1787513
0.0578	2132084
0.0677	2476630
0.0772	2821070
0.0868	3165563

Concentration: 200ppm
Tube: 0.018D

Q (cm^3/s)	ΔP ($dynes/cm^2$)
0.0499	441973
0.0862	786502
0.1227	1130761
0.1628	1475105
0.2015	1819232
0.2422	2163291
0.2830	2507256
0.3219	2851080
0.3612	3194830

Concentration: 200ppm
Tube: 0.018A1

Q (cm^3/s)	ΔP ($dynes/cm^2$)
0.0683	406511
0.1220	750937
0.1825	1095173
0.2399	1438806
0.2996	1782430
0.3569	2126188
0.4173	2469907

Flow of Polyox FRA Solutions in Silane-Treated Tubes

Concentration: 5ppm
Tube: 0.002C1

Q (cm^3/s)	ΔP ($dynes/cm^2$)
0.00006	365704
0.00011	710445
0.00016	1055186
0.00022	1399927
0.00027	1744668
0.00032	2089408
0.00038	2434132
0.00044	2778871
0.00049	3123609

Concentration: 5ppm
Tube: 0.006B2

Q (cm^3/s)	ΔP ($dynes/cm^2$)
0.00265	375819
0.00506	720343
0.00744	1065047
0.00982	1409736
0.01227	1754379
0.01459	2099047
0.01718	2443713
0.01951	2788373
0.02189	3133023

Concentration: 5ppm
Tube: 0.003C1

Q (cm^3/s)	ΔP ($dynes/cm^2$)
0.00029	366012
0.00056	710751
0.00083	1055489
0.00110	1400226
0.00137	1744962
0.00163	2089696
0.00193	2434430
0.00218	2779163
0.00245	3123893

Concentration: 5ppm
Tube: 0.008C2

Q (cm^3/s)	ΔP ($dynes/cm^2$)
0.00707	369779
0.01349	714468
0.01973	1059132
0.02611	1403766
0.03230	1748312
0.03849	2092876
0.04509	2437342
0.05100	2781863
0.05689	3126325

Concentration: 5ppm
Tube: 0.004C

Q (cm^3/s)	ΔP ($dynes/cm^2$)
0.00049	374704
0.00094	719442
0.00137	1064178
0.00182	1408912
0.00226	1753638
0.00270	2098353
0.00316	2443074
0.00359	2787799
0.00402	3132500

Concentration: 5ppm
Tube: 0.008B1

Q (cm^3/s)	ΔP ($dynes/cm^2$)
0.00561	375636
0.01056	720328
0.01547	1064996
0.02035	1409651
0.02525	1754256
0.03021	2098836
0.03544	2443399
0.04100	2787941
0.04488	3132476

Concentration: 5ppm
Tube: 0.008A1

Q (cm^3/s)	ΔP ($dynes/cm^2$)
0.00407	385329
0.00766	730031
0.01118	1074719
0.01477	1419317
0.01822	1763960
0.02185	2108587
0.02552	2453219
0.02902	2797801
0.03245	3142405

Concentration: 5ppm
Tube: 0.012E

Q (cm^3/s)	ΔP ($dynes/cm^2$)
0.0141	414278
0.0256	758936
0.0371	1103525
0.0488	1448089
0.0606	1792521
0.0716	2136825
0.0837	2481286
0.0945	2825712
0.1053	3170115

Concentration: 5ppm
Tube: 0.012F1

Q (cm^3/s)	ΔP ($dynes/cm^2$)
0.03031	377415
0.0572	721989
0.0839	1066485
0.1096	1410830
0.1351	1754935
0.1586	2099261
0.1836	2443436
0.2065	2787626
0.2284	3131671

Concentration: 5ppm
Tube: 0.018A1

Q (cm^3/s)	ΔP ($dynes/cm^2$)
0.0929	406574
0.1684	750891
0.2391	1094923
0.3078	1438760
0.3742	1782365
0.4412	2125628

Concentration: 5ppm
Tube: 0.012E1

Q (cm^3/s)	ΔP ($dynes/cm^2$)
0.0219	388167
0.0412	732798
0.0597	1077381
0.0785	1421924
0.0967	1766294
0.1150	2110681
0.1335	2455019
0.1497	2799327
0.1668	3143416

Concentration: 5ppm
Tube: 0.018C2

Q (cm^3/s)	ΔP ($dynes/cm^2$)
0.1417	387813
0.2579	731891
0.3653	1075713
0.4668	1419161

Concentration: 5ppm
Tube: 0.018D

Q (cm^3/s)	ΔP ($dynes/cm^2$)
0.0661	441779
0.1165	786199
0.1640	1130476
0.2121	1474678
0.2569	1818788
0.3024	2162769
0.3487	2506552
0.3919	2850364
0.4331	3194040

Concentration: 10ppm
Tube: 0.004C

Q (cm^3/s)	ΔP ($dynes/cm^2$)
0.00088	720495
0.00132	1065230
0.00174	1409963
0.00216	1754693
0.00259	2099420
0.00304	2444144
0.00346	2788863
0.00388	3133587

Concentration: 10ppm
Tube: 0.002C1

Q (cm^3/s)	ΔP ($dynes/cm^2$)
0.00006	366148
0.00011	710889
0.00016	1055630
0.00021	1400370
0.00026	1745111
0.00032	2089850
0.00038	2434590
0.00043	2779330
0.00048	3124069

Concentration: 10ppm
Tube: 0.006B2

Q (cm^3/s)	ΔP ($dynes/cm^2$)
0.00261	375638
0.00502	720354
0.00737	1065062
0.00975	1409748
0.01223	1754385
0.01453	2099065
0.01706	2443715
0.01935	2788361
0.02172	3132999

Concentration: 10ppm
Tube: 0.003C1

Q (cm^3/s)	ΔP ($dynes/cm^2$)
0.00029	366421
0.00056	711161
0.00082	1055899
0.00108	1400637
0.00137	1745372
0.00164	2090105
0.00192	2434838
0.00217	2779568
0.00243	3124296

Concentration: 10ppm
Tube: 0.008C2

Q (cm^3/s)	ΔP ($dynes/cm^2$)
0.00687	370976
0.01324	715649
0.01943	1060320
0.02572	1404969
0.03210	1749574
0.03812	2094160
0.04463	2438718
0.05063	2783231
0.05658	3127584

Concentration: 10ppm
Tube: 0.008B1

Q (cm^3/s)	ΔP ($dynes/cm^2$)
0.00542	376945
0.01030	721621
0.01522	1066277
0.02017	1410931
0.02501	1755529
0.03002	2100036
0.03504	2444618
0.03980	2789170
0.04456	3133502

Concentration: 10ppm
Tube: 0.012E1

Q (cm^3/s)	ΔP ($dynes/cm^2$)
0.0214	387975
0.0403	732606
0.0592	1077201
0.0780	1421777
0.0971	1766208
0.1148	2110547
0.1333	2454848
0.1497	2798753
0.1657	3142907

Concentration: 10ppm
Tube: 0.008A1

Q (cm^3/s)	ΔP ($dynes/cm^2$)
0.00393	385830
0.00745	730539
0.01094	1075233
0.01443	1419912
0.01796	1764593
0.02141	2109187
0.02509	2453803
0.02857	2798426
0.03193	3142941

Concentration: 10ppm
Tube: 0.012E

Q (cm^3/s)	ΔP ($dynes/cm^2$)
0.0139	414978
0.0254	759639
0.0368	1104279
0.0484	1448869
0.0597	1793422
0.0711	2137986
0.0833	2482323
0.0946	2826741
0.1053	3171095

Concentration: 10ppm
Tube: 0.012F1

Q (cm^3/s)	ΔP ($dynes/cm^2$)
0.0299	377409
0.0569	721966
0.0825	1066448
0.1085	1410883
0.1342	1755206
0.1579	2099489
0.1816	2443759
0.2040	2787748
0.2258	3131887

Concentration: 10ppm
Tube: 0.018A1

Q (cm^3/s)	ΔP ($dynes/cm^2$)
0.0923	406349
0.1683	750685
0.2399	1094949
0.3079	1438786
0.3713	1782440
0.4350	2126036

Concentration: 10ppm
Tube: 0.018C2

Q (cm^3/s)	ΔP ($dynes/cm^2$)
0.1416	388323
0.2579	732202
0.3618	1075628
0.4608	1418799

Concentration: 30ppm
Tube: 0.003C1

Q (cm^3/s)	ΔP ($dynes/cm^2$)
0.00027	365853
0.00053	710592
0.00079	1055330
0.00104	1400064
0.00129	1744799
0.00156	2089533
0.00183	2434265
0.00298	2778998
0.00233	3123720

Concentration: 10ppm
Tube: 0.018D

Q (cm^3/s)	ΔP ($dynes/cm^2$)
0.0655	441708
0.1162	786165
0.1656	1130510
0.2135	1474609
0.2598	1818606
0.3040	2162628
0.3493	2506312
0.3895	2850135
0.4315	3193753

Concentration: 30ppm
Tube: 0.004C

Q (cm^3/s)	ΔP ($dynes/cm^2$)
0.00045	377300
0.00087	722038
0.00128	1066776
0.00168	1411509
0.00210	1756243
0.00251	2100974
0.00294	2445704
0.00334	2790430
0.00375	3135157

Concentration: 30ppm
Tube: 0.002C1

Q (cm^3/s)	ΔP ($dynes/cm^2$)
0.00005	365397
0.00010	710139
0.00015	1054880
0.00020	1399620
0.00025	1744361
0.00036	2433841
0.00040	2778581
0.00046	3123318

Concentration: 30ppm
Tube: 0.006B2

Q (cm^3/s)	ΔP ($dynes/cm^2$)
0.00252	377046
0.00478	721771
0.00703	1066416
0.00929	1411125
0.01152	1755825
0.01387	2100503
0.01628	2445165
0.01853	2789836
0.02080	3134501

Concentration: 30ppm
Tube: 0.008C2

Q (cm^3/s)	ΔP ($dynes/cm^2$)
0.00660	371102
0.01815	1060338
0.02428	1404927
0.03029	1749560
0.03646	2093996
0.04278	2438500
0.04889	2782906
0.05464	3127391

Concentration: 30ppm
Tube: 0.012F1

Q (cm^3/s)	ΔP ($dynes/cm^2$)
0.0285	377747
0.0521	722340
0.0775	1066868
0.1026	1411339
0.1276	1755630
0.1533	2098150
0.1788	2443968
0.2023	2787712
0.2256	3131611

Concentration: 30ppm
Tube: 0.008B1

Q (cm^3/s)	ΔP ($dynes/cm^2$)
0.00516	376124
0.00983	720828
0.01440	1065510
0.01910	1410193
0.02383	1754848
0.02860	2099466
0.03358	2444073
0.03814	2788640
0.04293	3133178

Concentration: 30ppm
Tube: 0.012E1

Q (cm^3/s)	ΔP ($dynes/cm^2$)
0.0208	388644
0.0390	733281
0.0564	1077864
0.0737	1422395
0.0915	1766885
0.1099	2111151
0.1288	2455519
0.1462	2799631
0.1643	3143922

Concentration: 30ppm
Tube: 0.008A1

Q (cm^3/s)	ΔP ($dynes/cm^2$)
0.00378	386390
0.00717	731108
0.01041	1075808
0.01373	1420493
0.01707	1765157
0.02049	2109796
0.02407	2454436
0.02737	2798963
0.03060	3143563

Concentration: 30ppm
Tube: 0.012D*

Q (cm^3/s)	ΔP ($dynes/cm^2$)
0.0139	408574
0.0256	753226
0.0370	1097867
0.0484	1442469
0.0595	1787000
0.0710	2131562
0.0834	2476095
0.0944	2820629
0.1059	3165083

Concentration: 30ppm
Tube: 0.018A1

Q (cm^3/s)	ΔP ($dynes/cm^2$)
0.0863	406314
0.1581	750748
0.2285	1094970
0.3002	1438942
0.3718	1782675
0.4410	2126287

Concentration: 60ppm
Tube: 0.002C1

Q (cm^3/s)	ΔP ($dynes/cm^2$)
0.00010	711614
0.00015	1056355
0.00020	1401096
0.00025	1745837
0.00030	2090578
0.00034	2435318
0.00039	2780057
0.00044	3124797

Concentration: 30ppm
Tube: 0.018C2

Q (cm^3/s)	ΔP ($dynes/cm^2$)
0.1353	387881
0.2514	732043
0.3627	1075746

Concentration: 60ppm
Tube: 0.003C1

Q (cm^3/s)	ΔP ($dynes/cm^2$)
0.00027	367144
0.00052	711884
0.00074	1056619
0.00099	1401356
0.00125	1746092
0.00148	2090827
0.00176	2435562
0.00199	2780295
0.00225	3125027

Concentration: 30ppm
Tube: 0.018D

Q (cm^3/s)	ΔP ($dynes/cm^2$)
0.0622	441680
0.1105	786212
0.1575	1130647
0.2077	1474352
0.2550	1817975
0.3037	2162041
0.3539	2505989
0.3978	2849921
0.4391	3193702

Concentration: 60ppm
Tube: 0.004C

Q (cm^3/s)	ΔP ($dynes/cm^2$)
0.00042	376119
0.00082	720858
0.00121	1065595
0.00158	1410329
0.00197	1755058
0.00235	2099791
0.00278	2444522
0.00317	2789253
0.00357	3133979

Concentration: 60ppm
Tube: 0.006B2

Q (cm^3/s)	ΔP ($dynes/cm^2$)
0.00237	376063
0.00442	720787
0.00645	1065498
0.00862	1410208
0.01086	1754904
0.01308	2099597
0.01539	2444270
0.01759	2788955
0.01959	3133626

Concentration: 60ppm
Tube: 0.008A1

Q (cm^3/s)	ΔP ($dynes/cm^2$)
0.00359	386452
0.00662	731170
0.00968	1075874
0.01285	1420553
0.01606	1765232
0.01942	2109901
0.02263	2454557
0.02584	2799195
0.02896	3143816

Concentration: 60ppm
Tube: 0.008C2

Q (cm^3/s)	ΔP ($dynes/cm^2$)
0.00589	371212
0.01125	715919
0.01696	1060591
0.02272	1405250
0.02846	1749885
0.03429	2094503
0.04025	2439089
0.04574	2783661
0.05130	3128220

Concentration: 60ppm
Tube: 0.012F1

Q (cm^3/s)	ΔP ($dynes/cm^2$)
0.0260	377862
0.0496	722501
0.0733	1067044
0.0975	1411584
0.1214	1755983
0.1441	2100150
0.1701	2444530
0.1923	2788854
0.2148	3133173

Concentration: 60ppm
Tube: 0.008B1

Q (cm^3/s)	ΔP ($dynes/cm^2$)
0.00485	377148
0.00910	721861
0.01335	1066557
0.01782	1411230
0.02233	1755882
0.02673	2100481
0.03161	2445093
0.03599	2789656
0.04024	3134249

Concentration: 60ppm
Tube: 0.012E1

Q (cm^3/s)	ΔP ($dynes/cm^2$)
0.0192	388072
0.0357	732747
0.0524	1077276
0.0702	1421862
0.0877	1766351
0.1050	2110814
0.1232	2455286
0.1394	2799714
0.1565	3144058

Concentration: 60ppm
Tube: 0.012D*

Q (cm^3/s)	ΔP ($dynes/cm^2$)
0.0131	408481
0.0238	753177
0.0346	1097841
0.0456	1442475
0.0797	2476216
0.0907	2820678
0.1011	3165150

Concentration: 60ppm
Tube: 0.018D

Q (cm^3/s)	ΔP ($dynes/cm^2$)
0.0591	441887
0.1029	786373
0.1489	1130804
0.1946	1475064
0.2413	1819208
0.2874	2163184
0.3349	2507112
0.3804	2850795
0.4241	3194566

Concentration: 60ppm
Tube: 0.018C2

Q (cm^3/s)	ΔP ($dynes/cm^2$)
0.1198	388146
0.2277	732453
0.3343	1076467
0.4373	1420060
0.5374	1763500

Concentration: 200ppm
Tube: 0.002C1

Q (cm^3/s)	ΔP ($dynes/cm^2$)
0.00004	364877
0.00007	709618
0.00011	1054359
0.00015	1399100
0.00018	1743842

Concentration: 60ppm
Tube: 0.018A1

Q (cm^3/s)	ΔP ($dynes/cm^2$)
0.0794	406436
0.1492	750862
0.2159	1095065
0.2841	1439172
0.3522	1782813
0.4202	2126533

Concentration: 200ppm
Tube: 0.003C1

Q (cm^3/s)	ΔP ($dynes/cm^2$)
0.00019	365548
0.00038	710289
0.00056	1055028
0.00074	1399767
0.00169	3123439

Concentration: 200ppm
Tube: 0.004C

Q (cm^3/s)	ΔP ($dynes/cm^2$)
0.00031	377006
0.00061	721745
0.00091	1068476
0.00120	1411208
0.00149	1755941
0.00177	2100669
0.00206	2445397
0.00236	2790108
0.00264	3134814

Concentration: 200ppm
Tube: 0.008B1

Q (cm^3/s)	ΔP ($dynes/cm^2$)
0.00365	377004
0.00683	721693
0.01364	1411021
0.01728	1755612
0.02092	2100238
0.02469	2444790
0.02822	2789402
0.03166	3133995

Concentration: 200ppm
Tube: 0.006B2

Q (cm^3/s)	ΔP ($dynes/cm^2$)
0.00175	376492
0.00341	721219
0.00494	1065941
0.00664	1410652
0.00828	1755362
0.00997	2100070
0.01172	2444768
0.01351	2789453
0.01522	3134123

Concentration: 200ppm
Tube: 0.008A1

Q (cm^3/s)	ΔP ($dynes/cm^2$)
0.00261	386931
0.00503	731653
0.00732	1076313
0.00972	1421018
0.01227	1765711
0.01486	2110399
0.01758	2455074
0.02017	2799720
0.02274	3144371

Concentration: 200ppm
Tube: 0.008C2

Q (cm^3/s)	ΔP ($dynes/cm^2$)
0.00462	370651
0.00852	715341
0.01249	1060040
0.01745	1404726
0.02196	1749381
0.02641	2094021
0.03133	2438638
0.03573	2783239
0.04014	3127839

Concentration: 200ppm
Tube: 0.012F1

Q (cm^3/s)	ΔP ($dynes/cm^2$)
0.0181	377703
0.0362	722365
0.0547	1067000
0.0734	1411540
0.0920	1756076
0.1106	2100559
0.1308	2444880
0.1457	2789221
0.1627	3133428

Concentration: 200ppm
Tube: 0.012E1

Q (cm^3/s)	ΔP ($dynes/cm^2$)
0.0143	388250
0.0261	732941
0.0393	1077590
0.0521	1422209
0.0660	1766823
0.0797	2111278
0.0943	2455801
0.1066	2800268
0.1199	3144682

Concentration: 200ppm
Tube: 0.012D*

Q (cm^3/s)	ΔP ($dynes/cm^2$)
0.0096	408561
0.0171	753263
0.0256	1097950
0.0343	1442614
0.0431	1787256
0.0520	2131863
0.0616	2476468
0.0698	2821051
0.0792	3165572

Concentration: 200ppm
Tube: 0.018A1

Q (cm^3/s)	ΔP ($dynes/cm^2$)
0.0572	406193
0.1099	750504
0.1647	1094881
0.2174	1439075
0.2675	1783064
0.3227	2126860
0.3732	2470587

Concentration: 200ppm
Tube: 0.018C2

Q (cm^3/s)	ΔP ($dynes/cm^2$)
0.0860	388060
0.1703	732436
0.2531	1076403
0.3238	1420276
0.4024	1763806
0.4765	2107335

Concentration: 200ppm
Tube: 0.018D

Q (cm^3/s)	ΔP ($dynes/cm^2$)
0.0428	442012
0.0773	786594
0.1130	1131105
0.1477	1475535
0.1844	1819836
0.2166	2164102
0.2574	2508211
0.2903	2852251
0.3256	3196148

Additional Relevant Plots

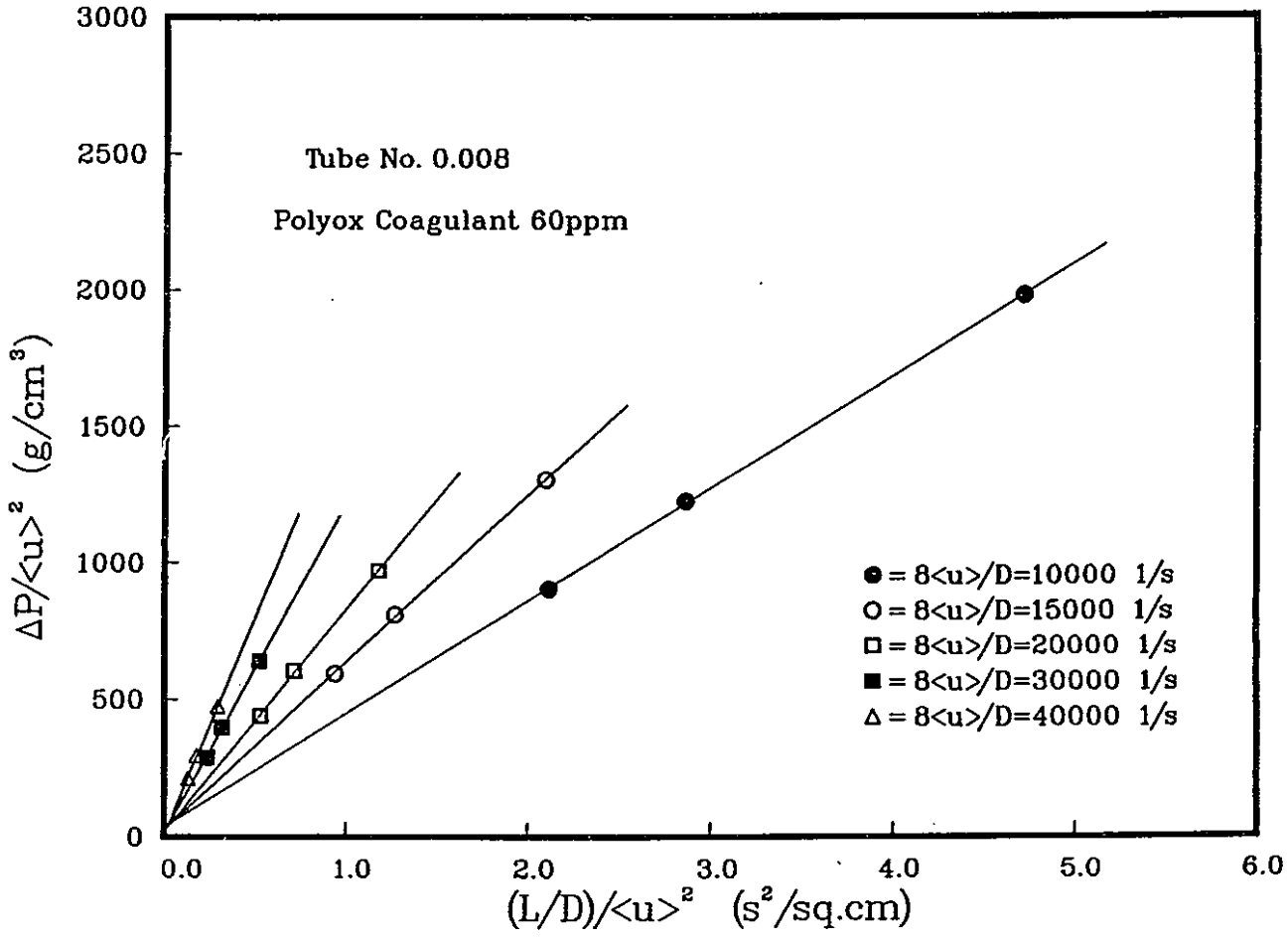

Figure G.1 Plot of $\Delta P/\langle u\rangle^2$ vs. $L/D/\langle u\rangle^2$ for 60ppm Polyox Coagulant solution, depicting end correction technique.

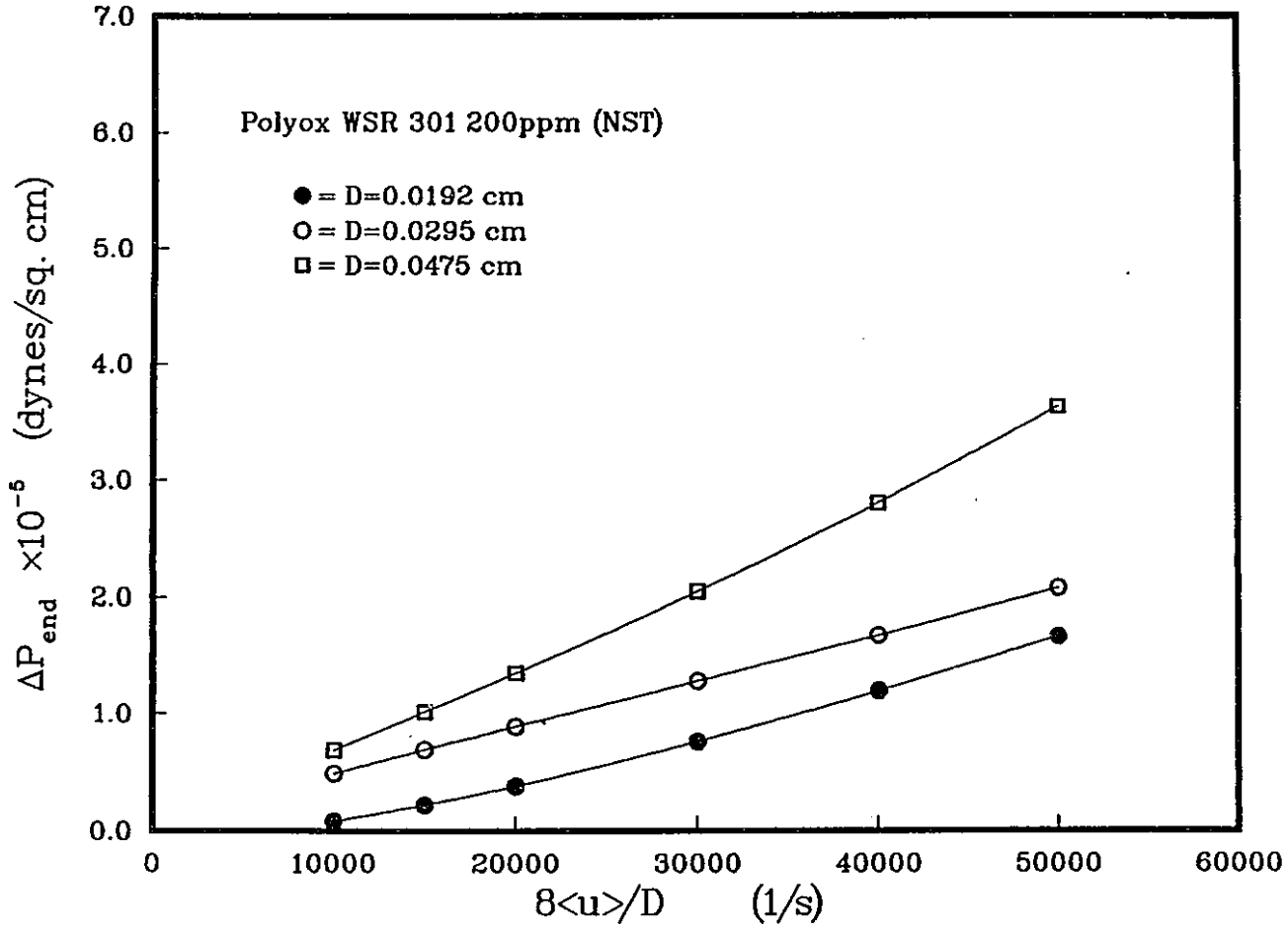

Figure G.2 Variation of ΔP_{end} with $8\langle u\rangle/D$ for capillary flow of 200 ppm WSR 301 solutions.

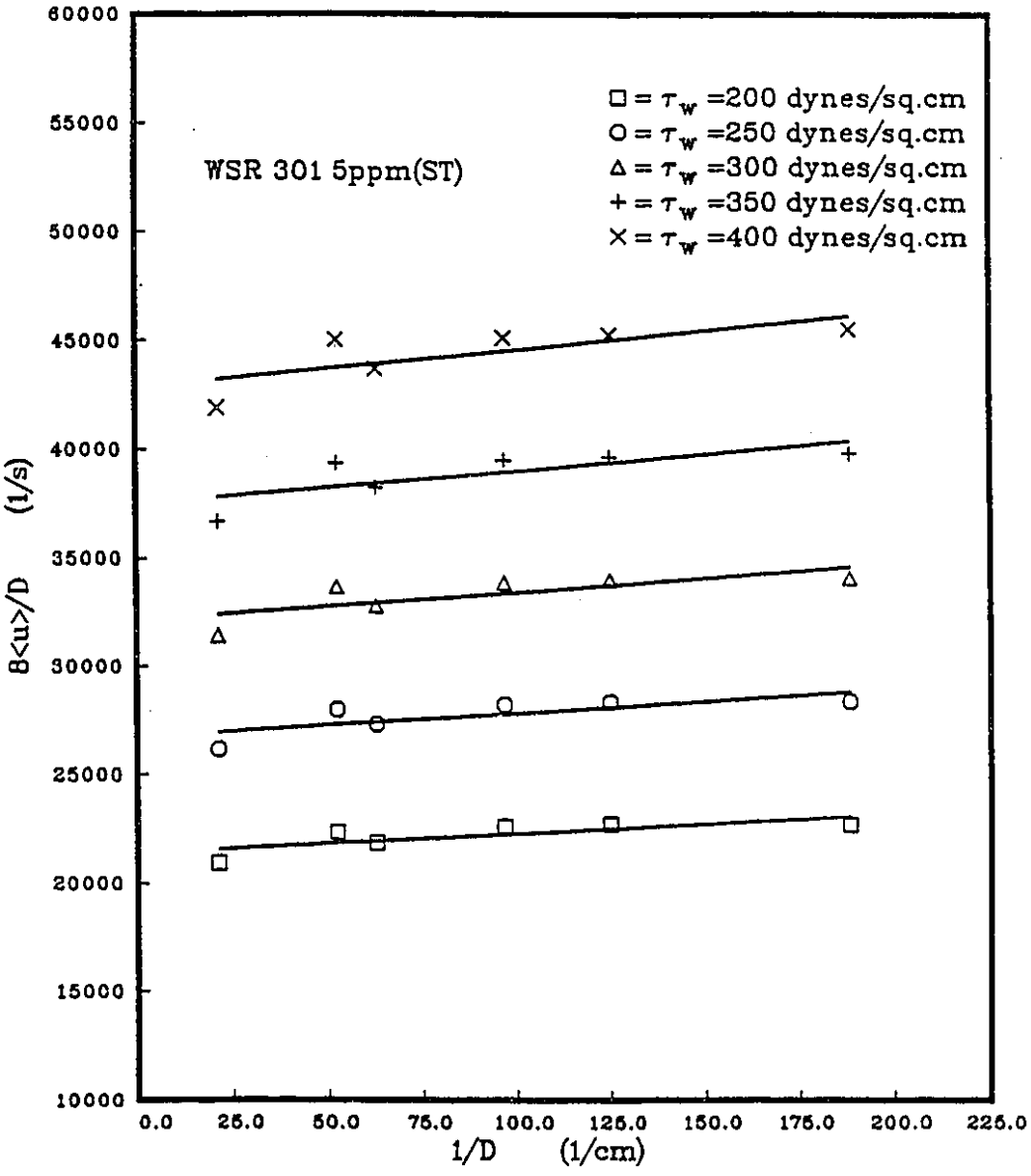

Figure G.3: Apparent shear rate vs. 1/D, 5 ppm Polyox WSR 301 (ST).

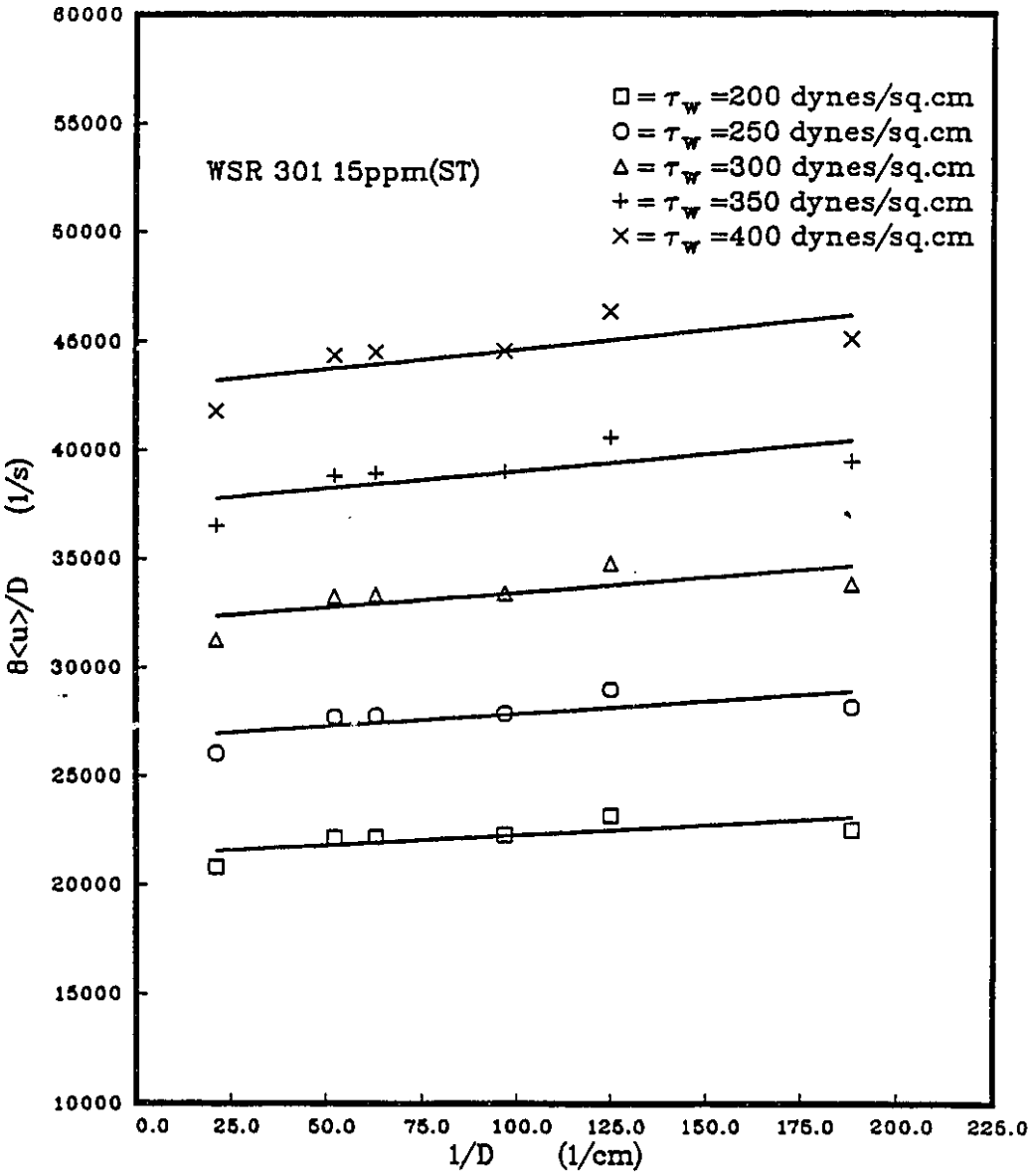

Figure G.4: Apparent shear rate vs. 1/D, 15 ppm Polyox WSR 301 (ST).

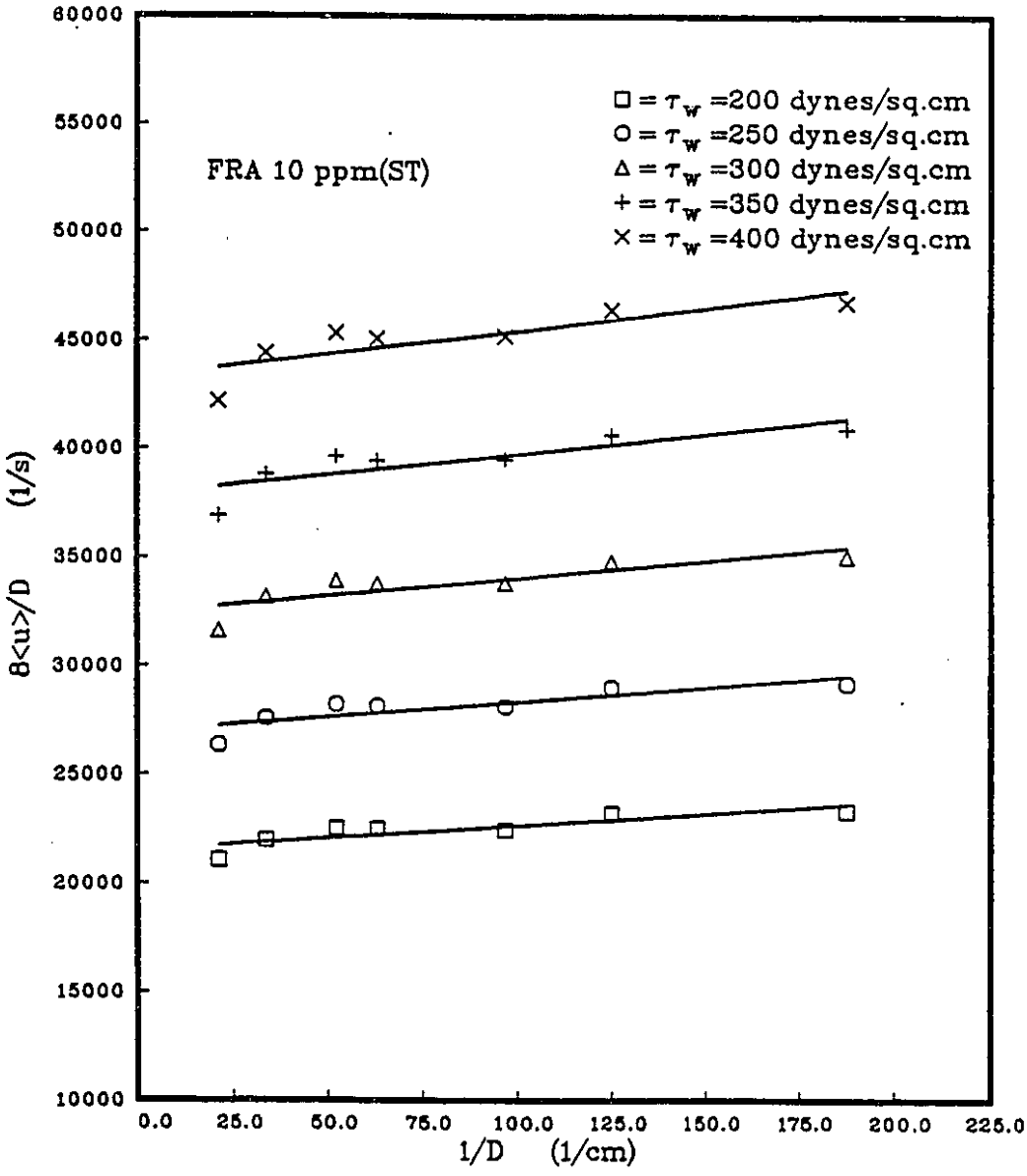

Figure G.5: Apparent shear rate vs. 1/D, 10 ppm Polyox FRA (ST).

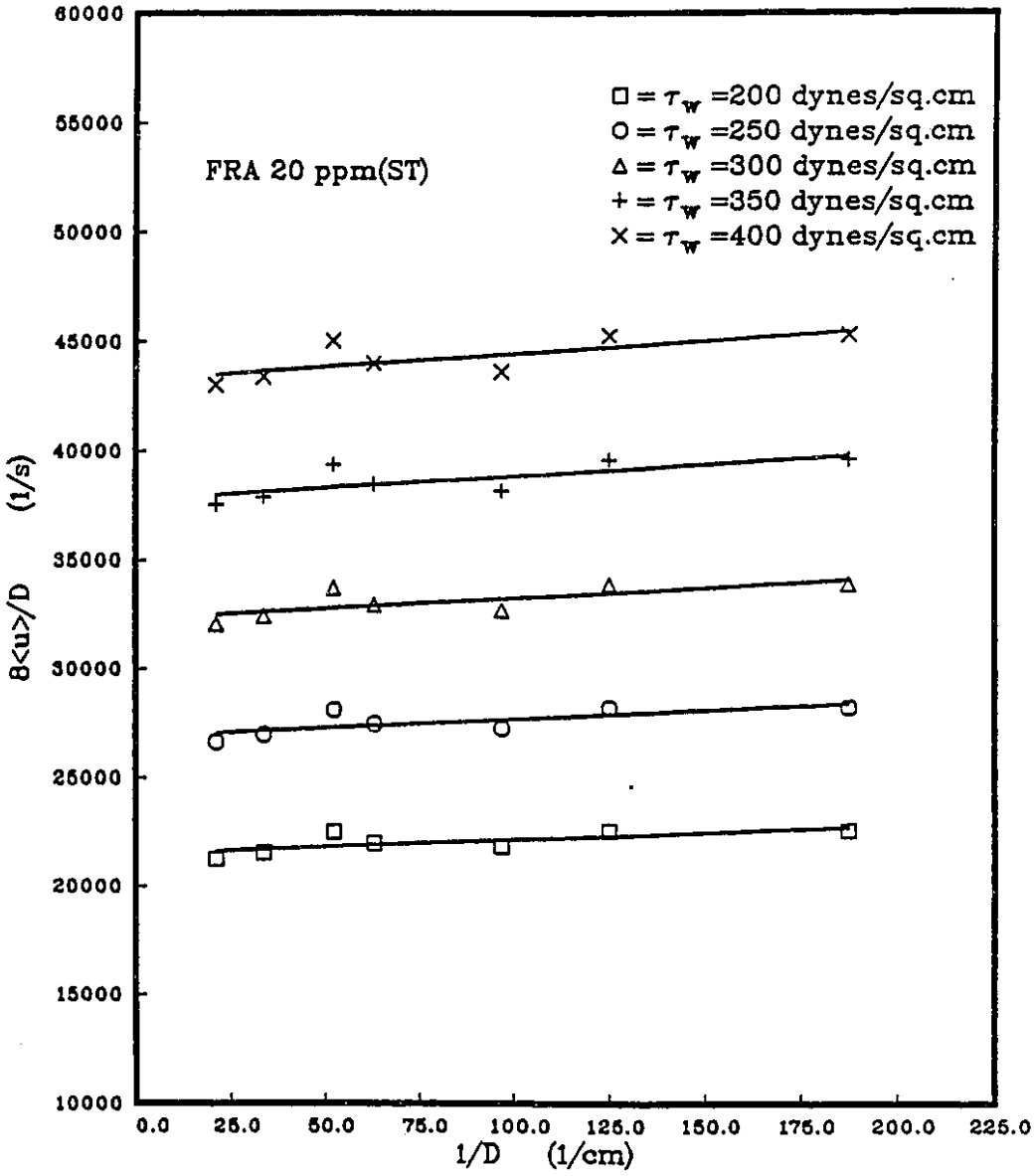

Figure G.6: Apparent shear rate vs. 1/D, 20 ppm Polyox FRA (ST).

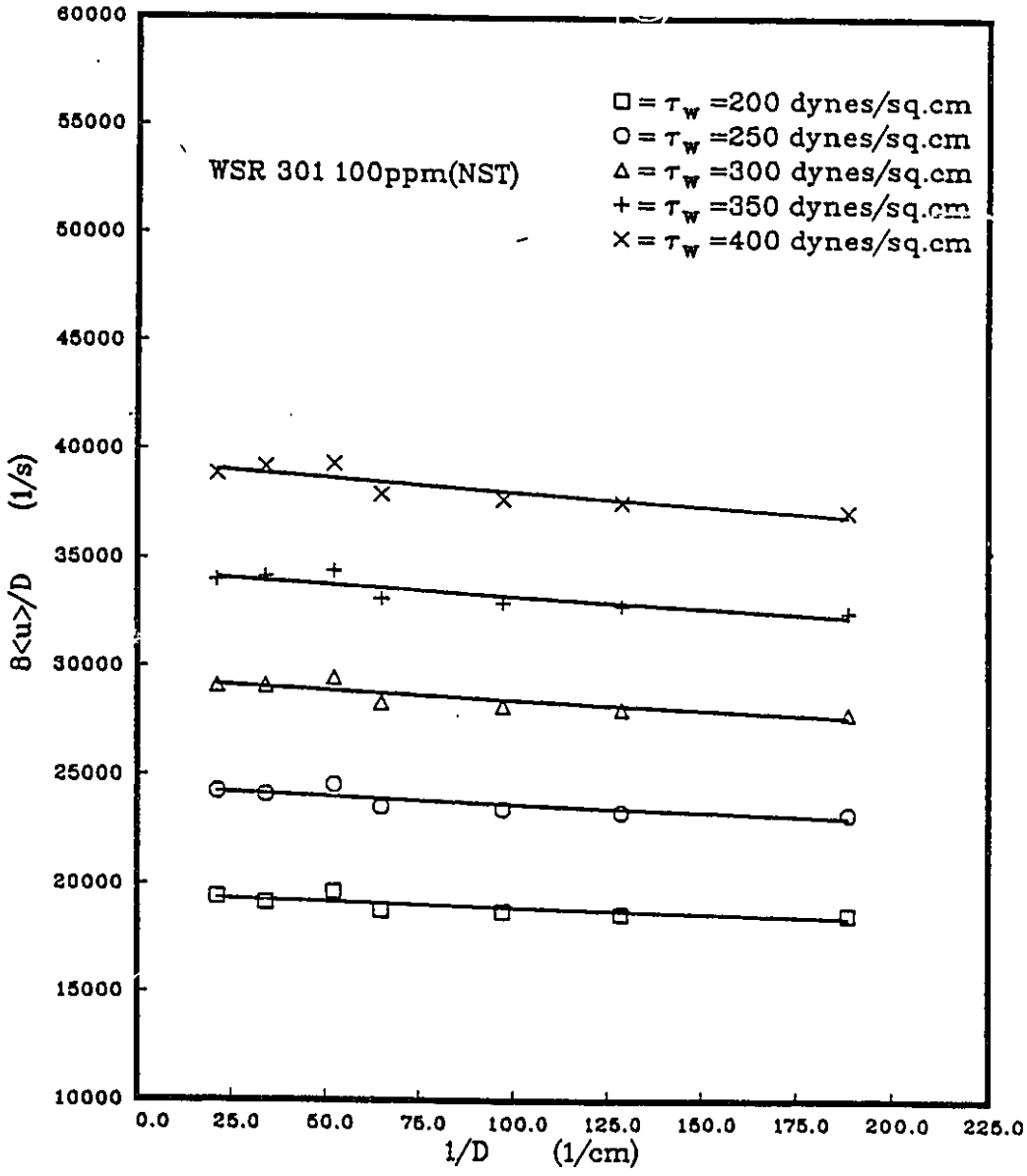

Figure G.7: Apparent shear rate vs. 1/D, 100ppm Polyox WSR 301 (NST).

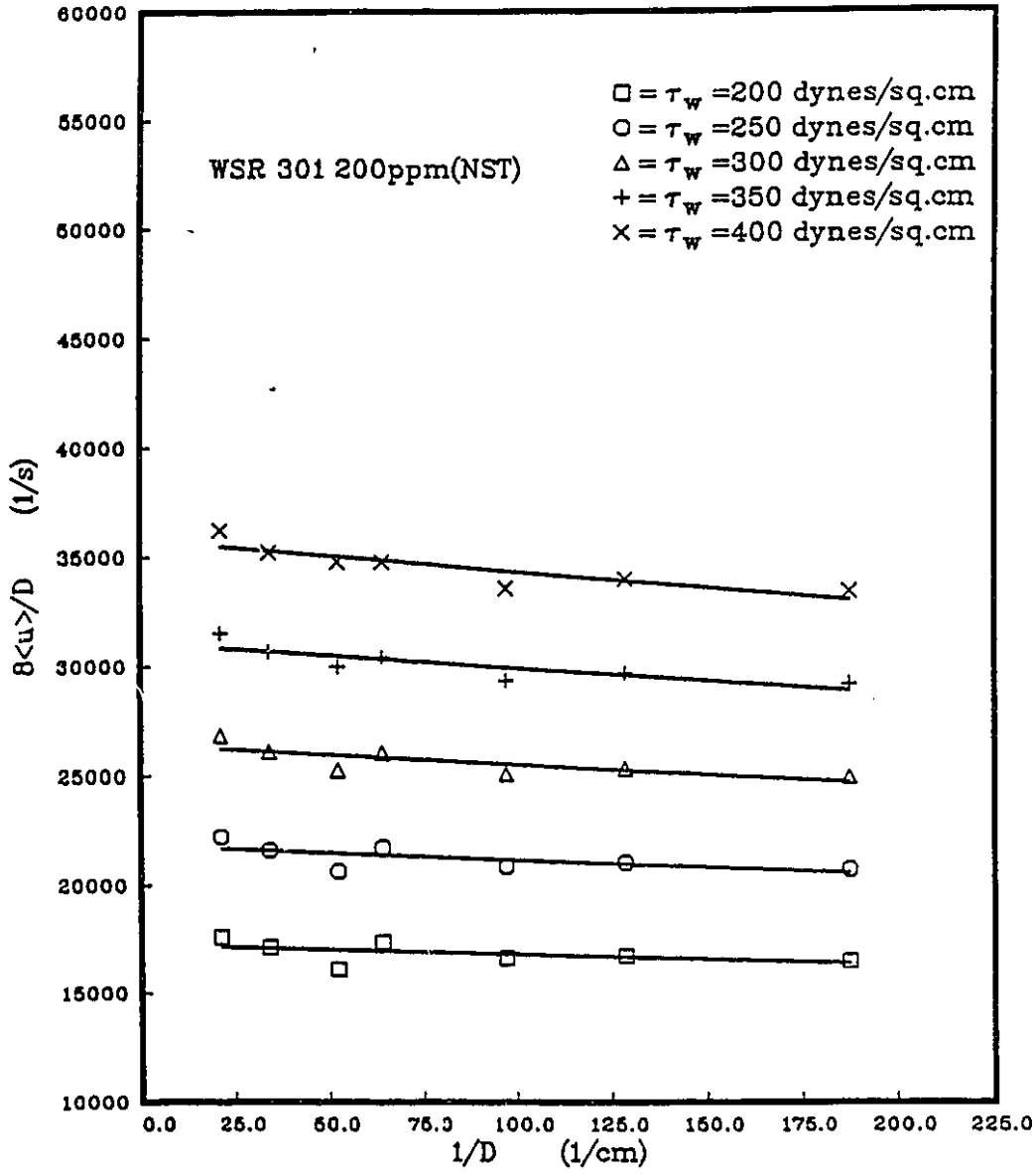

Figure G.8: Apparent shear rate vs. 1/D, 200ppm Polyox WSR 301 (NST).

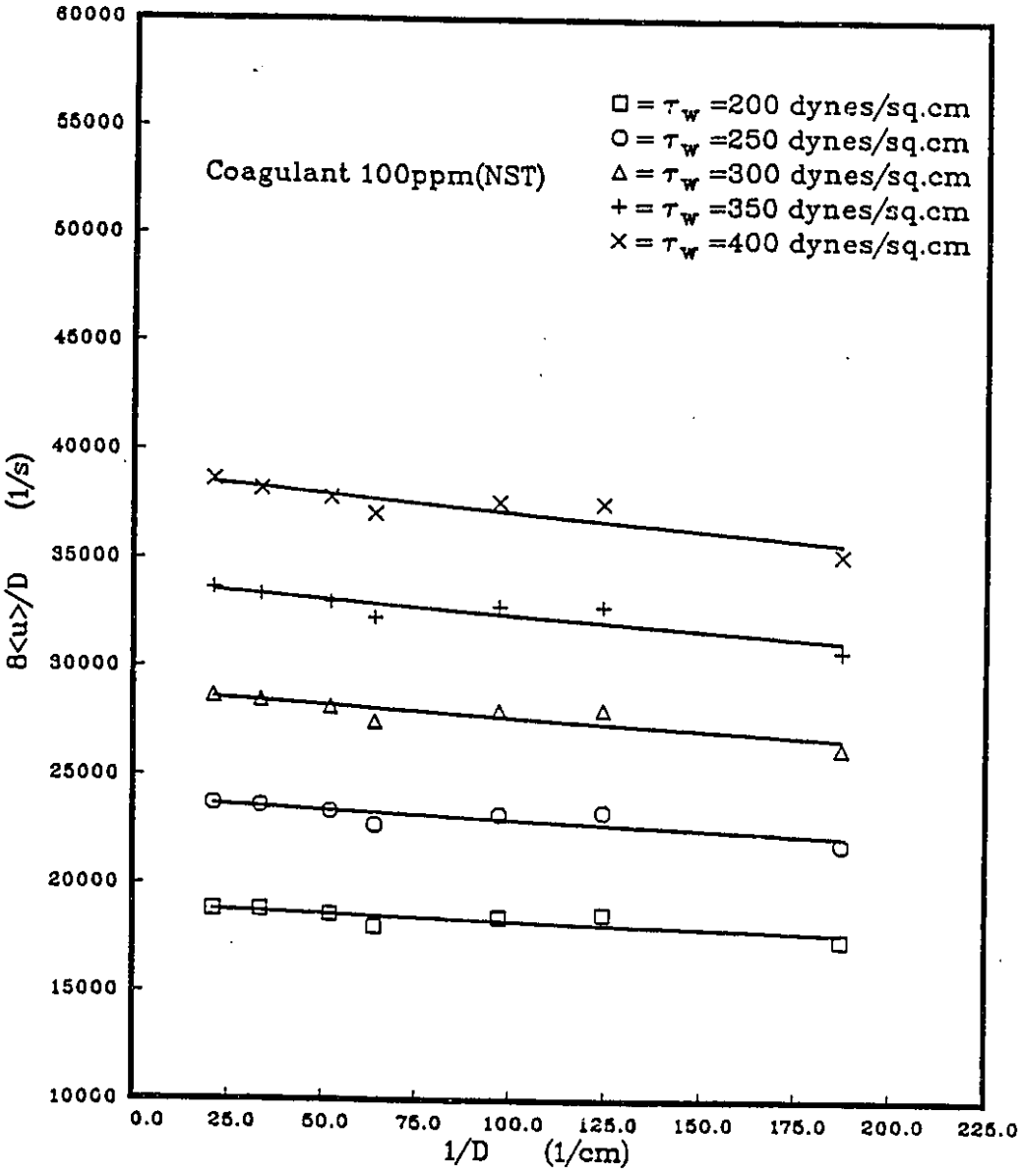

Figure G.9: Apparent shear rate vs. 1/D, 100ppm Polyox Coagulant (NST).

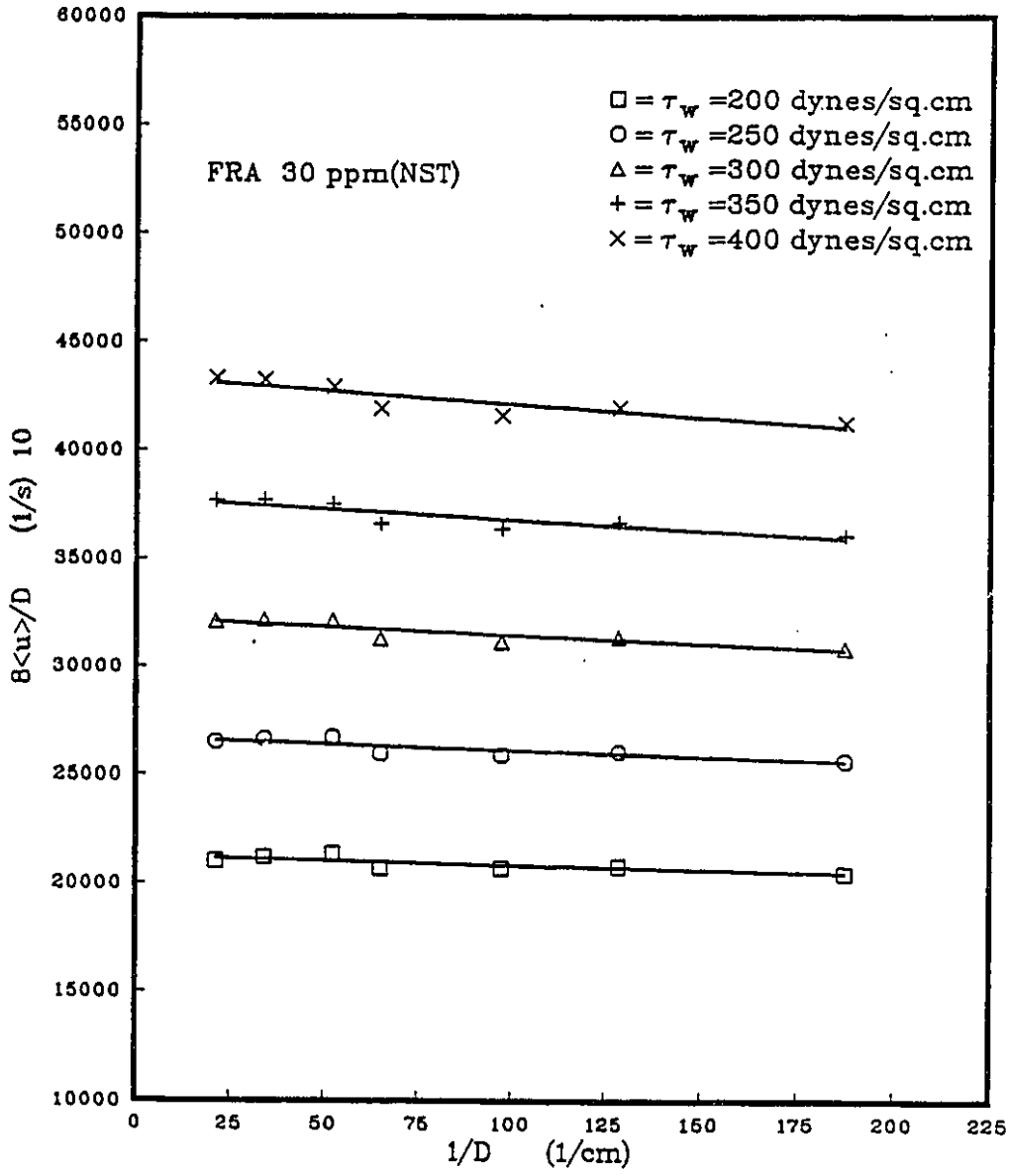

Figure G.10: Apparent shear rate vs. 1/D, 30ppm Polyox FRA (NST).

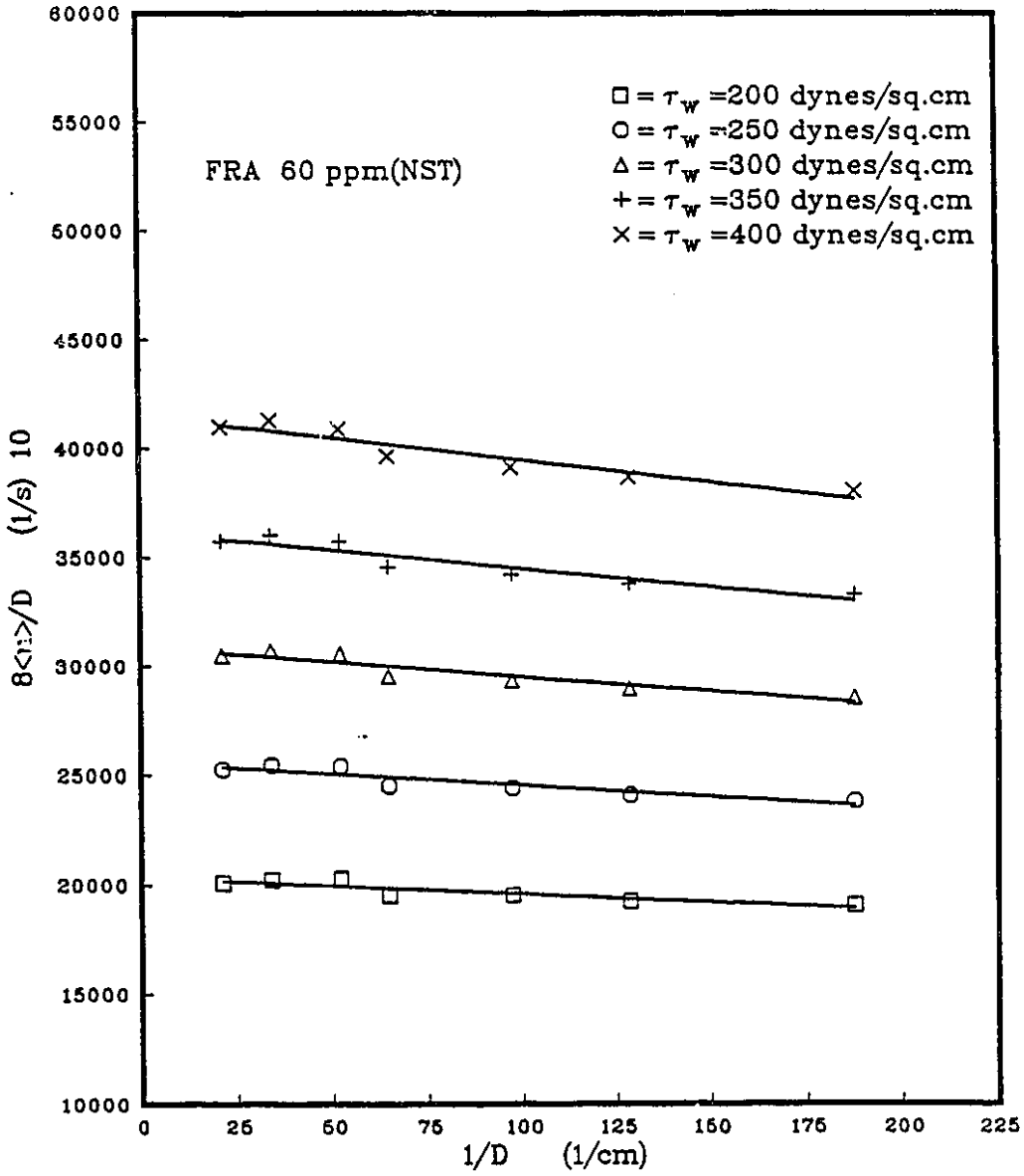

Figure G.11: Apparent shear rate vs. 1/D, 60ppm Polyox FRA (NST).

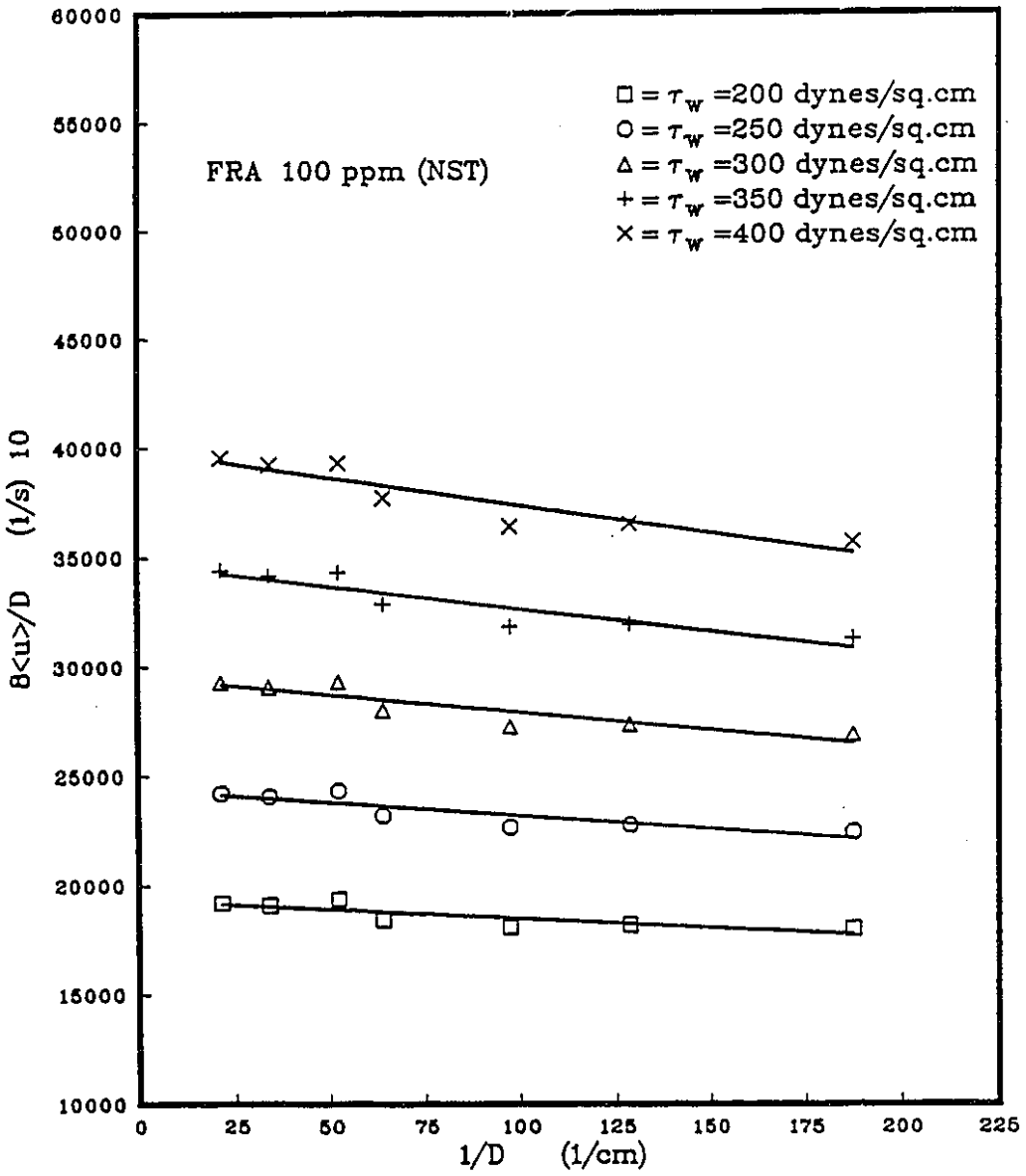

Figure G.12: Apparent shear rate vs. 1/D, 100ppm Polyox FRA (NST).

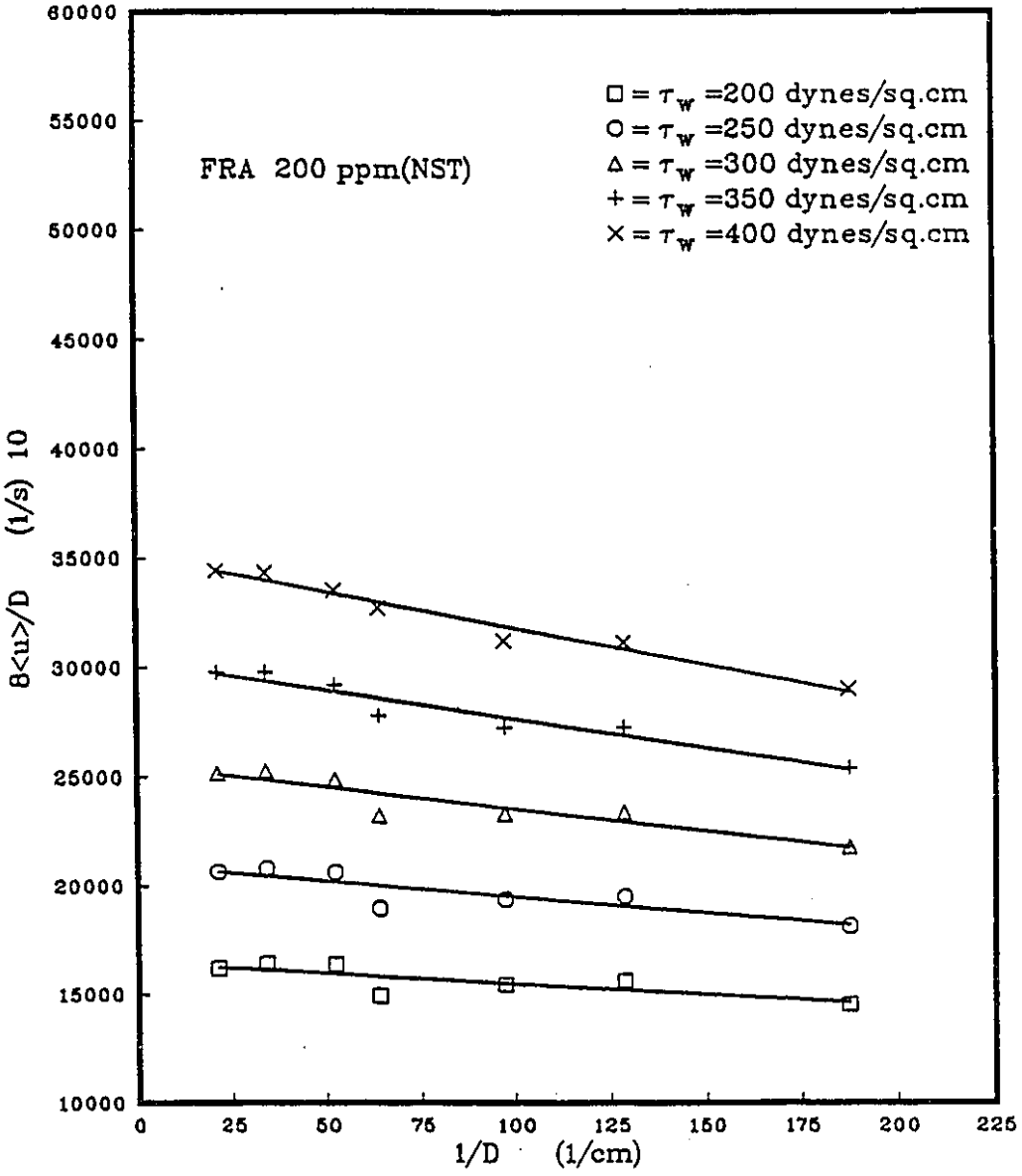

Figure G.13: Apparent shear rate vs. 1/D, 200ppm Polyox FRA (NST).

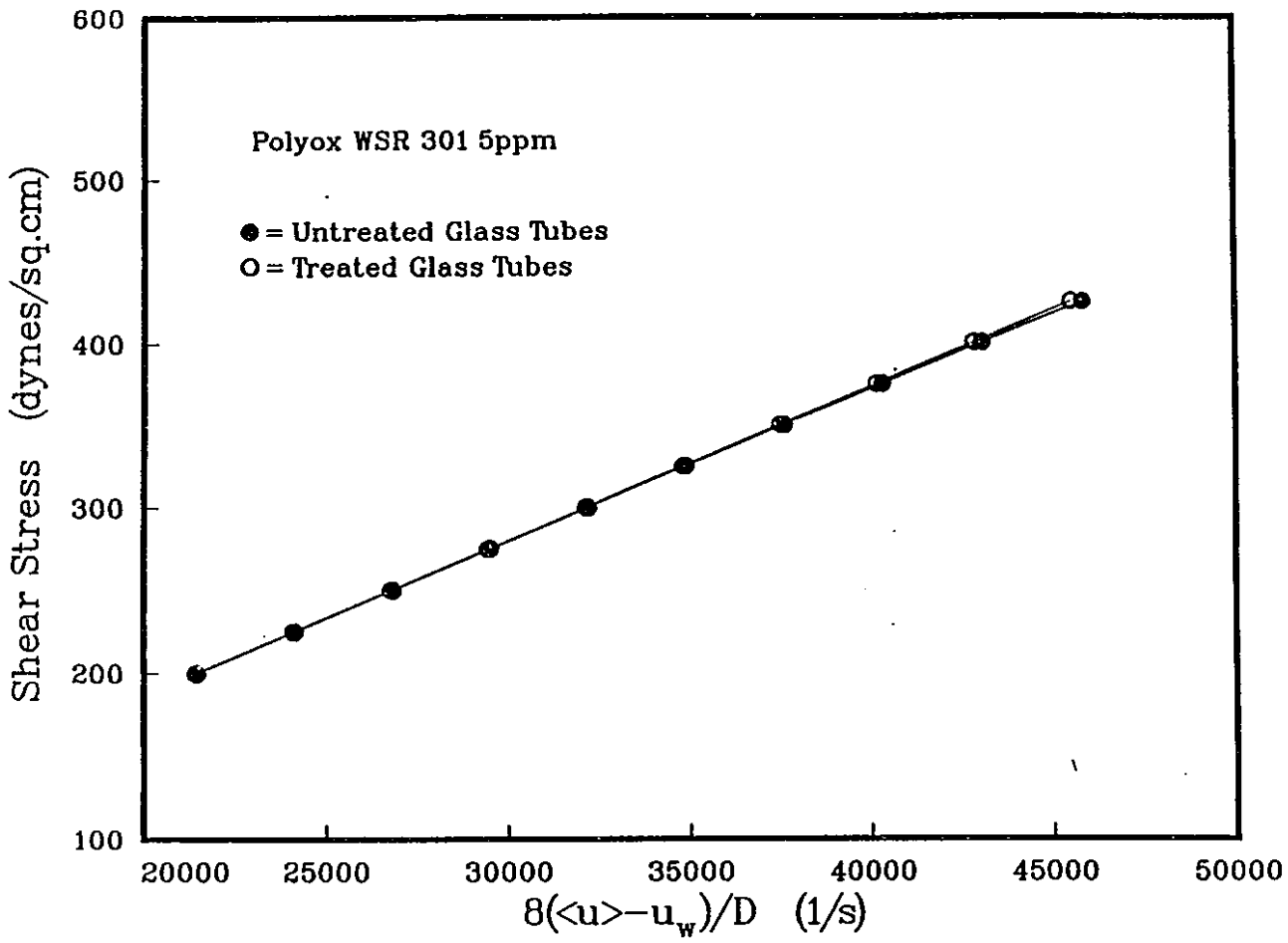

Figure G.14 Flow curves corrected for wall effects, for 5 ppm WSR 301 in treated and untreated tubes.

Appendix H

Computer Programs

This program is for evaluation of wall effects in capillary flow of polymer solutions, including end correction.

```
*************************************************************************PR000010
CC                    MAIN PROGRAMM                                      PR000020
                                                                         PR000030
CC                SURFACE PHENOMENA (POLYOX)                             PR000040
*************************************************************************PR000050
      CHARACTER*80 LAB1,LAB2,LAB3,LAB4,LAB5,LAB6,LAB7,LAB8,LAB9          PR000060
      CHARACTER*80 LAB10,LABX1,LABX2,LABX3,LABX4,LABY1,LABY2,LABY3       PR000070
      CHARACTER*80 LAB11(10),LAB22(10),LAB(400),LABY,SHEAD               PR000080
      REAL*4 SLD(10),N(10),K(10),SR(30),TW(30,30),P(30,30)               PR000090
     1,A,B,E(30),Y1(30),Y2(30),FTW(30),CSR(30),UW(30),SL(10)             PR000100
     2,PF(2,6),V8D(30),RVED(30),CK(30),CN(30),DALTA(30),C(30)            PR000110
     3,X1(30),X2(30),D(30),E1(30),LOD,EF,E2(30),S(30),TAW(30)            PR000120
     4,XX1(30,30),XXX1(30,30),AV8D(30,30),V8DL(30,30),DI(1000)           PR000130
     5,CB(30),CBB(30),DN(30),ENW(30,30),ENTO(30),TP(30),V(30)            PR000140
     6,CK1(30),CK2(30),CCK(30,30)                                        PR000150
      COMMON/FITT/ S1,S2,MMM,X1,Y1,A,B,DV,X2,Y2,BB                       PR000160
      COMMON/GRAPH1/ KKK,XX1,FTW,XXX1,C                                  PR000170
      COMMON/GRAPH2/ LABX1,LABX2,LABY1,LABY2,SHEAD,LAB                   PR000180
      COMMON/GRAPH3/LAB22                                                PR000190
      COMMON/GRAPH4/RVED,KK,AV8D,V8DL,LAB1                               PR000200
      COMMON/P3/CB,CBB,DN,VISIN,ENTO,CCK,ENW                             PR000210
      COMMON/ITER/III,DEFAT                                              PR000220
      COMMON DI                                                          PR000230
      READ(7,*) HEAD                                                     PR000240
      READ(7,*) SHEAD                                                    PR000250
      READ(7,*) KKK                                                      PR000260
      READ(7,*) (C(I),I=1,KKK)                                           PR000270
      READ(7,*) CB1,CB2,CN1                                              PR000280
        DO 9000 IJK1=1,KKK                                               PR000290
      READ(7,*) LAB1                                                     PR000300
      WRITE(8,90) LAB1                                                   PR000310
      READ (7,*) KK                                                      PR000320
        DO 456 IJ=1,KK                                                   PR000330
      READ(7,*) LAB2                                                     PR000340
      READ(7,*) LAB3                                                     PR000350
      READ(7,*) LAB4                                                     PR000360
      READ(7,*) M                                                        PR000370
      READ(7,*) (SL(I),I=1,M)                                            PR000380
      READ(7,*) (D(I),I=1,M)                                             PR000390
      READ(7,*) (N(I),I=1,M)                                             PR000400
      READ(7,*) (K(I),I=1,M)                                             PR000410
      READ(7,*) (SR(I),I=1,6)                                            PR000420
      AD=0.                                                              PR000430
        DO 15 I=1,M                                                      PR000440
      AD=1./D(I)+AD                                                      PR000450
15    SLD(I)=SL(I)/D(I)                                                  PR000460
      RVED(IJ)=AD/FLOAT(M)                                               PR000470
      IF (D(2).EQ.1.) GOTO 246                                           PR000480
      LAB5='    8<V>/D,       PEND/P              E          DV'         PR000490
CC    WRITE(8,90) LAB5                                                   PR000500
                                                                         PR000510
CC    ..................................................                 PR000520
CC    .                                                .                 PR000530
CC    . 1.  CALCULATION OF END EFFECT CORRECTION: EVC+EVE .              PR000540
CC    ..................................................                 PR000550
```

```
                                                                      PR000560
        DO 20 J=1,6                                                   PR000570
      LAB6='  8<V>/D   ,   PEND/TP   ,   EVE+EVC    , DV          '  PR000580
CC    WRITE(8,90) LAB6                                              PR000590
        DO 14 I=1,M                                                   PR000600
      TW(I,J)=K(I)*SR(J)**N(I)                                        PR000610
      P(I,J)=4.*SLD(I)*TW(I,J)                                        PR000620
      TP(J)=4.*2000.*TW(I,J)                                          PR000630
      V(I)=SR(J)*D(I)/8.                                              PR000640
      X1(I)=SLD(I)/(V(I)**2)                                          PR000650
      Y1(I)=P(I,J)/(V(I)**2)                                          PR000660
14    CONTINUE                                                        PR000670
      MMM=M                                                           PR000680
      A=1.                                                            PR000690
      CALL LINF                                                       PR000700
      E(J)=2*A/.9971                                                  PR000710
      EOP=A*V(1)**2/TP(J)                                             PR000720
      PEND=A*(SR(J)*D(1)/8.)**2                                       PR000730
      IF(E(J).GE.2.78) GOTO 1011                                      PR000740
      A=.5*0.9971*2.78                                                PR000750
      B=(S2-A*SM)/S1                                                  PR000760
1011  TAW(J)=B/4.                                                     PR000770
      WRITE(8,100) SR(J), PEND,EOP,D(1)                               PR000780
20    CONTINUE                                                        PR000790
                                                                      PR000800
CC    ..................................................              PR000810
CC    .                                                 .             PR000820
CC    . 2. ELLIS FITTING OF FLOW CURVE BEFORE WALL EFFECT CORRECT .   PR000830
CC    ..................................................              PR000840
        DO 1000 I=1,M                                                 PR000850
        OLD=9999.0                                                    PR000860
        ALPH=4.0                                                      PR000870
        DO 1400 JREP=1,57                                             PR000880
        ALPH=ALPH-.0500                                               PR000890
        DO 2000 J=1,6                                                 PR000900
      X1(J)=TAW(J)                                                    PR000910
      Y1(J)=SR(J)                                                     PR000920
      V(J)=SR(J)*D(I)/8.                                              PR000930
      X2(J)=(X1(J))**ALPH                                             PR000940
2000  CONTINUE                                                        PR000950
      MMM=6                                                           PR000960
      A=0.                                                            PR000970
      DEFAT=1.                                                        PR000980
      CALL LIN2F                                                      PR000990
      DIF=DV-OLD                                                      PR001000
      IF(DIF.GE.0.0 ) GOTO 1450                                       PR001010
      OLD=DV                                                          PR001020
      CN(IJ)=ALPH                                                     PR001030
      CK1(IJ)=B                                                       PR001040
      CK2(IJ)=BB                                                      PR001050
      B=1./B                                                          PR001060
1400  CONTINUE                                                        PR001070
1450  WRITE (8,100) B,BB,ALPH,DV,D(I)                                 PR001080
1000  CONTINUE                                                        PR001090
      GOTO 135                                                        PR001100
```

```
246     CK1(IJ)=0.0                                                     PR001110
        CN(IJ)=N(1)                                                     PR001120
        CK(IJ)=K(1)                                                     PR001130
        RVED(IJ)=1./D(1)                                                PR001140
135     KUANG=1                                                         PR001150
456     CONTINUE                                                        PR001160
                                                                        PR001170
CC     ..........................................                       PR001180
CC     .                                        .                       PR001190
CC     .  3.  FITTING OF 8<V>/D VS. 1/D  TO GET UW .                    PR001200
CC     .                                        .                       PR001210
CC     ..........................................                       PR001220
       CCC=175.                                                         PR001230
         DO 1500 IJK=1,10                                               PR001240
       CCC=CCC+25.                                                      PR001250
       FTW(IJK)= CCC                                                    PR001260
         DO 1200 JJ=1,KK                                                PR001270
       IF(CK1(JJ).EQ.0.0) GOTO 1105                                     PR001280
       V8D(JJ)=CK1(JJ)*FTW(IJK)+CK2(JJ)*FTW(IJK)**CN(JJ)                PR001290
       GOTO 1110                                                        PR001300
1105   V8D(JJ)=(FTW(IJK)/CK(JJ))**(1./CN(JJ))                          PR001310
1110   X1(JJ)=RVED(JJ)                                                  PR001320
       Y1(JJ)=V8D(JJ)                                                   PR001330
       AV8D(IJK,JJ)=V8D(JJ)                                             PR001340
1200   CONTINUE                                                         PR001350
       MMM=KK                                                           PR001360
       A=1.                                                             PR001370
       CALL  LINF                                                       PR001380
       CSR(IJK)=A                                                       PR001390
       UW(IJK)=8/8.                                                     PR001400
         DO 1480 JJ=1, KK                                               PR001410
       V(JJ)=V8D(JJ)/(RVED(JJ)*8.)                                      PR001420
       UWOU=UW(IJK)/V(JJ)                                               PR001430
1480   V8DL(IJK,JJ)=Y2(JJ)                                              PR001440
1500   CONTINUE                                                         PR001450
                                                                        PR001460
CC     ..............................................                   PR001470
CC     .                                            .                   PR001480
CC     . 4.  FITTING OF FINAL FLOW CURVE:  ELLIS MODEL                  PR001490
CC     ..............................................                   PR001500
                                                                        PR001510
CC   ......  8<U>/D=CK1*TAW+CK2*TAW**ALPH  ............                 PR001520
1888   LAB9=' ALPH ,    CK1  ,   CK2 IN ELLIS MODEL (FINAL VALUE)'      PR001530
CC     WRITE(8,90) LAB9                                                 PR001540
       ALPH=8.0                                                         PR001550
       OLD=40000.                                                       PR001560
         DO 1860 JREP=1,699                                             PR001570
       ALPH=ALPH-.01000                                                 PR001580
         DO 1850  JK=1,10                                               PR001590
       Y1(JK)= (CSR(JK))                                                PR001600
       X1(JK)=(FTW(JK))                                                 PR001610
       X2(JK)=(FTW(JK))**(ALPH)                                         PR001620
1850   CONTINUE                                                         PR001630
       MMM=10                                                           PR001640
       A=0.                                                             PR001650
       DEFAT=1.
```

```
      CALL LIN2F                                                        PR001660
      IF (DV.GE.OLD) GOTO 1860                                          PR001670
      ENTO(IJK1)=1./B                                                   PR001680
      FCK1=B                                                            PR001690
      FCK2=BB                                                           PR001700
      FCN=ALPH                                                          PR001710
      OLD=DV                                                            PR001720
1860  CONTINUE                                                          PR001730
1870  WRITE(8,100) ENTO(IJK1), OLD,ALPH,9999.                           PR001740
      LAB10=' TWA,    (8<U>-UW)/D          UW,      DALT ,    ENW  '  PR001750
CC    WRITE(8,90) LAB10                                                 PR001760
                                                                        PR001770
CC    ..................................................................PR001780
CC    .                                                                 PR001790
CC    . 5.  CALCULATION OF VISCOSITY & THICKNESS OF ANOMOLOUS LAYER .   PR001800
CC    ..................................................................PR001810
          DO 2800 KJ=1,10                                               PR001820
      CSR(KJ)=(FTW(KJ)*FCK1)+ FCK2*FTW(KJ)**FCN                         PR001830
      GG=FCK2*ENTO(IJK1)*(FCN+3.)/4.                                    PR001840
      ENW(KJ,IJK1)=ENTO(IJK1)/(1.+(FTW(KJ)**(FCN-1))*GG)                PR001850
      IF (UW(KJ).GT.0.) GOTO 1001                                       PR001860
      DALTA(KJ)=-UW(KJ)*ENW(KJ,IJK1)/FTW(KJ)                            PR001870
      GOTO 1002                                                         PR001880
1001  DALTA(KJ)= UW(KJ)/( FTW(KJ)*(1./.00893585-1./ENW(KJ,IJK1)))      PR001890
1002  WRITE(8,100) FTW(KJ),CSR(KJ), UW(KJ),ENW(KJ,IJK1),DALTA(KJ)      PR001900
2800  CONTINUE                                                          PR001910
                                                                        PR001920
CC    ..............................                                    PR001930
CC    FITTING OF UW=B*TW+BB*TW**DN                                      PR001940
CC    ..............................                                    PR001950
       DO 1111 III=1,10                                                 PR001960
       CALL GRP2                                                        PR001970
       DN(IJK1)=1.0                                                     PR001980
      OLD=99999.                                                        PR001990
        DO 2740 JREQ=1,50                                               PR002000
      DN(IJK1)=DN(IJK1)+0.05                                            PR002010
         DO 2850 KJ=1,10                                                PR002020
      X1(KJ)=FTW(KJ)                                                    PR002030
      X2(KJ)=FTW(KJ)**DN(IJK1)                                          PR002040
      Y1(KJ)=UW(KJ)                                                     PR002050
2850  CONTINUE                                                          PR002060
      MM=10                                                             PR002070
      A=0.0                                                             PR002080
      DEFAT=2.                                                          PR002090
      CALL LIN2F                                                        PR002100
      DIF=DV-OLD                                                        PR002110
      IF(DV.GE.OLD) GOTO 2740                                           PR002120
      OLD=DV                                                            PR002130
      DUMDT=B                                                           PR002140
      CB(IJK1)=B                                                        PR002150
      CCK(IJK1,III)=B                                                   PR002160
      CBB(IJK1)=BB                                                      PR002170
      BB=LOG(-BB)                                                       PR002180
C     WRITE(8,90) 'B         BB        DN        DV: UW=B*TAW+BB*TAW**DN' PR002190
      WRITE(8,100) B,BB,DN(IJK1),DV                                     PR002200
```

```
2740   CONTINUE                                                              PR002210
1111   CONTINUE                                                              PR002220
                                                                             PR002230
CC     ..............................................                        PR002240
CC     . VISCOSITY  AND ADSORBED LAYER AT ZERO SHEAR.                        PR002250
CC     ..............................................                        PR002260
CC       ....ENW0..FROM CANNON-FESKY MEASUREMENTS...                         PR002270
       ENW0=((CB1*C(IJK1)+CB2*C(IJK1)**CN1)+1.)*0.008936                     PR002280
         DO 2810 KJ=1,10                                                     PR002290
       STRESS=KJ*50.                                                         PR002300
       WVELO=CB(IJK1)*STRESS+CBB(IJK1)*STRESS**DN(IJK1)                      PR002310
2810   CONTINUE                                                              PR002320
         DO 2820 JH=1,10                                                     PR002330
       XXX1(IJK1,JH)=DALTA(JH)*10**4                                         PR002340
       XX1(IJK1,JH)=UW(JH)                                                   PR002350
2820   CONTINUE                                                              PR002360
9000   CONTINUE                                                              PR002370
CC.....ENTO=ENTS*(1+B*C)...FROM FLOW MEASUREMENT..                           PR002380
         DO 9500 I1=1,KKK                                                    PR002390
       Y1(I1)=(ENTO(I1)/0.008936)-1.0                                        PR002400
       WRITE(8,100) ENTO(I1)                                                 PR002410
9500   X1(I1)=C(I1)                                                          PR002420
       MMM=KKK                                                               PR002430
       A=0.                                                                  PR002440
       CALL LINF                                                             PR002450
       VISIN=B                                                               PR002460
       DO 9555 I2=1,KKK                                                      PR002470
       VISTY=0.008936*(1.+VISIN*C(I2))                                       PR002480
       ENW0=((CB1*C(I2)+CB2*C(I2)**CN1)+1.)*0.008936                         PR002490
       WRITE(8,100) VISTY,ENW0                                               PR002500
9555   CONTINUE                                                              PR002510
       CALL GRP22                                                            PR002520
100    FORMAT(5G13.5)                                                        PR002530
90     FORMAT(A/)                                                            PR002540
999    STOP .                                                                PR002550
       END                                                                   PR002560
                                                                             PR002570
*********************************************************************        PR002580
                                                                             PR002590
            SUBROUTINE  LINF                                                 PR002600
CC     ..............................                                        PR002610
CC     .                            .                                        PR002620
CC     .  LINEAR FITTING: Y=A+B*X   .                                        PR002630
CC     ..............................                                        PR002640
                                                                             PR002650
       COMMON/FITT/S1,S2,MMM, X1,Y1,A,B,DV,X2,Y2,BB                          PR002660
       REAL*4 S1, S2,S11, S12, Y1(30),X1(30),A,B,BB, X2(30),Y2(30)           PR002670
       S1=0.                                                                 PR002680
       S2=0.                                                                 PR002690
       S11=0.                                                                PR002700
       S12=0.                                                                PR002710
       DO 2221 J=1,MMM                                                       PR002720
       S2=Y1(J)+S2                                                           PR002730
       S12=Y1(J)*X1(J)+S12                                                   PR002740
       S1=X1(J)+S1                                                           PR002750
```

```
      S11=X1(J)**2+S11                                                  PRO02760
2221  CONTINUE                                                          PRO02770
      FM=FLOAT(MMM)                                                     PRO02780
      IF(A.EQ.0.) GOTO 2005                                             PRO02790
      B=(S12-S1*S2/FM)/(S11-S1**2/FM)                                   PRO02800
      A=(S2-S1*B)/FM                                                    PRO02810
      GOTO 2008                                                         PRO02820
2005  B=S2/S1                                                           PRO02830
2008  FF=0.                                                             PRO02840
      DO 2010 JJ=1,MMM                                                  PRO02850
      Y2(JJ)=A+B*X1(JJ)                                                 PRO02860
      X2(JJ)=X1(JJ)                                                     PRO02870
2010  FF=FF+(Y1(JJ)-A-B*X1(JJ))*(Y1(JJ)-A-B*X1(JJ))                    PRO02880
      DV=SQRT(ABS(FF/ FLOAT(MMM) ))                                     PRO02890
9991  RETURN                                                            PRO02900
      END                                                               PRO02910
                                                                        PRO02920
*****************************************************************     PRO02930
                                                                        PRO02940
      SUBROUTINE LIN2F                                                  PRO02950
                                                                        PRO02960
CC    ..............................                                    PRO02970
CC    LINEAR FITTING Y=A+B1*X1+B2*X2                                    PRO02980
CC    ..............................                                    PRO02990
      COMMON/FITT/S1,S2,MMM, X1,Y1,A,B,DV,X2,Y2,BB                     PRO03000
      COMMON/ITER/III,DEFAT                                             PRO03010
      REAL*4 X1(30),X2(30),Y1(30),Y2(30)                                PRO03020
      REAL*4 S10,S20,S11,S22,S12,S21,X1B,X2B,YB,A,B,BB                  PRO03030
      X1B=0.                                                            PRO03040
      X2B=0.                                                            PRO03050
      YB=0.                                                             PRO03060
       DO 55 I=1,MMM                                                    PRO03070
      X1B=X1B+X1(I)/FLOAT(MMM)                                          PRO03080
      X2B=X2B+X2(I)/FLOAT(MMM)                                          PRO03090
55    YB=YB+Y1(I)/FLOAT(MMM)                                            PRO03100
      S00=0.                                                            PRO03110
      S10=0.                                                            PRO03120
      S20=0.                                                            PRO03130
      S11=0.                                                            PRO03140
      S12=0.                                                            PRO03150
      S22=0.                                                            PRO03160
      S21=0.                                                            PRO03170
        DO 20 I=1,MMM                                                   PRO03180
      S00=S00+(Y1(I)-YB)**2                                             PRO03190
      S10=S10+(X1(I)-X1B)*(Y1(I)-YB)                                    PRO03200
      S20=S20+(X2(I)-X2B)*(Y1(I)-YB)                                    PRO03210
      S11=S11+(X1(I)-X1B)*(X1(I)-X1B)                                   PRO03220
      S12=S12+(X1(I)-X1B)*(X2(I)-X2B)                                   PRO03230
      S22=S22+(X2(I)-X2B)*(X2(I)-X2B)                                   PRO03240
      S21=S12                                                           PRO03250
 20   CONTINUE                                                          PRO03260
      BB=(S20*S11-S21*S10)/(S22*S11-S21*S12)                            PRO03270
      IF(DEFAT.EQ.1.) GOTO 201                                          PRO03280
      IF(DEFAT.EQ.2.) GOTO 202                                          PRO03290
      GOTO 203                                                          PRO03300
```

```
201     IF(BB.LT.0.0) BB=-BB                                                    PR003310
        GOTO 203                                                                PR003320
202     IF(BB.GT.0.0) BB=-BB                                                    PR003330
203     IF (A.EQ.0.) GOTO 25                                                    PR003340
        B =(S10-S12*BB)/S11                                                     PR003350
        A=YB-B*X1B-BB*X2B                                                       PR003360
        GOTO 26                                                                 PR003370
25      B=(YB-BB*X2B)/X1B                                                       PR003380
26      FF=0.                                                                   PR003390
          DO 65 J=1,MMM                                                         PR003400
        Y2(J)=A+B*X1(J)+BB*X2(J)                                                PR003410
65      FF=FF+(Y1(J)-Y2(J))*(Y1(J)-Y2(J))                                       PR003420
        DV=SQRT(ABS(FF/FLOAT(MMM)))                                             PR003430
        RETURN                                                                  PR003440
        END                                                                     PR003450
                                                                                PR003460
*****************************************************************************PR003470
        SUBROUTINE GRP2                                                         PR003480
                                                                                PR003490
CC     .....UWS=DLTA0* TAW....                                                  PR003500
                                                                                PR003510
        REAL*4 DN(30),ENT0(30),CCK(30,30),CB(30),CBB(30),ENW(30,30)             PR003520
        COMMON/P3/CB,CBB,DN,VISIN,ENT0,CCK,ENW                                  PR003530
        COMMON/ITER/III,DEFAT                                                   PR003540
         DN(1)=2.45                                                             PR003550
         DN(2)=3.90                                                             PR003560
         DN(3)=3.05                                                             PR003570
         DN(4)=3.00                                                             PR003580
         DN(5)=2.15                                                             PR003590
         DN(6)=1.540                                                            PR003600
         DN(7)=1.41                                                             PR003610
         DN(8)=1.585                                                            PR003620
        RETURN                                                                  PR003630
        END                                                                     PR003640
                                                                                PR003650
 ***************************************************************************** PR003660
        SUBROUTINE GRP22                                                        PR003670
                                                                                PR003680
        REAL*4 X1(30),X2(30),Y1(30),Y2(30),XXX1(30,30),XX1(30,30),C(30)         PR003690
     3,FTW(30),DN(30),ENT0(30),CB(30),CBB(30),CCK(30,30),ENW(30,30)             PR003700
     7,UWS(30,30),UWA(30,30),DALTAA(30,30)                                      PR003710
        COMMON/FITT/ S1,S2,MMM,X1,Y1,A,B,DV,X2,Y2,BB                            PR003720
        COMMON/GRAPH1/ KKK,XX1,FTW,XXX1,C                                       PR003730
        COMMON/P3/CB,CBB,DN,VISIN,ENT0,CCK,ENW                                  PR003740
        COMMON/ITER/III,DEFAT                                                   PR003750
CC      ..... ENT0 FROM SMOOTH CURVE.....                                       PR003760
        DO 1998 I9=1,1                                                          PR003770
        DO 9001  I=1,KKK                                                        PR003780
        ENT0(1)=0.00934                                                         PR003790
        ENT0(2)=0.009480                                                        PR003800
        ENT0(3)=0.009545                                                        PR003810
        ENT0(4)=0.009585                                                        PR003820
        ENT0(5)=0.00970                                                         PR003830
        ENT0(6)=0.01010                                                         PR003840
        ENT0(7)=0.01072                                                         PR003850
```

```
9001    ENT0(8)=0.01245                                                        PR003860
          DO 9100 I=1,8                                                        PR003870
        Y1(I)=ENT0(I)*CCK(I,III)                                               PR003880
        X1(I)=Y1(I)/C(I)                                                       PR003890
        X2(I)=(ENT0(I)/0.008936-1.)/C(I)                                       PR003900
9100    CONTINUE                                                               PR003910
        MMM=8                                                                  PR003920
        A=1.                                                                   PR003930
        DEFAT=0.                                                               PR003940
        CALL LIN2F                                                             PR003950
        DALTAP=-A                                                              PR003960
        FK=-B                                                                  PR003970
        DALTS1=-BB/B                                                           PR003980
        WRITE(8,90) '   DALTS1       DV       DALTAP     FK       III  '      PR003990
        WRITE(8,100) DALTS1,DV,DALTAP,FK,III,I9                                PR004000
          DO 9200 I=1,8                                                        PR004010
        DALTS0=DALTS1*(1.-C(I)/(FK+C(I)))                                      PR004020
        DALTA0=DALTAP*C(I)/(FK+C(I))                                           PR004030
        AA=Y2(I)/ENT0(I)                                                       PR004040
        WRITE(8,100) DALTA0,C(I),DALTS0,AA                                     PR004050
          DO 9155 JK=1,10                                                      PR004060
        SLIPC=DALTS0*(1./0.008936-1./ENT0(I))                                  PR004070
        UWS(JK,I)=FTW(JK)*DALTS0*(1./0.008936-1./ENT0(I))                      PR004080
        UWA(JK,I)=((-DALTA0/ENT0(I))*FTW(JK)+CBB(I)*FTW(JK)**DN(I))            PR004090
        DALTAA(JK,I)=-ENW(JK,I)*UWA(JK,I)/FTW(JK)                              PR004100
        WRITE(8,100) FTW(JK),UWS(JK,I),UWA(JK,I),DALTAA(JK,I),SLIPC            PR004110
9155    CONTINUE                                                               PR004120
9200    CONTINUE                                                               PR004130
1998    CONTINUE                                                               PR004140
100     FORMAT(5G13.5)                                                         PR004150
90      FORMAT(A/)                                                             PR004160
        RETURN                                                                 PR004170
        END                                                                    PR004180
```